Eloi da Silva Feitosa

Aspectos Físico-Químicos de Colóides de Associação em Solução e Interface

1910002804

TESE DE LIVRE DOCÊNCIA

ASPECTOS FÍSICO-QUÍMICOS DE COLÓIDES DE ASSOCIAÇÃO EM SOLUÇÃO E INTERFACE

Professor Doutor Eloi da Silva Feitosa

Departamento de Física

Instituto de Biociências, Letras e Ciências Exatas

Universidade Estadual Paulista "Júlio de Mesquita Filho" - UNESP

Câmpus de São José do Rio Preto

2804/14

BIBLIOTECA

2002

"É preciso muito tempo para se tornar jovem"

Pablo Picasso

Para Tainá, Lucas e Marília Beatriz

Para meus pais

Meus sinceros agradecimentos aos meus colaboradores e alunos que contribuíram com uma grande parcela no desenvolvimento dos meus projetos de pesquisa.

Meus agradecimentos especiais à minha família, especialmente aos meus filhos que sempre aguardavam o meu retorno da pesquisa com muita ansiedade, abraços e beijos.



Índice

Símbolos e abreviaturas 1

Lista de publicações 2

Resumo e apresentação 1

Introdução 6

- Micelas 9
- Surfactantes derivados de poli óxido de etileno 11
- Sais de bile 12
- Vesículas 14
- Interação polímero-surfactante 16
- Interação surfactante-surfactante 18

Métodos de investigação 21

- Espalhamento dinâmico de luz (EL) 21
- Crio-microscopia de transmissão de elétrons (cryo-TEM) 22
- Calorimetria 22
- Fluorescência 23
- Tensão superficial 26
- Condutividade 27
- Monocamadas em interface 28
- A equação de Poisson-Boltzmann (EPB) 29

Discussão dos resultados 30

- Interação de sal de bile com vesículas de DODAX 36
- Interação de surfactante com vesículas de DODAX 38
- Interação de polímero com surfactantes não-iônicos 42
- Efeito de eletrólitos nas vesículas e monocamadas de DODAX 45
- Considerações finais 48
- Bibliografia 49

Abstract 53

unesp

Símbolos e abreveaturas

α, grau de dissociação de contra-íons

$C_{12}E_n$, polietileno glicol n-dodecil mono-éter (n = 5, 7 e 8)

C_{16}TAS, sulfato de hexadeciltrimetilamônio

C_{16}TAB, brometo de hexadeciltrimetilamônio

C_{18}TAB, brometo de octadeciltrimetilamônio

DDAB, brometo de didodecildimetilamônio

DHP, fosfato de dihexadecil

DLS, espalhamento dinâmico de luz

DODAC, cloreto de dioctadecildimetilamônio

DODAB, brometo de dioctadecildimetilamônio

B4A, trans,trans-1,4-difenil-carboxi-propil-1,3-butadieno

DPB, trans,trans-1,4-difenil butadieno

DPH, trans,trans,trans-1,6-difenil hexatrieno

DPPC, Dipalmitoil fosfatidilcolina

EL, espalhamento de luz

EPB, equação de Poisson-Boltzmann

HPS, 1-(N-hexadecil, NN'dimetilamônio)-propano,3,sulfonato

NaC, colato de sódio

NaDOC, deoxicolato de sódio

NaGC, glicocolato de sódio

NaTDC, taurodeoxicolato de sódio

PC, fosfatidilcolina

RPE, ressonância paramagnética eletrônica

SAXS, espalhamento de luz a baixo ângulo

SDS, dodecil sulfato de sódio

T_c, temperatura de transição da fase gel para a fase líquido-cristalina

T_{cp}, temperatura de turvação

t-Dpo; trans-difenilpolienos

4H4A, trans,trans,trans-1,6-difenil-p'-n-butil-p-carboxi-propil-1,3,5-hexatrieno

cm 1 2 3 4 5 6 7 unesp 11 12 13 14 15 16 17 18

lista de publicações

I. Cuccovia, I. M.; Feitosa, E.; Chaimovich, H.; Sepulveda, L.; Reed, W. Size, Electrophoretic Mobility and Ion Dissociation of Vesicles Prepared with Synthetic Amphiphiles *J. Phys Chem*. **1990**, *94*, 3722-3725;

II. Feitosa, E.; Agostinho Neto, A.; Chaimovich, H. Integration of the non-linear Poisson-Boltzmann equation for charged vesicles in electrolytic solution. *Langmuir*, **1993**, *9*,702-707.

III. Feitosa, E.; Brown, W; Hansson, P. Interactions Between the Non-Ionic Surfactant $C_{12}E_5$ and Poly(ethylene oxide) Studied Using Dynamic Light Scattering and Fluorescence Quenching. *Macromolecules*, **1996**, *29*, 2169-2178.

IV. Feitosa, E.; Brown, W.; Vasilescu, M.; Swanson-Vethamuthu, M. Effect of Temperature on the Interaction Between the Nonionic Surfactant $C_{12}E_5$ and Poly(ethylene oxide) Investigated by Dynamic Light Scattering and Fluorescence Methods. *Macromolecules*, **1996**, *29*, 6837-6846.

V. Feitosa, E.; Brown, W.; Swanson-Vethamuthu, M. Interaction of the Nonionic Surfactant $C_{12}E_8$ with High Molar Mass Poly(ethylene oxide) Studied by Dynamic Light Sacttering and Fluorescence Quenching Methods. *Langmuir*, **1996**, *12*, 5985-5991.

VI. Feitosa, E.; Brown, W. Fragment and vesicle Structures in Sonicated Dispersions of Dioctadecyldimethylammonium Bromide *Langmuir* **1997**, *13*, 4810-4816.

VII. Feitosa, E.; Brown, W. Mixed micelles of sodium dodecyl sulphate and penta-ethyleneglycol mono n-dodecyl ether. *Langmuir* **1998**, *14*, 4460-4465.



VIII. Banatti, C. R.; Tiera, M. J.; Feitosa, E.; Olofsson, G. Phase Behavior of synthetic amphiphile vesicles invetigated by calorimetry and fluorescence methods. *Thermochim. Acta* **1999**, *328*, 137-142.

IX. Feitosa, E.; Barreleiro, P. C. A.; Olofsson, G. Phase transition in dioctadecyldimethylammonium bromide and chloride vesicles prepared by different methods. *Chem. Phys. Lipids* **2000**, *105*, 210-213.

X. Barreleiro, P. C. A.; Olofsson, G.; Feitosa, E. Vesicle-to-micelle transition in dioctadecyldimethylammonium bromide and dioctadecyldimethylammonium chloide dispersions induced by $C_{12}E_8$. An isothermal titration calorimetry study. *Progr. Colloid Sci.* **2000**, *116*, 33-36.

XI. Benatti, C. R. B.; Feitosa, E.; Fernandez, R. M.; Lamy-Freund, M. T. Structural and thermal characterization of dioctadecyldimethylammonium bromide dispersions by spins labels *Chem. Phys. Lipids* **2001**, *111*, 93-104.

XII. Cavalli, A.; Dynarovicz-Lakta, P.; Oliveira, O. N.; Feitosa, E. Using an effective to explain surface potential of Langmuir monolayers from dialkydimethylammonium halides with the Gouy-Chapman Theory. *Chem. Phys. Lett.* **2001**, *338*, 88-94.

cm 1 2 3 4 5 6 7 unesp 11 12 13 14 15 16 17 18

Resumo e apresentação

Neste trabalho apresentamos uma seleção de resultados obtidos nos últimos dez anos pelo nosso grupo de pesquisa (Grupo de Física de Colóides) em colóides de associação em solução contendo surfactantes simples e mistos, formadores de micelas e vesículas, na ausência e presença de polímero e eletrólitos, e na interface água/ar, e discutí-los à luz dos resultados existentes na literatura (vide lista de publicações na página 2). Os surfactantes investigados são catiônicos mono (C_{18}TAB) e dialquilado (DODAX, X = Br^- e Cl^-), aniônicos mono (SDS) e dialquilado (DHP), zwitteriônico (HPS) e não-iônicos (C_mE_n, m = 12 e n = 5 e 8). A estrutura química de alguns desses surfactantes é mostrado na Figura 1. Técnicas experimentais, como espalhamento de luz, SAXS, fluorescência, calorimetria, tensiometria, e métodos teórico-computacionais (equação de Poisson-Boltzmann) etc. foram usados neste estudo.

Os trabalhos aqui analisados tratam das propriedades físico-químicas de micelas catiônicas de C_{18}TAB (SWANSON-VETHAMUTHU *et al.*, 1998), de C_{16}TAS (FEITOSA *et al.*, 2001b), e micelas mistas de SDS/C_{16}TAB (VII), complexos polímero-surfactante para os sistemas PEO-$C_{12}E_5$ (III, IV) e de PEO-$C_{12}E_8$ (V, FEITOSA *et al.*, 2001), sendo PEO de grande e pequeno peso molecular (MW = 600 e 12 kDa), e vesículas catiônicas de DODAB e DODAC e aniônicas de DHP, preparadas por diferentes métodos, tais como sonicação, injeção clorofórmica, extrusão e espontaneamente (I, VI, VIII, IX, X, XI, LOPES *et al.*, 2001; FEITOSA e BARRELEIRO, 2001; BARRELEIRO *et al.*, 2001; FEITOSA *et al.*, 2001c). Dispersões mais concentradas de DODAX, DDAB e DHP foram investigadas por SAXS (FEITOSA e AMARAL, 2001). Usamos também SAXS no estudo da estrutura e tamanho da fosfolipase A_2 extraída do

veneno de cobra *Crotalus durissus terrificus* (ABREGO *et al.*, 2001), com o objetivo de darmos início ao estudo da interação de surfactante com proteína. As propriedades de filmes finos de DODAB, na presença de contra-íons com diferente eletronegatividade na subfase, também foram investigadas e a condensação da monocamada foi entendidas com base na teoria de Gouy-Chapman (XII), assim como a distribuição de íons e o potencial eletrostático nas vizinhanças das vesículas obtidos por solução numérica da equação de Poisson-Boltzmann (II).

Esclarecimento: anexamos a esta tese apenas os trabalhos publicados (enumerados de I a XII), os demais trabalhos, na forma de manuscritos, são citados como referências e estão disponíveis aos interessados.

Introdução

Colóides de associação, dos quais vesículas e micelas são exemplos, são importantes em muitas aplicações práticas, científicas e tecnológicas e estão presentes em solução de surfactantes. Vesículas são usadas, por exemplo, como agentes miméticos e no transporte de drogas em seres vivos (FENDLER, 1982), enquanto que as micelas são agentes solubilizantes poderosos usados na indústria de alimentos, cosméticos, tintas, detergentes etc. (JÖNSSON *et al.*, 1999). Estudos dos colóides de associação consistem essencialmente na obtenção de estruturas monodispersas, na caracterização de suas propriedades físico-químicas ou na determinação do diagrama de fase completo ou parcial.

A rica variedade estrutural de associação de surfactantes se deve à natureza física da interação entre seus monômeros, possibilitando que transições de fase ocorram pela variação da concentração do surfactante e de eletrólitos ou temperatura. Em geral, devido a critérios de empacotamento, surfactantes monoalquilados tendem a agregar-se em micelas esféricas a baixas concentrações, e, com o aumento da concentração, passam para as fases cúbica discreta, hexagonal, cúbica bicontínua, vesicular lamelar e as correspondentes estruturas reversas, obedecendo o diagrama de Fontell (FONTELL, 1990). Nem todos os surfactantes passam por todas essas fases, mas as mudanças de fase normalmente obedecem esta seqüência. O conhecimento do diagrama de fases de surfactantes é de grande importância para suas aplicações diversas, cujas soluções binárias são representadas por diagramas TX (temperatura vs. composição). Essas transições de fases ocorrem devido ao crescimento

cm 1 2 3 4 5 6 7 unesp 11 12 13 14 15 16 17 18

das micelas que adquirem a forma alongada em concentrações moderadas de surfactantes, podendo se ramificar e formar fases bicontínuas. A condição de empacotamento, segundo a qual o interior micelar é totalmente preenchido pelos hidrocarbonetos do surfactante, não permite crescimento radial das micelas. Com o aumento do tamanho das micelas aumenta também a polidispersidade.

Dispersões de vesículas são em geral polidispersa e meta-estáveis, e suas propriedades físico-químicas dependem do método de preparação das mesmas. Vesículas uni e multilamelares pequenas e grandes são encontradas em dispersões isotrópicas. Vesículas unilamelares predominantemente grandes são formadas espontaneamente pela mistura simples de surfactantes catiônicos em dispersões diluídas (IX), enquanto que os fosfolipídios naturais (zwitteriônicos) formam, mesmo a baixas concentrações, estruturas de bicamadas multilamelares (LASIC, 1993).

A mistura de surfactante, formadores de micelas, vesículas ou lamelas, constitui uma importante área de pesquisa, pois altera as propriedades físico-químicas dos surfactantes individuais e diagramas de fases. Polímeros, e co-solutos em geral, também alteram as propriedades e fases de dispersões de vesículas ou soluções micelares.

Nos últimos anos temos investigado o efeito de surfactantes não-iônicos derivados de polióxido de etileno ($C_{12}E_n$, n = 5, 7 e 8) nas propriedades das vesículas catiônicas de DODAX e observamos que $C_{12}E_n$ induz transição vesícula-micela e que essa transição ocorre em três estágios (X, BARRELEIRO *et al.*, 2001). Observamos também por DSC que $C_{12}E_n$ diminui a temperatura de transição de fase gel-líquido cristalina (T_c), tornando-a menos cooperativa. Um efeito oposto foi observado por PEG (12 kDa) que aumenta a T_c de DODAX (MARQUES, 2000), enquanto que sais de bile diminuem a T_c de DODAX (ALVES, 2001).



A interação entre PEG (12 e 600 kDa) com $C_{12}E_n$ (n = 5 e 8) também foi investigada (III, IV, FEITOSA *et al.*, 2001a). Basicamente observamos que, apesar do polímero e do surfactante serem neutros, existe interação com formação de complexos de PEG-$C_{12}E_n$ em água. Evidências dessa interação resultaram das medidas de espalhamento de luz, apesar de PEG não alterar significativamente a CMC de $C_{12}E_n$, e, na presença de PEG, o número de agregação das micelas de $C_{12}E_n$ ser menor, igual ou maior do que na ausência, dependendo da concentração das espécies na mistura. O estudo do efeito de co-solutos em vesículas está sendo estendido para polímeros de celulose (MARQUES, 2000), polissacarídeos (OLIVEIRA, 2001) outros surfactantes aniônicos, catiônicos e zwitteriônicos (TENGNOM, 2001)

Nosso trabalho também inclui estudos do efeito da eletronegatividade de contra-íons na pressão superficial e potencial de superfície de filmes finos de DODAB na interface água/ar (XII), e um estudo teórico-computacional do potencial eletrostático e distribuição de cargas (co- e contra-íons) na vizinhança, ou seja, nos compartimentos aquosos interno e externo das vesículas (II). A análise dos resultados da interação de co-solutos com vesículas catiônicas requereu um estudo detalhado das propriedades das vesículas de DODAX preparadas por diferentes métodos (I, VI, IX, XI, LOPES et al., 2001, FEITOSA *et al.*, 2001c).

Como este trabalho está essencialmente relacionado a micelas, vesículas e monocamadas, a seguir descreveremos, brevemente, o processo de formação e características principais dessas estruturas coloidais.

Micelas

Em solução aquosa diluída moléculas anfifílicas particionam-se preferencialmente na interface solvente/ar com a parte hidrofílica voltada para o solvente e a porção hidrofóbica expostas ao ar. A concentrações maiores, surfactantes formam espontaneamente agregados, denominados *micelas*, nos quais a cabeça polar dos monômeros fica voltada para a fase aquosa e a parte apolar imersa no interior do agregado, protegida de modo a minimizar a interação energeticamente desfavorável entre as cadeias de hidrocarboneto e a água. As interações hidrofóbicas são as principais responsáveis pela formação desses agregados (TANFORD, 1991). Ao contrário dos surfactantes, as micelas não são tensoativas, mas altamente solúveis em solventes polares, e são excelentes solubilizadores de moléculas apolares.

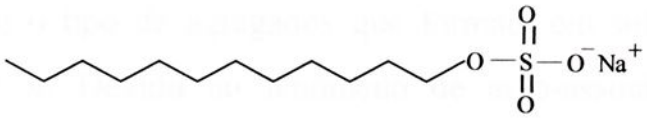
Surfactantes em solução podem formar uma variedade de agregados e fases, dependendo da natureza do surfactante e das condições do meio. O tipo de agregado formado pode ser previsto, aproximadamente, conhecendo o *parâmetro de empacotamento* do surfactante, $P = v/a_o l_c$, onde v e l_c são, respectivamente, o volume e o comprimento crítico (ligeiramente menor do que o comprimento das cadeias totalmente distendidas) das cadeias de hidrocarboneto, e a_o é a área efetiva do grupo de cabeça polar (ISRAELACHVILI, 1992). v e l_c são determinados semi-empiricamente através das equações $v = 0{,}027(n_c + n_{Me})$ e $l_c = 0.15 + 0.127n_c$ (em nm^3 e nm, respectivamente), onde n_c é o número de carbonos por cadeia de hidrocarbonetos e n_{Me} é número de grupos terminais metila (TANFORD, 1991), enquanto que a_o nem sempre pode ser determinado de forma trivial. Quando $P < 1/3$, micelas esféricas são formadas, e surfactantes monoalquilados em geral satisfazem esta condição, enquanto que bicamadas se formam quando $P \approx 1$, que em geral, são satisfeitas por

surfactantes dialquilados. $P > 1$ resulta na formação de estruturas reversas, onde pequenos volumes de água são solubilizados no meio predominantemente hidrofóbico formado pelas cadeias de hidrocarboneto. É possível, em sistemas binários surfactante/água, P variar numa extensa faixa de valores correspondentes à formação de estruturas que variam desde micelas normais a micelas reversas, quando se varia, p. ex., a concentração de surfactante; como v e l_c variam muito pouco com a concentração de surfactante, a_o é o principal responsável pela variação de P, daí a dificuldade de se determinar a_o com razoável precisão.

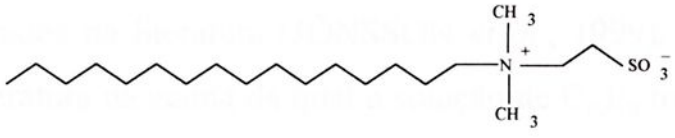
Micelas são formadas espontaneamente na região da *concentração micelar crítica*, CMC, que é tipicamente na faixa de alguns milimolares. A concentração de monômeros livres coexistindo com as micelas é da ordem da CMC e a troca de monômeros entre micelas é rápida, o tempo típico de residência de um monômero numa micela de alquilsulfato de sódio é da ordem de 1 ms (ANIANSSON *et al.*, 1976). Estas características são únicas e importantes na maioria das aplicações práticas de surfactantes.

Neste trabalho apresentamos resultados do estudo das micelas de C_{18}TAB em solução aquosa eletrolítica de NaBr (VI), das micelas de C_{16}TAS em solução aquosa de Na_2SO_4 (FEITOSA *et al.*, 2001b) das micelas mistas de C_{18}TAB/SDS em solução aquosa (VII), da interação de micelas não-iônicas de C_mE_n (n = 5 e 8) com polímeros neutros PEG de grande e baixo peso molecular (600 e 12 kDa) (III, IV, V, FEITOSA *et al.*, 2001a), e na interação de $C_{12}E_8$ com vesículas catiônicas de DODAB e DODAC (X, BARRELEIRO *et al.*, 2001). A Figura 1 mostra a estrutura molecular de alguns surfactantes monoalquilados, formadores de micelas, usados na nossa pesquisa.

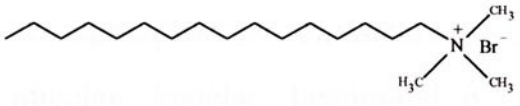
cm 1 2 3 4 5 6 7 unesp 11 12 13 14 15 16 17 18



Sulfato dodecil de sódio, SDS



Hexadecil propano sulfonato, HPS



Brometo de cetiltrimetilamônio, $C_{16}TAB$

tri-ethyleneglycol mono n-dodecyl ether, $C_{12}E_3$

Figura 1 - Estrutura molecular de alguns surfactantes formadores de micelas usados neste estudo.

Surfactantes derivados de poli óxido de etileno

Os surfactantes derivados de poli óxido de etileno (PEO) são importantes do ponto de vista de aplicação tecnológica e constituem um importante sistema para o estudo do fenômeno de auto-associação. São geralmente constituído por uma cadeia de hidrocarbonetos, C_m, em cuja extremidade se liga uma cadeia de PEO, E_m. Por isso, são, às vezes denominados co-polímeros diblocos AB. São, portanto, denotados por C_mE_n, e existem comercialmente para uma grande variedade de *m* e *n* variando de 3 a 18 ou mais.

Assim como PEO, os surfactantes C_mE_n exibem o fenômeno de turvação, e suas propriedades e o tipo de agregados que formam em solução aquosa dependem de *m* e *n*. Devido ao fenômeno de auto-associação desses surfactantes, os seus diagramas de fases são mais complexos do que dos polímeros puros de PEO. Os diagramas de fases desses surfactantes são facilmente encontrados na literatura (JÖNSSON *et al.*, 1999). O ponto de turvação é a temperatura na acima da qual a solução de C_mE_n torna-se turva resultante do fenômeno de separação da fase micelar isotrópica em duas fases: uma rica e a outra pobre em surfactante.

Dependendo da composição os surfactantes C_mE_n geralmente associam-se nas fases micelar, lamelar, hexagonal e cúbica. Estruturas reversas são encontradas nas fases ricas em surfactante. A fase lamelar é dominante para *n* pequenos, já para *n* grandes, a fase micelar predomina. O tamanho das micelas aumenta com a concentração e temperatura, ocorrendo um aumento pronunciado quando a temperatura se aproxima do ponto de turvação.

Os surfactantes C_mE_n são importantes em misturas ternárias com outros surfactantes em solução aquosa, nos sistemas mistos, cujas propriedades diferem, em geral, das propriedades dos sistemas binários correspondentes. Investigamos C_mE_n em misturas com outros surfactantes, SDS (VII), DODAB e DODAC (X, XVIII) e com o polímero neutro PEO (III, IV, V, FEITOSA *et al.*, 2001a).

Sais de bile

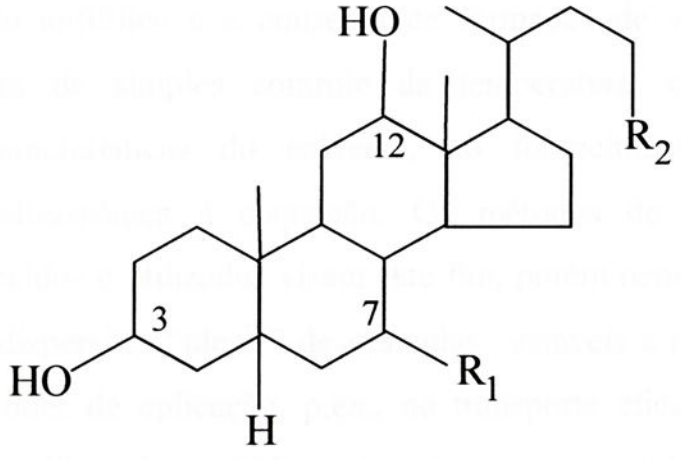
Os sais de bile constituem uma importante classe de surfactantes não usuais, fundamentais no processo de emulsificação de gordura no trato digestivo e auxiliam na eliminação de lecitina e colesterol do corpo (CAREY & SMALL, 1970; SMALL, 1971; BORGSTRÖM, 1977). Os sais

cm 1 2 3 4 5 6 7 unesp 11 12 13 14 15 16 17 18

de bile são derivados do ácido cólico e sua porção hidrofóbica consiste de anéis esteróides rígidos não-planares, contendo dois ou mais grupos hidroxila (OH^-), que lhes confere uma polaridade inserida na porção hidrofóbica. Os grupos OH^- estão no mesmo lado do anel que possui um lado polar (côncavo) e um lado apolar (convexo). A Figura 2 mostra a estrutura molecular de alguns sais de bile, NaC, NaDOC, NaTDC e NaGC. A rigidez da estrutura implica que o empacotamento dos sais de bile em micelas ou outras estruturas supramoleculares não pode ser do modo convencional. A associação de sais de bile é de baixa cooperatividade, e a CMC é pouco definida (LINDMAN *at al.*, 1976; MYSELS, 1984). Na região da CMC os sais de bile agregam-se através de interações hidrofóbicas em agregados mais ou menos esféricos com número de agregação (N_{ag}) muito menor do que os de surfactantes convencionais, tipicamente N_{ag} = 4 a 10 (SMALL, 1971; CAREY & SMALL, 1970; MAZER *et al.*, 1979; KRATOHVIL, 1986; LI & MCGOWN, 1994). Estas pequenas micelas são denominadas *micelas primárias*. Com o aumento da concentração do sal de bile, os agregados primários associam-se em micelas maiores e mais complexas, as *micelas secundárias*, nas quais as pontes de hidrogênio entre os sítios hidrofílicos das várias moléculas desempenham importante papel. No entanto, é possível que a força responsável pela agregação seja de natureza essencialmente hidrofóbica. O processo de agregação e tipo de interação ainda é um assunto de muita controvérsia.

Outro aspecto peculiar do comportamento interfacial dos sais de bile é o modo como eles adsorvem em interfaces. Tem-se mostrado que eles adsorvem preferencialmente na posição achatada na interface água-ar (ie., paralelamente à interface), com a parte côncava voltada para a água (parte convexa exposta para o ar) (KRATOHVIL *et al.*, 1986). O mesmo tipo de

orientação plana ocorre nas monocamadas planas de lecitina-sal de bile e na interface da mistura de sal de bile com bicamada de lecitina (ULMIUS, 1982) e micelas catiônicas (NICHOLS, 1990; HJELM, 1992), com a porção apolar convexa voltada para o caroço hidrofóbico dos agregados. Comportamento semelhante deve ocorrer na interação de sais de bile com as vesículas de DODAB e DODAC.



Sal de bile	R_1	R_2
NaC	OH	COO^-Na^+
NaDOC	--	COO^-Na^+
NaTDC	--	$CONHCH_2CH_2SO^-_3Na^+$
NaGC	OH	$CONHCH_2COO^-Na^+$

Figura 2 - Estrutura molecular dos sais de bile colato de sódio (NaC), deoxicolato de sódio (NaDOC), tauro deoxicolato de sódio (NaTDC) e glico colato de sódio (NaGC).

Vesículas

Estruturas vesiculares (bicamadas anfifílicas fechadas) são muito importantes em muitas aplicações científicas e tecnológicas, e estão presentes em muitas dispersões de anfifílicos em solução aquosa. Por isso, o estudo de dispersões de vesículas tem atraído crescente interesse de

pesquisadores. Em muitos sistemas, as vesículas estão em equilíbrio com outras estruturas mais complexas, por exemplo, em concentrações mais elevadas de surfactantes. Um dos grandes desafios da pesquisa de hoje em sistemas vesiculares consiste em preparar dispersões de vesículas estruturalmente homogêneas, monodispersas e estáveis. Estas estruturas nem sempre se formam espontaneamente na mistura de anfifílicos com o solvente, mas requerem métodos que promovam ou facilitem a solubilização do anfifílico e a conseqüente formação de vesículas. Estes métodos variam de simples controle da temperatura, composição do anfifílico e características do solvente, ao fornecimento de energia mecânica ou ultrassônica à dispersão. Os métodos de preparação de vesículas conhecidos e utilizados visam este fim, porém nem todos são bem sucedidos. As dispersões "ideais" de vesículas –estáveis e monodispersas– teriam maior poder de aplicação, p.ex., no transporte eficiente de drogas para células específicas do corpo humano, para uso em terapia gênica.

Um dos maiores desafios da pesquisa dos colóides de associação é ter o controle do tamanho, geometria e estabilidade das vesículas, a fim de que elas tenham maior poder de aplicação. Dentre os principais métodos de preparar vesículas destacamos: sonicação com probe ou a banho, extrusão, injeção orgânica, remoção do anfifílico, e formação espontânea (LASIC, 1993).

Um ponto em comum destes métodos consiste na temperatura de preparação das vesículas ser acima da T_c do anfifílico e que, uma vez formada, as vesículas em geral se mantêm estáveis após resfriar a amostra para uma temperatura abaixo da T_c. Isto é particularmente destacável em vesículas de anfifílicos, cuja T_c está acima da temperatura ambiente (*eg.*, DODAB), na qual muitas medidas experimentais são realizadas. Nem sempre as vesículas permanecem estáveis abaixo da T_c, é o caso de

unesp

dispersões aquosas de brometo de dihexadecildimetilamônio (DHDAB), T_c = 41 °C; acima da qual as vesículas são estáveis, mas à temperatura ambiente temos água mais cristais hidratados do surfactante. A Figura 3 ilustra a estrutura molecular de alguns surfactantes e fosfolipídios comumente usados na preparação de vesículas.

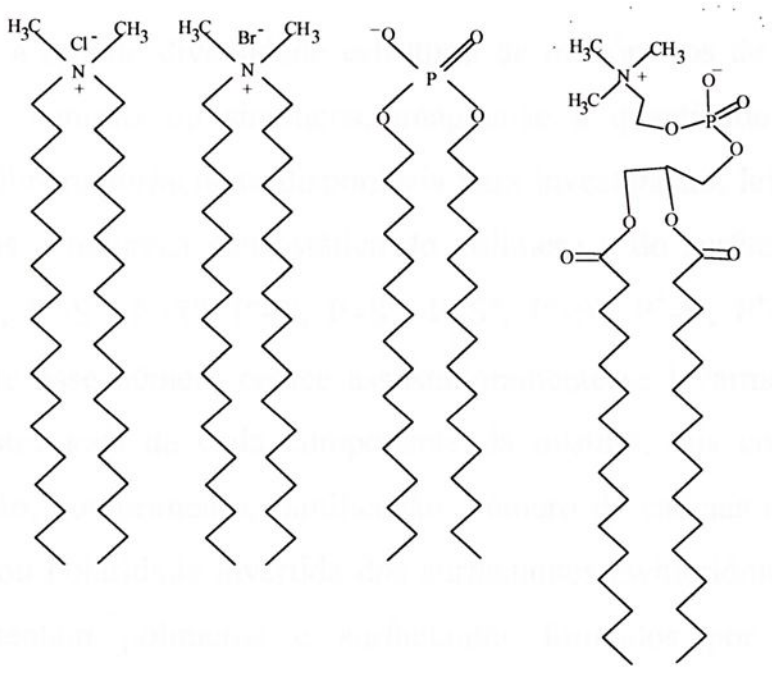


Figura 3 – Estrutura molecular de DODAX (X = Cl^- e Br^-), DHP e DPPC, formadoras de vesículas catiônicas, aniônicas e zwitteriônicas, respectivamente.

Interação polímero-surfactante

Misturas de polímeros com surfactantes em solução aquosa têm aplicação em áreas diversas de pesquisas científicas e tecnológicas (GODDARD e ANANTHAPADMANABHAN, 1993; BREUER e ROBB, 1972). Em sistemas biológicos, p.ex., lipídios dificilmente encontram-se dissociadas de alguma outra biomolécula (proteína, açúcar, colesterol etc.). O

surfactante pode alterar a capacidade de aderência do polímero a superfícies e, alternativamente, o polímero aumentar o poder de solubilidade do surfactante, evidenciado pela redução da CMC do surfactante pelo polímero. A adição de surfactante em solução de polímero modifica, em geral, as propriedades do polímero devido à interação entre os componentes e a conseqüente formação de complexos.

Dada a grande diversidade estrutural de monômeros de polímeros e surfactantes, naturais ou sintéticos, imagina-se a quantidade enorme de sistemas polímero-surfactante disponíveis para investigação, levando-se em conta apenas a natureza eletrostática do polímero e do surfactante: P^{o}-S^{o}, P^{o}-S^{-}, P^{o}-S^{+}, P^{o}-$S^{\pm}$, P^{-}-S^{o}, P^{-}-S^{-}, P^{-}-S^{+}, P^{-}-$S^{\pm}$, P^{+}-S^{o}, P^{+}-S^{-}, P^{+}-S^{+} e P^{+}-$S^{\pm}$. Naturalmente esse número cresce assustadoramente se levarmos em conta variantes estruturais de cada componente da mistura, tais como grau de polimerização, comprimento, ramificação, número de cadeias alquílicas do surfactante ou polaridade invertida dos surfactantes zwitteriônicos. Aqui, P e S representam polímeros e surfactantes formados por monômeros aniônicos (-), catiônicos (+), neutros (o) e zwitteriônicos (±).

A "driving force", de complexação, isto é, de formação de "clusters" de surfactantes no interior do polímero em solução aquosa, tem sido descrita como sendo forte, fraca e ou nula, dependendo da natureza química e estrutural dos componentes, inclusive do solvente (GODDARD E ANANTHAPADMANABHAN, 1993). A intensidade de interação costuma ser "medida" monitorando-se uma dada propriedade física do sistema, p. ex., a CMC ou CAC, o número de agregação das micelas na presença e ausência de polímero, condutividade ou viscosidade, entre outras. Regra geral, para um dado polímero neutro, a intensidade de

cm 1 2 3 4 5 6 7 unesp 11 12 13 14 15 16 17 18

interação com surfactantes decresce com a natureza polar do surfactante na seqüência: aniônico > catiônico > neutro (GODDARD, 1986).

Para um dado surfactante neutro, a intensidade de interação tende a aumentar com a hidrofobicidade do polímero (BRACKMAN e ENGBERTS, 1993). A natureza hidrofóbica do polímero limita, porém, a sua aplicabilidade a pequenas massas molares, devido a problemas de solubilidade. Por outro lado, para um dado polímero, a afinidade aumenta com o aumento do tamanho das micelas (GODDARD, 1986), o que tem sido observado por nós para sistemas de PEO-C_mE_n-água, nos quais o tamanho das micelas varia dependendo da razão n/m do anfifílico; para os casos até aqui investigados, fixamos $m = 12$ e $n = 5$ e 8.

A natureza da "driving force" responsável pela complexação de polímeros com surfactantes ainda é pouco conhecida. Por exemplo, surfactantes com a mesma porção hidrofóbica (C_{12}), porém com diferente polaridade têm afinidade distinta a polímeros neutros; em geral, surfactantes aniônicos (SDS) interagem mais fortemente com PEO do que surfactantes catiônicos (C_{16}TAB), apesar da interação eletrostática ser igualmente dominante em ambos os sistemas. A diferença na interação desses sistemas tem sido atribuída ao tamanho diferenciado das cabeças polares dos surfactantes (GODDARD, 1986).

Interação surfactante-surfactante

A mistura de surfactantes também é muito interessante e funciona como estabilizador de fases e no controle da carga elétrica e tamanho dos agregados formados. O efeito de surfactante na transição vesícula-micela, apesar de muito investigado, ainda não é bem entendido.

cm 1 2 3 4 5 6 7 unesp 11 12 13 14 15 16 17 18

A mistura de surfactante com lipídios naturais é muito explorada na formação de vesículas, e tem múltiplas aplicações. Na extração de proteína de membrana o surfactante deve ter grande poder de solubilização dos lipídios e baixo potencial de desnaturação protéica. O estudo da interação proteína/surfactante e lipídio/surfactante é, portanto, relevante no processo de extração e purificação de proteínas de membrana e mimetização de membranas naturais (GODDARD e ANANTHAPADMANABHAN, 1993).

A transição estrutural de vesícula para micela induzido por adição de surfactante se deve à interação das espécies tensoativas na solução, e a razão molar surfactante/lipídeo da transição depende das características dos componentes individuais. Em geral, a adição de surfactante na dispersão de vesículas induz mudança estrutural no processo de transição vesícula-micela que ocorre em três estágios (LOPEZ *et al.*, 1998): (i) a baixas concentrações os surfactante se distribuem essencialmente entre as vesículas, formando vesículas mistas, (ii) a concentrações intermediárias há uma mistura de micelas e vesículas, e (iii) a elevadas concentrações do surfactante ocorre a formação somente de micelas mistas (Figura 4).

O tamanho e a forma das estruturas intermediárias dependem da estrutura molecular dos anfifílicos (surfactantes) que formam as vesículas e micelas, e também do método utilizado na obtenção das vesículas, ou seja, da estrutura inicial das vesículas. O efeito de surfactantes na transição morfológica das vesículas é usualmente investigado com relação à estabilidade das vesículas, permeabilidade, espalhamento de luz, fusão ou agregação, além do efeito na incorporação de drogas, cujo controle de dosagem reduz efeitos colaterais alérgicos, tóxicos e imunológicos.

As técnicas mais usadas para investigar mudanças morfológicas de vesículas, na ausência ou presença de aditivos em geral, são: espalhamento

cm 1 2 3 4 5 6 7 unesp 11 12 13 14 15 16 17 18

dinâmico e estático de luz, NMR, calorimetria de varredura (DSC), microscopia de transmissão eletrônica por criogênese (cryo-TEM), fluorescência e tensão superficial (EDWARDS *et al.*, 1989).

Temos investigado a mistura de surfactantes formadores de micelas, SDS e $C_{12}E_8$ (VII) e na mistura de surfactantes formadores de vesículas, DODAB e DODAC, com surfactantes formadores de micelas, $C_{12}E_8$ e sais de bile (resultados mostrados nesta tese), e de DODAB com SDS, C_mTAB (m = 12 e 16) (TENGNOM, 2001).

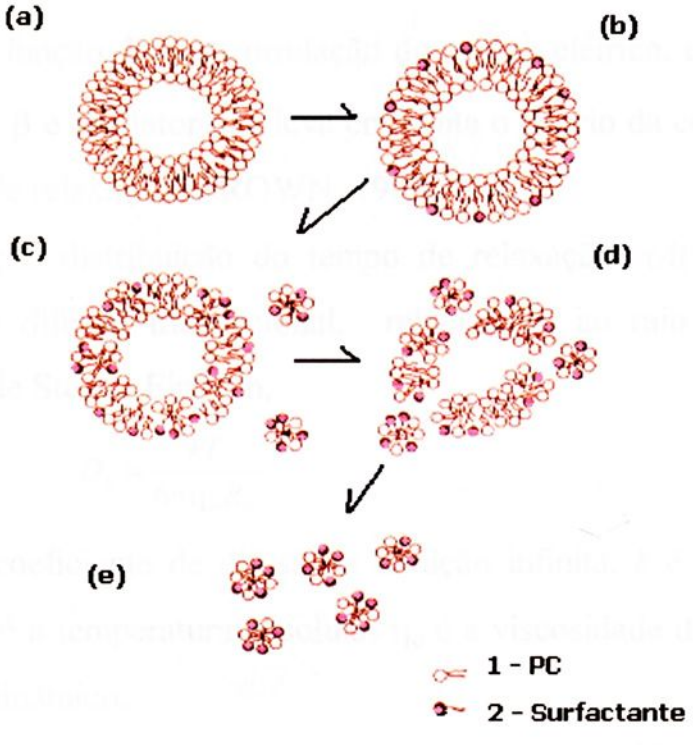


Figura 1 - Modelo de três estágios proposto para as estruturas formadas na mistura de fosfatidil colina PC-surfactante na transição vesícula-micela: (a) vesícula em meio aquoso, (b) vesícula mista, (c) mistura de vesícula e micela mistas, (d) desintegração das vesículas mistas, (e) micelas mistas.

Métodos de investigação

Usamos vários métodos experimentais e teóricos no estudo dos colóides de associação, cujos princípios e conceitos básicos são aqui discutidos.

Espalhamento dinâmico de luz (EL)

A partir da função de autocorrelação da intensidade da luz espalhada, $g_2(t)$, medida obtém-se, através da transformada inversa de Laplace, a função distribuição do tempo de relaxação, $A(\tau)$,

$$g_1(t) = \int_{-\infty}^{+\infty} \tau A(\tau) \exp(t/\tau) d \ln \tau \qquad (1)$$

onde $g_1(t)$ é a função de autocorrelação do campo elétrico, dado por $g_2(t) - 1 = \beta |g_1(t)|^2$, β é um fator que leva em conta o desvio da correlação ideal, e t é o tempo de relaxação (BROWN, 1993).

Da função distribuição do tempo de relaxação, $\tau A(\tau)$, obtém-se o coeficiente de difusão translacional, relacionado ao raio hidrodinâmico pela equação de Stokes-Einstein,

$$D_o = \frac{kT}{6\pi\eta_o R_h} \qquad (2)$$

onde D_o é o coeficiente de difusão a diluição infinita, k é a constante de Boltzmann, T é a temperatura absoluta, η_o é a viscosidade do solvente e R_h é o raio hidrodinâmico.

A técnica de EL é excelente para o estudo de colóides de associação. Temos usado esta técnica no estudo de micelas (SWANSON-VETHAMUTHU *et al.*, 1998, FEITOSA *et al.*, 2001b), vesículas (VI, X, XIV, LOPES *et al.*, 2001) e da interação de polímeros neutros com surfactantes não-iônicos (III, IV, V, FEITOSA *et al.*, 2001a) em solução.

unesp

Crio-microscopia de transmissão de elétrons (cryo-TEM)

Imagens diretas de alta resolução de macromoléculas individuais podem ser obtidas por microscopia de transmissão de elétrons (TEM). O experimento requer alto vácuo no microscópio (< 10^{-6} torr) e filmes finos da amostra (< 0,25 μm) a fim de permitir que feixes de elétrons o atravessem. Esta técnica consiste em preparar um filme fino (de 10 a 500 nm) em uma câmara ambiental, com condições de temperatura e humidade controladas. Para detalhes da técnica, vide BELLARE et al., 1988. O filme é vitrificado da temperatura desejada por congelamento rápido e então transferido em etano líquido para o microscópio de transmissão de elétrons (temos usado o Zeiss EM 902, da Universidade de Uppsala) para o exame da amostra. A fim de evitar perturbação da amostra e formação de cristais de gelo, as amostras foram mantidas a 108 K durante a transferência e o processo de observação. Todas as observações foram feitas a uma voltagem de aceleração eletrônica de 80 kV.

Calorimetria

Dentre os métodos termométricos para o estudo de macromoléculas em solução, destacam-se os de calorimetria diferencial de varredura (DSC) e de calorimetria por titulação isotérmica (ITC).

No DSC, calor é fornecido ou retirado, à mesma taxa, da amostra e da referência (solvente) colocados em celas gêmeas, e o calor é retirado da amostra ou fornecido para ela, a fim de manter a amostra e referência à mesma temperatura. O termograma é registrado em termos da variação do calor específico da amostra em função da temperatura. Transições de fases são caracterizados por picos no termograma centrado no valor da temperatura de transição. A área sob o pico fornece a entalpia associada à

transição, e a largura do pico é inversamente proporcional à cooperatividade da transição (VIII, IX).

No ITC, o calor de reação é medido após cada adição (titulação) de uma solução de macromoléculas (ex., solução de micelas) a um solvente ou solução de uma segunda macromolécula (ex., micela, vesícula , polímero, proteína etc.), a fim de investigar a entalpia de reação entre essas macromoléculas (X, SWANSON-VETHAMUTHU *et al.*, 1998, FEITOSA *et al.*, 2001b). O método é excelente para se obter a CMC ou CAC de surfactantes, respectivamente na ausência e presença de um polímero, além de verificar se duas espécies tensoativas interagem em solução formando agregados. A entalpia, a energia livre e a entropia do sistema podem ser facilmente obtidas por este método.

Fluorescência

Fluorescência de estado estacionário – A razão do primeiro pelo terceiro picos vibrônicos de um cromóforo (eg., pireno), I/III, reflete a micropolaridade do meio no qual está solubilizado, e pode ser usado para obter a CMC, número de agregação e polaridade desse meio (KALYANASUNDARAM, 1987). Abaixo da CMC os cromóforos estão localizadas no volume aquoso ou em agregados pré-micelares, resultando em valores elevados de I/III; na CMC, os cromóforos solubilizam-se no interior das micelas, reduzindo drasticamente o valor de I/III. Da curva de I/III em função da concentração de surfactante obtém-se a CMC.

O número de agregação, N_{ag}, de micelas pode ser determinado pelo método de Turro-Yekta (TURRO e YEKTA, 1978),

$$[M] = \frac{[S_m]}{N_{ag}} \qquad (3)$$

onde $[M]$ e $[S_m]$ são, respectivamente, as concentrações molares de micela e de surfactantes micelizados, relacionados às intensidades de fluorescência

dos cromóforos, I e I_o, na ausência e presença de supressor, respectivamente, através da equação

$$\ln \frac{I_o}{I} = \frac{[Q]}{[M]} \tag{4}$$

onde $[Q]$ é a concentração molar do supressor. A Eq. 4 é válida considerando que o cromóforo e o supressor estão no caroço hidrofóbico micelar e obedecem a distribuição de Poisson, e que o cromóforo fluoresce apenas na ausência do supressor (KALYANASUNDARAM, 1977). Pireno e cloreto de cetilpiridino são muito usados, respectivamente como sonda supressor de fluorescência. A Figura 4 mostra algumas sondas fluorescentes usadas em nossa pesquisa.

A anisotropia de fluorescência, r, é importante no estudo da polaridade da região hidrofóbica de micelas e vesículas. Obtém-se r por medidas da radiação de excitação e emissão vertical e horizontalmente polarizada do cromóforo. Para uma radiação de excitação verticalmente polarizada, a emissão vertical ($I_{//}$) e horizontalmente ($I_{\perp}$) polarizada é medida; e para uma radiação de excitação horizontalmente polarizada, a emissão vertical ($i_{\perp}$) e horizontalmente ($i_{//}$) polarizada é medida. O valor médio da anisotropia de fluorescência, $\langle r \rangle$, é dado pela Eq. 5:

$$\langle r \rangle = (I_{//} - GI_{\perp})/(I_{//} + 2GI_{\perp}) \tag{5}$$

onde $G = i_{\perp}/i_{//}$ é um fator de correção que leva em conta o canal de emissão simples do espectrofotômetro tipo "L" (LAKOWICZ, 1983).

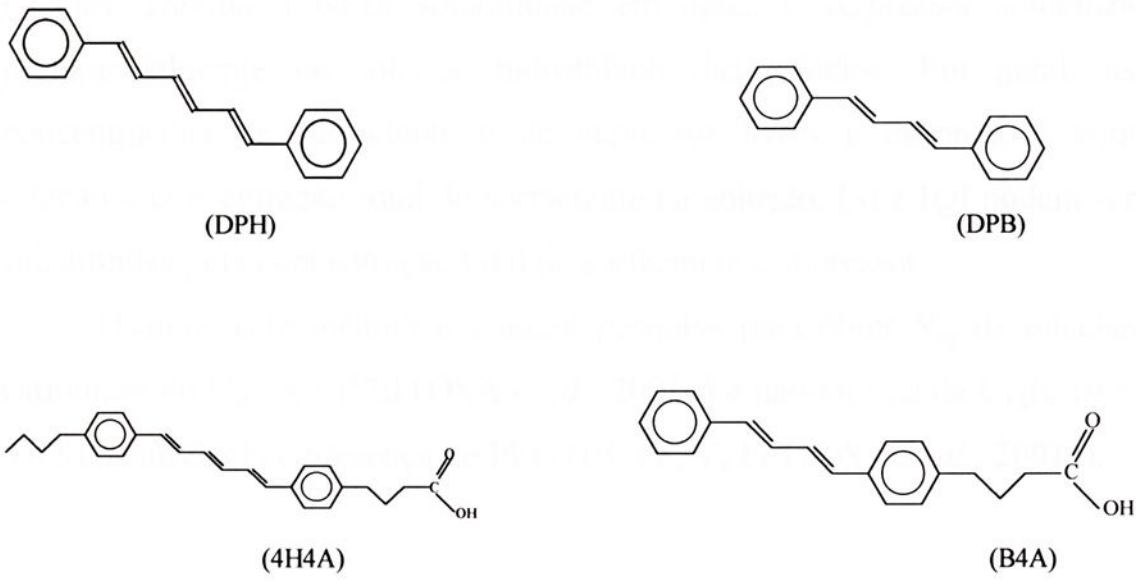


Figura 4 - Estrutura molecular de algumas sondas fluorescentes trans-difenilpolienos (*t*-Dpo).

Fluorescência resolvida no tempo - A curva de decaimento de fluorescência do cromóforo (pireno), na presença de supressor (3,4-dimethylbenzophenone, DMBP) é ajustada através do modelo de Infelta-Tachiya (INFELTA *et al.*, 1974):

$$F(t) = F(0)\exp[-t/\tau_0 + \langle n\rangle\{\exp(-k_q t) - 1\}] \qquad (6)$$

onde $F(t)$ descreve a evolução temporal da intensidade de fluorescência do cromóforo e supressor que obedece a distribuição de Poisson. $F(0)$ é a intensidade de fluorescência no instante inicial; τ_0 é o tempo de vida natural do cromóforo sem o supressor, $\langle n\rangle$ é o número médio de supressor nas micelas, e k_q é a constante de reação de primeira ordem do supressor. O número de agregação, N_{ag} é calculado usando a Eq. 7

$$N_{agg} = \langle n \rangle \frac{[S]}{[Q]} \qquad (7)$$

onde [*S*] e [*Q*] são as concentrações molares do surfactante e supressor nas micelas. Devido à baixa solubilidade em água, o surpressor solubiliza preferencialmente no interior hidrofóbico das micelas. Em geral, as concentrações de surfactante e de supressor livres é desprezível com relação à concentração total de surfactante na solução, [*S*] e [*Q*] podem ser substituídas pela concentração total de surfactante e supressor.

Usamos este método em nossa pesquisa para obter N_{ag} de micelas catiônicas de $C_{16}TAS$ (FEITOSA *et al.*, 2001b) e não-iônicas de $C_{12}E_n$ (n = 5 e 8) na ausência e presença de PEO (III, IV, V, FEITOSA *et al.*, 2001a).

Tensão superficial

A tensão superficial, γ, de líquidos é uma força tangencial atrativa entre moléculas adjacentes que mantém o líquido unido. Essa força atrativa é a *fonte de condensação do vapor de um líquido e tem origem nas forças de* dispersão, dipolo-dipolo e nas pontes de hidrogênio. No interior do líquido uma molécula sofre a mesma força atrativa em todas as direções, mas na região existe uma assimetria nessas forças que resultam na energia de superfície e se manifesta na tensão superficial que é, portanto, a força de coesão do líquido.

À temperatura ambiente a água tem uma grande tensão superficial, 72 mN/m, enquanto que γ de álcoois é baixo, de 20 a 22 mN/m. Solventes em geral, γ está na faixa de 20 a 30 mN/m. Existem diferentes modos de se medir a tensão superficial, γ, de uma solução. Medidas de γ de soluções de surfactante permitem obter a CMC e a área ocupada por surfactante na região da interface. No método de du Noüy (método do anel), mede-se a força F necessária para remover um anel de platina (raio R) e a tensão superficial γ é obtida através da Eq. 8:



$$\gamma = \frac{\beta F}{4\pi R} \tag{8}$$

onde β é um fator de correção obtido da medida da tensão superficial da água (72.0 mN/m at 25°C). Da curva de tensão superficial contra o logarítmo da concentração de surfactante obtemos a CMC, que corresponde ao intercepto das curvas ajustadas e a área por surfactante, a_o, na interface de saturação, usando a equação de adsorção de Gibbs (EVANS E WENNESTRÖM, 1999):

$$\Gamma = \frac{-1}{nRT}\frac{d\gamma}{d\ln C} \tag{9}$$

onde Γ (mol/área) = $1/N_A a_o$ é o excesso de superfície do surfactante na interface, C é a concentração molar de surfactante, N_A é a constante de Avogadro, R é a constante dos gases, T é a temperatura absoluta, e n é um número que leva em conta a valência do contra-íon, n = 1 para surfactantes não-iônicos, e n = 2 ou 3 para contra-íons mono ou divalentes, respectivamente. A Eq. 9 se aplica no limite de $C \rightarrow$ cmc.

Usamos este método no estudo de micelas catiônicas de C_{18}TAB (SWANSON-VETHAMUTHU *et al.*, 1998) e C_{16}TAS (FEITOSA *et al.*, 2001b).

Condutividade

É uma técnica muito útil para se obter a CMC e o grau de dissociação de contra-íons (α) de micelas iônicas. O intercepto das curvas ajustadas dá a CMC, enquanto que a razão entre as inclinações das curvas acima e abaixo da CMC á o valor de α (ZANA, 1980). A técnica consiste em medir a resistência R da solução de micelas, que está relacionada à condutância específica $\sigma = k/R$, onde k é a constante da cela (k = 1,0 cm^{-1}, em nosso caso).

unesp

Monocamadas na interface

A balança de superfície de Lagmuir-Adam (ou cuba de Langmuir) é a mais usada no estudo de monocamadas na interface água-ar. A monocamada é formada sobre a superfície de um líquido espalhando uma solução orgânica do surfactante entre duas barreiras, uma fixa e a outra móvel, e evaporando o solvente orgânico. A área da monocamada pode variar movendo-se a barreira móvel. A presença da monocamada de surfactante na superfície diminui a tensão superficial (γ) relativamente à tensão superficial da superfície "limpa" (γ_o), sem o surfactante, originando uma pressão superficial (π) sobre as barreiras na direção da superfície limpa, definida por

$$\pi = \gamma_o - \gamma \qquad (10)$$

A pressão superficial pode ser obtida medindo-se a força por unidade de comprimento sobre a barreira fixa, ou, alternativamente, medindo-se por métodos convencionais (*eg.* de Wilhelmy) a tensão superficial na ausência e presença do surfactante.

A medida do potencial de superfície usando um eletrodo posicionado acima e próximo à interface e um eletrodo de referência posicionado na subfase. O potencial entre os eletrodos é medido usando um eletrômetro de alta impedância, na presença (V) e na ausência da monocamada (V_o). O potencial de superfície, ΔV, é definido como

$$\Delta V = V - V_o \qquad (11)$$

e reflete a polaridade e a orientação dos dipolos da superfície. Para um dipolo μ formando um ângulo θ com a normal à superfície, ΔV é dado por

$$\Delta V = \frac{n\mu\cos\theta}{D\varepsilon_o} \qquad (12)$$

onde n é a densidade de moléculas por unidade de área na monocamada, D é a constante dielétrica do meio e ε_o é permissividade do vácuo.

Medimos o potencial de superfície e a isoterma pressão-área de DODAB contendo solução aquosa de diferentes eletrólitos na subfase (XII).

A equação de Poisson-Boltzmann (EPB)

Na teoria de campo médio, a EPB relaciona o potencial eletrostático médio, $\phi(r)$, de um macro-íon (*eg.* Micela ou vesícula) em solução eletrolítica, cujos íons provêm da dissociação do macro-íon ou pela adição de eletrólitos à solução, à densidade de cargas, $\rho(r)$, distribuídas radialmente na dupla camada elétrica de Gouy-Chapman adjacente ao macro-íons, segundo a EPB:

$$\Delta\phi = -(kT/\varepsilon)\Sigma(n_{io}z_i)\exp(-z_i e\phi/kT) \qquad (13)$$

onde Δ é o operador laplaciano, n_{io} é a densidade numérica de íons no ponto de referencia, onde o potencial é nulo (na borda da cela, no modelo da cela), $\varepsilon = D\varepsilon_o$ é a permissividade do meio, D é a constante dielétrica do meio, ε_o é a permissividade do vácuo, z_i é a valência do íon i, e é a carga elementar, k é a constante de Boltzmann e T é a temperatura absoluta. A EPB (Eq. 13) é uma equação não-linear de 2ª ordem e, em geral, não possui solução analítica simples, podendo em muitos casos ser resolvida numericamente. Através de condições de contorno apropriadas (II). Na Ref. II resolvemos numericamente, usando o modelo da cela, a EPB para vesículas catiônicas de DODAB.

cm 1 2 3 4 5 6 7 unesp 11 12 13 14 15 16 17 18

discussão dos resultados

As propriedades de uma série de colóides de associação foram investigadas por nós, usando uma variedade de técnicas e métodos discutidos acima. Uma das maiores contribuições do nosso grupo para a pesquisa das vesículas catiônicas consiste, a meu ver, na formação e caracterização de vesículas espontâneas de DODAB e DODAC, obtidas pela mistura simples desses surfactantes em água. Em baixas concentrações essas vesículas são grandes e unilamelares. Quando preparadas em solução iso-osmolar de sal (NaBr ou NaCl) essas vesículas são menores e uni, bi ou trilamelares. As Figuras 5 a 10 mostram algumas típicas fotos cryo-TEM de vesículas espontâneas, sonicadas e extrudadas de DODAB e DODAC preparadas em água ou em solução iso-osmolar de NaBr.

Algumas conclusões podem ser traçadas. As vesículas sonicadas a banho têm o formato de lentes, semelhantemente às sonicadas com probe (ANDERSSON *et al.*, 1995), mostrando que esses dois métodos de sonicação levam à formação de vesículas com a mesma forma e tamanho. As dispersões de vesículas sonicadas possuem duas populações de estruturas características de vesículas pequenas e fragmentos, pois o tamanho destas estruturas não é grande o suficiente para formar vesículas (VI). O tamanho das vesículas extrudadas depende naturalmente do diâmetro efetivo do poro da membrana de extrusão, podendo ser menor ou maior; para $\phi = 200$ nm, o diâmetro das vesículas é aproximadamente igual ϕ, para ϕ menores as vesículas são maiores e, para ϕ maiores, as vesículas são menores do que ϕ (LOPES *et al.*, 2001). Interessante notar que as vesículas de DODAC tendem a ser mais esféricas e menores do que as de DODAB. Além disso, vesículas unilamelares de DODAC se formam a concentrações muito maiores do que as de DODAB. Quando preparadas



em solução iso-osmolar de NaCl, p. ex., as vesículas catiônicas têm maior curvatura e são principalmente uni, bi ou trilamelares Nas Figuras 6 e 10 comparamos as cryo-fotos de duas dispersões espontâneas de DODAB 5.0 mM, de onde vemos claramente que as vesículas na presença de sal são muito mais definidas. Importante observar que em 5.0 mM as vesículas espontâneas de DODAB apresentam uma grande fração de agregados, enquanto que as vesículas de DODAC são mais homogêneas, esféricas e não formam agregados (Figura 5).

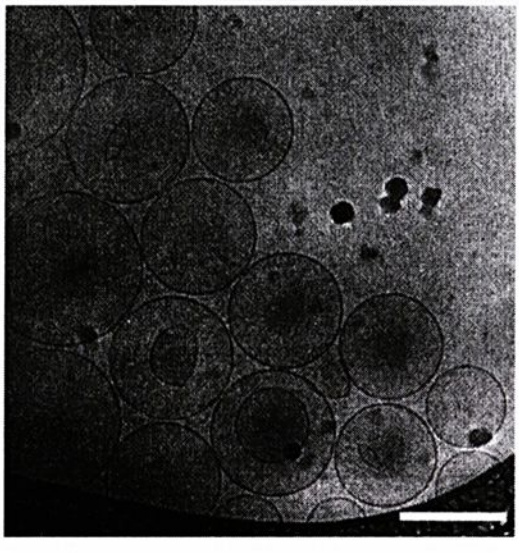


Figura 5 - Cryo-TEM de DODAC 5.0 mM em água. Amostra vitrificada de 25 °C. Barra = 200 nm.

A T_c de DODAB e DODAC exibem o fenômeno de histerese, ou seja, a T_c é sempre maior quando obtida por aquecimento do que por resfriamento da amostra, com essa diferença chegando a 6,4 °C para DODAC (Figura 11); uma histerese menor, de 4,8 °C, foi obtida para DODAB. A razão da histerese ainda não é bem entendida e está sendo investigada pelo nosso grupo. Um valor similar da T_c de DODAC (47 °C) e DODAB (45 °C) também foi obtida por medidas de ressonância

paramagnética eletrônica, RPE (XI) e turbidez em função da temperatura (Figura 12). A rápida variação na turbidez na região da T_c mostra que a transição é cooperativa, resultando no estreito pico no termograma DSC (Figura 11). Vimos que a T_c de DODAX diminui com o aumento da curvatura (a extrusão diminui a T_c). A sonicação, no entanto, aumenta a T_c de DODAX, provavelmente devido a anomalias ou defeitos causada pela força das ondas ultrassônicas (IX).



Figura 6 - Cryo-TEM de dispersão espontânea de DODAB 5.0 mM em água. Amostra vitrificada de 25 °C.



Figura 7 - Cryo-TEM de DODAB 2.0 mM em dispersão aquosa espontânea. Barra = 100 nm.

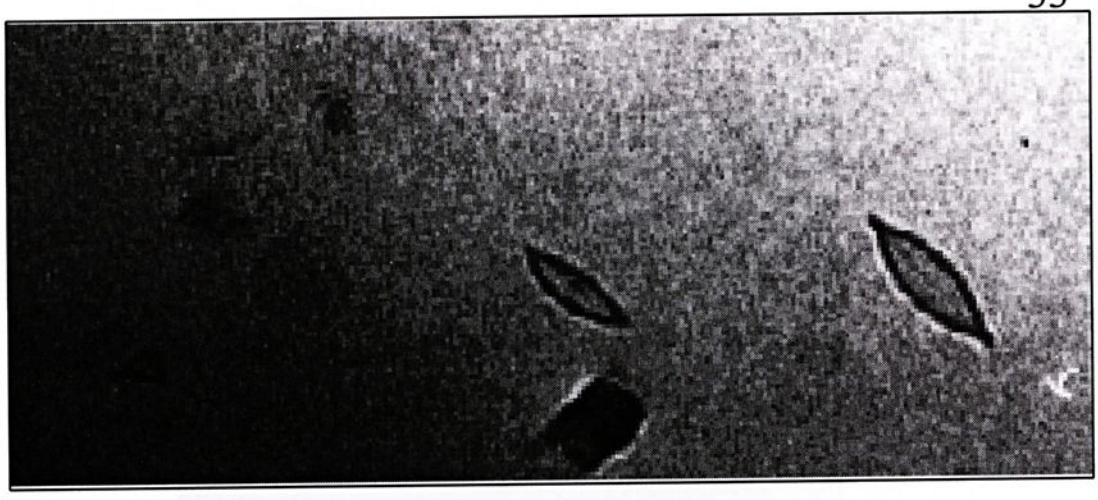


Figura 8 - Cryo-TEM de DODAB 1.0 mM em água. Vesículas preparadas por sonicação a banho (2,5 h).

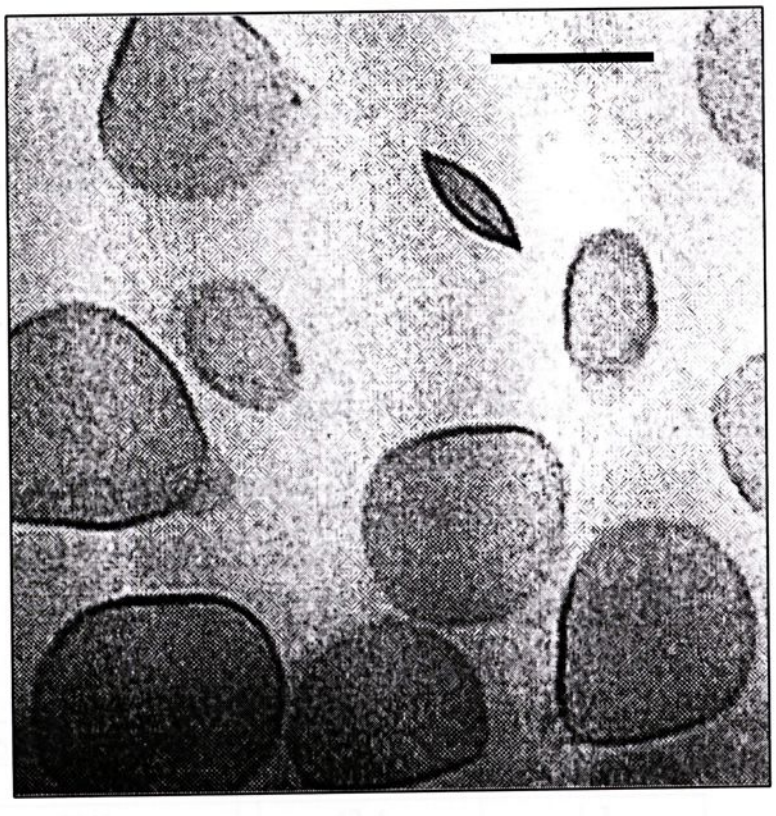


Figura 9 - Cryo-TEM de vesículas de DODAB 1 mM extrudadas (ϕ = 100 nm) em água. Barra = 100 nm.

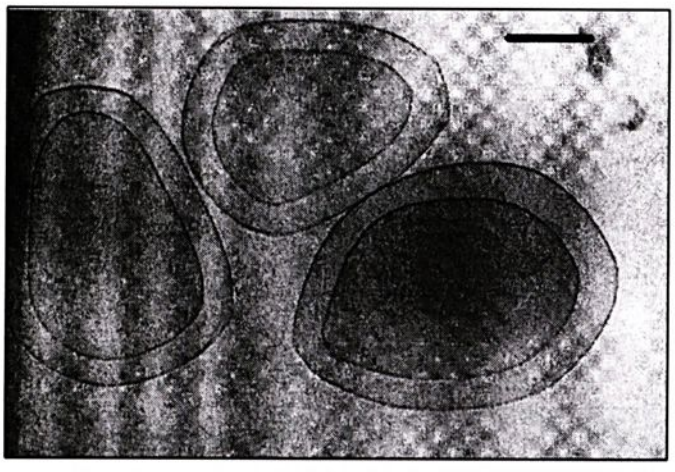
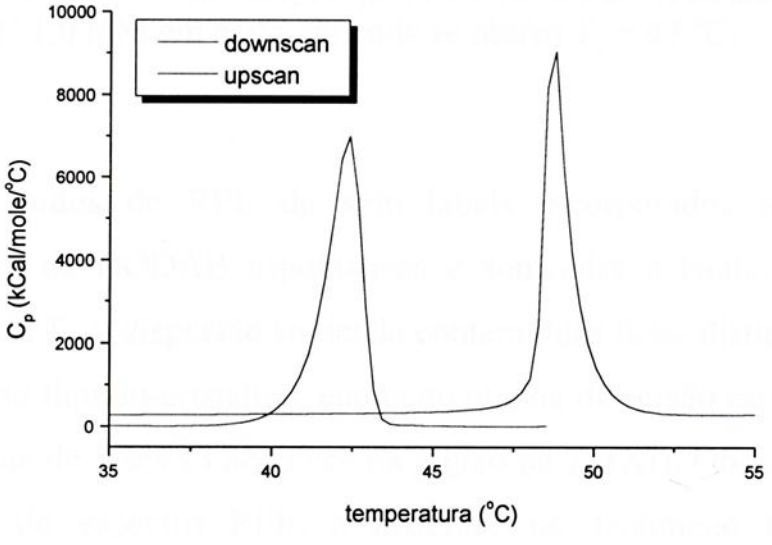


Figura 10 - Cryo-TEM de dispersão espontânea de DODAB 5.0 mM em 1,2 mM de NaCl. Amostra vitrificada de 25 °C. Barra = 100 nm.



varredura	ΔH (kcal/mol)	T_c (°C)	$T_{1/2}$ (°C)
up	10,0	48.8	0.8
down	10,0	42.4	1.3

Figura 11 – Termogramas DSC de dispersão espontânea de DODAC, obtidos por aquecimento e resfriamento da amostra. Valores de T_c, $T_{1/2}$ e ΔH da transição de fase principal são mostrados na Tabela.

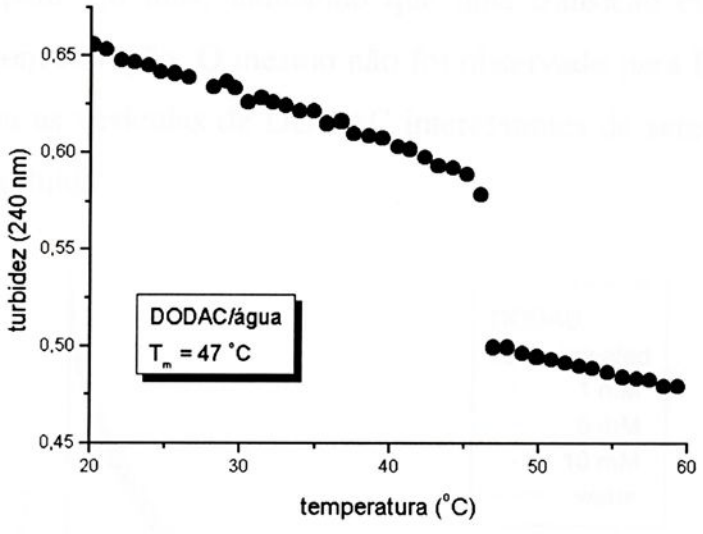


Figura 12 – Efeito da temperatura na turbidez de vesículas espontâneas de DODAC 1,0 mM em água, de onde se obtém $T_c = 47\ ^oC$.

Estudos de RPE de spin labels incorporados na bicamada de vesículas de DODAB espontâneas e sonicadas a banho revelaram que, abaixo da T_c, a dispersão sonicada contém duas fases distintas, uma gel e a outra tipo líquido-cristalina, enquanto que na dispersão espontânea esta co-existência de fases só acontece na região da T_c (XI). Observamos também, através do espectro RPE, a histerese no fenômeno termotrópico de vesículas de DODAB (XI).

Uma outra característica importante das vesículas catiônicas é que os surfactantes tendem a formar estruturas multilamelares com o aumento da concentração. Isso foi observado para brometo de didodecildimetilamônio, DDAB, (MARQUES, 1993) e DODAX (FEITOSA e AMARAL, 2001). A Figura 13 mostra as curvas de intensidade de espalhamento de raios-X a baixo ângulo, SAXS, de dispersões espontâneas de DODAB. O pico de Bragg característico de estruturas multilamelares aparece para DODAB 5,0

mM, mas não para 1,0 mM, indicando que uma transição estrutural ocorre nesta faixa de concentração. O mesmo não foi observado para DODAC até 20 mM, o que torna as vesículas de DODAC interessantes de serem investigadas no sistema semidiluído.

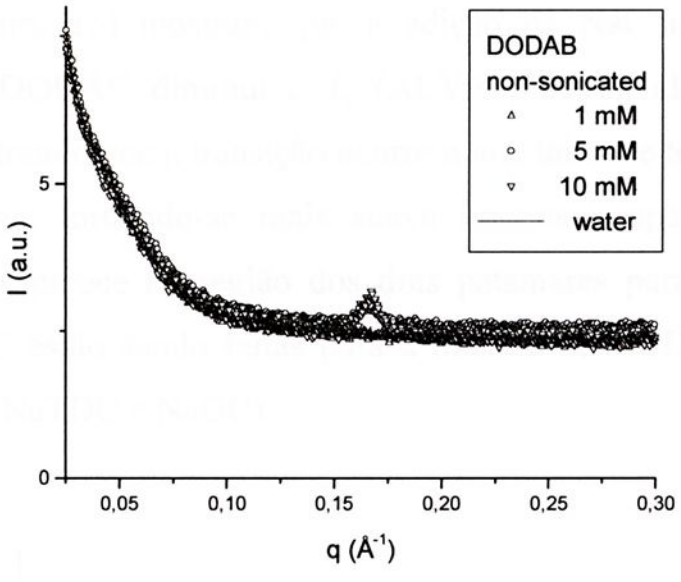


Figura 13 – Intensidade SAXS de dispersões espontâneas de DODAB em água medida à temperatura ambiente. O pico de Bragg começa a aparecer em torno de 5 mM.

Interação de sal de bile com vesículas de DODAB e DODAC

A Figura 14 mostra o modo como os sais de bile NaC, NaDOC, NaTDC e NaGC afetam a turbidez da dispersão de vesículas de DODAC preparadas espontaneamente em água. Vemos que o efeito final independe da natureza do sal de bile; porém, o modo como esse estado final é alcançado depende da estrutura molecular do sal de bile. O alto valor final da turbidez, e o aspecto turvo da dispersão, sugere a formação de estruturas macromoleculares gigantes, provavelmente não-lamelar, pois os

termogramas DSC nessas condições não apresentam pico de transição de fase característico de estruturas lamelares (resultados não mostrados), podendo ser estruturas micelares alongadas; este assunto está sendo investigado pelo nosso grupo (ALVES, 2001). Interessante que apenas NaC e NaGC induzem a formação de micelas mistas (valores baixos de turbidez na Figura 14) antes de ocorrer a transição para a fase final, turva. Medidas de DSC (Figura 15) mostram que a adição de NaC na dispersão de vesículas de DODAC diminui a T_c (ALVES, 2001), alarga o pico da transição mostrando que a transição ocorre numa faixa de temperatura cada vez mais larga, tornando-se mais suave (menos cooperativa). O pico finalmente desaparece na região dos dois patamares para NaC e NaGC (medidas DSC estão sendo feitas para a mistura de DODAC e DODAB com NaDOC, NaTDC e NaGC).

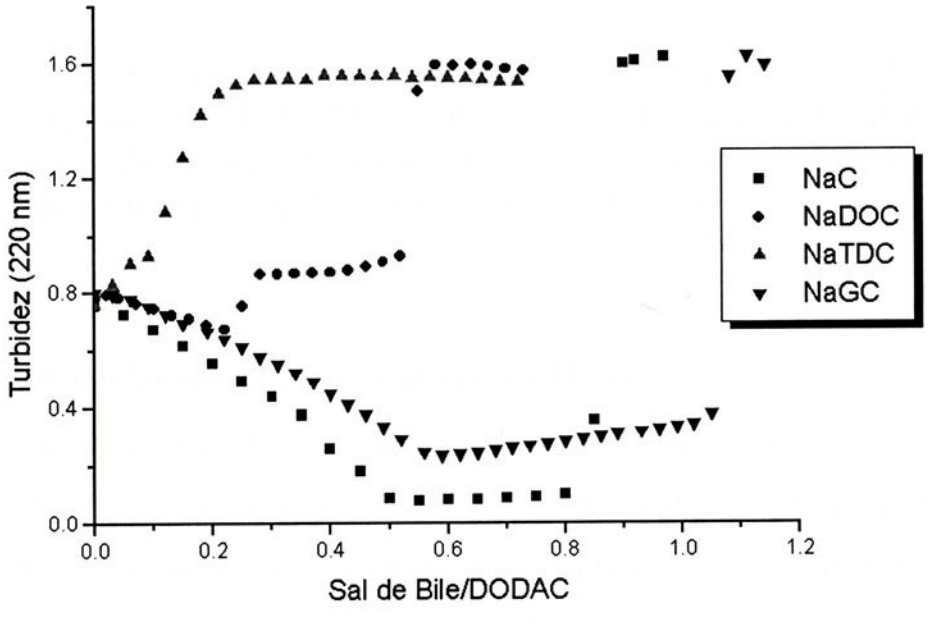
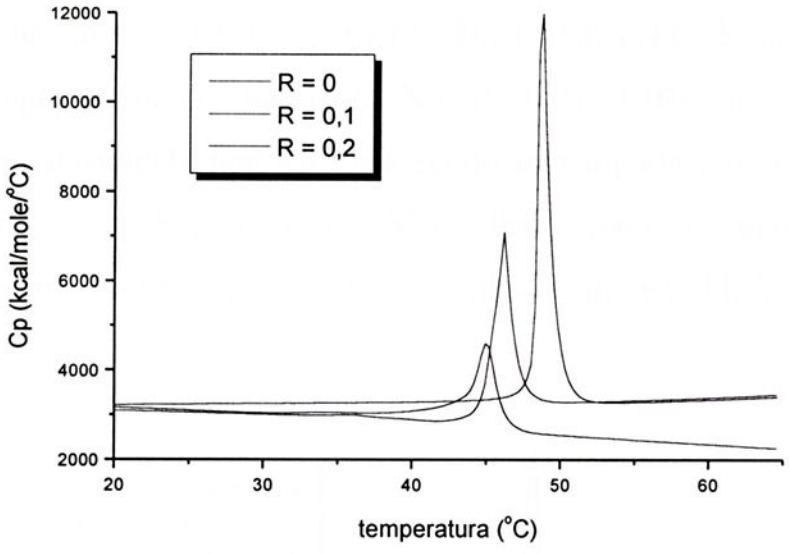


Figura 14 – Efeito da razão de concentração molar R = sal de bile/DODAC na turbidez (220 nm) da dispersão. Medidas realizadas (25 °C) por titulação do sal de bile em dispersão de DODAC 1,0 mM.



NaC/DODAC	ΔH (kcal/mol)	T_c (°C)	$T_{1/2}$ (°C)
0	10,0	48,8	0.77
0.1	6,5	46,2	1.28
0.2	5,6	44,9	1.52

Figura 15 – Efeito de colato de sódio (NaC) no termograma DSC de dispersões espontâneas de DODAC, obtido por aquecimento da amostra, para três valores de R = NaC/DODAC, 0, 0,1 e 0,2. Valores de ΔH, T_c e $T_{1/2}$ e da transição de fase principal são mostrados na Tabela.

Interação de surfactantes com vesículas de DODAX

Nossos resultados têm mostrado que o efeito de surfactantes não-iônicos, zwitteriônicos e aniônicos na transição da fase gel para a líquido-cristalina de DODAX é semelhante ao efeito de surfactante não-iônico em vesículas de fosfolipídio (EDWARDS et al., 1989). A Figura 16 mostra o efeito do surfactante zwitteriônico HPS no termograma DSC de DODAC 1,0 mM. Analogamente ao efeito de sal de bile (Figura 15), HPS diminui a T_c e ΔH da transição de fase de DODAC, porém, numa menor taxa (Tabela 1). Em

todos esses casos a transição vesícula-micela pode ser explicada com base no modelo de três estados de Lichtenberg (LICHTENBERG, 1985), conforme proposto por nós nas Refs. X e BARRELEIRO *et al.*, 2001. A transição vesícula-micela também está sendo investigada para os sistemas DODAX/$C_{12}E_n$, n = 5 a 8 (BONASSI, 1999), para os quais também obtemos o mesmo comportamento geral do observado para HPS.

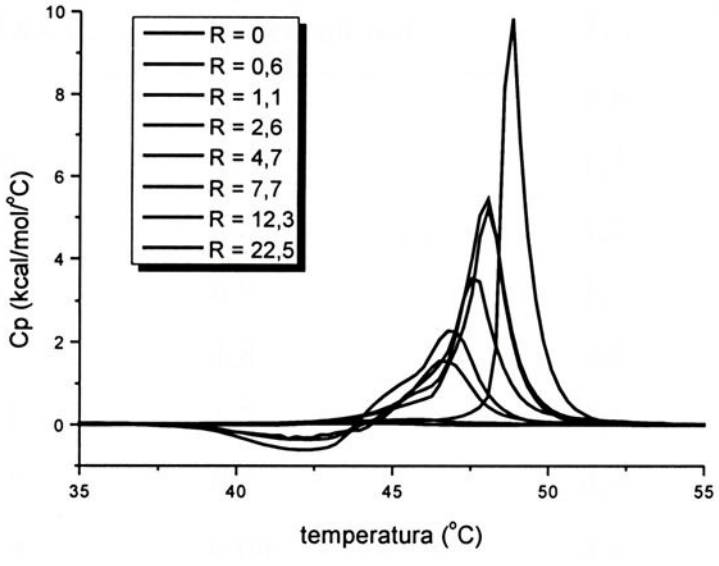


Figura 16 – Termograma DSC de vesículas espontâneas de DODAC em água, na presença de HPS, para diferentes razões de concentrações molares, R. A concentração inicial de DODAB é de 1,0 mM.

Medidas de turbidez da mistura $C_{12}E_n$/DODAX têm se mostrado muito útil na determinação de valores críticos de concentrações críticas nas quais ocorrem mudanças de estrutura na mistura de surfactantes. Na Figura 17 comparamos as curvas para $C_{12}E_5$/DODAX e $C_{12}E_8$/DODAX. Notamos que n afeta muito pouco a razão crítica de saturação (R = $C_{12}E_n$/DODAX), R_{sat}, correspondente ao ponto de saturação das vesículas pelo surfactante não-iônico, mas a razão crítica de solubilização, R_{sol}, na qual a transição

vesícula-micela se completa, aumenta com o aumento de *n*, ou seja, com a diminuição da hidrofobicidade do surfactante. Este resultado é facilmente previsto pelo princípio de auto-associação dos surfactantes C_mE_n. A Tabela 2 resume os valores das razões críticas R_{sat} e R_{sol}.

Tabela 1 - Valores de ΔH, T_c e $T_{1/2}$ de vesículas espontâneas de DODAC 1,0 mM, na ausência e presença de HPS.

HPS/DODAC	ΔH (kcal/mol)	$T_{1/2}$	T_c (°C)
0	11,3	0,8	48,8
0,6	11,0	1,5	48,1
1,1	10,3	1,3	48,2
2,6	6,9	1,5	47,6
4,7	4,8	2,1	46,8
7,7	1,7	2,1	46,3
12,3	0,7	4,7	45,8
22,5	0,09	4,1	45,6

Tabela 2 – Valores das razões molares críticas de saturação e de solubilização de dispersões espontâneas de DODAX (X = Cl^- e Br^-), com $C_{12}E_n$ (*n* = 5 e 8), para diferentes intervalos de tempo Δt entre as medidas.

sistema	Δt (min.)	R_{sat}	R_{sol}
$C_{12}E_8$/DODAB	5	0,5	6,2
$C_{12}E_8$/DODAC	5	0,3	5,1
$C_{12}E_8$/DODAB	15	0,3	6,2
$C_{12}E_8$/DODAC	15	0,2	5,1
$C_{12}E_5$/DODAB	15	0,3	3,2
$C_{12}E_5$/DODAC	15	0,3	3,2



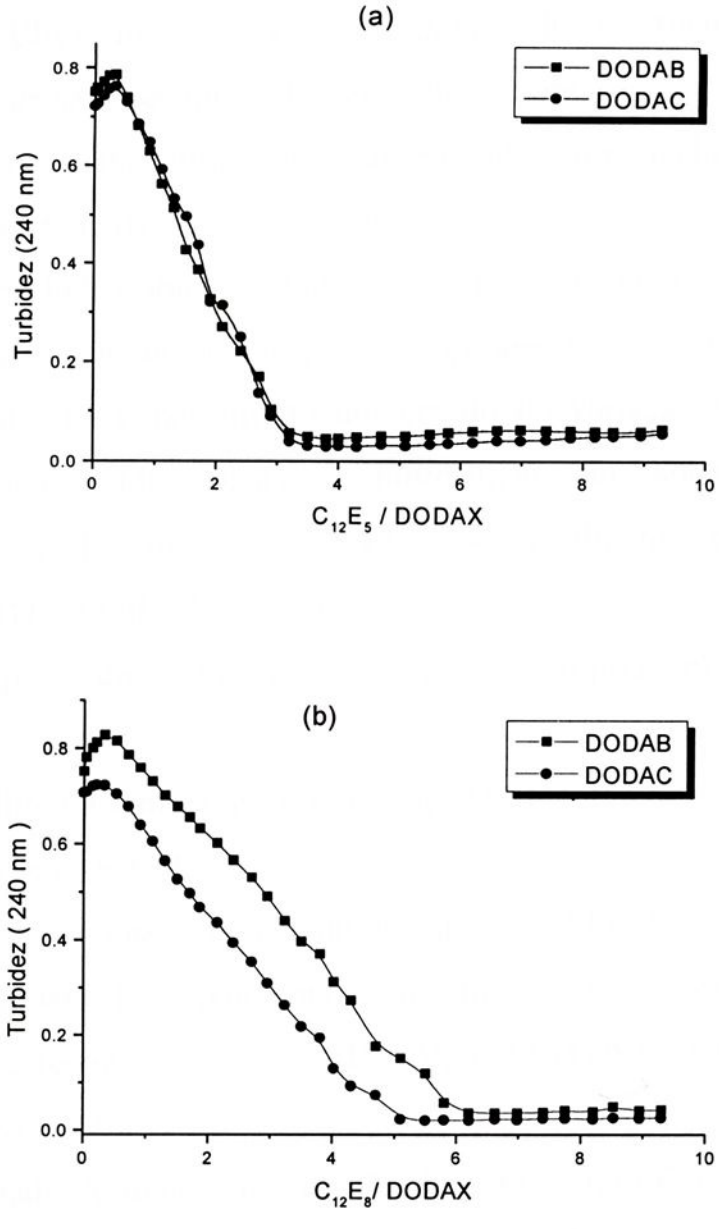


Figura 17 – Turbidez de vesículas espontâneas de DODAX (X = Cl^- e Br^-) em função da concentração de $C_{12}E_5$ (a) e $C_{12}E_8$ (b) medidas em intervalos de 15 min. Medidas realizadas à temperatura ambiente (22 °C).

Interação de polímero com surfactantes não-iônicos

Sistemas de PEO com surfactante de poli(óxido de etileno) (C_mE_n) são interessantes de se investigar pelas seguintes razões:

a) são sistemas ainda muito pouco investigados, provavelmente devido à fraca afinidade entre os componentes,

b) as porções hidrofóbica e hidrofílica do surfactante são facilmente modificadas podendo-se variar o comprimento dos segmentos apolar (C_m) e polar (E_n), permitindo um estudo de variação sistemática das características hidrofóbicas e hidrofílicas do surfactante; e as propriedades das micelas formadas são facilmente encontradas na literatura (DEGIORGIO, 1985),

c) a porção polar do surfactante (C_mE_n) é ela própria um seguimento de PEO,

d) PEO modifica a temperatura de turvação (temperatura na qual a solução torna-se turva) de C_mE_n.

Nossas conclusões do estudo dos sistemas PEO-C_mE_n-água baseiam-se nas medidas de espalhamento de luz e fluorescência de estado estacionário e resolvida no tempo (III, IV, V, FEITOSA *et al.*, 2001a):

1) PEO interage com C_mE_n;

2) a intensidade de interação é função de porção hidrofílica (cabeça polar) do surfactante, da massa molar do polímero e da temperatura, e aumenta com a massa molar do polímero, mas diminui com o aumento do número de segmentos de PEO da porção hidrofóbica do surfactante, provavelmente devido à diminuição no tamanho das micelas ou aumento da temperatura de turvação (T_{cp});

cm 1 2 3 4 5 6 7 unesp 11 12 13 14 15 16 17 18

3) a intensidade de interação aumenta com a temperatura quando esta se aproxima de T_{cp}; a temperaturas bem inferiores à T_{cp} a intensidade diminui com a temperatura até um valor mínimo;
4) para uma dada concentração de PEO, o número de agregação (N_{ag}) das micelas no complexo é menor, igual ou maior do que das micelas na ausência do polímero, dependendo da concentração de surfactante. N_{ag} aumenta com a concentração de surfactante, mas a uma taxa maior na presença do polímero, de modo que a pequenas concentrações de surfactante, N_{ag} é menor na presença do que na ausência do polímero (como acontece para o sistema PEO-SDS-água), mas é maior a concentrações maiores, contrariando a expectativa para sistemas iônicos;
5) a CMC do surfactante é a mesma na ausência e na presença do polímero, ou seja, CMC = CAC para os sistemas PEO-C_mE_n-água, sugerindo que os agregados micelares, e não os monômeros são os principais responsáveis pela complexação;

Esses resultados são impressionantes quando comparados a sistemas polímero neutro-surfactante iônico, para os quais a CMC é sempre menor do que a CMC e N_{ag} é menor na presença do que na ausência de polímero, propriedades essas comumente usadas como indicadores de complexação e da intensidade da "driving force". Polímeros neutros relativamente hidrofóbicos apesar de interagir com surfactantes não-iônicos também não alteram a CMC (BRACKMAN e ENGBERTS, 1993).

Questões ainda não respondidas sobre complexos polímero-surfactante neutros diz respeito ao efeito da temperatura e da concentração ou da massa molar do polímero no tamanho do complexo. Por exemplo, uma dada concentração de PEO com diferentes massas molares os complexos têm tamanhos diferentes? Esses polímeros afetam igualmente a temperatura de turvação do surfactante? Ou, como levar em conta o efeito

da temperatura nas propriedades do complexo formado por PEO com surfactantes da série C_mE_n que tenham T_{cp} distintas? A que temperatura devemos comparar o tamanho dos agregados desses surfactantes com PEO de modo que a temperatura exerça o mesmo efeito? Para um dado sistema, convém escolher uma temperatura T de modo que $(T_{cp} - T)/T_{cp}$ seja igual para os sistemas. Pretendemos no futuro monitorar a T_{cp} de surfactantes C_mE_n numa faixa de concentração dos componentes maior das investigadas nas Refs. III, IV, V e FEITOSA *et al.*, 2001a. Procuraremos também propor um modelo definitivo para os complexos de PEO-C_mE_n em solução, pois, até o momento, apesar do nosso esforço, isso ainda não foi possível.

Apesar da importância dos surfactantes zwitteriônicos, presentes em abundância nas membranas naturais, são pouquíssimos os trabalhos publicados em misturas de polímero com surfactante zwitteriônico. Temos investigado a interação de HPS com PEG (BRAZOLIN, 1999). Medidas de fluorescência e de tensão superficial mostram que PEO (PM = 12 kDa) alteram muito pouco a CMC de HPS e C_{16}TAS (BRAZOLIN, 1999), embora resultados conclusivos da interação desses sistemas requerem o uso de outras técnicas, como espalhamento dinâmico de luz e calorimetria por titulação isotérmica (ITC).

Além dos trabalhos acima descritos de caracterização de vesículas de DODAB e DODAC, das micelas de C_{18}TAB e de C_{18}TAS, das micelas mistas de SDS/$C_{12}E_8$, e dos sistemas mistos PEO/$C_{18}E_n$ (n = 5 e 8), DODAX/$C_{18}E_8$, incluímos neste trabalho um estudo, através da solução numérica da equação de Poisson-Boltzmann (EPB), da distribuição de íons e potencial eletrostático nos compartimentos aquosos interno e externo das vesículas de DODAX (II). Naturalmente que o método numérico proposto pode ser aplicado ao estudo de vesículas aniônicas. Investigamos também o efeito da eletronegatividade de contra-íons na distribuição de potencial e

pressão de superfície em filmes finos DODAB contendo solução eletrolítica na subfase (XII).

Efeito de eletrólitos nas vesículas e monocamadas de DODAB

Vimos acima que, em quantidade moderada, eletrólitos simples aumentam a curvatura de vesículas de DODAB. Numa tentativa de entendermos melhor esse efeito, investigamos o efeito de eletrólitos no comportamento termotrópico de fase de dispersões de DODAX (Figura 18) e no potencial eletrostático de superfície e de pressão interfacial em filmes finos (monocamadas) de DODAB (XII). A Figura 18a mostra o efeito de NaBr no termograma DSC das vesículas espontâneas de DODAB, onde vemos que a intensidade e posição dos picos das transições principais e da pós-transição variam de modo inverso com a força iônica. Na Figura 18b vemos que NaCl aumenta a T_c de DODAB e NaBr tende a diminuir, o que é consistente com o fato da T_c ser maior para DODAC do que para DODAB.

É importante notar que nosso estudo mostra que a T_c, das vesículas de DODAX depende não apenas da força iônica, mas também da concentração de surfactante e do método de preparação das vesículas (IX).

O surfactante C_{18}TAB, homólogo a DODAB, mas com uma única cauda, forma micelas aproximadamente esféricas na presença de pequenas concentrações de NaBr, mas forma bicamada (e não micelas cilíndricas) em concentrações elevadas de NaBr, eg. 80 mM. A transição micela-bicamada induzida por NaBr foi por nós observada por medidas de espalhamento dinâmico de luz, tensão superficial e calorimetria por titulação isotérmica (SWANSON-VETHAMUTHU *et al.*, 1998). Esse comportamento não usual se deve à longa cadeia de hidrocarboneto desse surfactante.

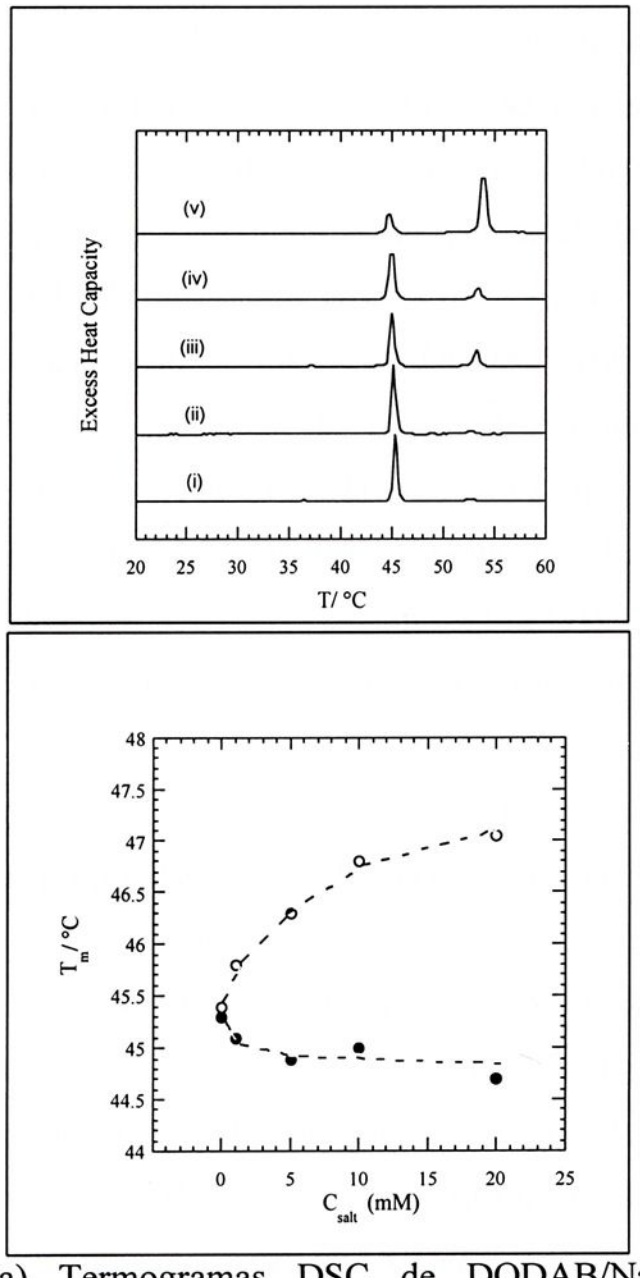


Figura 18 – (a) Termogramas DSC de DODAB/NaBr/water nas concentrações de NaBr: 0 (i) 1 (ii), 5 (iii), 10 (iv) and 20 mM (v). (b) Efeito de NaCl (❍) e NaBr (●) na T_c de DODAB.

O surfactante C_{18}TAB, homólogo a DODAB, mas com uma única cauda, forma micelas aproximadamente esféricas na presença de pequenas

concentrações de NaBr, mas forma bicamada (e não micelas cilíndricas) em concentrações elevadas de NaBr, eg. 80 mM. A transição micela-bicamada induzida por NaBr foi por nós observada por medidas de espalhamento dinâmico de luz, tensão superficial e calorimetria por titulação isotérmica (SWANSON-VETHAMUTHU *et al.*, 1998). Esse comportamento não usual se deve à longa cadeia de hidrocarboneto desse surfactante.

Medidas da pressão superficial e do potencial de superfície de monocamadas de DODAB mostraram, através da teoria de Gouy-Chapman que na interface água/ar, a monocamada de DODAB não está totalmente ionizada. A densidade superficial de carga efetiva aumenta com a eletronegatividade do contra-íon na subfase devido à ligação seletiva dos íons à interface, afetando não apenas o potencial de superfície da monocamada, mas também a isoterma área-pressão (XII). A monocamada de DODAB é muito condensada quando a subfase contém I^- e muito expandida quando contém F^-.

A distribuição de íons nas vizinhanças de micelas e vesículas determinam as suas propriedades e estabilidade. O potencial de superfície de colóides de associação iônicos podem ser determinados experimentalmente, p.ex. através de medidas da mobilidade eletroforética, ou por sondas espectroscópicas (I), ou teoricamente, resolvendo a equação de Poisson-Boltzmann, EPB (II), ou por simulação de Monte Carlo (STEVENS *et al.*, 1996). Resolvemos numericamente a EPB para as vesículas catiônicas (esféricas) de DODAX, modeladas como uma casca esférica com carga nas superfícies interna e externa proveniente da dissociação de contra-íons e da adsorção específica de íons adicionados ao sistema, e observamos que existe uma assimetria na distribuição radial do potencial eletrostático e da carga elétrica (II).

cm 1 2 3 4 5 6 7 unesp 11 12 13 14 15 16 17 18

Considerações finais

O trabalho aqui apresentado no campo dos colóides de associação mostra que existe um amplo campo de pesquisa com aplicação de colóides de associação em ciência e tecnologia.

Assim, este trabalho constitui um esforço de avanço na investigação da interação de diferentes macromoléculas com interesses de aplicações diversas, tais como micelas, vesículas, polímeros naturais e sintéticos e proteínas. A mistura desses componentes visa caracterizar fisicoquimicamente os complexos de macromoléculas formados em misturas dessas espécies, além de investigar a estabilidade das diversas fases. É por essa razão que procuramos diferentes alternativas de estudo da estabilidade em sistemas contendo surfactantes, muitos dos quais ainda não investigados.

O trabalho, claro, não se esgota aqui, mas requer continuidade, na busca de um entendimento cada vez maior das propriedades das micelas, vesículas e monocamadas, em sistemas simples ou mistos. A pesquisa está continuando dentro do mesmo espírito de envolvimento de colaboradores e alunos interessados no assunto.

unesp

bibliografia

ABREGO, J. R. B.; BROGNARO, D. P.; FEITOSA, E.; , GIGLIO, J. R.; ARNI, R. K., 2001. Small Angle X-ray Scattering Study of the Phospholipase A_2 from *Crotalus durissus terrificus* and Comparison with Other Snake Venon Phospholipases in the Crystalline State. *J. Appl. Cryst.* (Submetido).

ALVES, F. R., 2001. Projeto de Mestrado, IBILCE/UNESP, São José do Rio Preto.

ANDERSSON, M.; HAMMARSTRÖM, L.; EDWARDS, K., 1995. *Phys. Chem.* **99**, 1431.

BARRELEIRO, P. C. A.; OLOFSSON, G.; BROWN, W.; EDWARDS, K.; BONASSI, N. M.; FEITOSA, E., 2001. Interaction of octaethylene glycol n-dodecyl mono-ether with dioctadecyldimethylammonium bromide and chloride vesicles. *Langmuir* (Submetido).

BELLARE, J. R.; DAVIS, H. T.; SCRIVEN, L. E.; TALMON, Y., 1988. *J. Electron Microsc.* **10**, 87.

BONASSI, N. M., 1999. Projeto de Doutorado, IBILCE/UNESP, São José do Rio Preto.

BORGSTRÖM, B., 1977. *Int. Rev. Physiol.* **12**, 305.

BRACKMAN, J. C.; ENGBERTS, J. B. F. N., 1993. *Chem. Soc. Rev.* *22*, 8.

BRAZOLIN, M. S., 1999. Projeto de Mestrado, IBILCE/UNESP, São José do Rio Preto.

BREUER, M. M.; ROBB, I. D., 1972. *Chem. Ind* (Londres) **13**, 530.

BROWN, W., 1993. (Ed.) "Dynamic Light Scattering. The Method and Some Applications." Clarendon Press, Oxford.

CAREY, M. C.; SMALL, D. M., 1970. *Amer. J. Med.* **49**, 590.

DEGIORGIO, V., 1985. **In** *Physics of Amphiphiles. Micelles, Vesicles and Microemulsions*; Degiorgio, V.; Corti, M. (Eds.); North-Holland: Amsterdam, p. 303.

EDWARDS, K.; ALMGREN, M.; BELLARE, J.; BROWN, W., 1989. *Langmuir* **5**, 473.

EVANS, D. F.; WENNESTRÖM, H., 1999. The Colloidal Domain. Where Physics, Chemistry, and Biology Meet. 2nd ed., Wiley-VCH, Nova Iorque,.

FEITOSA, E.; BROWN, W.; WANG, K.; BARRELEIRO, P. C. A., 2001a. Interaction between poly(ethylene glycol) and $C_{12}E_8$ investigated by dynamic light scattering, time-resolved fluorescence quenching, and calorimetry. *Macromolecules* (no prelo).

FEITOSA, E.; BRAZOLIN, M. R. S. B.; NAAL, R. M. Z. G.; DEL LAMA, M. P. F. M.; LOPES, J. R.; LOH, W.; VASILESCU, M.; BROWN, W., 2001b. Structural organization of cetyltrimethylammonium sulfate in Na_2SO_4 aqueous solution. *Langmuir* (Submetido).

FEITOSA, E.; KARLSSON, G.; EDWARDS, K., 2001c. Unilamellar Vesicles Obtained by Simply Mixing Dioctadecyldimethylammonium Chloride and Bromide with Water. *J. Colloid Interface Sci.* (Submetido).

FEITOSA, E.; BARRELEIRO, P. C. A., 2001. The effect of ionic strength on the structural organization of dioctadecyldimethylammonium bromide in semi-dilute aqueous solution. *Langmuir* (Submetido).

FEITOSA, E.; AMARAL, L. Q., 2001 Structural organization of synthetic double-chain surfactants in semi-dilute aqueous dispersions. (Manuscrito em preparação).

FENDLER, J. H., 1982. *Membrane Mimetic Chemistry*, Wiley-Interscience: Nova Iorque.

FONTELL, K., 1990. *Colloidal Polymer Sci.* **268**, 264.

2804/14

BIBLIOTECA

GODDARD, E. D., 1986. *Coll. Surf.* **19**, 255 e 301.

GODDARD, E.; ANANTHAPADMANABHAN, K. P., 1993. *Interactions of surfactants with polymers and Proteins*; CRC Press: Boca Raton, FL.

HJELM, R. P.; THIYAGARAYAN, P.; ALKAN-ONYUKSEL, H., 1992. *J. Phys. Chem.* **96**, 8653.

INFELTA, P. P.; GRÄTZEL, M.; THOMAS, J. K. *J. Phys. Chem.* **1974**, **78**, 190.

ISRAELACHVILI, J., 1992. *Intramolecular and Surface Forces*, 2ª ed., Academic Press: Londres.

JÖNSSON, B.; LINDMAN, B.; HOLMBERG, K.; KRONBERG, B.. 1999. *Surfactants and Polymers in Aqueous Solution*, John Wiley & Sons, Nova Iorque.

KALYANASUNDARAM, K.; THOMAS, J. K., **1977.** *J. Am. Chem. Soc. 99*, 2039.

KALYANASUNDARAM, K., 1987. *Photochemistry in Microheterogeneous Systems*. Academic Press: Orlando.

KRATOHVIL, J. P., 1986. *Adv. Colloid Interface Sci.* **26**, 131.

LAKOWICZ, J. R., 1983. *Principles of Fluorescence Spectroscopy*, Plenum Press, Nova Iorque.

LASIC, D. D., 1993. *Liposomes: From Physics to Application.* Elsevier, Amdsterdam.

LI, G.; MCGOWN, L. B. J., 1994. *J. Phys. Chem.* **98**, 13711.

LICHTENBERG, D., 1985. *Biochim. Biophys. Acta* **821**, 470.

LINDMAN, B.; KAMENKA, N.; BRUN, B., 1976. *J. Colloid Interface Sci.* **56**, 238.

cm 1 2 3 4 5 6 7 unesp 11 12 13 14 15 16 17 18

LOPES, A.; BARRELEIRO, P. C. A.; EDWARDS, K.; FEITOSA, E., 2001. Characterization of extruded cationic vesicles: a light scattering and cryo-tem study. *Langmuir* (Submetido).

LOPEZ, O.; MAZA, A.; CODERCH, L.; LÓPEZ-IGLESIAS, C.; WEHRLI, E., 1998, *FEBS Lett.* **426**, 314.

MARQUES, E.; KHAN, A.; MIGUEL, M. G.; LINDMAN, B., 1993. *J. Phys. Chem.* **97**, 4729.

MARQUES, C. , 2000. Projeto de Doutorado, IBILCE/UNESP, São José do Rio Preto.

MAZER, N. A.; CAREY, M. C.; KWASNICK, R. F.; BENEDEK, G. B., 1979. *Biochemistry* **18**, 3064.

MYSELS, K. J., 1984. *Hepatology* **4**, 805.

NICHOLS, J. W., 1990. *Biochemistry* **29**, 4600.

OLIVIERA, S. R., 2001. Projeto de Doutorado, IBILCE/UNESP, São José do Rio Preto.

SMALL, D. M., 1971. *The Bile Acids*. Nair, P. P.; Kritchevsky, D. (Eds.), Plenum Press, Nova Iorque.

STEVENS, M. J.; FALK, M. L.; ROBBINS, M. O., 1996. *J. Chem. Phys*. **104**, 5209.

TANFORD, C., 1991. *The Hydrophobic Effect: Formation of micelles and biological membranes*. 2ª ed., Wiley: Nova Iorque, 1991.

TENGNOM, D. L., 2001. Dissertação de Mestrado, IBILCE/UNESP, São José do Rio Preto.

TURRO, N. J.; YEKTA, A., 1978. *J. Am. Chem. Soc.* **78**, 5951.

ULMIUS, J.; LINDBLOM, G.; WENNESTRÖM, H.; JOHANSSON, L. B.-Å; FONTELL, K.; SÖDERMAN, O.; ARVIDSON, G., 1982. *Biochemistry* **29**, 1553.

ZANA, R., 1980. *J. Colloid Interface Sci.* **78**, 330.

cm 1 2 3 4 5 6 7 unesp 11 12 13 14 15 16 17 18

abstract

In this work we present a series of results obtained in the last ten years by our research group (Group of Colloid Physics) on association colloids in bulk solution containing micele- and vesicle-forming single and mixed surfactants, in the presence of polymers and electrolytes, and at the air/water interface. The results discussion is based on the existing ones in the literature (see list of publications on page 2). The surfactants investigated are cationic single (C_{18}TAB) and double-chain (DODAX, X = Br^- and Cl^-), anionic single (SDS) and double-chain (DHP), and non-ionics (C_mE_n, n = 5 and 8). The chemical structures of some of these surfactants are shown in Figure 1. Experimental techniques, such as light scattering, SAXS, fluorescence, calorimetry, tensiometry, as well as computer methods based on the Poisson-Boltzmann equation, were used in this study.

This work mainly concerns with the physico-chemical properties of cationic micelles of C_{18}TAB (SWANSON-VETHAMUTHU *et al.*, 1998) and C_{16}TAB (FEITOSA *et al.*, 2001b), mixed micelles of SDS/C_{16}TAB (VII), polymer-surfactant complexes of PEO-$C_{12}E_5$ (III, IV) and of PEO-$C_{12}E_8$ (V, FEITOSA *et al.*, 2001), for PEO with high and low molecular weight (M_W = 600 and 12 kDa), and cationic and anionic vesicles of DODAB, DODAC and DHP prepared by different methods, such as sonication, chloroform injection, extrusion and spontaneously (I, VI, VIII, IX, X, XI, LOPES *et al.*, 2001, FEITOSA and BARRELEIRO, 2001, BARRELEIRO *et al.*, 2001, FEITOSA *et al.*, 2001c). We also investigated by SAXS more concentrated dispersions of DODAX, DDAB and DHP (FEITOSA and AMARAL, 2001) and the shape and size of phospholipase A_2 from snake venom of *Crotalus durissus*

terrificus (ABREGO *et al.*, 2001) as a tempt for our group to start investigating protein-surfactant interactions.

The properties of thin films of DODAB in the presence of electrolytes with different electronegativity in the subphase were also investigated and the monolayer condensation were understood on the basis of the Gouy-Chapman theory (XII), as well as the charge and potential distributions about cationic vesicle surfaces obtained by numerical integration of the Poisson-Boltzmann equation.

Warning: We enclose in this Thesis only the published papers (numbered I through XII), whereas the manuscripts are referred in the Bibliography section and are available to those who are interested.

unesp

artigo I

Size, Electrophoretic Mobility, and Ion Dissociation of Vesicles Prepared with Synthetic Amphiphiles

Iolanda Midea Cuccovia,*,† Eloi Feitosa,†,‡ Hernan Chaimovich,† Luis Sepulveda,§,∥ and Wayne Reed⊥

Departamento de Bioquimica, Instituto de Quimica, Universidade de Sao Paulo, Caixa Postal 20780, Sao Paulo, SP, Brazil CEP 01498, Departamento de Fisica, UNESP, Rio Preto, Brazil, Departamento de Quimica, Facultad de Ciencias, Universidad de Chile, Santiago, Chile, and Physics Department, Tulane University, New Orleans, Louisiana 70118 *(Received: July 17, 1989)*

Vesicles prepared with synthetic amphiphiles (dioctadecyldimethylammonium bromide and chloride, dihexadecyl phosphate and its sodium salt) were obtained by sonication, ethanol injections, and chloroform injections. The hydrodynamic diameter of vesicles (D_h), estimated from the diffusivity measured by quasielastic light scattering, ranged from 230 to 3000 Å. The electrophoretic mobility (U_m) was measured by free-flow electrophoresis. The zeta potential (ζ) and the degree of counterion dissociation (α) of the vesicles were calculated from U_m and conductivity data. α decreased with increasing D_h of the vesicles, probably due to the decreasing headgroup area and the increasing counterion association needed to relax the surface electrostatic potential. The electrophoretic mobility was also calculated (U_c) according to an impenetrable, nonconducting sphere model with a spherically symmetric charge distribution approximation. Within the limits of the experimental error(s) of the (different) methods employed and the assumptions made in the calculations, the fact that the U_m/U_c ratio ranged from 1.3 to 7.5 was considered to be a good agreement between the calculated and the experimental values.

Introduction

Vesicles prepared with both natural and synthetic amphiphiles are convenient systems for the study of structural and functional properties of bilayers as well as carriers of drugs and genetic information into cells.[1] Particularly, synthetic amphiphile vesicles are extremely efficient catalysts for both ground- and excited-state reactions.[1] The rate of vesicle-modified reactions can be controlled by substrate compartmentalization and changes in the composition of the reaction medium.[2,3] The size of vesicles can be varied from 250 to 5000 Å in diameter by use of different preparation methods.[4] Several features, such as solubilization and permeability, are strictly related to vesicle size. Not only the association constants but also the relative positions of bound substrates vary with vesicle size.[5] These data led us to investigate the degree of counterion dissociation (α) as a function of vesicle size. This parameter is essential for the quantitative analysis of kinetic data using models such as the pseudophase ion exchange.[6] Moreover, the determination of the parameters needed for the calculation of α of synthetic amphiphile vesicles of different sizes (e.g., hydrodynamic radius, electrophoretic mobility, zeta potential) may be of relevance for the understanding of the (several) differences between lipid and synthetic amphiphile bilayers.

Here we have used free-flow electrophoresis to determine, for the first time, the degree of ion dissociation from vesicles as a function of their size (measured by quasielastic light scattering). The experimental values of electrophoretic mobility of vesicles were lower than those calculated according to theory,[7] and this discrepancy was analyzed. For both positively and negatively charged amphiphiles the degree of ion dissociation decreased with increasing size of the vesicle.

Materials and Methods

Dioctadecyldimethylammonium chloride (DODAC) (Herga Industrias Quimicas, Rio de Janeiro, Brazil) and dioctadecyldimethylammonium bromide (DODAB) (Eastman Kodak) were purified by recrystallization.[8] Dihexadecyl phosphate (DHPH) (Sigma Chemical Co.) was used as received. The sodium salt of DHPH (DHPNa) was prepared by neutralization of a hexane solution of DHPH with NaOMe in MeOH. After solvent stripping the solid was recrystallized from ethanol:acetone. 1-[(2-methylphenyl)azo]-2-naphthol (Orange OT) was obtained from *o*-toluidine and 2-naphthol (Aldrich) according to standard procedures.[9] All other reagents were of analytical grade. Deionized, twice-distilled water was used throughout.

Vesicle preparation. (1) Sonication: Enough amphiphile to give a final concentration of ca. 10 mM was weighed in a sonication tube, water (or aqueous NaCl) was added, and the tube was maintained for 10 min above the phase transition temperature (T_c) of the (corresponding) bilayer. The mixture was then sonicated at the T_c for 1 h (DODAC) or 1.5 h (DODAB) in a bath sonicator (Branson do Brazil, Sao Paulo, Brazil, MSX-10). Sonication was also performed with a tip sonifier (Braunsonic 1510) for 20 min (above the T_c), and mixtures were later centrifuged at 10000g, for 30 min. (2) Chloroform injection: Large DODAC and DODAB vesicles were prepared by injection of chloroform solutions of DODAX (X = Cl^- or Br^-) into water or aqueous salt as previously described.[10] (3) Ethanol injection: 1.0 mL of an ethanolic solution of DODAC (0.2 M) was slowly injected into 19.0 mL of either water or aqueous NaCl maintained at 50 °C.

Conductivity was determined (30 °C) in a digital apparatus (Digimed, Sao Paulo, Brazil) with a cell constant of 1.00. Absorbance was measured in a Beckman M25 spectrophotometer at 495 nm. To minimize light scattering errors, vesicles were destroyed before absorbance measurements by addition of detergent and incubation at 60 °C for 5 min. For DODAC or DODAB we used hexadecyltrimethylammonium bromide (CTAB), and for DHPH or DHPNa we used sodium dodecyl sulfate (SDS). DODAB and DODAC concentrations were measured by halide titration,[11] and DHPH was determined, after

* Address correspondence to this author.
† Universidade de Sao Paulo.
‡ UNESP.
§ Universidad de Chile.
∥ Deceased 1989.
⊥ Tulane University.

(1) Fendler, J. H. *Membrane Mimetic Chemistry*; Wiley-Interscience: New York, 1982.
(2) Moss, R. A.; Swarup, S.; Zhang, H. *J. Am. Chem. Soc.* **1988**, *110*, 2914.
(3) Cuccovia, I. M.; Kawamuro, M. K.; Krutman, A. K.; Chaimovich, H. *J. Am. Chem. Soc.* **1989**, *111*, 365.
(4) Lasic, D. D. *Biochem. J.* **1988**, *256*, 1.
(5) Abuin, E.; Lissi, E. *J. Colloid Interface Sci.* **1988**, *122*, 201.
(6) Quina, F. H.; Chaimovich, H. *J. Phys. Chem.* **1979**, *83*, 1844.
(7) Booth, F. *Proc. R. Soc. London* **1950**, *A203*, 514.
(8) Cuccovia, I. M.; Quina, F. H.; Chaimovich, H. *Tetrahedron* **1982**, *38*, 917.
(9) Vogel, A. I. *Textbook of Practical Organic Chemistry*, 4th ed.; Longman Scientific & Technical: London, England, 1978.
(10) Ribeiro, A. M. C.; Yoshida, L. S.; Sesso, A.; Chaimovich, H. *J. Colloid Interface Sci.* **1984**, *100*, 433.
(11) Schales, O.; Schales, S. S. *J. Biol. Chem.* **1941**, *140*, 879.

0022-3654/90/2094-3722$02.50/0 © 1990 American Chemical Society

TABLE I

methods and conditions[a]	D_h, Å	$(d\lambda/dc)/f$ ($\times 10^2$)	α
	DODAC		
EtOH injection[b]			
no salt (0.92)	230	4.47	0.29
no salt (8.0)	220	4.47	0.35
5 mM NaCl (9.0)	250	2.83	0.23
sonication			
no salt (5.0)	530 (484[c])	3.32	0.21
no salt (1.0)	530	3.32	0.22
0.93 mM NaCl (5.0)		2.80	0.20
2.42 mM NaCl (5.0)		2.35	0.17
4.76 mM NaCl (5.0)	380	1.73	0.13
9.27 mM NaCl (5.0)	400	1.40	0.11
$CHCl_3$ injection			
no salt (0.3)	2850 (5000,[d] 3000[e])	0.61	0.044
4.4 mM NaCl (0.3)	3500		
9.0 mM NaCl (0.3)	3500		
	DODAB		
sonication			
no salt (5.0)	650	1.64	0.13
$CHCl_3$ injection (0.3)	2750	0.58	0.043
	DHPNa		
sonication (5.0)	673 (508[f])	2.50	0.22
	DHPH		
sonication (4.0)	1162 (500,[g] 900[f])	2.92	0.068
	CTAB		
NaBr 0.025 M, 30 °C	61 (64.4[h])	2.73	0.203
	SDS		
25 °C	51[i]	2.52	0.26
30 °C		2.69	0.24

[a] Amphiphile concentrations (mM) in parentheses. [b] 5% (v/v) EtOH. [c] Reference 28. [d] Reference 10. [e] Reference 19. [f] Reference 29. [g] Reference 30. [h] Reference 31. [i] Reference 32.

hydrolysis, by measuring inorganic phosphate.[12]

Electrophoretic mobility (U_m) was determined according to the procedure described by Hoyer et al.[13] as modified by Sepulveda and Cortes.[14] The agar (2%) bridge contained 0.2 M NaCl. Labelling was done by adding 20 μL of an acetonitrile solution of Orange OT (0.025 M) to vesicle preparations to yield 5×10^{-5} M final dye concentration. Current was measured with a Keithley 197 multimeter. The applied voltage (300 V) was maintained with a Shandon SAE 2761 source. The silver electrodes (tapes $1 \times 10 \times 0.1$ cm, generously supplied by Degussa S. A. Brasil) were immersed in NaCl (0.2 M). During electrophoresis the temperature was maintained at 30.0 ± 0.02 °C with a thermostating–circulating pump (Quimis Brasil) in a 50 L water bath. U_m was calculated from the equation[13]

$$U_m = \frac{\lambda(A_i - A_f)v}{itA_i} \quad (1)$$

where A_i and A_f are the initial and final absorbances, respectively, of the Orange OT labeled vesicle solution contained in a capillary of volume (v) = 3.71 cm^3; t is the time (in seconds) during which the current (i, amperes) was measured; λ is the conductivity of the sample (mho per centimeter).

Dynamic light scattering measurements were made at 25 °C in an apparatus equipped with a Coherent Innova 90-5 argon ion laser operating at 488 nm and a Thorn EMI 9863Q-35 phototube with an APED-II amplifier for single photon detection, connected to a Brokhaven PI-2030 digital correlator. Vesicle solutions were passed through nylon filters before quasielastic light scattering (QELS); for sonicated and ethanolic vesicles the filter cutoff was 2200 Å and for chloroformic vesicles it was 8000 Å.

(12) Houser, G.; Fleischer, S.; Yamamoto, A. *Lipids* **1970** *5*, 494.
(13) Hoyer, H. W.; Mysels, K. J.; Stigler, D. *J. Phys. Chem.* **1954**, *58*, 385.
(14) (a) Sepulveda, L.; Cortes, J. *J. Phys. Chem.* **1985**, *89*, 5322. (b) Czerniawski, M. *Rocz. Chem.* **1967**, *41*, 817.

Results and Discussion

Results are presented in Tables I and II. Vesicles of various sizes have been prepared with lipids (for a review see ref 4), and some of the methods used for lipids have been adapted for synthetic amphiphiles.[8,10] In particular, dialkyldimethylammonium (DODA) amphiphiles form aggregates of different architecture (e.g., micelles or vesicles) depending not only on the preparation method but also on the alkyl chain length and counterion type.[15] Size determinations using QELS depend on several assumptions, including corrections for particle–particle interactions.[16] The reported hydrodynamic diameters (D_h) were estimated from the diffusivity measured by QELS using the Stokes–Einstein relation.[17] We note that for all reported D_h's the polydispersity index, Q,[18] ranged from 0.1 to 0.2. In the case of micelles, extrapolation to the critical micelle concentration (cmc) generally affords consistent sizes from QELS data.[16] The apparent sizes of sonicated vesicles varied little with concentration up to 10 mM amphiphile (not shown). Hence, for the purpose of this work, we elected to report all D_h's at a single amphiphile concentration (Table I). The micellar D_h of CTAB was extrapolated to the cmc and agrees with published data.[16]

Ethanol injection (DODAC) produced aggregates with an D_h of 230 Å with or without added salt. Sonicated DODAC vesicles exhibited a D_h of 520 Å when prepared in water. Sonication of DODAC in salt ($(5–10) \times 10^{-3}$ M) produced smaller vesicles (D_h = 380–400 Å). For vesicles obtained by chloroform injection the presence of salt in the preparation medium led to an increase in D_h from 2850 Å (no salt) to 3500 Å ($(4–9) \times 10^{-3}$ M NaCl). Comparison of the values obtained here for D_h with published data (presented in Table I) show good agreement for sonicated vesicles. In the case of large (chloroformic) vesicles the present values are smaller than those obtained by electron microscopy[10] but similar to those obtained by QELS.[19] Since these vesicles are salt-sensitive,[10] it is probable that the difference in the sizes reflects the effect of the staining salt used for contrast in electron microscopy. A limited study of the size of DHPH vesicles was also undertaken (Table I). It should be noted that the size of DHPH vesicles was extremely sensitive to the nature of the counterion. Sonicated DHPH vesicles exhibited a D_h of 1162 Å while for DHPNa D_h was 673 Å. This difference is probably related to the formation of intrabilayer hydrogen bonds[20] in the DHPH bilayer which could prevent the formation of small vesicles.

Measured mobilities are sensitive functions of both amphiphile and salt concentrations.[21] Without added salt the values of U_m of large vesicles were 30–50% lower than those of small (sonicated) vesicles irrespective of the nature of the counterion. The mobility of positively charged vesicles was similar to those of DHPNa and DHPH vesicles and to micelles (Table II). In spite of the remarkable size difference between the amphiphilic structures, ranging from 40 to 5000 Å in diameter, the maximum difference in U_m was ca. 2-fold. The data in Table I suggest that there is no relationship between particle size and electrophoretic mobility. This lack of relationship could be expected for particles in which the size increases were accompanied by a decrease in ion dissociation, e.g., a decrease in effective surface potential (vide infra).

From the electrophoretic mobility (U_m) we estimated the streaming potential (ξ) of the particles using a simple Smoluchovski model. The ξ value calculated by using the (uncorrected) Smoluchovsky expression is known to yield a minimum estimate of the streaming potential.[22] There are serious doubts that ξ values can be calculated from U_m data even using more rigorous data-

(15) Israelachvili, J. N. *Intramolecular and Surface Forces*; Academic Press: London, 1985.
(16) Biresaw, G.; McKenzie, D. C.; Bunton, C. A.; Nicolli, D. F. *J. Phys. Chem.* **1985**, *89*, 5144.
(17) Berne, B. J.; Pecora, R. *Dynamic Light Scattering*; Wiley: New York, 1976.
(18) Reed, C. E., Li, X.; Reed, W. F. *Biopolymers*, in press.
(19) Moss, R. A.; Swarup, S. *J. Org. Chem.* **1988**, *53*, 5860.
(20) Carmona-Ribeiro, A. M. *J. Phys. Chem.* **1989**, *93*, 2630.
(21) Stigter, D.; Mysels, K. J. *J. Phys. Chem.* **1955**, *59*, 55.
(22) McLaughlin, S. *Curr. Top. Membr. Transp.* **1977**, *9*, 71.

TABLE II

methods and conditions[a]	U_m (×10⁴), cm²/(V s)	U_c (×10³), cm²/(V s)	U_c/U_m	U_c/U_m[b]	ξ,[c] mV
		DODAC			
EtOH injection[d]					
no salt (0.92)	8.2	4.3	5.2	2.7	96.4
no salt (8.04)	4.5	3.4	7.5	6.6	52.9
5 mM NaCl (9.42)	4.0	1.4	3.4	3.0	47.0
sonication					
no salt (1.0)	7.2				85.0
no salt (5.0)	7.8	4.1	5.3	3.3	91.5
0.93 mM NaCl (5.0)	6.2				72.6
2.42 mM NaCl (5.0)	5.9				70.1
4.76 mM NaCl (5.0)	4.9	0.92	1.3	1.1	57.9
9.27 mM NaCl (5.0)	4.6	0.86	1.9	1.6	54.1
$CHCl_3$ injection					
no salt (5.0)	5.4	2.8	5.2	4.2	63.6
		DODAB			
sonication					
no salt (5.0)	6.7	3.0	4.5	3.2	78.4
$CHCl_3$ injection					
no salt (5.0)	5.1	2.4	4.5	3.8	60.4
		DHPNa			
sonication (4–10)	6.6	4.6	5.8		77.9 (77–127[e])
		DHPH			
sonication (4.0)	8.3	2.9	3.6	1.8	97.3
		CTAB			
25 mM NaBr (5.0)	5.0 (2.45,[f] 4.75[g])	0.94	1.9	1.6	58.9
		SDS			
25 °C (16)	4.8 (4.5[h])	0.8	1.7	1.4	56.2
30 °C (16)	5.6	0.8	1.5	1.1	66.2

[a] Amphiphile concentrations (mM) in parentheses. [b] Corrected U_c values; see text. [c] Calculated from U_m; see text. [d] 5% v/v EtOH. [e] Reference 33. [f] Reference 14a. [g] Reference 14b. [h] Reference 21.

analysis models. Nevertheless, the calculations were considered to be illustrative for comparative purposes. ξ was calculated by using the expression[22]

$$\xi = \frac{\eta U_m}{\epsilon_r \epsilon_0} \qquad (2)$$

where η is the water viscosity (7.975×10^{-3} (dyn s/cm²)), ϵ_0 the permissivity of free space ($8.857\,17 \times 10^{-7}$ dyn/V²), and ϵ_r the dielectric constant of water (76.55) at 30 °C. The calculated ξ values (Table II) ranged from 50 to 90 mV, well within the range published for similar supramolecular aggregates of this type at low salt concentration.[22]

From U_m and conductance data we calculated the relative counterion dissociation of the supramolecular aggregate (α)[23] using the relationship

$$\alpha = \frac{10^3\, d\lambda/dc}{F(U_m + U_x)f} \qquad (3)$$

where the Faraday constant (F) is equal to 96 500, U_x is the mobility of the counterion, and $d\lambda/dc$ is the slope of the conductance vs total amphiphile concentration plot. For micelles $d\lambda/dc$ was taken above the cmc.[14] In the case of vesicles $d\lambda/dc$ was corrected for the fraction of amphiphiles residing in the external surface (f). The dissociation of ions from the internal surface should not contribute to the measured conductance.[24] Hence f is 1.0 for micelles and was taken as 0.7, 0.6, and 0.5 for vesicle diameters up to 250 Å, from 250 to 700 Å, and greater than 700 Å, respectively.[10] The conductances of solutions of large vesicles were significantly lower than those containing smaller structures. In some cases a deviation from linearity in the λ vs c plots was observed. The values of $d\lambda/dc$ are presented in Table I. Vesicles of DHPNa and DHPH exhibited similar $d\lambda/dc$. However, since the specific conductance of H^+ is larger than that of Na^+, the calculated value of α for DHPH was much lower than that of DHPNa. Function-dependent changes due to replacement of H^+ in DHPH monolayers have been described for intra- and interlayer forces.[20]

As previously observed for micelles,[14] the degree of counterion dissociation (α) from small DODAX vesicles was larger with Cl^- ion than with Br^- ion. The difference in α, however, is negligible when Cl^- ion and Br^- ion are compared in large DODAX vesicles (Table I). Ion dissociation from the large vesicles was very small, and the detection of minor differences in α (between DODAC and DODAB) in large vesicles would be outside the sensitivity of the present method. The salt dependence of α, especially in the small DODAC vesicles, suggests that ion dissociation in vesicles is affected by ionic strength more strongly than in micelles. It is attractive to speculate that the effective size of the ion pair at the surface[15] affects both ion dissociation and vesicle size. The size dependence of α is probably partially due to the difference in headgroup packing in the bilayer as a function of changing radius of curvature. Abuin and Lissi[5] have observed marked changes in the partition coefficients of neutral substrates as a function of vesicle size and interpreted their data in terms of a lesser monomer packing in the small vesicles. Lesser packing should reduce the electrostatic repulsion at the surface and permit a larger extent of ion dissociation as observed. The values of α presented here were utilized to analyze quantitatively vesicle size dependent catalytic effects on chemical reactions and resulted in excellent fits.[25] The large differences in α, varying by as much as a factor of 8 (Table I), cannot be wholly explained by changes in headgroup area. The latter is not expected to exceed a factor of about 2 in going from a vesicle diameter of 220 Å to 2850 Å.[26]

(23) Keh, E.; Gavach, C.; Guastalla, J. C. R. *Acad. Sci. Paris, Ser. C* **1966**, *263*, 1488.
(24) McNeil, R.; Thomas, J. K. *J. Colloid Interface Sci.* **1980**, *73*, 522.
(25) Cuccovia, I. M.; Kawamuro, M. K.; Chaimovich, H. Submitted for publication.

The surface potential (ψ) of the vesicle should be roughly proportional to

$$\frac{\alpha R}{(1 + \kappa R)}$$

where κ is the Debye–Hückel inverse screening length and R is taken as half of D_h. At very low salt concentration the interaction energy between an ion and the surface would increase with increasing vesicle size to levels well above kT unless some counterions condense back to the headgroups; i.e., α must decrease with increasing vesicle size in order to maintain the thermal distribution of bound and free counterions.

Vesicles, because they can be prepared with a number of different monomers in varied sizes and charge distributions, are interesting systems to test theories for particle movement as well as particle–particle interactions in solution. Although a completely satisfactory model for the relationship between electrophoretic mobility, polyion parameters, and solution parameters does not exist, the impermeable sphere model should be a better approximation for vesicles and micelles than for polymeric polyelectrolytes. In the approximation of an impenetrable, nonconducting sphere with a spherically symmetric charge distribution, the leading term for the expression of electrophoretic mobility is given by[7]

$$U_e = z\epsilon X(kR)/[(6\pi\eta R)(1 + kR)] \quad (4)$$

Here k is the Debye–Hückel parameter, R is the radius of the sphere, and $X(kR)$ is a sigmoidal function which varies from 1.0 to 1.5 over the range of kR from zero to infinity. The hydrodynamic radii were used for R in the above equation.

In order to estimate the mobility according to eq 4, it was necessary to make approximations for the values of z and k in the cases of no added electrolyte. Two assumptions were used to estimate z: First, the headgroup area per monomer in all the vesicles was taken as 75 Å^2. Literature values for the surface areas of monomers in bilayers range from 40 to 100 Å^2 for amphiphiles as different as DODAC to (a number of) naturally occurring lipids.[27] Thus, while headgroup area is expected to decrease with increasing radius, the (constant) value chosen should not affect z by more than a factor of 2 in any of the cases. Second, the value of α was used to compute the net charge via

$$z = \alpha(\pi D_h^2)/75 \quad (5)$$

where D_h is measured in angstroms. This equation implicitly assumes that only the dissociated headgroups on the external surface contribute to the vesicles' net charge and mobility.

In the cases of added NaCl the usual prescription for the inverse Debye–Hückel screening length was used:

$$k = (I)^{1/2}/(3.04) \quad (6)$$

where I is the ionic strength in terms of moles and k has the units of inverse angstroms.

In the case where no added salt was present, the value of k was estimated by assuming the ionic strength to be due to the concentration of (external) unassociated counterion, e.g., to αf [amphiphile]/2. No attempt is made to justify this procedure since in the absence of added salt the applicability of the assumptions of Debye–Hückel theory is uncertain. It is important to note that by this estimation even low effective free counterion concentrations, on the order of 0.1 mM lead to ionic atomsphere radii on the order of the vesicles' radii and hence to appreciable values for kR in eq 4.

The shortest interparticle distance (800 Å) was calculated for ethanol-injected vesicles (8 mM DODAC, Table I), and even in this case, the screening length (100 Å) was lower than the intervesicle distance. As the size of the particle increases, at the amphiphile concentrations used, the interparticle distances increase. Thus, for the large DODAC vesicles (0.3 mM DODAC, Table I) the intervesicle distance was ca. 1.36×10^4 Å and the screening length was 409 Å. It is therefore clear that the assumption of no interparticle repulsions, in the calculation of α, was adequate.

Table II shows the values for the calculated mobilities (U_c) and the ratio U_c/U_m. The latter values range from 1.3 to 7.5. Even this level of agreement is surprising given the number of approximations. In the case of all vesicles the U_c values are larger than U_m values. Booth[7] carried out the expansion in terms of zeta potential to third order for the electrophoretic mobility of impenetrable, uniformly charged, nonconducting spheres in symmetric electrolytes and found that for potentials above about 40 mV the mobility begins to deviate downward from the linear relation of eq 4. For a potential of 100 mV the linear fit overestimates the mobility by a factor of 2. In light of this correction, all of the U_c values in Table II can be revised downward. Table H shows the values of U_c/U_m with U_c corrected to third order using Booth's graphical summary.[7] Since Booth's theory also only applies in the case of added symmetric electrolyte, it is most interesting to see the effect of the correction on the case of 5 mM salt for sonicated DODAC in the Table II, using the associated estimate for the zeta potential. The revised value was within 10% of the measured value (Table II). The good agreement between measured and calculated values for the micelles is probably due to the fact that the error inherent in the approximation of k has a relatively small effect on the value of kR, since the micellar radius is quite small. The larger deviations for the ethanolic vesicle preparations may have to do with differences in dielectric constant around the vesicles due to the (unknown) distribution of the ethanol between the bulk and vesicular pseudophases.

Given the good agreement between experiment and theory in the case of the sonicated DODAC vesicles and added NaCl, it would be interesting to conduct more extensive tests on vesicles or liposomes that are stable at high ionic strengths.

Acknowledgment. We are indebted to the BID/USP Program for Human Resources (W.R. and H.C.), FINEP, CNPq (H.C. and I.M.C.), and CAPES (E.F.) for support. We thank The Louisiana Board of Reagents for partial support.

Registry No. DODAC, 107-64-2; DODAB, 3700-67-2; DHPH, 2197-63-9; DHPNa, 60285-46-3.

(26) Cadenhead, D. A. In *Structures and Properties of Cell Membranes*; Benga, G., Ed.; CRC Press: Boca Raton, FL, 1985; Vol. III, p 21.
(27) Mason, J. T.; Huang, C. *Ann. N.Y. Acad. Sci.* **1987**, *308*, 29.
(28) Pileni, M. P. *Chem. Phys. Lett.* **1980**, *71*, 317.
(29) Tricot, Y. M.; Furlong, D. N.; Sasse, W. H. F.; Daivis, P.; Snook, I.; van Megen, W. *J. Colloid Interface Sci.* **1984**, *97*, 380.
(30) Mortara, R. A.; Quina, F. H.; Chaimovich, H. *Biochem. Biophys. Res. Commun.* **1978**, *81*, 1080.
(31) Dorshow, R.; Briggs, J.; Bunton, C. A.; Nicolli, D. F. *J. Phys. Chem.* **1982**, *86*, 2388.
(32) Corti, M.; Degiorgio, V. *J. Phys. Chem.* **1981**, *85*, 711.
(33) Ben Chaabane, T.; Bernas, A.; Grand, D.; Hautecloque, S. *J. Phys. Chem.* **1987**, *91*, 6055.

artigo II

Reprinted from LANGMUIR, 1993, 9.
Copyright © 1993 by the American Chemical Society and reprinted by permission of the copyright owner.

Integration of the Nonlinear Poisson–Boltzmann Equation for Charged Vesicles in Electrolytic Solutions

Eloi Feitosa,† Augusto Agostinho Neto,† and Hernan Chaimovich*,‡

Departamento de Física, IBILCE/UNESP, São José do Rio Preto, SP, Brasil, and Departamento de Bioquímica, Instituto de Química, Universidade de São Paulo, São Paulo, SP, Brasil

Received October 5, 1992. In Final Form: December 22, 1992

The Poisson–Boltzmann equation (PBE), with specific ion–surface interactions and a cell model, was used to calculate the electrostatic properties of aqueous solutions containing vesicles of ionic amphiphiles. Vesicles are assumed to be water- and ion-permeable hollow spheres and specific ion adsorption at the surfaces was calculated using a Volmer isotherm. We solved the PBE numerically for a range of amphiphile and salt concentrations (up to 0.1 M) and calculated co-ion and counterion distributions in the inside and outside of vesicles as well as the fields and electrical potentials. The calculations yield results that are consistent with measured values for vesicles of synthetic amphiphiles.

Introduction

In excess water natural amphiphiles, such as phospholipids, associate spontaneously forming a variety of supramolecular aggregates.[1] Synthetic amphiphiles form many of the complex structures obtained with phospholipids furnishing, therefore, unique opportunities to study the relationships between the structure of the monomer and the architectural and functional properties of the aggregate(s).[1,2] We have been interested in the preparation and properties of synthetic amphiphile vesicles,[2c,3] a general denomination of closed spherical particles enclosed by a single bilayer.[1] In vesicles, as in other charged supramolecular or polymeric assemblies, knowing the charge density is essential information for understanding structural as well as functional properties.

Electrostatic potential functions, and corresponding ion distributions, have been analyzed using both the linearized and nonlinearized Poisson–Boltzmann equations (PBE) in the planar, cylindrical, and spherical symmetries for polyelectrolytes and different supramolecular aggregates, including vesicles.[4–14] In a solution containing vesicles, ions can reside in the intervesicular bulk solution, at the inner and outer bilayer interfaces and in the internal aqueous compartment. In these compartments the PBE has to be integrated under conditions where the geometry of the systems affords no analytical solution; hence several simplifying approximations have been employed to obtain numerical solutions. The PBE has been integrated for vesicles under conditions such as (a) no added salt,[4] (b) low amphiphile and/or salt concentrations,[5] (c) assuming electroneutrality in the vesicle's inner compartment,[5] (d) vesicles with no curvature,[6,7] and (e) hard instead of hollow spheres (shells).[5,14] Bentz has presented approximated solutions of the PBE for concentric planar, cylindrical, and spherical surfaces with large inner radius (R_a), relative to the inverse Debye screening length (κ), ie. $R_a\kappa \geq 10$, with aqueous electrolyte between the surfaces.[14]

Solutions of the PBE for macromolecular assemblies that do not take into account specific (nonelectrostatic) ion binding lead to unrealistic high surface potentials.[5] Several assumptions can be used to approximate the calculated to the experimental values including nonelectrostatic counterion ion adsorption which partially neutralizes the surface charge of the aggregate, yielding lower surface potentials and more realistic ion concentrations at the surface.[15]

Here we present a new approach for describing ion distribution and electrical potential functions inside and outside vesicles. This description, based on the use of a cell model, the Poisson equation, and the Boltzmann ion distribution, is applicable for a wide range of conditions. The model includes specific (nonelectrostatic) ion–bilayer interactions using a Volmer isotherm, leading to realistic values for the electrical potentials and ion concentrations at the vesicular surfaces.

Theoretical Model

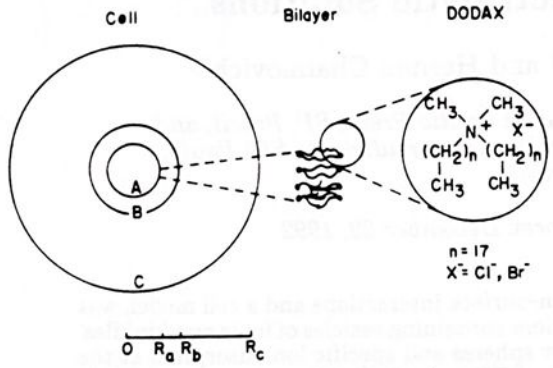
The model developed here applies to systems containing vehicles prepared with charged amphiphiles, for example, dioctadecyldimethylammonium halides (DODAX) (where X = Cl^- or Br^- ion).[1] Vesicles are treated as semipermeable nonconducting spherical cells, with internal and external radii R_a and R_b, respectively (Scheme I). Surface charges

† IBILCE/UNESP.
‡ Universidade de São Paulo.

(1) (a) Fendler, J. H. *Membrane Mimetic Chemistry*; Wiley: New York, 1982. (b) Israelachvili, J. N. *Intramolecular and Surface Forces*; Academic Press: London, 1985.
(2) (a) Bangham, A. D.; Hill, M. W.; Miller, N. G. A. *Methods Membr. Sci.* **1974**, *1*, 1. (b) Kunitake, T.; Okahata, Y.; Tamaki, K.; Kumamuru, F.; Yakayanagi, M. *Chem. Lett.* **1977**, 387. (c) Mortara, R. A.; Quina, F. H.; Chaimovich, H. *Biochem. Biophys. Res. Commun.* **1978**, *81*, 1080.
(3) (a) Carmona-Ribeiro, A. M.; Yoshida, L. S.; Sesso, A.; Chaimovich, H. *J. Colloid Interface Sci.* **1984**, *100*, 433. (b) Cuccovia, I. M.; Feitosa, E.; Chaimovich, H.; Sepulveda, L.; Reed, W. *J. Phys. Chem.* **1990**, *94*, 3722. (c) Kawamuro, M. K.; Chaimovich, H.; Abuin, E. B.; Lissi, E.; Cuccovia, I. M. *J. Phys. Chem.* **1991**, *95*, 1458.
(4) Lampert, M. A.; Martinelli, R. U. *Chem. Phys.* **1984**, *88*, 399.
(5) (a) Mille, M.; Vanderkooi, G. *J. Colloid Interface Sci.* **1977**, *59*, 211. (b) Mille, M.; Vanderkooi, G. *J. Colloid Interface Sci.* **1977**, *61*, 455.
(6) Linse, P.; Gudmundur, G.; Jonsson, B. *J. Phys. Chem.* **1982**, *86*, 413.
(7) Oshima, H.; Makino, K.; Kondo, T. *J. Colloid Interface Sci.* **1986**, *113*, 369.
(8) Bell, G. M.; Dunning, A. J. *Trans. Faraday Soc.* **1970**, *66*, 500.
(9) Loeb, A. L.; Overbeek, J. T. G.; Wiersema, P. H. *The Electrical Double Layer around a Spherical Colloid Particle*; M. I. T. Press: Cambridge, MA, 1961.
(10) Wall, F. T.; Berkowitz, J. *J. Chem. Phys.* **1957**, *26*, 114.
(11) McLaughlin, S. *Curr. Top. Membr. Transp.* **1977**, *9*, 71.
(12) Gujeron, M.; Weisbuch, G. *Biopolymers* **1980**, *19*, 353.
(13) Fixman, M. *J. Chem. Phys.* **1979**, *70*, 4995.
(14) Bentz, J. *J. Colloid Interface Sci.* **1982**, *90*, 164.
(15) (a) Frahm, J.; Diekman, S. *J. Colloid Interface Sci.* **1979**, *70*, 440. (b) Fernandez, M. M.; Fromherz, P. *J. Phys. Chem.* **1977**, *81*, 1755. (c) Lelievre, J.; Haddad-Fahed, O.; Gaboriaud, R. *J. Chem. Soc., Faraday Trans. 1* **1986**, *82*, 2301. (d) Bunton, C. A.; Moffatt, J. R. *J. Phys. Chem.* **1986**, *90*, 538. (e) Bunton, C. A.; Moffatt, J. R. *J. Phys. Chem.* **1988**, *92*, 2896. (f) Karpe, P.; Ruckenstein, E. *J. Colloid Interface Sci.* **1990**, *137*, 408.

0743-7463/93/2409-0702$04.00/0 © 1993 American Chemical Society

Scheme I. Schematic Representation of a Dioctadecyldimethylammonium Chloride (DODAC) Vesicle in a Cell Model[a]



[a] A, B, and C indicate the inner, bilayer, and outer compartments, respectively. The inner and outer vesicle and cell radii are R_a, R_b, and R_c, respectively.

are assumed to be smeared uniformly on the inner and outer surfaces. The mobile ions (halide counterions and added salt) in both the internal and external aqueous compartments are assumed to be univalent point charges distributed radially, according to the Boltzmann distribution.[16] Mobile ions and water are allowed to freely cross the bilayer, i.e. the bilayer contains nonselective ion channels and the ion concentration in the bilayer is assumed to be negligible. The external compartment is bounded by a spherical cell wall of radius R_c containing one vesicle (Scheme I). We have used SI units throughout.

In the mean field theory, the PBE relates the mean electrostatic potential $\psi(r)$ of a (spherical) macroion (e.g. ionic micelle or vesicle) immersed in electrolytic solution to the net charge density $\rho(r)$ of charges (counter- and co-ions), radially distributed in the Gouy–Chapman electrochemical double-layer adjacent to the macroion, according to[16,17]

$$\Delta\phi = -(kT/\epsilon)\sum_i (z_i n_i^0) \exp(-z_i\phi) \qquad (1)$$

n_i^0 is the number concentration of ions (ions per liter) at the cell boundary, where the potential is zero. Δ is the Laplace operator. The permittivity of the medium (ϵ) is related to the permittivity of vacuum (ϵ_0) by

$$\epsilon = \Pi\epsilon_0 \qquad (2)$$

where Π is the dielectric constant of the medium. The charge of the ion i of valence z_i is

$$q_i = z_i e \qquad (3)$$

where e is the elementary charge. The reduced (unitless) potential ϕ is expressed as

$$\phi = e\psi/kT \qquad (4)$$

where k is the Boltzmann constant and T the absolute temperature (degrees Kelvin).

Integrating eq 1 over the volume and using the relation

$$\text{div } \mathbf{E} = -\text{div grad } \psi \equiv -\Delta\psi$$

where $\mathbf{E}$ is the radially oriented electric field (V/m) and Gauss' law of divergence, eq 1 can be written as

$$\epsilon_w r^2 E = \sum_i q_i n_i^0 \int_0^r r'^2 \exp(-z_i\phi)\, dr' \qquad (r < R_a) \quad (5a)$$

$$\epsilon_h r^2 E = \sum_i q_i n_i^0 \int_0^{R_a} r'^2 \exp(-z_i\phi)\, dr' + Q_a/4\pi\epsilon_h r^2 \qquad (R_a < r < R_b) \quad (5b)$$

$$\epsilon_w r^2 \mathbf{E}_c = \sum_i q_i n_i^0 \left[\int_0^{R_a} r'^2 \exp(-z_i\phi)\, dr' + \int_{R_b}^{r} r_i'^2 \exp(z_i\phi)\, dr'\right] + (Q_a + Q_b)/4\pi\epsilon_w r^2 \qquad (R_b < r < R_c) \quad (5c)$$

The charges of the vesicles' head groups (fixed charges) at the internal (Q_a) and external (Q_b) interfaces, containing N_a and N_b monomers, respectively, are

$$Q_a = e\Phi_a N_a \quad \text{and} \quad Q_b = e\Phi_b N_b \qquad (6)$$

Q_a and Q_b are taken as positive. The inner (Φ_a) and outer (Φ_b) degrees of ion dissociation are expressed as the fraction of (mobile) counterions not bound specifically to the vesicle interfaces.[1b,17]

Specifically bound ions are calculated by a Volmer isotherm

$$\Gamma_a = 1 - \Phi_a = \frac{\delta_a \exp(-\Gamma_a/(1-\Gamma_a))\,[X^-]}{1 + \delta_a \exp(-\Gamma_a/(1-\Gamma_a))\,[X^-]} \qquad (7)$$

Γ_a is the fractional coverage at the inner monolayer and $[X^-]$ is the mean concentration of counterions within an aqueous layer of thickness ω adjacent to the inner surface. In our calculations ω was taken to be 0.25 nm.[15d,e] An equivalent expression was used for Γ_b, the fraction of coverage at the outer vesicle surface ($\Gamma_b = 1 - \Phi_b$). Volmer isotherms have been employed for the PBE description of ion distributions in micellar solutions of single chain surfactants with quaternary ammonium head groups similar to those of DODAX.[15d] The parameter δ was taken as characteristic of the counterion–amphiphile interaction. Here δ is zero for co-ions; ie., no specific coion adsorption was allowed.

Equations 5a–c give the electrostatic field at any point from the vesicle center to the cell wall. The potential can be obtained from the relation

$$E(r) = -\text{grad } \phi(r) \text{ or } \phi(r) = -\int E\, dr \qquad (8)$$

To integrate these equations we have assumed that the potential through each interface is continuous and can be described by the following set of conditions:

$$\Pi_w\left(\frac{\partial\phi}{\partial r}\right)_{r=R_a-0} - \Pi_b\left(\frac{\partial\phi}{\partial r}\right)_{r=R_a+0} = \frac{\sigma_a}{\epsilon_0} \qquad (9a)$$

$$\Pi_w\left(\frac{\partial\phi}{\partial r}\right)_{r=R_b-0} - \Pi_b\left(\frac{\partial\phi}{\partial r}\right)_{r=R_b+0} = \frac{\sigma_b}{\epsilon_0} \qquad (9b)$$

Π_w and Π_b are, respectively, the dielectric constants of the electrolyte solution and the bilayer. The inner (σ_a) and outer (σ_b) surface charge densities are

$$\sigma_a = Q_a/4\pi R_a^2; \qquad \sigma_b = Q_a/4\pi R_b^2 \qquad (10)$$

Our boundary condition is that the potential, as well as its grad, is null at the cell boundary:

$$\phi_c = 0, \qquad \text{at } r = R_c \qquad (11a)$$

$$E_c = 0, \qquad \text{at } r = R_c \qquad (11b)$$

The choice of a null field at the cell boundary is justified by the electroneutrality of the whole system. The fact that, by construction, the cell interior is electroneutral does not imply, however, that the inner or outer vesicle compartments are also electroneutral. The field at the

(16) Hill, T. L. *Statistical Mechanics*; Addison-Wesley: Reading, MA, 1960.
(17) Verwey, E. J. W.; G. Overbeek, J. Th. G. *Theory of Stability and Lyophobic Colloids*; Elsevier: Amsterdam, 1948.

cm 1 2 3 4 5 6 7 8 unesp 12 13 14 15 16 17 18 19

vesicle center is, by symmetry, null. Within the bilayer the electrical potential varies with the inverse of the distance. The field within the bilayer satisfies eq 5b and is null only when the net sum of ions in the inner compartment is equal (and of opposite charge) to the total net charge in the inner surface, that is, when the vesicle interior is electrically neutral.

A computer program, appropriate for the numerical integration of the PBE in the integrated form (eqs 5), was developed.[18] The integral equation was solved using the cell model (Scheme I) with each vesicle isolated in a spherical compartment of radius R_c given by[5]

$$(4/3)\pi R_c^3 = 10^3 N/(LC_a) \qquad (12)$$

where L is the Avogadro's constant and C_a the total amphiphile concentration in moles per liter. The number of monomers in the vesicle (N) is equal to the sum of monomers in the internal (N_a) and external (N_b) monolayers. N_a and N_b were calculated from

$$N_a = 4\pi(R_a^2/s); \quad N_b = 4\pi(R_b^2/s) \qquad (13)$$

We have assumed that the area per monomer (s) is 75 Å^2 in a bilayer of 45 Å thickness (l).[20,21,22a] The bilayer thickness, as well as the area per monomer, were taken as fixed parameters. In a closed vesicle of finite size the percentage of monomers in each monolayer are a function of the diameter of the particle. For R_b = 265 Å (R_a = 220 Å), 59.2% of the monomers reside in the outer monolayer. The cell radius (R_c) was calculated using eq 12. The amphiphile, and salt concentrations, were varied from 10^{-4} to 0.10 M. All calculations were done at 298 K.[18]

The internal, external, and cell radii, as well as the amount of added (monovalent) salt, were used as input data to obtain the potential, field, and ion distribution as a function of radial distance to the center of the vesicle.

Results and Discussion

The value of the dielectric constant within a lipid bilayer is uncertain.[22,23] In our calculations we used Π_w = 78.54 (25 °C) for the bulk solution and different values for the bilayer dielectric constant: Π = 2.5, 15, and 40, (Π is about 2.5 for a hydrocarbon medium).[22] As expected from our model, which assumes free ion permeation, changes of the value of Π of the bilayer, did not alter considerably the calculated potentials. Varying the value of Π in the bilayer from 2.5 to 40 produced a decrease in ψ of no more than 0.9%.

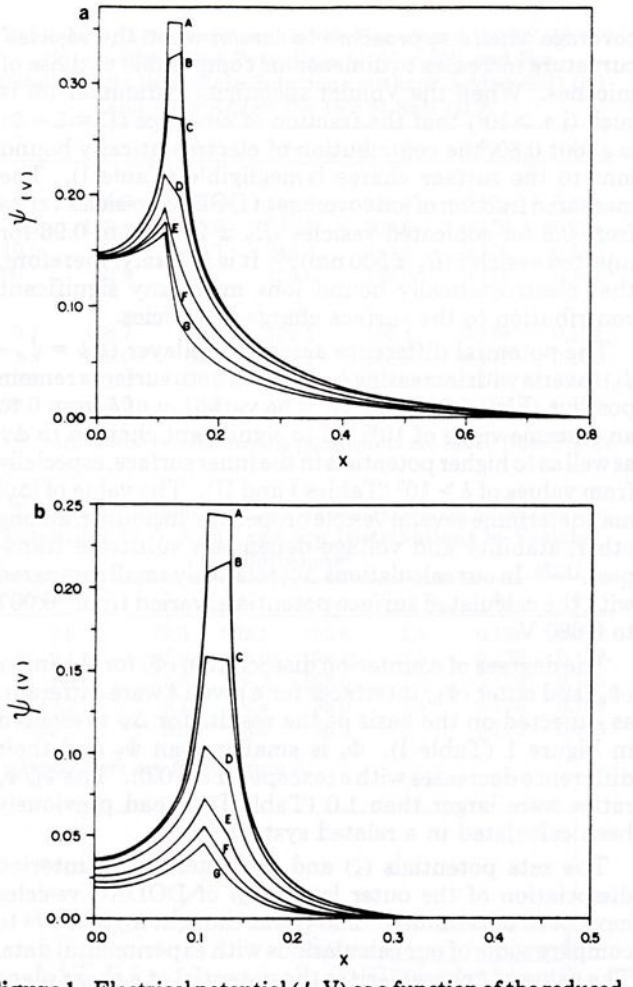


Figure 1. Electrical potential (ψ, V) as a function of the reduced distance ($x = r/R_c$) from the vesicle center for different values of the Volmer isotherm parameter (δ) in the absence (a) and presence (b) of added salt (1×10^{-3} M). Curves A through G were calculated with the following values of δ: 0.0 (A); 1.0 (B); 10^3 (C); 10^{10} (D); 10^{20} (E); 10^{30} (F); 10^{40} (G). The parameters used in the calculations were R_a = 220 Å, R_b = 265 Å, R_c = 1990 Å, s = 75 Å^2, and $C_a = 1.0 \times 10^{-3}$ M.

Table I. Electrical Potentials (ψ, V × 10^3) and Ion Distributions in Vesicle Solutions without Added Salt Calculated with Different Values of the Volmer Binding Parameters (δ, M^{-1})

δ	ψ_0	ψ_a	ψ_b	$\psi_a - \psi_b$	Φ_a	Φ_b
0.0	148.0	356.7	355.3	1.4	1.0	1.0
1.0	147.7	321.4	328.1	−6.7	0.495	0.594
10^3	146.9	271.8	269.0	2.8	0.179	0.196
10^{10}	144.8	218.8	197.1	21.7	0.054	0.057
10^{20}	143.2	189.8	141.7	48.1	0.025	0.026
10^{30}	142.0	175.0	107.1	68.6	0.016	0.017
10^{40}	141.9	166.5	85.4	81.1	0.012	0.012

In the absence of added salt the potential at the vesicle center (ψ_0) was not null and did not vary sharply with the value of the Volmer parameter δ (Figure 1a, Table I). The potentials and fields on the surfaces decreased significantly with increasing counterion affinity (Figure 1a). In the bilayer region, with no mobile ions, the potential decreased with the inverse of the distance (r).

The counterions bound electrostatically within a water layer of an arbitrary thickness (ω = 0.25 nm, see Theoretical Model)[24] only contribute significantly to the surface

(18) The computer program is basically an iterative routine. Initial values for the field are set arbitrarily at some space point; from this field an electrostatic potential is build up and so is the mobile ionic charge distribution. The ion distribution, together with the surface charge densities, yield another field that builds up another potential and a new charge distribution and so a new field. The process continues until a criteria of convergence is obtained. In these calculations, the solution was said to be attained when the fields of the two last computations differ, at every point, by a relative value less than 10^{-5}, i.e. $[|E_{N-1}(r) - E_N(r)|]/|E_N(r)| < 10^{-5}$, where N is the iteration number. The final results did not depend on the initial value taken for the field, but the number of iterations and CPU time did. Details on the computer calculations can be found elsewhere.[19] All calculations were done in a SparcStation II (SUN Microsystems Inc.)

(19) Feitosa, E. Ph.D. Thesis, Departamento de Química Fundamental. Instituto de Química da Universidade de São Paulo, São Paulo, SP, Brasil, 1990.

(20) Johnson, S. M. *Biochim. Biophys. Acta* **1973**, *307*, 27.

(21) Marra, J. *J. Phys. Chem.* **1986**, *90*, 2145.

(22) (a) Tanford, C. *The Hydrophobic Effect*; Wiley: New York, 1973. (b) Israelachvili, J. N.; Marcelja, S.; Horn, R. G. *Q. Rev. Biophys.* **1980**, *13*, 121. (c) Jain, M. K. *The Bimolecular Lipid Membrane: A System*; van Nostrand Reinhold Co.: New York, 1972; Chapter 4.

(23) Cevc, G.; Marsh, D. *Phospholipid Bilayers, Physical Principles and Models*; J. Wiley & Sons: New York, 1987.

(24) The value of ω should be related to the hydrated size of the ions adjacent to the inner and outer hydrocarbon–water interfaces.

(25) Romsted, L. S. PhD thesis, Indiana University, Bloomington, IN, 1975.

coverage when δ approaches to zero or when the vesicles' curvature increases to dimensions comparable to those of micelles. When the Volmer specificity parameter (δ) is such (i.e. $>10^3$) that the fraction of coverage ($\Gamma = 1 - \Phi$) is about 0.80, the contribution of electrostatically bound ions to the surface charge is negligible (Table I). The measured fraction of ion coverage of DODAC vesicles varies from 0.8 for sonicated vesicles ($R_b \cong 20$ nm) to 0.96 for injected vesicles ($R_b \cong 500$ nm).[3b] It is unlikely, therefore, that electrostatically bound ions make any significant contribution to the surface charge in vesicles.

The potential difference across the bilayer ($\Delta\psi = \psi_a - \psi_b$) inverts with increasing δ, although both surfaces remain positive (Figure 1, Table I). The variation of δ from 0 to an extreme value of 10^{40} led to significant changes in $\Delta\psi$ as well as to higher potentials in the inner surface, especially from values of $\delta > 10^3$ (Tables I and II). The value of $|\Delta\psi|$ may determine several vesicle properties, including, among other, stability and voltage-dependent substrate transport.[11,22c] In our calculations $\Delta\psi$, relatively small compared with the calculated surface potentials, varied from −0.007 to 0.080 V.

The degrees of counterion dissociation (Φ) for the inner (Φ_a) and outer (Φ_b) interfaces for a given δ were different, as expected on the basis of the results for $\Delta\psi$ presented in Figure 1 (Table I). Φ_a is smaller than Φ_b and their difference decreases with δ (except for $\delta = 0.0$). The Φ_b/Φ_a ratios were larger than 1.0 (Table I) as had previously been calculated in a related system.[5b]

The zeta potentials (ζ) and the extent of counterion dissociation of the outer layer (α_b) of DODAC vesicles have been determined[3b] and it was thought instructive to compare some of our calculations with experimental data. The value of ζ characterizes the potential at a shear plane located at some distance from R_b.[9,11] Our calculations explicitly yield values of ψ at any distance from the vesicle surface; therefore, the choice of a particular distance for the purpose of comparing our calculations with values of ζ is arbitrary. In some of our calculations a value of δ was chosen such that Φ_b or the potential at the external surface (ψ_b) corresponded to experimental values for the extent of counterion dissociation of the outer layer (α_b) or zeta potentials (ζ), respectively.[3b,24] For DODAC vesicles, of comparable radii without added salt, values of ζ, measured by electrophoresis, ranged from 0.050 to 0.100 V, while α_b ranged from 0.2 to 0.35.[3b] In the absence of added salt, no single value of δ gave Φ's or ψ's comparable to the measured α_b and corresponding ζ. Using a value of δ yielding a Φ_b equal to α_b furnishes a value of ψ_b higher than that described for ζ. A value of δ yielding a ψ_b corresponding to ζ results in a value of α_b smaller than that observed. In the absence of salt the calculated external potentials were, in general, higher than the values reported for the zeta potentials. The calculated potentials at a distance from the surface likely to correspond to the ζ plane were also higher than the measured values of ζ (Figure 1).

The addition of a (very) moderate amount of salt (10^{-3} M added salt with the same total amphiphile concentration) produces major changes in the calculated values (Figure 1b, Table II). Even without nonelectrostatic binding ($\delta = 0$), the potential at the surface decreases markedly and ψ_0 falls to values below 0.040 V. The values of ψ_0 with added salt are more sensitive to the value of δ (Figure 1b, Table II). The calculated potentials at the vesicle surface, or at a distance which is likely to represent the measured ζ (2.5–5 Å),[23] fall in the 0.100 V range if $\delta > 10^3$ and decrease sharply with distance (Figure 1b, Table II). The measured values for 5×10^{-3} M DODAC vesicles with added 1×10^{-3} M salt fall in the 0.070-V range.[3b] Moreover the value of Φ_b ($\delta = 10^3$) was 0.195, comparable with the value of $\alpha = 0.2$, determined for DODAC at the same salt concentration (see Table II). Thus this model reproduces, simultaneously, experimental values of α and ζ with added salt when δ is about 10^3.

Calculated electrical potentials at the vesicular surfaces in the absence of added salt are highly concentration dependent, as expected for ionic amphiphiles contributing free ions to the bulk solution (Figure 2a).[26] This very high dependence of the external potential on the vesicle

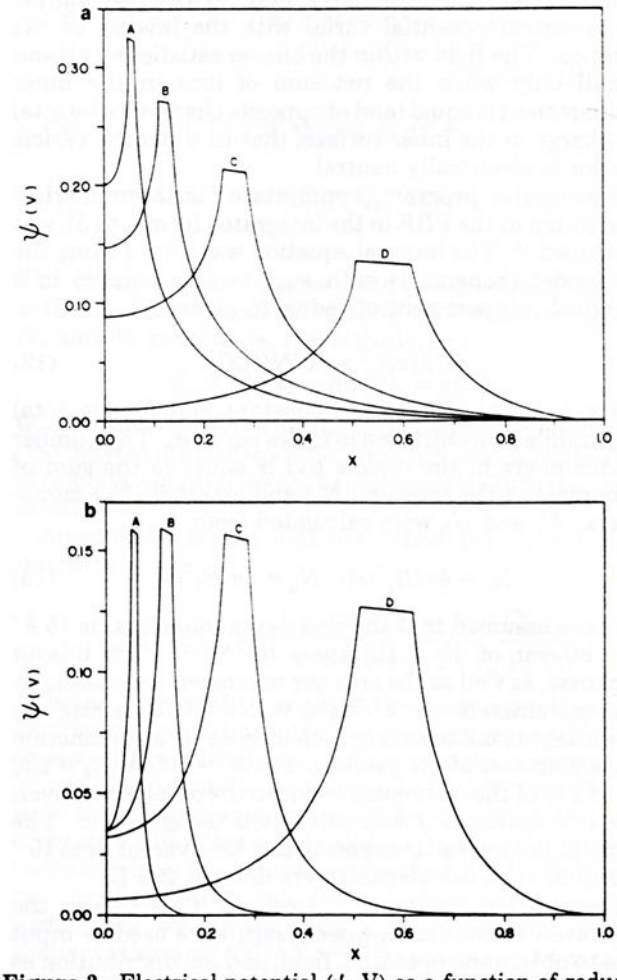


Figure 2. Electrical potential (ψ, V) as a function of reduced distance ($x = r/R_c$) from the vesicle center, for different amphiphile concentrations in the absence (a) and presence (b) of added salt (1×10^{-3} M). Curves A through D correspond to 0.1×10^{-3} (A), 1.0×10^{-3} (B), 10.0×10^{-3} (C), and 100×10^{-3} M (D) amphiphile, respectively. Corresponding R_c's were 428.7, 199.0, 92.4, and 42.9 nm, respectively. The value of δ was 10^3 M^{-1}. R_a, R_b, and s are as in Figure 1.

Table II. Electrical Potentials (ψ, V × 10^3) and Ion Distributions in Vesicle Solutions with Added 1.0×10^{-3} M Salt Calculated with Different Values of the Volmer Binding Parameter (δ, M^{-1})

δ	ψ_0	ψ_a	ψ_b	$\psi_a - \psi_b$	Φ_a	Φ_b
0.0	36.3	244.3	242.9	1.4	1.0	1.0
1.0	36.0	208.9	215.7	−6.8	0.495	0.593
10^3	34.7	158.9	156.5	2.4	0.179	0.195
10^{10}	31.0	104.2	89.2	15.0	0.054	0.056
10^{20}	26.0	72.3	51.4	20.9	0.025	0.026
10^{30}	22.0	55.7	35.0	20.7	0.016	0.016
10^{40}	18.8	45.2	26.2	19.0	0.012	0.012

(26) Quina, F. H.; Chaimovich, H. *J. Phys. Chem.* **1979**, *83*, 1844.

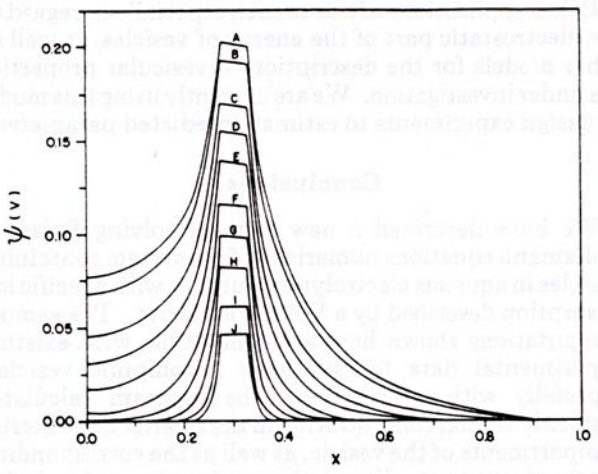


Figure 3. Salt effects on the electrical potential (ψ, V) of vesicles as a function of the reduced distance ($x = r/R_c$) from the vesicle center. Amphiphile concentration was 0.015 M. Curves A to J correspond to 0×10^{-3} (A), 0.1×10^{-3} (B), 0.5×10^{-3} (C), 1×10^{-3} (D), 2×10^{-3} (E), 5×10^{-3} (F), 10×10^{-3} (G), 20×10^{-3} (H), 50×10^{-3} (I), and 100×10^{-3} M (J) added salt, respectively. R_a and R_b are as in Figure 1, $\delta = 10^{-3}$ M^{-1}.

concentration in the absence of added salt may be one of the sources of the differences between our calculated values and the experimental results obtained with a limited set of vesicle concentrations. Because of experimental limitations, electrophoretic measurements of the zeta potential of DODAC vesicles in the absence of salt were obtained only at amphiphile concentrations between (1 and 9) $\times 10^{-3}$ M.[3b] Note that for vesicles of external diameter of 265 Å and $s = 75$ Å^2, the (1–9) $\times 10^{-3}$ M concentration range corresponds to a variation in the vesicle concentration between (0.5 and 4.5) $\times 10^{-7}$ M.

The addition of 10^{-3} M salt nearly eliminates the surface potential dependence (ψ_a and ψ_b) on vesicle concentration below 0.010 M amphiphile (Figure 2b). High values of C_a give small values of R_c (eq 12) and the aqueous space is taken by the mobile ions, leading to a decrease in the potential (Figure 2).

The effect of monovalent salt on the vesicle potential is shown in Figure 3. The potential difference $\Delta\psi = \psi_a - \psi_b$ is always positive, without inversion and approaches zero as the salt concentration increases. The potential–distance function becomes symmetric at high salt (Figure 3). It is worth noting that the numerical method of solution of the PBE works very well even at 0.1 M added salt.[27] The value of the Φ_b/Φ_a ratio decreases slightly with salt concentration (Table IV). A similar effect has been described previously over a more limited salt concentration range.[5b]

Co-ion and counterion distributions inside and outside the vesicle are shown in Figure 4. Above 5×10^{-5} M added salt the concentrations of co-ions and counterions are equal at the cell boundary. The concentrations of co-ions and counterions at the vesicle center become equal only for salt concentration higher than 5.0×10^{-3} M. The distribution of counterions changes slightly in the inner compartment; that is not the case for the distribution of co-ions. The counterion concentration in the vicinity of both the inner and outer interfaces does not depend on the salt concentration (Figure 4). The co-ion concentration, however, varies sharply with added salt at both outer and inner surfaces (Figure 4). Co-ion variation and

(27) In this range of salt concentrations the radius of the vesicles was assumed to be constant, although the effect of ionic strength on the vesicles' size is not well understood.[3b,19]

Table III. Effect of Amphiphile Concentration (C, M $\times 10^3$) on Electrical Potentials (ψ, V $\times 10^3$) and Ion Distributions in Vesicle Solutions without Added Salt (A) and with Added 1×10^{-3} M Salt (B)[a]

C	R_c	ψ_0	ψ_a	$\psi_a - \psi_b$	Φ_a	Φ_b
			A			
0.1	438.7	300.4	335.3	331.0	0.179	0.195
1.0	199.0	145.9	271.8	269.6	0.179	0.198
10.0	92.4	88.7	213.6	210.8	0.179	0.195
100	42.9	10.7	135.6	133.0	0.179	0.194
			B			
0.1	428.7	38.0	159.1	156.4	0.179	0.194
1.0	199.0	34.7	158.9	156.8	0.179	0.196
10.0	92.4	32.6	156.6	154.1	0.179	0.195
100	42.9	6.0	127.1	124.7	0.179	0.193

[a] R_c (nm) is the cell radius, the parameters are taken from Figure 2.

Table IV. Effect of Salt Concentration on Electrical Potentials (ψ, V $\times 10^3$) and Ion Distributions in Vesicle Solutions[a]

salt (M $\times 10^3$)	ψ_0	ψ_a	ψ_b	$\psi_a - \psi_b$	Φ_a	Φ_b
0.0	77.3	202.1	199.6	2.5	0.179	0.196
0.1	67.8	192.6	190.1	2.5	0.179	0.196
1.0	31.3	155.2	153.0	2.2	0.179	0.195
10.0	0.7	99.4	98.0	1.4	0.178	0.194
100	0.0	46.3	46.3	0	0.173	0.183

[a] Parameters are from Figure 3.

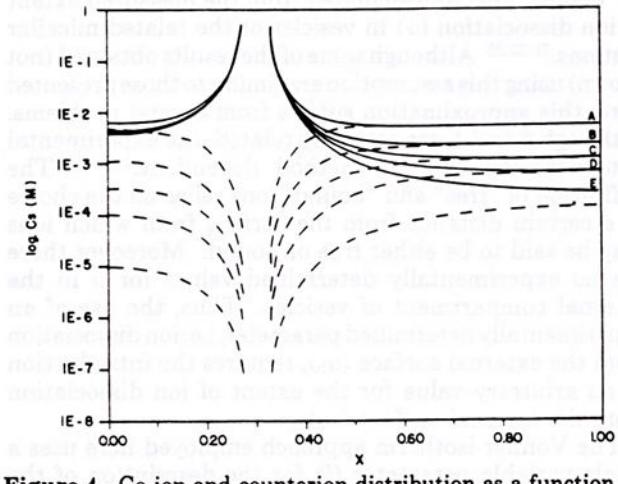


Figure 4. Co-ion and counterion distribution as a function of the reduced distance ($x = r/R_c$) from the vesicle center: co-ion (– – –), counterion (——). Added salt concentrations were 0.1×10^{-3} (E), 0.5×10^{-3} (D), 1.0×10^{-3} (C), 2.0×10^{-3} (B), and 5.0×10^{-3} M (A), respectively. Amphiphile concentration = 0.015 M. R_a, R_b, and δ are as in Figure 3.

counterion constancy with added salt have been also calculated, as well as experimentally measured in micellar systems.[28]

Figure 5 shows the magnitude and shape of the electrostatic field in all the vesicle compartments, for three concentrations of salt ((0.5, 10.0, and 100) $\times 10^{-3}$ M). The magnitude of the field near the interfaces is ca. 6.0×10^7 V/m and decreases sharply with the distance. The function relating field with distance is increasingly symmetric as the salt concentration increases and it is discontinuous in the bilayer region.

In addition to considering specific counterion adsorption, described here by a Volmer isotherm, we also have varied the vesicular surface charges using a totally different assumption for obtaining a lower electrical potential. An

(28) Bunton, C. A.; Mahala, M. M.; Moffatt, J. R. *J. Phys. Chem.* **1989**, *93*, 7851.

cm 1 2 3 4 5 6 7 8 unesp 12 13 14 15 16 17 18 19

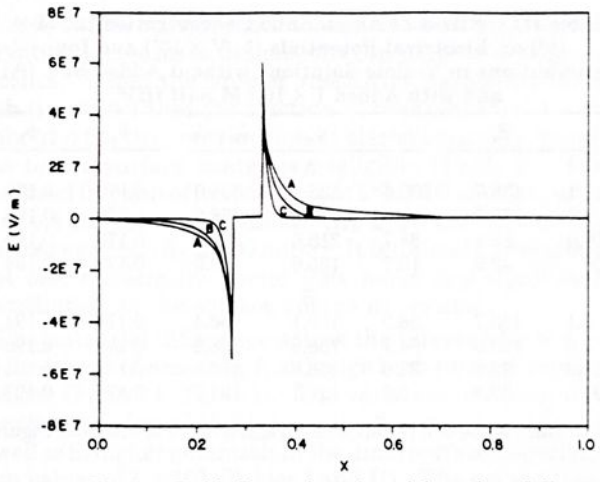


Figure 5. Electric Field (E) as a function of the reduced distance ($x = r/R_c$) from the vesicle center: A, 0.5×10^{-3}; B, 10×10^{-3}; C, 100×10^{-3} M salt, respectively. Amphiphile concentration, R_a, R_b, and δ are as in Figure 3.

arbitrary degree of charge neutralization due to specific (nonelectrostatic) binding of a fixed proportion of ions may be introduced as an initial value for ionic fractional coverage (Γ). This approach has been used, with the added assumption that the interior of the vesicle was neutral.[5b] The value of Γ may be taken to be equal to the fraction of "bound" ions (β) calculated from the measured extent of ion dissociation (α) in vesicles or the related micellar systems.[3b,25,26] Although some of the results obtained (not shown) using this assumption are similar to those presented here, this approximation suffers from several problems. Although β and Γ are certainly related, the experimental determination of α is method dependent.[1a,9,22] The definition of "free" and "bound" ions relies on the choice of a certain distance from the surface from which ions may be said to be either free or bound. Moreover there are no experimentally determined values for α in the internal compartment of vesicles. Thus, the use of an experimentally determined parameter, i.e. ion dissociation from the external surface (α_b), requires the introduction of an arbitrary value for the extent of ion dissociation from the internal surface (α_a).

The Volmer isotherm approach employed here uses a single variable parameter (δ) for the description of the specific ion–surface association and relies on a clear definition of what is considered to be a bound ion. The assumption that δ is equal in the inner and outer surfaces is reasonable for the present model. We should point out, however, that as the size of the vesicle varies, the value of δ should be different, especially for smaller vesicles. We have shown that ion dissociation from the outer bilayer of DODAC decreases with the increase in vesicle diameter.[3b] The size dependence of the ion dissociation is related to the difference in head group packing as a function of changing radius of curvature.[1b] As the vesicle diameter decreases, the radius of curvature of the outer and inner monolayers increasingly differ; therefore, δ_a may differ from δ_b. We also note that in biological systems the lipid composition in the inner and outer leaflets of the bilayer are generally different.[22c] Attention should be given, therefore, to the fact that ion affinities in the interior and exterior of (lipid) unsymmetrical vesicles may vary appreciably.

Other applications of this model, especially in regard to the electrostatic part of the energy of vesicles, as well as other models for the description of vesicular properties are under investigation. We are currently using this model to design experiments to estimate predicted parameters.

Conclusions

We have described a new form of solving Poisson–Boltzmann equations numerically for a system containing vesicles in aqueous electrolytic solutions, with specific ion adsorption described by a Volmer isotherm. The sample computations shown here are compatible with existing experimental data for synthetic amphiphile vesicles, especially with added salt. The program calculates explicitly the ion concentration in the interior and exterior compartments of the vesicle, as well as the corresponding degree of counterion dissociation, and can be used to design experimental conditions in order to measure ion distributions in aqueous ionic solutions containing vesicles.

Glossary

α	experimentally determined fraction of ion dissociation
β	experimentally determined fraction of ion coverage ($\beta = 1 - \alpha$)
δ	specificity parameter in the Volmer isotherm
e	elementary charge ($e = 1.602189 \times 10^{-19}$ C)
ϵ	permittivity of the medium
ϵ_0	permittivity of vacuum ($\epsilon_0 = 8.854188 \times 10^{-12}$ C^2/(N m^2))
Π	dielectric constant
Φ	fraction of ion dissociation
Γ	fraction of ion coverage ($\Gamma = 1 - \Phi$)
ψ	electrostatic potential
ρ	charge density
n_i^0	concentration of ion i in the bulk solution
k	Boltzmann constant ($k = 1.380662 \times 10^{-23}$J/deg)
T	absolute temperature
E	electric field
Q	electric charge
N	number of monomers
ω	length of a water layer adjacent to the surface
σ	charge density
L	Avogadro's number
C	total amphiphile concentration
s	area/monomer
R_a, R_b	internal and external radius of a vesicle, respectively
R_c	radius of the cell
q_i	charge of ion i
ϕ	reduced potential
ζ	zeta potential
z_i	valence of ion i

Acknowledgment. This work was supported by grants from the following Brazilian agencies: FINEP (PADCT, QU), FAPESP (Projeto Temático), and CNPq (Projecto Integrado). We thank Professor C. A. Bunton and Dr. I. M. Cuccovia for their help with this text, Ms. Soraia Soares for the drawings, and two anonymous reviewers for their analysis of an earlier version of this manuscript.

artigo III

Interactions between the Non-ionic Surfactant $C_{12}E_5$ and Poly(ethylene oxide) Studied Using Dynamic Light Scattering and Fluorescence Quenching

Eloi Feitosa,† Wyn Brown,* and Per Hansson

Department of Physical Chemistry, University of Uppsala, Box 532, 751 21 Uppsala, Sweden

Received April 17, 1995; Revised Manuscript Received September 22, 1995®

ABSTRACT: Dynamic light scattering measurements have been made to elucidate changes in the coil conformation of a high molecular weight poly(ethylene oxide) (PEO) fraction when the non-ionic surfactant $C_{12}E_5$ is present in dilute solutions. The measurements were made at 20 °C as functions of (a) the $C_{12}E_5$ concentration at constant PEO concentration, (b) the PEO concentration at constant $C_{12}E_5$ concentration, and (c) the $C_{12}E_5$/PEO concentration ratio. The influence of temperature on the interactions in terms of the relaxation time distributions was also examined up to the cloud point. It was found that when the $C_{12}E_5$/PEO weight ratio was >2 and when the temperature was >14 °C, the correlation functions became bimodal with well-separated components. The fast mode derives from individual surfactant micelles which are present in the solution at high number density. The appearance of the slow mode, which dominates the scattering, is interpreted as resulting from the formation of micellar clusters due to an excluded-volume effect when the high molar mass ($M = 6 \times 10^5$) PEO is added to the surfactant solution. It is shown that the micellar clusters form within the PEO coils and lead to a progressive swelling of the latter for steric reasons. The dimensions of the PEO/$C_{12}E_5$ complex increase with increasing surfactant concentration to a value of $R_H \approx 94$ nm ($R_g \approx 208$ nm) at $C_{C_{12}E_5} = 3.5\%$. Fluorescence quenching measurements show that the average aggregation number of $C_{12}E_5$ increases significantly on addition of the high molar mass PEO. With increasing temperature toward the cloud point the clusters increase in number density and/or become larger. The cloud point is substantially lower than that for $C_{12}E_5$ in water solution and is strongly dependent on the PEO concentration.

Introduction

The interactions between surfactants and polymers are a subject of great interest which also has important technological implications; see, for example, recent reviews.[1−3] Adding a surfactant to a polymer solution with formation of a surfactant/polymer complex can substantially alter the physical properties of the starting polymer, for example, by imparting polyelectrolyte characteristics to a neutral polymer such as poly(ethylene oxide) (PEO) by addition of SDS (see, for example, refs 4 and 5) or by partial neutralization of the intrinsic polyelectrolyte charge by adding CTAB of opposite charge to solutions of sodium polystyrene sulfonate.[6,7] Pronounced changes in coil conformation occur in these cases. It is generally accepted[1−3] that an ionic surfactant interacts with the polymer chain as small micellar aggregates, which are first formed at the critical aggregation concentration (cac); the latter is substantially lower than the critical micelle concentration (cmc) of the pure surfactant in solution. The interactions may involve electrostatic, hydrophobic, and steric interactions, which together serve to considerably modify the overall coil conformation of the original polymer chain. Ricka and co-workers[8] have illustrated this in the case of SDS added to solutions of poly(*N*-isopropylacrylamide) with considerable modification of the coil-to-globule transition. Almost all the prior work has involved addition of a charged surfactant either to a neutral polymer or to a polyelectrolyte. In general, there is a much stronger affinity between anionic surfactants and neutral polymers compared to cationic surfactants and neutral polymers[3].

There is, however, ambiguous and less well-documented experimental evidence for interactions between the neutral counterparts. According to the review of Saito,[2] hydrophilic polymers such as poly(vinyl alcohol) (PVA), PEO, and poly(vinylpyrrolidone) (PVP) show no signs of interaction with the polyethoxylated non-ionic surfactants, C_mE_n. However, the latter type of non-ionic surfactants was shown to interact weakly with poly(carboxylic acids).[2] Subsequently, a number of communications have appeared detailing interactions between uncharged polymers and non-ionic surfactants (see ref 3 for a review). For example, Brackman et al.[9] described microcalorimetric measurements on solutions of poly(propylene oxide) (PPO), $M = 1000$, containing the non-ionic surfactant *n*-octyl thioglucoside micelles (OTG). Although the cmc was identical with and without the polymer, the results gave clear evidence for an endothermic interaction between the components.

Winnik[10] studied the interaction between pyrene-labeled hydroxypropyl-cellulose and OTG using fluorescence measurements. From measurements of the ratio of the pyrene monomer emission to the pyrene excimer emission intensity and its changes with surfactant concentration, the author reported the first unambiguous detection of complex formation between neutral polymers and neutral surfactants. Cohen-Addad and di Meglio[11] also described foam stabilization in the $C_{12}E_5$/PEO system and again the results were interpreted in terms of polymer/surfactant interaction.

Thus, although non-ionic surfactants have the same value for the cmc in the presence of the polymer as in water, in contrast to the considerably lower cac when ionic surfactants interact with uncharged polymers, this need not unequivocally mean the absence of interaction. It probably does mean, however, that the interactions do not involve the same type of specificity in the binding of surfactant micelles to the polymer chain as for example in the PEO/SDS system mentioned above. Nevertheless, the solution properties of the polymeric component may still be strongly changed in the presence

† Permanent address: Departamento de Física, IBILCE/UNESP, São José do Rio Preto, SP, Brazil.

® Abstract published in *Advance ACS Abstracts*, February 1, 1996.

0024-9297/96/2229-2169$12.00/0 © 1996 American Chemical Society

unesp

of the surfactant since, as pointed out by Winnik,[10] polymer/polymer aggregates are disrupted and the conformation of the polymer is modified. Since light scattering measurements provide a non-invasive means of probing conformational changes we chose to apply dynamic light scattering (DLS) and fluorescence quenching measurements to elucidate such changes in the interaction pattern in mixtures of a high molecular weight fraction of PEO and the non-ionic surfactant $C_{12}E_5$ (which itself contains a PEO segment as the hydrophilic entity) in aqueous solution. It will be noted that the binary aqueous solutions of the components are in themselves not straightforward in terms of their solution properties. $C_{12}E_5$ shows a pronounced tendency for micellar growth with both temperature and concentration change while high molar mass PEO almost invariably reveals the presence of clusters in its solutions. As will be discussed below, however, the mixtures in solution display features that are not present in the binary solutions.

Experimental Section

Materials. $C_{12}E_5$ and PEO are from, respectively, Nikko Chemicals, Tokyo, Japan, and Toya Soda, Ltd. Tokyo, Japan, and were used without further purification. PEO has $M_w = 5.94 \times 10^5$ and $M_w/M_n = 1.04$. Solutions were prepared using purified water (Milli-Q plus) and filtered through 0.22-μm Millipore filters directly into the scattering ampules. The results are presented in terms of weight percent (1% w/w is equivalent to 2.46×10^{-2} M for $C_{12}E_5$ and 0.23 M in terms of the PEO monomer). The cmc of $C_{12}E_5$ is 2.64×10^{-3}% (65 μM) at 25 °C.[12]

Clouding temperatures (T_c) of the PEO/$C_{12}E_5$ mixtures were measured by slowly heating the sample in a thermostat and visually observing the sharp demixing at various compositions.

Dynamic Light Scattering. Polarized (VV) DLS measurements, in the self-beating (homodyne) mode, were made using a 633 nm He–Ne laser and detector optics employing an ITT FW130 photomultiplier, the output of which was digitized by an ALV-PM-PD amplifier–discriminator. The signal analyzer was an ALV-5000 digital multiple-tau correlator, Langen GmbH, with 288 exponentially spaced channels. It has a minimum real-time sampling time of 0.2 μs and a maximum of ~100 s. The intensity autocorrelation function, $g^{(2)}(t)$, was measured at different angles. The scattering cells (10 mL sealed cylindrical ampules) were immersed in a large-diameter thermostated bath of index-matching liquid (decalin). The temperature was controlled to within ±0.02 °C.

Data Analysis. The DLS data were analyzed by nonlinear regression procedures. The function fitted was the intensity autocorrelation function described as

$$g^{(2)}(t) - 1 = \beta|g^{(1)}(t)|^2 \quad (1)$$

where β is a nonideality factor accounting for deviation from ideal correlation. $g^{(1)}(t)$ can be written as the Laplace transform of the distribution of relaxation rates, $G(\Gamma)$:

$$g^{(1)}(t) = \int_0^\infty G(\Gamma) \exp(-\Gamma t)\, d\Gamma \quad (2)$$

For relaxation times, τ, this is expressed

$$g^{(1)}(t) = \int_{-\infty}^{\infty} \tau A(\tau) \exp(-t/\tau)\, d \ln \tau \quad (3)$$

where t is the lag time. $\tau A(\tau)$ was obtained by inverse Laplace transformation (ILT) using a constrained regularization calculation algorithm called REPES as incorporated in the analysis package GENDIST.[14] This algorithm directly minimizes the sum of the squared differences between experimental and calculated $g^{(2)}(t)$ functions. It allows the selection of a smoothing parameter "probability to reject" (P). The higher the P, the greater the smoothing.

The choice of P was optimized for each inversion although the initial value of $P = 0.5$ was chosen as standard in the analyses. Diffusion coefficients are calculated from the ILT moments as $D = (\Gamma/q^2)_{q\to 0}$, where q is the magnitude of the scattering vector.

Time-Resolved Fluorescence Quenching (TRFQ). Fluorescence decay data were collected with the single-photon-counting technique. A detailed description of the experimental technique and equipment used is given elsewhere.[6] All measurements were performed in equilibrium with air. Pyrene and dimethylbenzophenone were used as probe and quencher, respectively.

The TRFQ data were fitted to the Infelta–Tachiya equation:[15,16]

$$F(t) = A_1 \exp[-A_2 t + A_3\{\exp(-A_4 t) - 1\}] \quad (4)$$

where $F(t)$ describes the time evolution of the fluorescence intensity. When probe and quencher are stationary in the micelles during the lifetime of the probe, the parameters A_1–A_4 can be interpreted as follows: $A_1 = F(0)$, $A_2 = 1/\tau_0$, $A_3 = \langle n \rangle$, and $A_4 = k_q$. $F(0)$ is the intensity at zero time, τ_0 the natural lifetime of the probe, $\langle n \rangle$ the average number of quenchers in a micelle, and k_q the intramicellar quasi-first-order quenching constant. This interpretation demands a Poisson distribution of the quencher over the micelles. In the fitting procedure, the A_2 parameter was fixed to $1/\tau_0$, as estimated from separate experiments without quencher. The surfactant aggregation number, N, was calculated from $C_{s,m}$ and $C_{q,m}$, the concentration of surfactant and quencher in micelles, respectively, and $\langle n \rangle$ using the relationship

$$N = \langle n \rangle C_{s,m}/C_{q,m} \quad (5)$$

At the surfactant concentratons used in this study, the free concentrations of surfactant and quencher are negligible. Thus, $C_{s,m}$ and $C_{q,m}$ can be replaced by the total concentration of surfactant and quencher, respectively. The free concentration of the probe is also completely negligible.

Results and Discussion

Binary Systems (a) $C_{12}E_5$/Water. Figure 1a shows a typical correlation function and an ILT relaxation time distribution for $C_{12}E_5$ in water at 20 °C at a concentration of 0.5% (w/w). The correlogram is very close to a single exponential, although a small-amplitude faster component is present. The evaluated relaxation rate (Γ) is linearly dependent on q^2 demonstrating a diffusive process.

Figure 1b shows the diffusion coefficients for $C_{12}E_5$ as a function of concentration at 20 °C. The strong initial decrease in the mutual diffusion coefficient D has been described earlier[13,17,18] and has also been observed in pulsed-field gradient (PFG) NMR experiments.[17] Similar trends have been also noted for other non-ionic surfactants ($C_{12}E_7$ and $C_{12}E_8$) with the depth of the minimum diminishing as the ethylene oxide moiety increased in length. Since the mutual diffusion coefficient is related to the thermodynamic interaction in the system, it was proposed in refs 13 and 18 that there are strong changes in the intermicellar interactions at concentrations in the vicinity of the minimum D value and that pronounced micellar shape changes occur with concentration change. The initial decrease in D suggests strong micellar growth over a narrow range of concentration starting at $c < 1.5$%. At concentrations above the minimum in D where the semidilute concentration range is entered, the long micelles give rise to a large excluded-volume effect and the slope is strongly positive.

An approximate value for R_H can be obtained by extrapolating the curved portion in Figure 1b to infinite dilution. This gives 11.9 nm for the main micellar

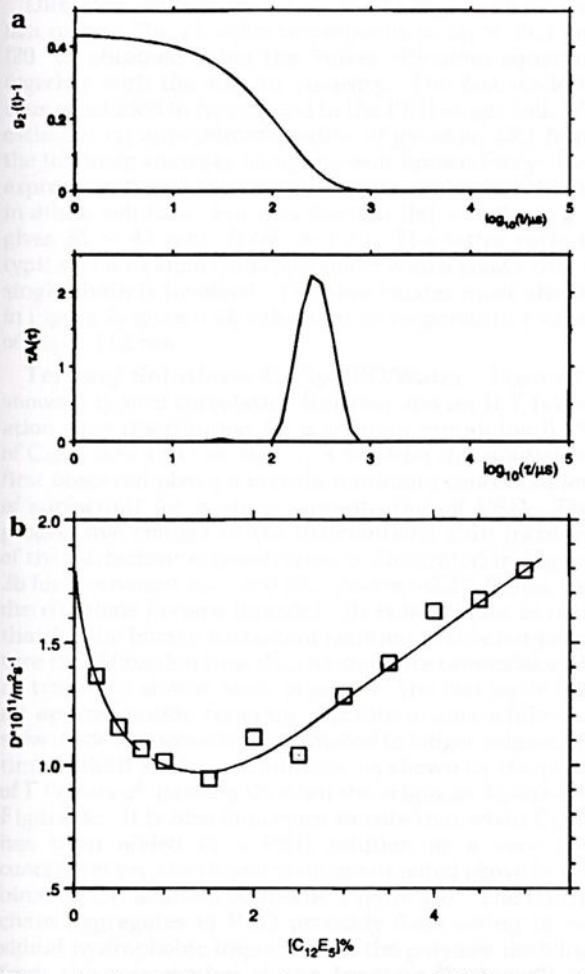


Figure 1. (a, top) Autocorrelation function ($g^2(t)$) (top) and ILT relaxation time distribution (bottom) for a 0.5% solution of $C_{12}E_5$ at 20 °C; measurements at $\theta = 90°$. (b, bottom) Diffusion coefficients for $C_{12}E_5$ as a function of C in the for $C_{12}E_5$ solutions; 20 °C.

component (using $D_0 = 1.8 \times 10^{-11}$ m^2 s^{-1} at 20 °C). PFG NMR data gave $R_H \approx 7$ nm using the data summarized in Figure 3 of ref 13. The lower value is probably the result of considerable polydispersity since D from PFG NMR approximates a number-averaged quantity and DLS the higher z-averaged quantity. The DLS value agrees, however, with that previously given (12 nm) in ref 13. (Extrapolation of the present $C_{12}E_5$ data at 20 °C to infinite dilution from the linear part of the curve at the higher concentrations, on the other hand, would give $R_H \approx 40$ nm, a value that is unrealistically large for the micellar radius.) Although the extrapolated value is uncertain, $R_H = 12$ nm will be used for comparisons with the dimensions of the free micelles in the polymer/surfactant mixed systems. It was concluded in ref 13 that below 10 °C the $C_{12}E_5$ micelles are large and rodlike. At ~15 °C, the micelles are substantially smaller than at low temperatures but then grow with increasing temperature. Thus the minimum in Figure 1b is displaced to lower concentration with increasing temperature. Kato et al.[18] also showed that the correlation length increases with increasing temperature, demonstrating micellar growth.

(b) PEO/Water. Figure 2a shows a typical correlation function for PEO in water at $c = 0.5\%$ and the resulting ILT relaxation time distribution. This is

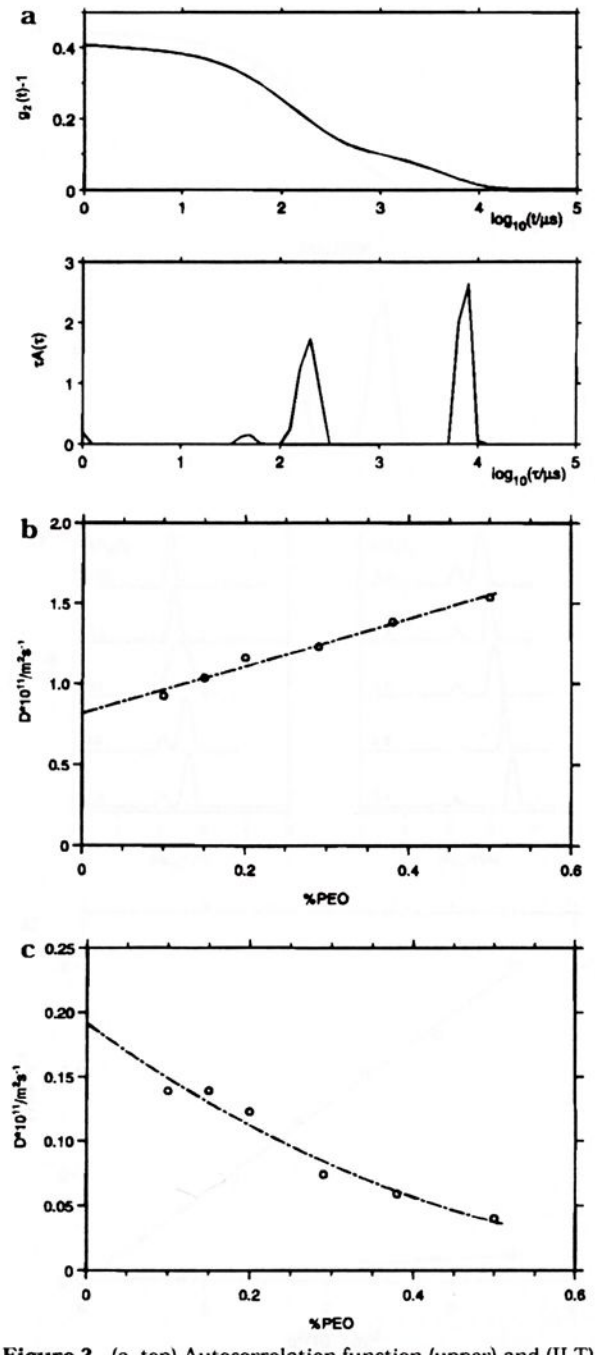


Figure 2. (a, top) Autocorrelation function (upper) and (ILT) distribution (lower) for PEO ($M_w = 5.9 \times 10^5$) at $c = 0.5\%$ and 20 °C; $\theta = 90°$. (b, middle) Diffusion coefficients for the fast PEO mode (single coil) as a function of concentration at 20 °C. (c, bottom) Concentration dependence of the slow PEO mode at 20 °C.

bimodal. Both modes are diffusive, as was established by the linear dependence of the relaxation rate (Γ) on q^2. The slow "cluster" mode has been considered characteristic of dilute solutions of PEO in both water and non-aqueous solvents.[19] However, recent papers[20,21] have reported that it is possible to prepare aggregate-free PEO solutions in water by the use of very "tight" filters, e.g., 0.02- or 0.05-μm pore size, whereas the usually employed 0.22-μm filters do not remove this component.

Diffusion coefficients are shown in Figure 2b for the fast mode. The D_0 value corresponds to $R_H = 26.3$ nm (20 °C) obtained using the Stokes–Einstein equation together with the solvent viscosity. The fast mode is thus concluded to correspond to the PEO single coil. We estimate an approximate radius of gyration (R_g) from the intrinsic viscosity using the well-known Flory–Fox expression for the intrinsic viscosity of flexible chains in dilute solution. For this fraction ($[\eta] = 418$ mL g^{-1} gives $R_g = 43$ nm), $R_g/R_H = 1.74$. The latter ratio is typical of a flexible Gaussian coil,[22] which shows that a single chain is involved. The slow cluster mode shown in Figure 2c gives a D_0 value that corresponds to a value of $R_H = 112$ nm.

Ternary Solutions: $C_{12}E_5$/PEO/Water. Figure 3a shows a typical correlation function and an ILT relaxation time distribution for a solution containing 0.5% of $C_{12}E_5$ and PEO at 20 °C. A bimodal distribution is first observed above a certain minimum concentration of surfactant for a given concentration of PEO. The progressive change in the distributions with increase of the surfactant concentration is illustrated in Figure 3b for a constant $c_{PEO} = 0.2\%$. Above ~0.2% $C_{12}E_5$, the distributions become bimodal. (It is important to note that for the binary surfactant solution at this temperature the relaxation time distributions are unimodal with no trace of a slower mode present.) The fast mode has an approximately constant relaxation time while the slow mode is successively displaced to longer relaxation times. Both modes are diffusive as shown by the plots of Γ versus q^2, passing through the origin as dipicted in Figure 3c. It is also important to note that when $C_{12}E_5$ has been added to a PEO solution at a very low concentration, the cluster component noted above in the binary PEO solution is absent (Figure 2a). The multichain aggregates of PEO probably form owing to residual hydrophobic impurities in the polymer deriving from the preparation of the fractions.[21] As will be pointed out below in the discussion of the ternary systems, addition of the surfactant removes the "cluster" peak in PEO solutions, probably because these hydrophobic impurities are incorporated into the micellar core. Inhibition of polymer cluster formation by surfactant was previously noted[7] for poly(styrene sulfonate) in the presence of the ionic surfactant CTAB. In this latter case, however, the surfactant serves to screen the charge interactions that lead to the aggregate formation, which is a well-known feature in polyelectrolytic solutions.

Figure 4 shows the diffusion coefficients obtained from the distributions in Figure 3b as a function of surfactant concentration at three constant levels of PEO concentration. The relaxation time of the fast mode is approximately constant with change in the PEO concentration, and the concentration dependence is small. From the infinite dilution value, it is estimated that the free micelles thus have an approximate size of R_H = 12 nm which agrees well with the value for the surfactant in binary solution. These data scatter strongly, probably owing to poorer resolution due to partial overlap of the ILT peaks. The relaxation time for the slower mode increases with increasing $C_{12}E_5$. The intercepts at $c_{C_{12}E_5} \to 0$ yield the apparent hydrodynamic radii of the slow mode, i.e., the radius at a given constant value of PEO concentration. The approximate values estimated by extrapolating to zero surfactant concentrations are as follows: 0.1% PEO, 25.8 nm; 0.15% PEO, 30.6 nm, and 0.2% PEO, 34.8 nm.

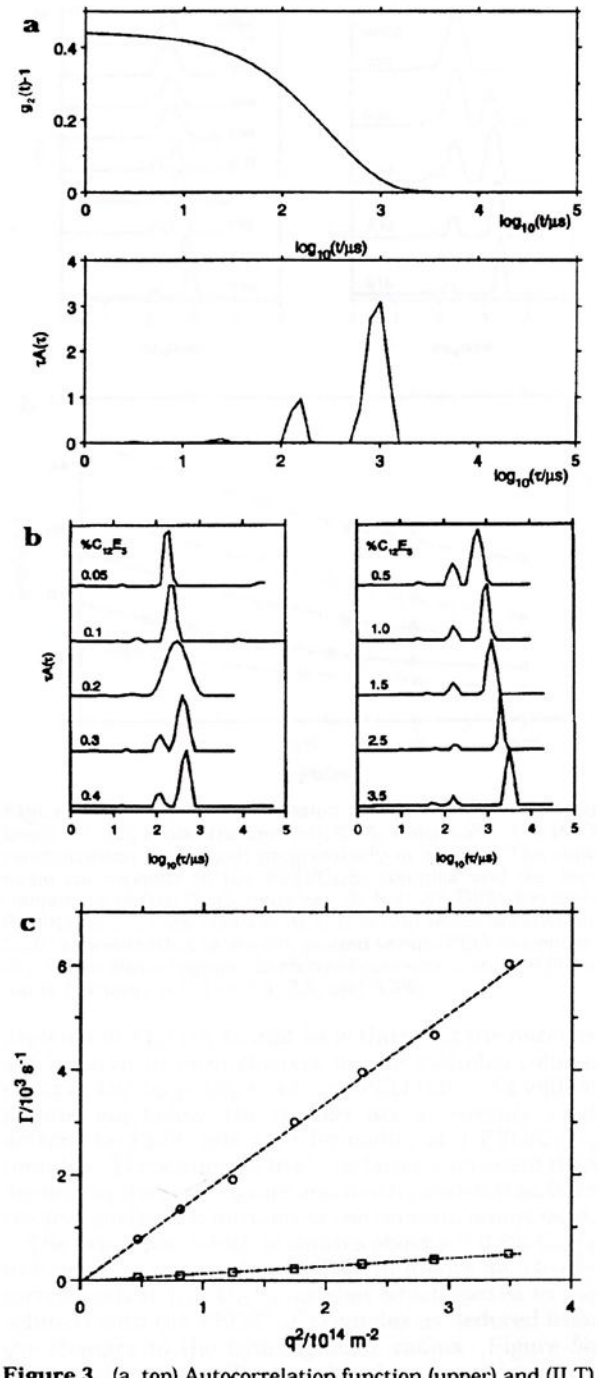


Figure 3. (a, top) Autocorrelation function (upper) and (ILT) distribution (lower) for a $C_{12}E_5$/PEO mixture in solution at equal concentrations of 0.5%; measurements at 20 °C and θ = 90°. (b, middle) ILT relaxation time distributions for constant PEO concentration (0.2%) with successive increase of $C_{12}E_5$ concentration at 20 °C. (c, bottom) Dependence of the relaxation rate (Γ) versus the square of the scattering vector (q^2) for the ternary system (2.5% $C_{12}E_5$, 0.2% PEO; 20 °C).

Figure 5 shows analogous relaxation time distributions for solutions in which the surfactant concentration is held constant and the PEO concentration is increased. In Figure 5a, left, with $c_{C_{12}E_5} = 0.5\%$, the ILT distributions become bimodal above $c_{PEO} \approx 0.08\%$. The slow component again becomes progressively slower in relaxation time, whereas the fast component has an approximately constant value. At $c_{C_{12}E_5} = 3.5\%$ (Figure

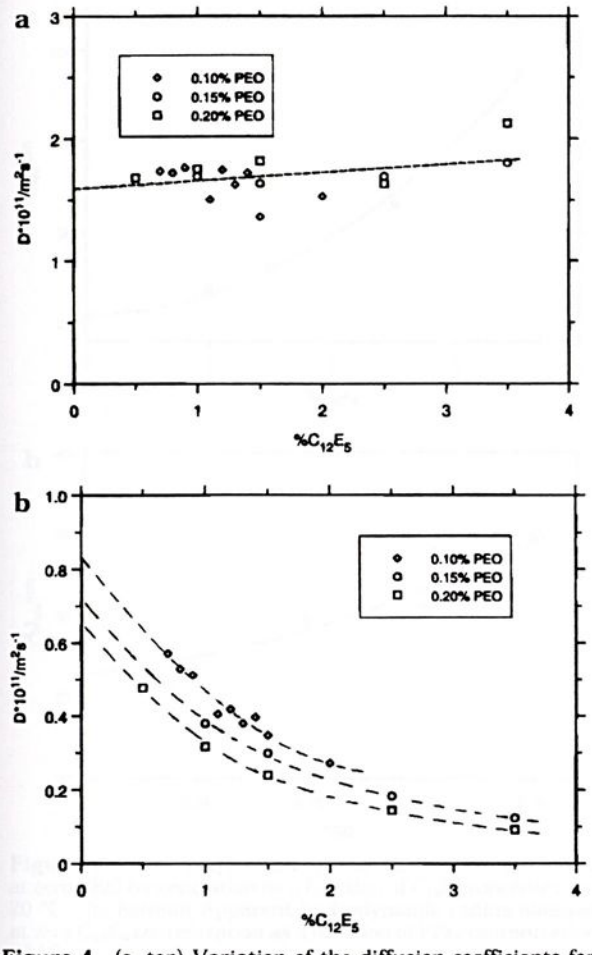


Figure 4. (a, top) Variation of the diffusion coefficients for the fast mode with increasing surfactant concentration at constant PEO concentrations of 0.1, 0.15, and 0.2% and 20 °C. (b, bottom) Diffusion coefficients for the complex mode as a function of surfactant concentration at constant PEO concentrations at 20 °C.

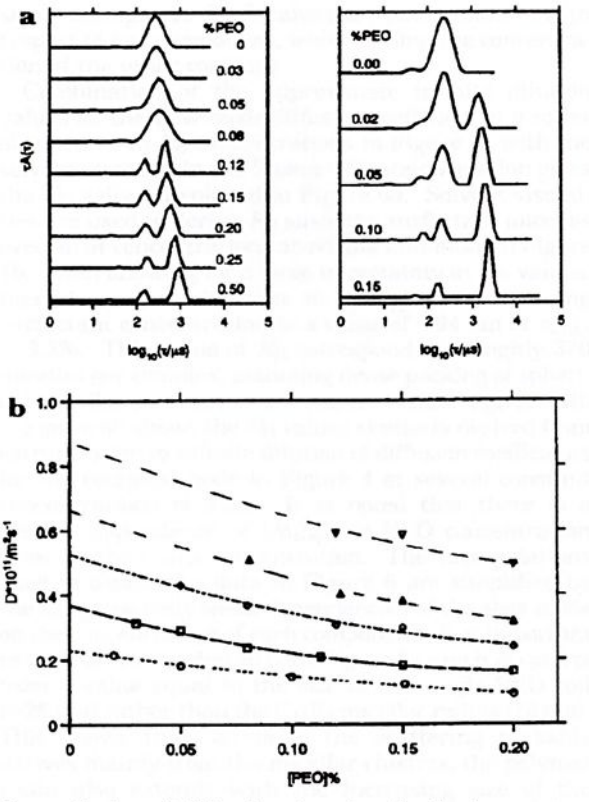


Figure 5. (a, top) ILT relaxation time distributions at two levels of $C_{12}E_5$ concentration: left, 0.5%; right 3.5%. The PEO concentration is changed progressively as shown. The slow mode corresponds to the PEO/$C_{12}E_5$ complex and the fast component to free $C_{12}E_5$ micelles. (b, bottom) Diffusion coefficients for the slow component at different levels of constant $C_{12}E_5$ concentration as shown, plotted versus PEO concentration in the dilute regime. Surfactant concentrations are (from top to bottom): 0.5, 1.0, 1.5, 2.5, and 3.5%.

5a, right), splitting into two modes has already occurred below $c_{PEO} = 0.02\%$. The results reported in the earlier paper,[13] and discussed above with regard to the binary $C_{12}E_5$/water solutions, show that this surfactant has a strong tendency to micellar growth as functions of both concentration and temperature. Although, as pointed out below in the discussion of the temperature dependence, $C_{12}E_5$ itself in aqueous solution shows no tendency for micellar cluster formation all the way up to the cloud point, it was shown in ref 13 that other non-ionic micellar systems display a low-intensity component with long relaxation time. The relative amplitude of this cluster peak increases as the cloud point is approached, indicating a sensitive equilibrium between the individual micelles and their clusters. The analogous cluster peak is not observed with $C_{12}E_5$ owing to the proximity of the overlap point (the overlap concentration is low (~1.5%)). Thus it is to be expected that the addition of high molecular weight PEO with an associated large excluded volume to the system will displace such an equilibrium and induce cluster formation of the micellar component. Coupled with the well-known weak or negligible energetic interactions between non-ionic surfactants and neutral polymers, this interpretation means that the effect is primarily entropic. A plausible interpretation of the data for the slow mode depicted in Figures 4b and 5a is thus that the micelles are induced to form clusters by the excluded-volume effect of the large ($R_g \approx 43$ nm) PEO coils. As will be pointed out below, the clusters are apparently sited within the PEO coils with formation of a PEO/$C_{12}E_5$ complex. The scattering from the latter component then dominates the correlogram and much exceeds that from the free surfactant micelles at the concentrations used.

The fast mode, which separates above $c > 0.2\%$ $C_{12}E_5$ in Figure 3b and $c > 0.08\%$ PEO in Figure 5a, clearly corresponds to free $C_{12}E_5$ micelles which coexist in the solution with the PEO/$C_{12}E_5$ complex as deduced from the changes in the hydrodynamic radius. Figure 5b shows diffusion coefficients for the slow mode as a function of PEO concentration, where the data have been obtained by holding the surfactant concentration constant at different levels of $C_{12}E_5$ between 0.5 and 3.5%. The PEO concentration range was selected so that $c < c^*$, where the overlap concentration for this PEO fraction was estimated using $c^* = 1/[\eta] = 0.24\%$.[27]

Conventionally, the concentration dependence of the diffusion coefficient in binary polymeric dilute solutions is given by

$$D = D_0(1 + k_D c + ...) \quad (6)$$

where k_D is related to the second virial coefficient, i.e., to the pair interaction potential, by $k_D = 2A_2M - k_f - 2\nu_2$; k_f describes the concentration dependence of the

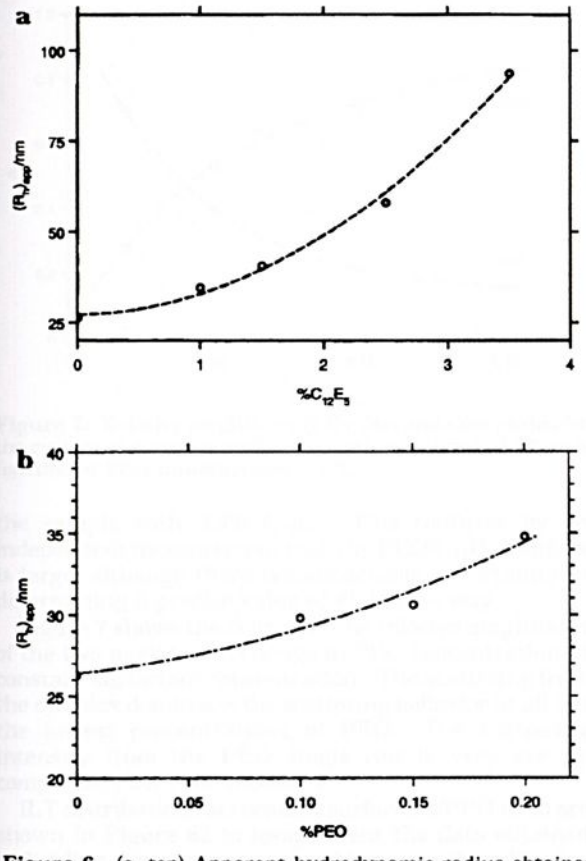


Figure 6. (a, top) Apparent hydrodynamic radius obtained at zero PEO concentration as a function of $C_{12}E_5$ concentration; 20 °C. (b, bottom) Apparent hydrodynamic radius obtained at zero $C_{12}E_5$ concentration as a function of PEO concentration; 20 °C.

friction factor and ν_2 is the partial specific volume of the particle. In the presence of PEO, however, the concentration dependences become nonlinear and negative and, in analogy with binary systems, imply attractive interactions between the micellar clusters induced in the system by addition of PEO. This behavior may be contrasted with the positive value of k_D for the binary PEO solutions shown in Figure 2b. In binary systems, a negative concentration dependence would mean that association or aggregation occurs. Micellar systems are more complex in that extensive changes in size (molecular weight) and shape can take place, depending on the system and the location in the phase diagram. Since, as we shall show below, the PEO/$C_{12}E_5$ complex grows with increasing concentration of both the components (Figure 6), as well as the temperature, we conclude even in this case that (i) micellar cluster formation is favored, (ii) the cluster size probably increases with increasing concentration, and (iii) the overall PEO/$C_{12}E_5$ complex as a result also expands with increasing concentration. The negative concentration dependence is also consistent with the strongly lowered cloud point observed for $C_{12}E_5$ when PEO is present in the solutions in comparison with the pure surfactant at the same concentration—see below. Both c and k_D in eq 6 should refer to the PEO/$C_{12}E_5$ complex, but the complex concentration is inaccessible in the absence of quantitative information on the association. For this reason we do not evaluate k_D. The structure of the complex is shown to be dependent on the concentration of both components. Thus, it is necessary to successively extrapolate the D values to infinite dilution with respect to one component, while holding the concentration of the other constant.

Combination of the approximate infinite dilution values for the slow-mode diffusion coefficient at a series of constant $C_{12}E_5$ concentrations in Figure 5b with the solvent viscosity in the Stokes–Einstein equation gives the R_H values displayed in Figure 6a. Solvent viscosities are used to derive R_H since the surfactant micelles overlap at concentrations above the minimum in Figure 1b. Even allowing for a large uncertainty in the values, there is a strong increase in $(R_H)_{app}$ with increasing surfactant concentration to a value of ~94 nm at $c_{C_{12}E_5}$ = 3.5%. This value of R_H corresponds to roughly 370 micelles per complex, assuming dense packing of spherical micelles in a cluster of micelles within a given coil.

Figure 6b shows the R_H values similarly derived from extrapolation to infinite dilution of diffusion coefficients for the complex mode in Figure 4 at several constant concentrations of PEO. It is noted that there is a weaker dependence of $(R_H)_{app}$ on PEO concentration than on the $C_{12}E_5$ concentration. The extrapolations used to obtain the data in Figure 6 are simplified by the comparatively weak dependencies of the slow mode on the concentration of each component. It is important to note, however, that in both Figure 6a and b R_H starts from a value equal to the size of the single PEO coil (~26 nm) rather than the $C_{12}E_5$ micellar radius (12 nm). This shows that, although the scattering probably derives mainly from the micellar clusters, the polymer chain also extends with the increasing size of the clusters, i.e., there is a progressive uncoiling of the PEO chain which apparently occurs to accomodate cluster growth, finally yielding a PEO/$C_{12}E_5$ complex. Presumably, nonspecific interactions between polymer and micelles lead to a preferred environment for the surfactant. This conclusion is substantiated by the increase in the average aggregation number of the $C_{12}E_5$ micelles in the presence of PEO—see below. Similarly, PPO has been found to uncoil in the presence of OTG by Brackman et al.[9] Thus, the surfactant micelles apparently nucleate, forming clusters of micelles within the polymer coil, with the surfactant micellar cluster surrounded by a meandering PEO chain, rather than a model in which relatively compact PEO coils are interspersed by segregated surfactant clusters. The PEO chain used here has a contour length of the magnitude 2400 nm if a meander conformation is assumed with the chain twisted into an expanded helical form and using a dimension for the ethylene oxide unit of ~1.8 Å.[23]

This "coil/cluster" model for the complex is considered reasonable since, as is discussed below, fluorescence quenching measurements show that the average aggregation number increases significantly on adding PEO

Total intensity measurements on the solutions used to assemble the data in Figure 5b showed that, for the slow mode depicted, there is excess low-angle scattered intensity and the concentration dependence of the reduced scattered intensity is negative and nonlinear. Estimates of R_g from the initial slope of the reciprocal intensity showed that $qR_g > 1$ for all angles used; i.e., the data lie outside of the Guinier range. The Debye function

$$P(X) = (2/X^4)[\exp(-X^2) + X^2 - 1] \qquad (7)$$

with $X = qR_g$, was thus used to evaluate R_g at each measurement angle, and the values were extrapolated to zero angle. The value of 208 nm was obtained for

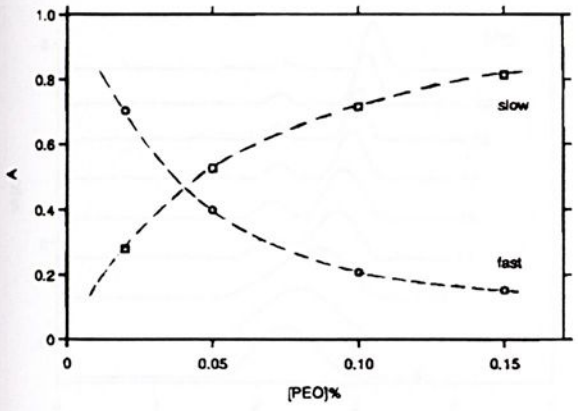


Figure 7. Relative amplitudes of the fast and slow modes for the system at constant surfactant concentration of 3.5% as a function of PEO concentration; 20 °C.

the sample with 3.5% $C_{12}E_5$. This confirms by an independent measurement that the PEO/$C_{12}E_5$ complex is large, although there is considerable uncertainty in determining a precise value of R_g in this way.

Figure 7 shows the change in the relative amplitudes of the two modes with change in PEO concentration at constant surfactant concentration. The scattering from the complex dominates the scattering behavior at all but the lowest concentrations of PEO. The scattering intensity from the PEO single coil is very low by comparison with the mixtures.

ILT distributions at constant surfactant/PEO ratio are shown in Figure 8a to complement the data obtained by holding the components fixed in succession. Similar trends are discerned as described above: thus, the ILT distributions are bimodal above a concentration of 0.2% and the relative amplitude of the slow-mode peak increases with increasing concentration. Figure 8b shows the corresponding fast mode diffusion coefficients for surfactant/polymer ratios of 2 and 4. The fast-mode relaxation rate at infinite dilution again corresponds to the hydrodynamic radius of the free micelles, i.e., $R_H \approx$ 12 nm.

Figure 8c illustrates the strong, non-linear, negative concentration dependence of the cluster mode at the same ratios as in Figure 8b.

Figure 9 presents ILT relaxation time distributions as a function of temperature at equal PEO and $C_{12}E_5$ concentrations of 0.5% (w/w) (i.e., $R = 1$). The broad single peak at 8−12 °C becomes asymmetric above ~12 °C and at 14 °C has split into two modes. The normalized relaxation time for the fast mode (which again corresponds to $R_H \approx 12$ nm for the free micelles) changes only weakly with temperature, while the relaxation time for the complex increases more strongly. It is relevant to note that this behavior is strikingly different from that of the binary $C_{12}E_5$/water system. For the latter, with increasing temperature, the relaxation time distribution remains closely single modal all the way up to the cloud point in the vicinity of 32 °C. There is no indication of the formation of micellar clusters. This contrasts with the complex formation promoted by the presence of high molecular weight PEO at the same temperature in the ternary systems. However, the relaxation time of the single micellar peak increases strongly with temperature. Since the concentration dependence is small, this shows that the $C_{12}E_5$ micelles grow and that this growth continues up to the cloud point due to enhanced attractive interactions. This

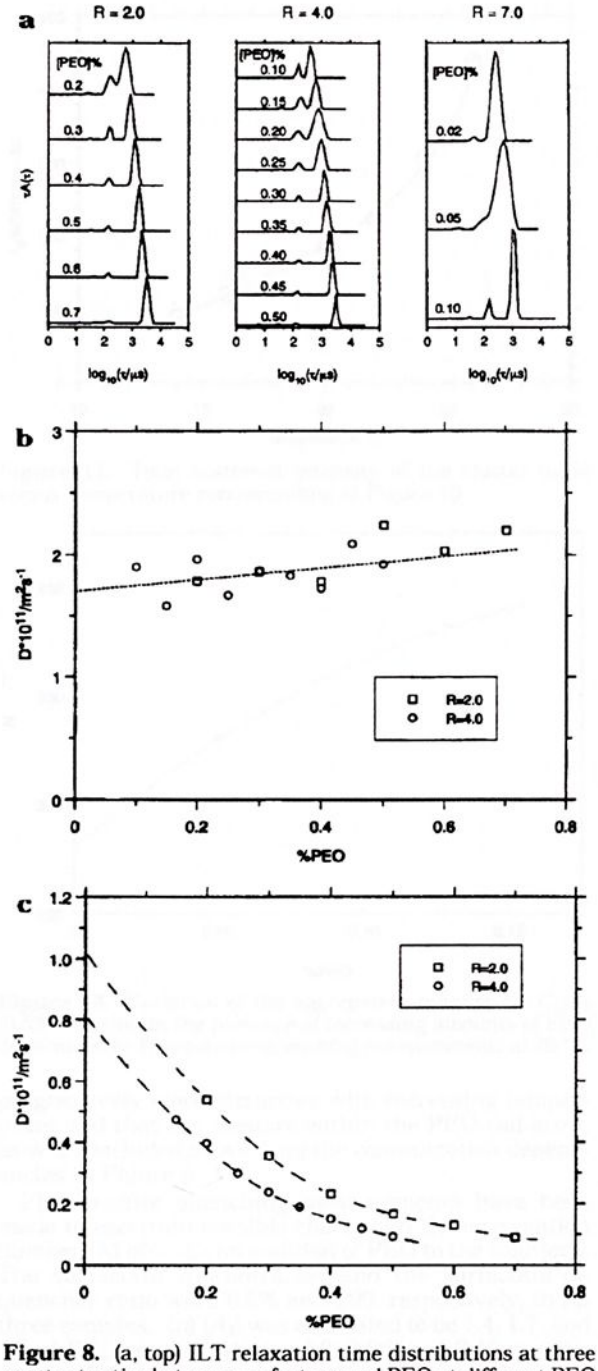


Figure 8. (a, top) ILT relaxation time distributions at three constant ratios between surfactant and PEO at different PEO concentrations at 20 °C. (b, middle) Dependence of fast diffusion coefficient at constant surfactant/polymer ratios of 2 and 4 on PEO concentration at 20 °C. (c, bottom) Dependence of the complex diffusion coefficient at constant surfactant/PEO ratios $R = 2$ and 4 on PEO concentration at 20 °C.

behavior is illustrated in Figure 10, which shows that the diffusion coefficients normalized by (η_0/T) have a strong dependence on temperature for both the binary $C_{12}E_5$/water system and the systems in the additional presence of PEO (a constant ratio surfactant/polymer $R = 1$ at two total concentrations (0.5 and 1%)). The trend follows those data earlier presented on $C_{12}E_5$ in ref 13, where it was noted that above 15 °C in the binary $C_{12}E_5$/water system the second virial coefficient from static light scattering decreases monotonically with

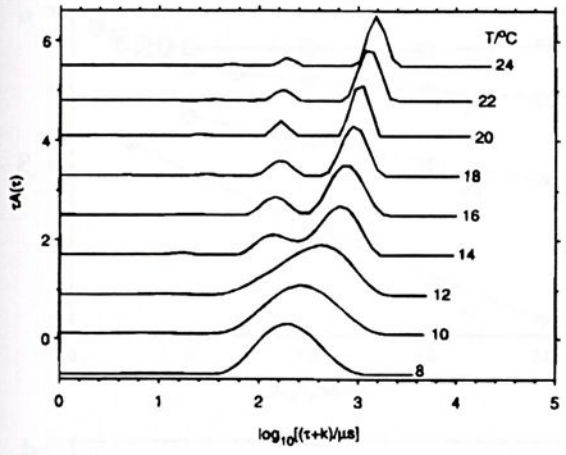


Figure 9. ILT distributions for $C_{12}E_5$/PEO mixtures, ratio $R = 1$ at a concentration of 0.5% at different temperatures shown. The distributions are shifted on the log τ axis by (T/η); $\theta = 90°$.

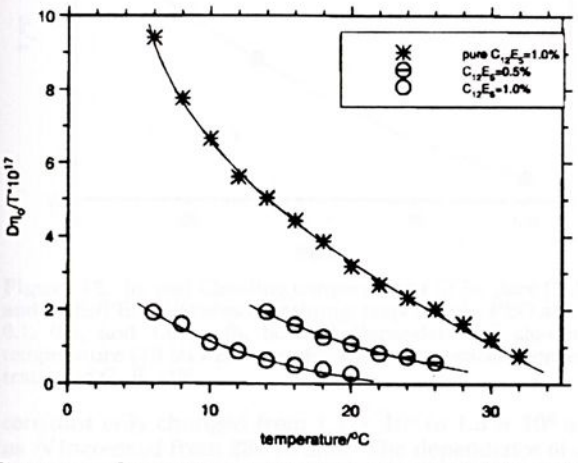


Figure 10. Comparison of reduced slow-mode diffusion coefficients ($D\eta_o/T$) versus temperature for pure $C_{12}E_5$, $c = 1\%$, and two $C_{12}E_5$/PEO mixtures wth $R = 1$ at $c = 0.5$ and 1%.

increasing temperature while the weight-average molar mass simultaneously increases as the temperature moves toward the cloud point at ~32 °C. (A similar trend was shown by the other surfactants investigated: $C_{12}E_8$ and $C_{12}E_7$).

Taken together, the present data establish that the intermicellar attractive interactions are augmented by the presence of PEO and increase strongly with both temperature and concentration. We note here that Piculell and co-workers[24] have recently determined the characteristics of the phase diagram for the $C_{12}E_5$/PEO system. The two-phase area increases with increasing temperature. They concluded that the phase behavior is segregative. Wormuth[26] examined the phase behavior of similar amphiphiles (i.e., ethoxylated alcohols) in the presence of PEO. They showed that the miscibility decreases strongly upon increasing the chain lengths of the segments in the amphiphile and also the molar mass of the PEO and found that there are similarities to the phase behavior of two polymers in a solvent.

Figure 11 shows that the scattering intensity of the PEO/$C_{12}E_5$ complex mode—calculated by apportioning the total intensity using the relative amplitudes of the two modes seen in Figure 9—also increases strongly with increasing temperature. This shows that the mutual interactions between micellar clusters become

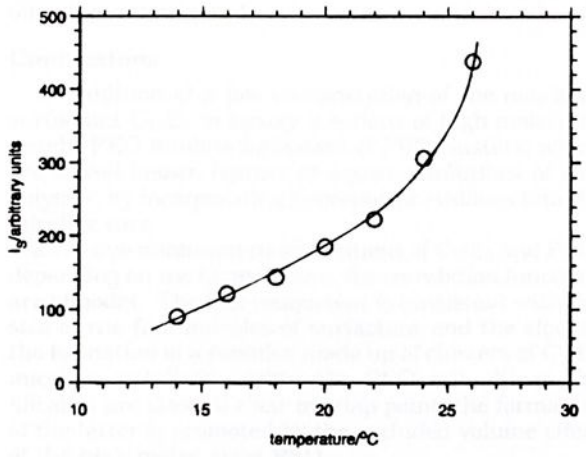


Figure 11. Total scattered intensity of the cluster mode versus temperature corresponding to Figure 10.

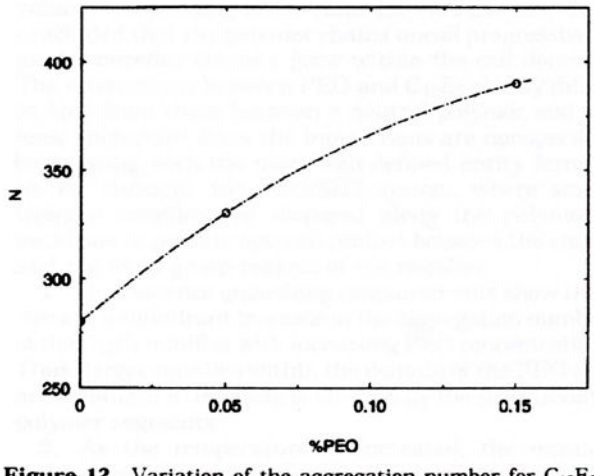


Figure 12. Variation of the aggregation number for $C_{12}E_5$ (0.5%) micelles in the presence of increasing amounts of PEO determined by fluorescence quenching measurements at 20 °C.

progressively more attractive with increasing temperature and that the clusters within the PEO coil grow, as was concluded above from the concentration dependencies in Figure 6.

Fluorescence quenching measurements have been made to ascertain possible changes in the aggregation number (N) of $C_{12}E_5$ on addition of PEO to the solutions. The surfactant concentration and the surfactant-to-quencher ratio were 0.5% and 200, respectively, in all three samples. $\langle n \rangle$ (A_3) was estimated to be 1.4, 1.7, and 1.9 at PEO concentrations of 0, 0.05, and 0.15, respectively. The quality of the fit was acceptable (reduced χ^2, 1.1−1.2). The results in Figure 12 show that there is a significant increase in N with increasing PEO concentration. The aggregation numbers are quite large. This is expected for this surfactant at 20 °C. The TRFQ data were analyzed with the assumption of no migration of the quencher (A_2 fixed). The time window for the experiment was not enough for the quenched decays to completely develop into the stationary state characteristic of quenching in small micelles. We cannot, therefore, rule out the possibility of migration of the quencher. An analysis of the data with a model that allows for migration (A_2 as a free parameter) gave somewhat smaller aggregation numbers, but the trend was the same as in Figure 12. The fluorescence lifetime for pyrene (solutions in equilibrium with air) was 185 ns at all PEO concentrations used. The quenching rate

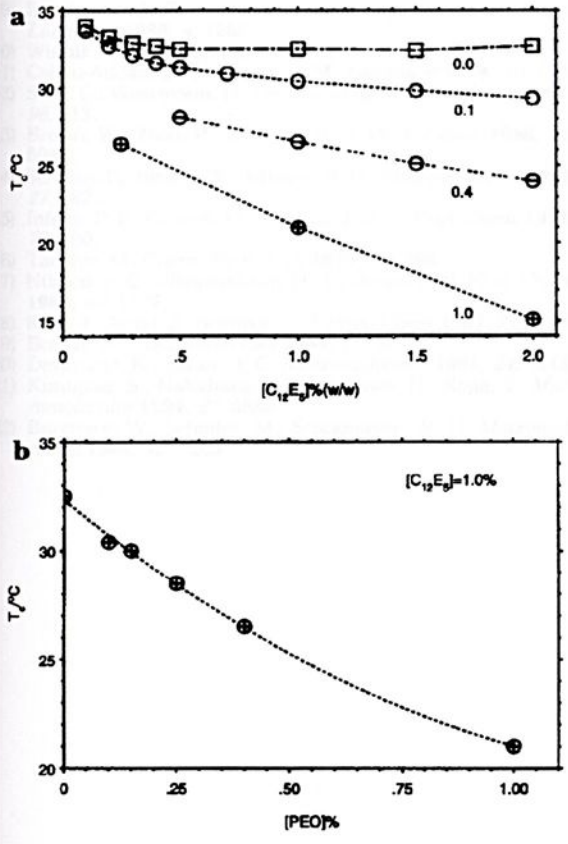


Figure 13. (a, top) Clouding temperature (T_c) for pure $C_{12}E_5$ and $C_{12}E_5$/PEO mixtures containing, respectively, PEO at c = 0.1, 0.4, and 1.0%. (b, bottom) Dependence of clouding temperature (T_c) on PEO concentration at a constant concentration of $C_{12}E_5$, 1%.

constant only changed from 1.4×10^6 to 1.3×10^6 s^{-1} as N increased from 280 to 380. The dependence of k_q (A_4) on N is larger in pure surfactant solutions.[30] However, when the polymer is present, k_q is generally smaller for a given N than in the absence of polymer.[31-33]

Figure 13a shows how the clouding temperature (T_c) for a solution of pure $C_{12}E_5$ in water varies with surfactant concentration and compares these data with the corresponding cloud points for similar solutions containing 0.1, 0.4, and 1% PEO. We find a value of T_c = 32.5 °C for pure $C_{12}E_5$ at a concentration of 1%, which is is good agreement with literature values.[11] The addition of PEO to a solution of $C_{12}E_5$ thus decreases T_c as shown in Figure 13b at an arbitrarily chosen concentration of 1% $C_{12}E_5$. The decrease is a strong function of the concentration of PEO. $C_{12}E_5$/PEO mixtures exhibit a pronounced decrease in T_c as the PEO concentration is increased at constant surfactant concentration. Above a PEO concentration of ~1.5%, the solution clouds at room temperature. For equal concentrations of PEO and $C_{12}E_5$ of 1%, T_c = 21 °C; T_c then increases on dilution of the solution. Similar behavior was noted for $C_{12}E_8$ together with PEO[28] and also a hydrophobized PEO sample.[25] These observations support the conclusion of micellar cluster formation within the PEO coil domains. If there had been the type of surfactant/polymer interaction which occurs in PEO/SDS solutions in which small micelles are bound to the polymer chain, one would anticipate that the cloud point would have increased. The interactions between neutral polymers and non-ionic surfactants is a subject of on-going investigation.

Conclusions

1. Addition of a low concentration of the non-ionic surfactant $C_{12}E_5$ to binary solutions of high molecular weight PEO inhibits formation of PEO clusters, which are a well-known feature of aqueous solutions of this polymer, by incorporating hydrophobic residues into the micellar core.

2. Above minimum concentrations of $C_{12}E_5$ and PEO, depending on the temperature, the correlation functions are bimodal. The fast component is consistent with the size of the free micelles of surfactant and the slow to the formation of a complex made up of clusters of $C_{12}E_5$ micelles stabilized within the PEO coil. Since the micelles are close to their overlap point, the formation of the latter is promoted by the excluded-volume effect of the high molar mass PEO.

3. R_H for the PEO/$C_{12}E_5$ complex increases strongly with increasing surfactant concentration from an initial value corresponding to the value for the PEO coil. It is concluded that the polymer chains uncoil progressively as the micellar clusters grow within the coil domain. The interactions between PEO and $C_{12}E_5$ clearly differ in kind from those between a neutral polymer and an ionic surfactant since the interactions are nonspecific, contrasting with the more well-defined entity formed in, for example, the PEO/SDS system, where small charged micelles are disposed along the polymeric backbone to provide optimal contact between the chain and the head group regions of the micelles.

4. Fluorescence quenching measurements show that there is a significant increase in the aggregation number of the $C_{12}E_5$ micelles with increasing PEO concentration. Thus, larger micelles within the domain of the PEO coil are stabilized in the form of clusters by the surrounding polymer segments.

5. As the temperature is increased, the mutual interaction between $C_{12}E_5$ micelles becomes more attractive. The cluster number density/size increase strongly toward the cloud point. The clouding temperature (T_c) is found to decrease and to be a strong function of the concentration of added PEO.

Acknowledgment. This work has been supported by the Swedish National Board for Technical Development (NUTEK) and the Swedish Technical Research Council (TFR). E.F. thanks the Conselho Nacional de Desenvolvimento Científico e Tecnológico (CNPq) for a stipendium (Grant 201720/93-0).

References and Notes

(1) *Interactions of Surfactants with Polymers and Proteins*; Goddard, E. D., Ananthapadmanabhan, K. P., Eds.; CRC Press: Boca Raton, FL, 1993.
(2) Saito, S. Polymer–surfactant interactions. In *Non-ionic Surfactants*; Schick, M. J., Ed.; Marcel Dekker: New York, 1987.
(3) Lindman, B.; Thalberg, K. In *Interactions of Surfactants with Polymers and Proteins*; Goddard, E. D., Ananthapadmanabhan, K. P. CRC Press: Boca Raton, FL, 1993.
(4) (a) Cabane, B. *J. Phys. Chem.* **1977**, *81*, 1639. (b) Cabane, B.; Duplessix, R. *J. Phys.* **1982**, *43*, 1529.
(5) Brown, W.; Fundin, J.; da Graça Miguel, M. *Macromolecules* **1992**, *25*, 7192.
(6) Almgren, M.; Hansson, P.; Mukhtar, E.; van Stam, J. *Langmuir* **1992**, *8*, 2405.
(7) Brown, W.; Fundin, J. *Macromolecules* **1994**, *27*, 5024.
(8) (a) Ricka, J.; Meewes, M.; Nyffenegger, R.; Binkert, Th., *Phys. Rev. Lett.* **1990**, *65*, 657. (b) Meewes, M.; Rika, J.; de Silva, M.; Nyffenegger, R.; Binkert, Th. *Macromolecules* **1991**, *24*, 5811.

(9) Brackman, J. C.; van Os, N. M.; Engberts, J. B. F. M. *Langmuir* **1988**, *4*, 1266.
(10) Winnik, F. M. *Langmuir* **1990**, *6*, 522.
(11) Cohen-Addad, S.; di Meglio, J.-M. *Langmuir* **1994**, *10*, 773.
(12) Sinn, C.; Woermann, D. *Ber. Bunsenges. Phys. Chem.* **1992**, *96*, 913.
(13) Brown, W.; Zhou, P.; Rymdén, R. *J. Phys. Chem.* **1988**, *92*, 6086.
(14) Schillén, K.; Brown, W.; Johnsen, R. M. *Macromolecules* **1994**, *27*, 4825.
(15) Infelta, P. P.; Grätzel, M.; Thomas, J. K. *J. Phys. Chem.* **1974**, *78*, 190.
(16) Tachiya, M. *Chem. Phys. Lett.* **1975**, *33*, 289.
(17) Nilsson, P. G.; Wennerström, H.; Lindman, B. *J. Phys. Chem.* **1983**, *87*, 1377.
(18) Kato, T.; Anzai, S.; Seimiya, T. *J. Phys. Chem.* **1987**, *91*, 4655.
(19) Brown, W. *Macromolecules* **1984**, *17*, 66.
(20) Devanand, K., Selser, J. C. *Macromolecules* **1991**, *24*, 5943.
(21) Kinugasa, S.; Nakahara, H.; Fudagawa, N.; Koga, Y. *Macromolecules* **1994**, *27*, 6889.
(22) Burchard, W.; Schmidt, M.; Stockmayer, W. H. *Macromolecules* **1980**, *13*, 1265.
(23) Rosch, M. In *Non-ionic Surfactants*; Surfactant Science series 1; Schick, M. J., Ed.; Marcell Dekker: New York, 1987; pp 753–793.
(24) Piculell, L., private communication.
(25) Alami, E.; Brown, W.; Almgren, M.; Francois, J. *Macromolecules*, in press.
(26) Wormuth, K. R. *Langmuir* **1991**, *7*, 1622.
(27) Brown, W.; Mortensen, K. *Macromolecules* **1988**, *21*, 420.
(28) Feitosa, E.; Brown, W.; Swanson-Vethamuthu, M., submitted to *Macromolecules*.
(29) Zana, R.; Weill, C. *J. Phys. Lett.* **1985**, *46*, 953.
(30) Almgren, M. In *Kinetics and Catalysis in Microheterogeneous Systems*, Grätzel, M., Kalyanasundaram, K. Eds.; Marcel Dekker: New York, 1991.
(31) Zana, R.; Lianos, L.; Lang, J. *J. Phys. Chem.* **1985**, *89*, 41.
(32) Zana, R.; Binana-Limbelé, W.; Kamenka, N.; Lindman, B. *J. Phys. Chem.* **1992**, *96*, 5461.
(33) van Stam, J.; Almgren, M.; Lindblad, C. *Progr. Colloid Polym. Sci.* **1991**, *84*, 13.

MA950516G

artigo IV

Effect of Temperature on the Interaction between the Nonionic Surfactant $C_{12}E_5$ and Poly(ethylene oxide) Investigated by Dynamic Light Scattering and Fluorescence Methods

Eloi Feitosa,† Wyn Brown,* Marilena Vasilescu,‡ and Martin Swanson-Vethamuthu

Department of Physical Chemistry, University of Uppsala, Box 532, 751 21 Uppsala, Sweden

Received January 19, 1996; Revised Manuscript Received July 1, 1996®

ABSTRACT: The interaction between the nonionic surfactant $C_{12}E_5$ and a high molar mass ($M = 5.94 \times 10^5$) poly(ethylene oxide) (PEO) in aqueous solution has been examined as a function of temperature by dynamic light scattering and fluorescence methods over a broad concentration range. Clusters of small surfactant micelles form within the PEO coil, leading to its extension. The hydrodynamic radius of the complex increases strongly with temperature as well as with the concentrations of surfactant and polymer. At high concentrations of the surfactant, the coil/micellar cluster complex coexists with free $C_{12}E_5$ micelles in the solution. Fluorescence quenching measurements show a moderate micellar growth from 155 to 203 monomers in PEO-free solutions of $C_{12}E_5$ over a wide concentration range (0.02−2.5%) at 8 °C. Below 0.25% $C_{12}E_5$, the average aggregation number (N) of the micelles is smaller in the presence of PEO than in its absence. However, N increases with increasing surfactant concentration up to a plateau value of about 270 at about 1.2% (ca. 30 mM) $C_{12}E_5$. At high surfactant concentrations, N is larger in the presence of polymer than in its absence, a finding which is connected to a significant lowering of the clouding temperature due to the PEO at these compositions. Similar results of increasing aggregation number followed by a plateau were also found at a fixed concentration of surfactant (2.5%) and varied PEO.

Introduction

There is increasing interest in ternary surfactant/polymer systems from both theoretical[1] and experimental[2] points of view. PEO is a favored polymer for such studies due to its unusual solubility properties, but the extension of the knowledge gained to other surfactant/polymer systems is not straightforward. Thus, although the general features of the interactions in various such systems have been extensively examined, it is difficult to delineate general rules since the interactions are strongly system dependent, depending on the hydrophobic/hydrophilic and/or structural and charge characteristics of the components.[3] While neutral polymers such as PEO are known to interact comparatively strongly with anionic surfactants, such as sodium dodecyl sulfate (SDS),[2] they interact only weakly with cationic surfactants such as the alkyltrimethylammonium bromides.[7−9] However, cationic surfactants form complexes with polymeric acids which are weakly ionized, such as poly(acrylic acid) at low pH.[10] The relative surfactant/polymer composition, and the temperature influence the interaction between surfactant and polymer. The physical properties of the micellar aggregates, such as the cloud point, critical micelle concentration (cmc), and the micellar size (aggregation number),[4−6] are highly dependent on the relative lengths of the polar and apolar portions of the surfactant, which also determine the strength of interaction with polymers.

The nature and extent of the interactions between neutral polymers and nonionic surfactants have also been controversial and in some aspects are still ambiguous. In an initial approach to this problem, the earlier paper[11] dealt with the ternary system containing the nonionic surfactant $C_{12}E_5$ and a PEO fraction of high molar mass ($M = 5.94 \times 10^5$). There it was established that, in contrast to the interactions of this polymer with SDS, where a complex is formed in which small micelles are strung along the chain, clusters of small surfactant micelles form within the PEO coil, leading to its extension for steric reasons. Thus, the excluded volume effect resulting on addition of high molar mass polymer to the system drives formation of nonionic surfactant micellar clusters.

The role of the system composition was examined[11] and it was found, for example, that on addition of the high molar mass PEO fraction there is a pronounced decrease in the cloud point in comparison with the binary $C_{12}E_5$−water system. The relatively low clouding temperature of $C_{12}E_5$ in water (≈32 °C), combined with the decreasing polarity of PEO with increasing temperature, makes this system an interesting one for investigating the influence of temperature on the polymer−surfactant interactions.

The present work thus extends the measurements described in the previous paper[11] to wider ranges of concentration and in particular focuses on the role of temperature change. Dynamic light scattering (DLS) measurements have been made on the ternary $C_{12}E_5$−PEO−water system at temperatures varying from 4 °C up to the cloud point (T_c) of the system in two different ways: (1) maintaining consecutively constant each of the solution components and varying the other; and (2) varying the concentration of both the solution components but keeping the ratio (R) between them constant.

Fluorescence probing methods have also been used to obtain additional information regarding the polymer−surfactant interaction, especially on the cmc (or cac) and the micellar aggregation number to examine the variation of the micellar size on addition of polymer to the system. At low concentrations of surfactant, the average aggregation number of the $C_{12}E_5$ micelles is found to decrease on adding PEO, as already described.[11]

† Permanent address: Departamento de Física, IBILCE/UNESP, São José do Rio Preto, SP, Brazil.

‡ Permanent address: Institute of Physical Chemistry, Romanian Academy, Spl. Independentei Nr. 202, Bucharest, Romania.

® Abstract published in *Advance ACS Abstracts,* September 15, 1996.

S0024-9297(96)00077-0 CCC: $12.00 © 1996 American Chemical Society

unesp

Materials and Methods

$C_{12}E_5$ (pentaethylene glycol mono-*n*-dodecyl ether) was purchased from Nikko Chemicals, Japan, and PEO ($M_w = 5.94 \times 10^5$ g/mol; $M_w/M_n = 1.03$) was from Toyo Soda, Ltd., Japan, and used without purification. The cmc of $C_{12}E_5$ is 2.64×10^{-3}% (w/w) (65 μM) at 25 °C.[4] Concentrations of the surfactant are expressed either in % (w/w) or moles/liter (M) (1% of $C_{12}E_5$ corresponds to 24.6 mM).

Pyrene and 3,4-dimethylbenzophenone 99% (DMBP), from Aldrich, were recrystallized from ethanol. Probes and quencher were transferred from stock solutions to empty flasks and the solvent evaporated. The surfactant or surfactant−polymer solutions were then added and the mixtures were magnetically stirred. Measurements were performed after 24 h to ensure that equilibrium was attained. The pyrene concentration was kept below 10^{-6} M to avoid excimer formation. The quencher concentration was such that it approximated one DMBP molecule per aggregate and ranged between 10^{-5} and 10^{-4} M.

Dynamic Light Scattering Measurements. DLS measurements were made using the apparatus described briefly in ref 12. An ALV wide-band, multi-τ, digital autocorrelator was used for data collection. The measured intensity autocorrelation function $g_2(t)$ is related to the field correlation function $g_1(t)$ by

$$g_2(t) = B[1 + \beta|g_1(t)|^2]$$

where β is a factor accounting for deviations from ideal correlation and B is a baseline term.

For a continuous distribution of relaxation times, corresponding to an infinite range of particle sizes, the inverse Laplace transform (ILT) may be used:

$$g_1(t) = \int_0^\infty A(\tau)e^{-t/\tau}\,d\tau$$

ILT analysis was performed using a constrained regularization routine, REPES.[13] Although similar to CONTIN,[14] the algorithm REPES differs in that it directly minimizes the sum of the squared differences between the experimental and calculated intensity−intensity autocorrelation functions $g_2(t)$ using nonlinear programming and allows the selection of the "smoothing parameter" P (probability to reject).[15] Analysis of data encompassing 288 exponentially spaced grid points and a grid density of 12 per decade can be rapidly performed on an IBM AT desk top computer. Representation of the relaxation time distributions in the form of an $\tau A(\tau)$ versus log τ plot, with $\tau A(\tau)$ in arbitrary units, provides an equal-area representation.

Fluorescence Measurements. Time-resolved fluorescence decay data were collected by means of the single-photon-counting technique. Fluorescence excitation was achieved by a Nd-YAG mode-locked laser which pumped a dye laser (DCM as dye and a KDP crystal for frequency doubling). The excitation and emission wavelengths, selected by monochromators, were 320 and 395 nm, respectively. The technique and data analysis are described elsewhere.[16-18] Fluorescence steady-state spectra were recorded on a SPEX Fluorolog 1680 combined with a SPEX Spectroscopy Laboratory Coordinator DM1B. Measurements were carried out at controlled temperatures, in air-equilibrated solutions.

The time-resolved fluorescence quenching method (TRFQ) in microheterogeneous solutions is well described in the literature[19-21] and is based on the equation[22]

$$\ln[F(t)/F(0)] = -A_2t + A_3[\exp(-A_4t) - 1] \qquad (1)$$

where $A_2 = k_0 + k_q k_- n/(k_q + k_-)$, $A_3 = nkq^2/(k_q + k_-)^2$, and $A_4 = k_q + k_-$, k_q standing for the first-order quenching rate constant, k_- for the exit rate constant of a quencher leaving the micelle, and n for the average number of quenchers per micelle.

If k_- is much less than k_q and k_0, eq 1 becomes

$$\ln[F(t)/F(0)] = -k_0t + n[\exp(-k_qt) - 1] \qquad (2)$$

This is the ideal case for determination of the aggregation number. Fitting the experimental data to eq 2 yields the values of n and k_q. The aggregation number (N) is given by

$$N = n[S]_{mic}/[Q]_{mic} \qquad (3)$$

where $[S]_{mic}$ and $[Q]_{mic}$ are the surfactant and quencher concentrations in the micelles, respectively; $[S]_{mic} = [S]_t - [S]_f$, where $[S]_t$ is the total surfactant concentration. One usually considers $[S]_f = [S]_{cmc}$. Because DMBP has a low solubility in water, the quencher concentration in the micelles is corrected

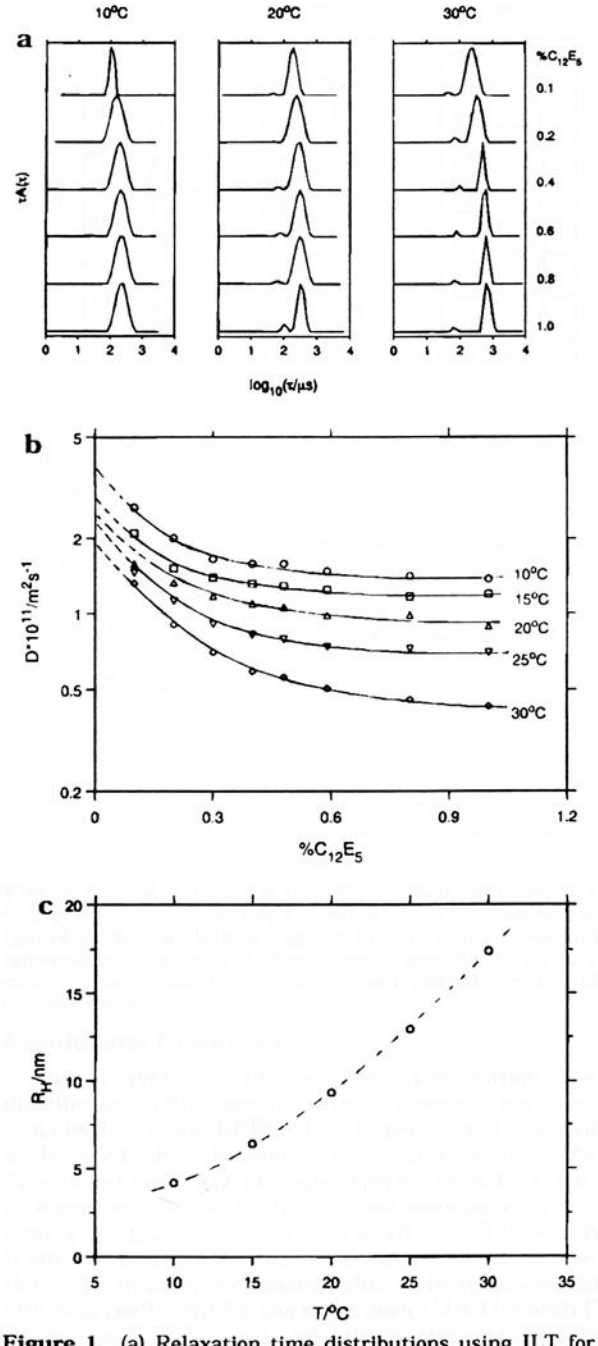


Figure 1. (a) Relaxation time distributions using ILT for binary $C_{12}E_5$ aqueous solutions at different surfactant concentrations and at three temperatures. Data at angle 90°. (b) Translational diffusion coefficients versus concentration for the binary $C_{12}E_5$/water system at the temperatures indicated. (c) Hydrodynamic radii for the binary $C_{12}E_5$ system as a function of temperature.

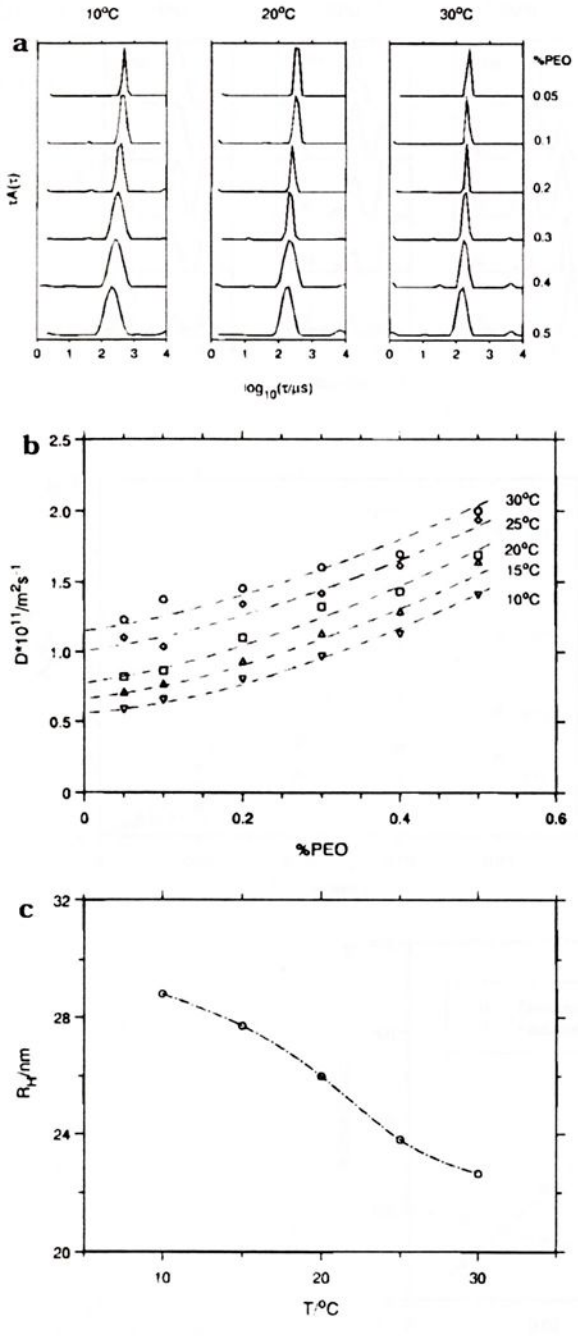


Figure 2. (a) Relaxation time distributions (ILT) for the binary PEO/water system at the different PEO concentrations and temperatures indicated. (b) Diffusion coefficients versus concentration for the binary PEO/water system at the temperatures indicated. (c) Temperature dependence of the hydrodynamic radius for the binary PEO/water system as a function of temperature.

by the equation

$$[Q]_{mic} = [Q]_t\{k_D[S]_{mic}\}/\{k_D[S]_{mic} + 1\} \quad (4)$$

where $[Q]_t$ is the total quencher concentration and k_D the rate constant for DMBP distribution between the micelles and the aqueous phase. The value of k_D for DMBP in 1% $C_{12}E_5$ was determined as 2525 M^{-1} at 10 °C by the method described in ref 23 and used in the analysis.

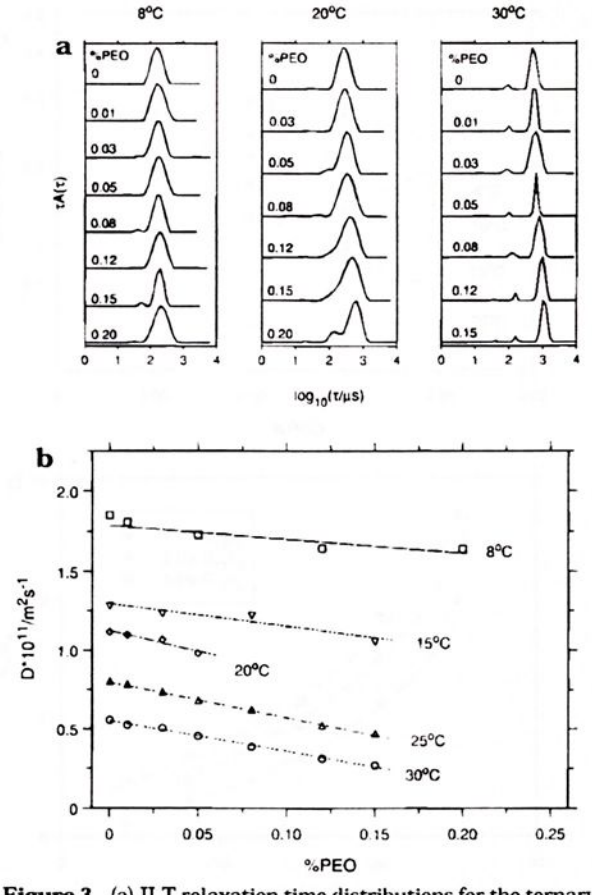


Figure 3. (a) ILT relaxation time distributions for the ternary $C_{12}E_5$/PEO/water system at a constant surfactant concentration of 0.5%. The data are at the PEO concentrations and temperatures shown. (b) Diffusion coefficients for the ternary system in (a), at the temperatures shown, plotted versus PEO concentration.

Results and Discussion

Binary Systems. Figure 1a shows relaxation time distributions obtained from the autocorrelation functions by ILT using REPES (see Experimental Section) for binary $C_{12}E_5$ solutions at three temperatures. The distributions are close to single exponential at 10 °C but, as noted previously,[11] contain a low-amplitude component with short relaxation time at 20 and 30 °C which is enhanced in intensity at higher surfactant concentration. The strongly decreasing value of the translational diffusion coefficient for the main peak ($D = \Gamma/q^2$ with Γ the relaxation rate $= \tau^{-1}$ and q the scattering vector) is shown as a function of surfactant concentration in the log–lin plot in Figure1b. The strong curvature in the concentration range below about 0.5%. was earlier interpreted[11,24,25] as deriving from micellar growth/intermicellar interactions. Approximate values of the hydrodynamic radii (R_H) were obtained from the estimated zero-concentration value of D at each temperature using the Stokes–Einstein equation:

$$R_H = kT/6\pi\eta_0 D_0 \quad (5)$$

and this parameter is shown in Figure1c as a function of temperature. The solvent viscosity at the relevant temperature, η_0, has been used in eq 5. Kato et al. [25] found that the correlation length, similarly estimated but for concentrations above the overlap concentration, also increases with increasing temperature.

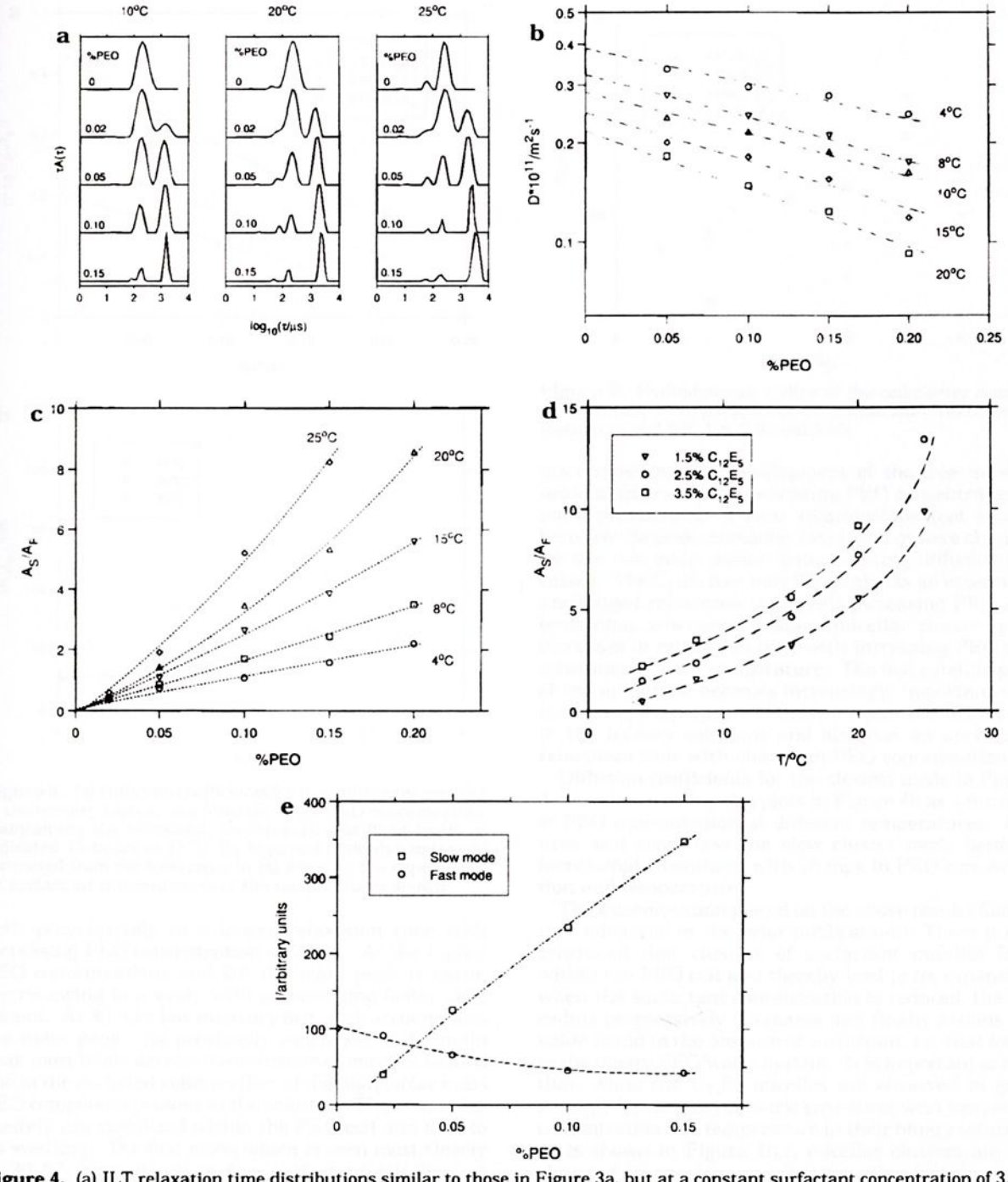


Figure 4. (a) ILT relaxation time distributions similar to those in Figure 3a, but at a constant surfactant concentration of 3.5%. The distributions are shown at different PEO concentrations and temperatures as indicated. (b) Diffusion coefficients plotted versus PEO concentration for a constant surfactant concentration of 3.5% at the temperatures indicated. (c) The intensity of the slow cluster mode and the fast micellar mode as a function of the PEO concentration at C (surfactant) = 3.5% and 25 °C. (d) Variation of the DLS amplitude ratio of slow to fast modes with temperature at the concentrations of surfactant shown in the insert and concentration PEO of 0.1%. (e) DLS measurements: intensities of slow and fast modes as a function of PEO concentration for surfactant concentration 3.5% at 25 °C.

Figure 2a shows examples of ILT relaxation time distributions for the PEO fraction in dilute solution at three temperatures. The single-coil diffusion coefficients derived from the peak moments are shown as a function of concentration in Figure 2b.

Hydrodynamic radii estimated from the intercepts using eq 5 are shown in Figure 2c as a function of temperature. R_H decreases with increasing temperature in the range 8–30 °C. This behavior is well known for PEO in aqueous solution and is understood to derive from the more compact conformation adopted by the oxyethylene chain at elevated temperature due to a higher population of unfavorable states.[26]

Ternary Systems. Figure 3a shows ILT results at three temperatures for the ternary PEO–$C_{12}E_5$–water solutions at a constant $C_{12}E_5$ concentration of 0.5% and with increasing PEO concentration. The distributions are essentially single modal at 8 and 20 °C and then

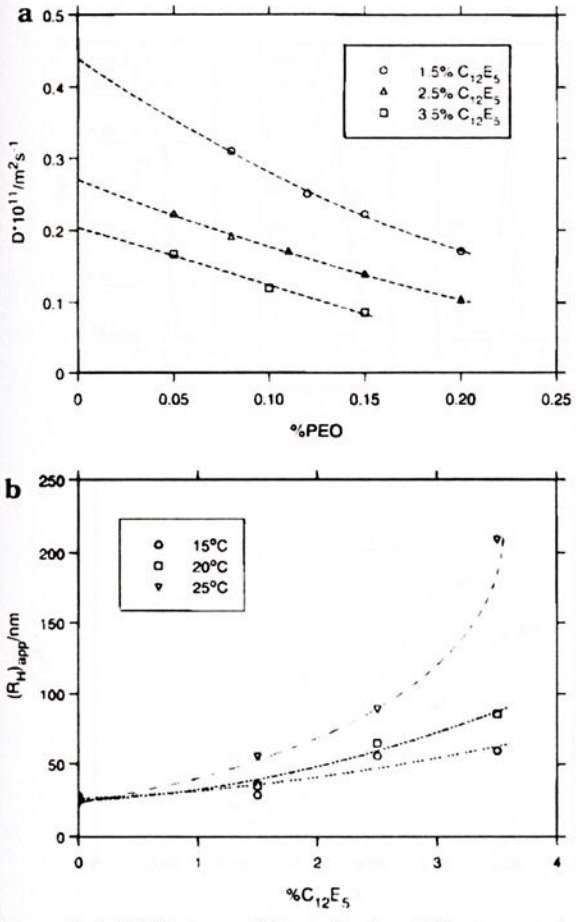


Figure 5. (a) Diffusion coefficients for the coil/cluster complex in the ternary system as a function of the PEO concentration, maintaining the surfactant concentration at fixed levels as indicated. Data are at 25 °C. (b) Apparent hydrodynamic radii estimated from the intercepts in (a) showing the dependence on surfactant concentration at the temperatures shown.

shift progressively to a longer relaxation time with increasing PEO concentration at 30 °C. At the higher PEO concentrations and 20° the main peak is asymmetric owing to overlap with an emerging faster component. At 30 °C a low intensity fast peak accompanies the main peak. As previously concluded,[11] the main peak most likely derives from clusters of micelles formed due to the excluded volume effect of the high molar mass PEO component present in the solution. These micellar clusters are stabilized within the PEO coil and lead to its swelling. The fast mode which is seen most clearly at 30 °C, corresponds to free surfactant micelles, as deduced from the hydrodynamic radius.

Figure 3b depicts the diffusion coefficients corresponding to the main peak in Figure 3a as a function of PEO concentration at different temperatures. The points included for zero PEO concentration are data interpolated at the surfactant concentration of 0.5% in Figure 1b for the binary surfactant system. It is noted that temperature strongly influences the D-value, while the approximately constant negative slope suggests a weak attractive interaction between the complex particles which is of similar magnitude over the temperature interval examined.

Figure 4 a shows analogous ILT results to those in Figure 3a but here they refer to a fixed surfactant concentration of 3.5%. A similar overall patttern is

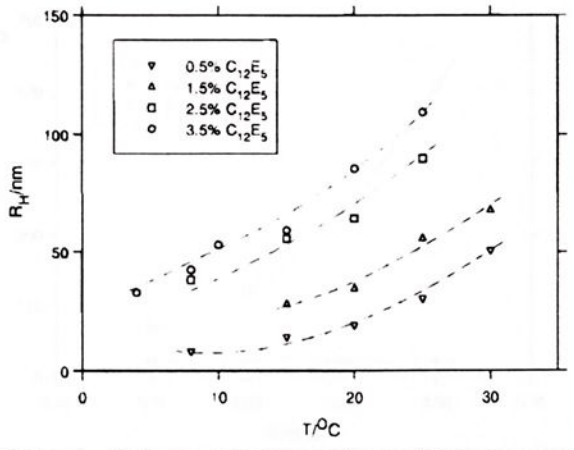


Figure 6. Hydrodynamic radius of the coil/cluster complex as a function of temperature at the surfactant concentrations (bottom to top) 0.5, 1.5, 2.5, and 3.5%.

discernible but the development of the free micellar mode amplitude with increasing PEO concentration is more pronounced. Linear relationships (not shown) between the peak relaxation rate Γ and q^2 were obtained for the two main modes demonstrating diffusive processes. The $C_{12}E_5$ free micellar peak has an essentially unchanged relaxation time with increasing PEO concentration, whereas the slow "micellar cluster" peak increases in relaxation time with increasing PEO concentration at each temperature. The fast satellite peak of low amplitude becomes increasingly important with increasing temperature both for the pure surfactant and in the ternary solutions and also has an unchanged relaxation time with change in PEO concentration.

Diffusion coefficients for the slowest mode in Figure 4a are shown as log−lin plots in Figure 4b as a function of PEO concentration at different temperatures. Figures 4c,d show how the slow cluster mode becomes increasingly dominant with change in PEO concentration and temperature.

The interpretation placed on the above results follows that advanced in the prior publication.[11] There it was concluded that clusters of surfactant micelles form within the PEO coil and thereby lead to its expansion: when the surfactant concentration is reduced, the coil radius progressively decreases and finally attains the value found in the absence of surfactant, i.e. that found in the binary PEO/water system. It is important to note that, while the $C_{12}E_5$ micelles are observed to grow strongly forming asymmetric structures with increasing concentration and temperature in their binary solutions as is shown in Figure 1b,c, micellar clusters are not observed in the binary solutions: this is true at all temperatures up to the cloud point at about 32 °C. Cluster formation is a phenomenon only found in the ternary system in the presence of the large PEO coils which, through the excluded volume effect, drive cluster formation in the surfactant system. Figure 4e shows the enhancement of the absolute intensity of the cluster mode at different PEO concentrations at a constant concentration of $C_{12}E_5 = 3.5\%$, and this contrasts with the approximately constant intensity of the free micellar peak.

Diffusion coefficients at three constant $C_{12}E_5$ concentrations are extrapolated to infinite dilution PEO in Figure 5a. From the intercepts, the apparent coil dimension (R_H) at finite $C_{12}E_5$ concentrations has been estimated using eq 5. These radii are summarized in

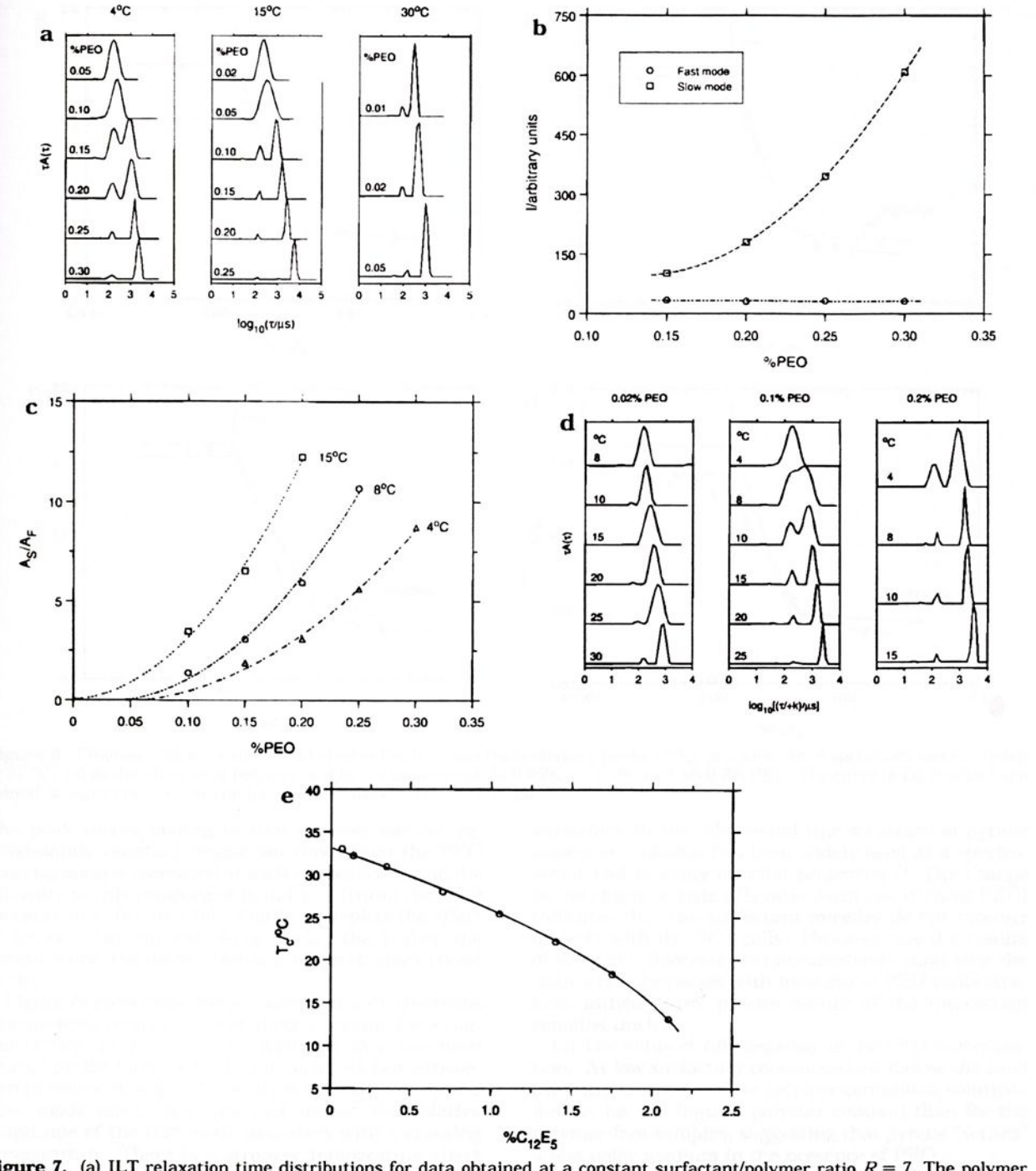


Figure 7. (a) ILT relaxation time distributions for data obtained at a constant surfactant/polymer ratio $R = 7$. The polymer concentration is indicated. (b) Intensity of fast and slow modes in (a) as a function of PEO concentration for constant surfactant/PEO ratio $R = 7$ at 8 °C. (c) Effect of PEO concentration on the ratio between the slow and fast mode amplitudes at constant surfactant/polymer ratio $R = 7$ and the temperatures shown. (d) Relaxation time distributions (ILT) at different temperatures and concentrations of PEO for $R = 7$. The log(time) axis has been shifted by the factor (T/η) to facilitate comparison. (e) The variation in the clouding temperature (T_c) with surfactant concentration at surfactant/PEO ratio $R = 7$.

Figure 5b as a function of surfactant concentration at 8, 25, and 30 °C. These data would indicate that (a) the coil expands as the surfactant concentration increases and also that (b) the coil expansion is greater the higher the temperature. Data points at zero surfactant concentration are taken from Figure 2c for the binary PEO system.

Figure 6 shows the corresponding trends in the apparent R_H for the PEO/micellar cluster complex with change in temperature for selected concentrations of $C_{12}E_5$. These data demonstrating coil expansion, taken together, substantiate the earlier interpretation[11] of micellar clustering within the polymer coil.

Constant Surfactant/Polymer Ratio. Complementary measurements were also made on the ternary system at a constant ratio $R = C_{12}E_5/PEO = 7$ as a function of temperature. Figure 7 a shows ILT results for various PEO concentrations at three temperatures.

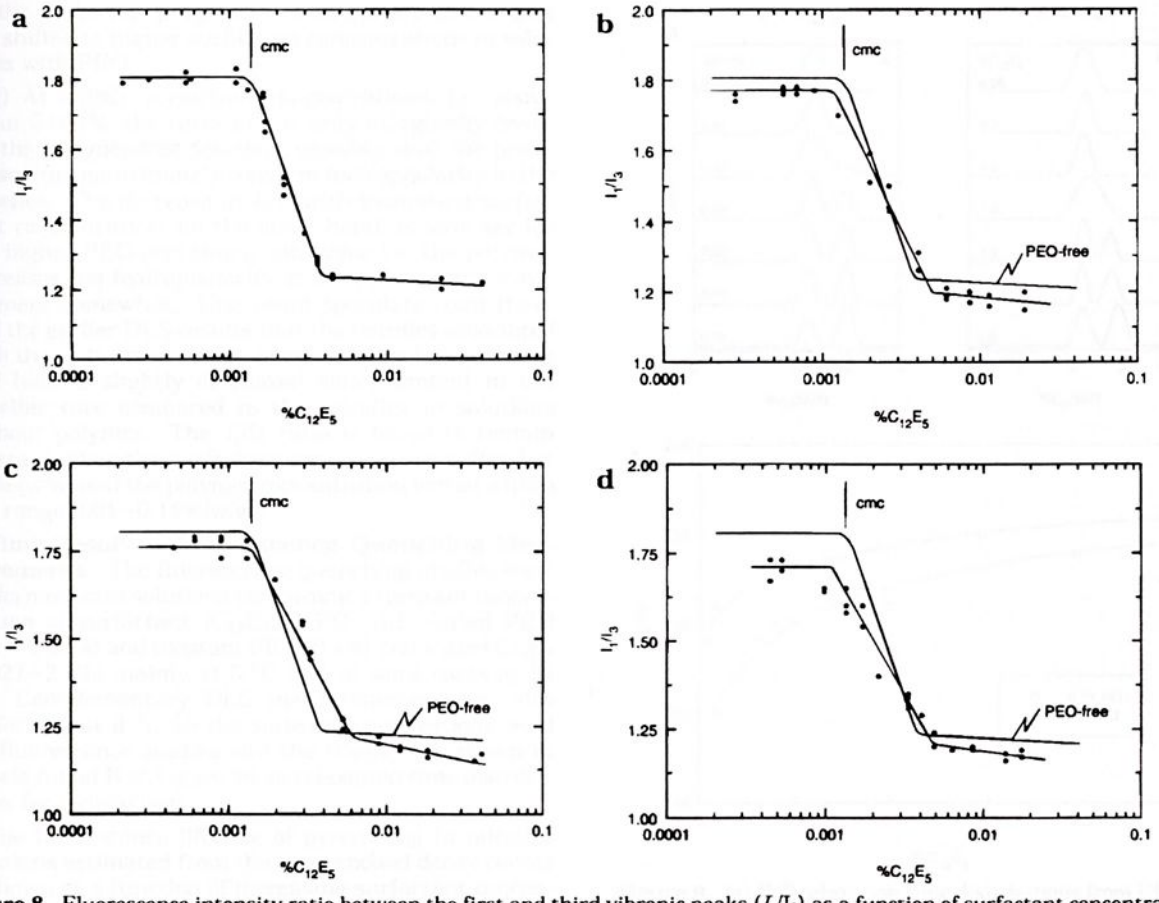


Figure 8. Fluorescence intensity ratio between the first and third vibronic peaks (I_1/I_3) as a function of surfactant concentration at 22 °C: (a) in the absence of polymer and in the presence of (b) 0.05%, (c) 0.1%, and (d) 0.2% PEO. The curve in (a) (without the points) is superimposed for comparison purposes in (b), (c), and (d).

The peak corresponding to free micelles has an approximately constant relaxation time when the PEO concentration is increased at each temperature, and the intensity of this component is independent of the PEO concentration (Figure 7b). Figure 7c depicts the effect of temperature on the A_S/A_F ratio: the higher the temperature, the more dominant is the complex (slow) mode.

Figure 7d shows how the relaxation time distributions change with temperature at three constant PEO concentrations at $R = 7$. The log(time) axis has been shifted by the factor $k = (T/\eta)$ to facilitate comparison. Temperature change affects the relaxation time of the slow mode more than the fast mode: the relative amplitude of the fast mode decreases with increasing temperature. There is a stronger temperature effect than observed at a $C_{12}E_5$ concentration of 3.5% shown in Figure 4e.

Measurements of the clouding temperature were made at constant ratio surfactant/polymer = 7 as a function of the surfactant concentration. These data are summarized in Figure 7e. T_c decreases strongly with increasing $C_{12}E_5$ concentration.

Steady-State Fluorescence Measurements. The fluorescence intensity ratio between the first and third vibronic peaks (I_1/I_3) of excited state monomeric pyrene emission was determined over a wide range of $C_{12}E_5$ concentration (0.004−0.04%) both in the absence of PEO (Figure 8a) and in the presence of 0.05% PEO (Figure 8b) at 22 °C. Similar determinations were also made at 0.1% (Figure 8c) and 0.2%PEO (Figure 8d). The variations in the vibrational fine structure of pyrene monomer emission has been widely used as a spectroscopic tool to study micellar properties.[21] The change in the characteristic I_1/I_3 ratio (with and without PEO) indicates that the surfactant micelles do not interact directly with the PEO coils. However, the the results of the static fluorescence measurements show that the interaction increases with increase in PEO concentration, although the precise nature of the interaction remains unclear.

(a) The value of I_1/I_3 depends on the PEO concentration. At low surfactant concentrations (below the cmc) the ratio is lower for the polymer-containing solutions (lowest for the highest polymer content) than for the polymer-free samples, suggesting that pyrene "senses" a less polar medium in the presence of PEO.

(b) After micellization begins, pyrene is increasingly partitioned into the hydrophobic domains leading to a sharper decrease in the I_1/I_3 ratio for the polymer-free case. For polymer-containing solutions, the decrease is less steep and is dependent on the PEO concentration (i.e. the concentration interval of the slope increases with increase in PEO). This behavior reveals the existence of interactions between PEO and $C_{12}E_5$. Similar results have been observed for interactions with PEO and cationic surfactant.[8] Taking the cmc or cac as the concentration at which the ratio starts to decrease (as is usual for nonionic surfactants), no significant dependence of the cac on adding PEO was noted. However, changes in the slope of the curve above the cmc or cac probably reflect the extent of interaction felt

by the probe (i.e. progressive changes are slower and are shifted to higher surfactant concentrations in solutions with PEO.

(c) At higher surfactant concentrations, i.e. above about 0.004%, the ratio I_1/I_3 is only marginally lower for the polymer-free solution, showing that the probe senses an approximately constant hydrophobicity in the micelles. The decrease in I_1/I_3 with increasing surfactant concentration, on the other hand, is stronger for the higher PEO-containing solutions; i.e. the polymer increases the hydrophobicity of the pyrene microenvironment somewhat. One could speculate from these and the earlier DLS results that the micelles associated with the coils are probably more compact (compressed) and have a slightly decreased water content in the micellar core compared to the micelles in solutions without polymer. The I_1/I_3 ratio is found to remain constant when the surfactant concentration is fixed at 2.5% (w/w) and the polymer concentration varied within the range 0.01−0.15%(w/w).

Time-Resolved Fluorescence Quenching Measurements. The fluorescence quenching studies were performed with solutions containing a constant concentration of surfactant ($C_{12}E_5$; 2.5%) with varied PEO (0.01−0.15%) and constant PEO (0.1%) and varied $C_{12}E_5$ (0.027−2.5%) mainly at 8 °C and in some cases at 15 °C. Complementary DLS measurements were also performed at 8 °C on the series of compositions used for fluorescence studies and the results are shown in panels A and B of Figure 9a as relaxation time distributions for comparison.

The fluorescence lifetime of pyrene (τ_0) in micellar solutions estimated from the unquenched decay curves is shown as a function of increasing surfactant concentration both with and without 0.1%PEO at 8 °C in Figure 9b Although the data points scatter somewhat, the results indicate that τ_0 does not change significantly on addition of PEO but is only marginally higher for solutions with PEO (224−230 ns) as opposed to 220−230 ns for PEO-free samples in line with the slight decrease in the I_1/I_3 ratio found in polymer-containing solutions above the cmc (Figures 8b-d). The small increase in lifetime suggests a slightly better shielding of micelle-solubilized pyrene associated with the PEO chains. At higher surfactant concentrations (≥1.5%), τ_0 remains nearly constant (228 ± 3 ns) in the polymer and polymer-free solutions showing no particular shielding effects. Increasing the temperature to 15 °C did not show significant differences in pyrene lifetime for the above two cases but instead gave a nearly constant lifetime of 200 ±3 ns (figure not shown). The corresponding τ_0 for solutions with fixed $C_{12}E_5$ (2.5%) and varied PEO was found to lie between 230−236 ns at 8 °C. The lack of sharp variations in the lifetime data suggests that pyrene senses a similar micellar microstructure and packing within the composition ranges studied. Typical TRFQ decay curves from micelles with probes and with different quencher concentrations are shown in Figure10a (upper panel, without PEO; right panel, with PEO). Curve 1 is for micelles with only probe molecules while in curves 2 and 3, the initial rapid quenching is from micelles with both probe and quencher followed by a linear exponential tail at long times for micelles with only pyrene present. The decays were also recorded using a longer time window of 2 μs to check for quenching of excited-state pyrene in quencher-free micelles by quencher molecules migrating from neighboring micelles or the bulk phase, but no significant migration effects were detected.

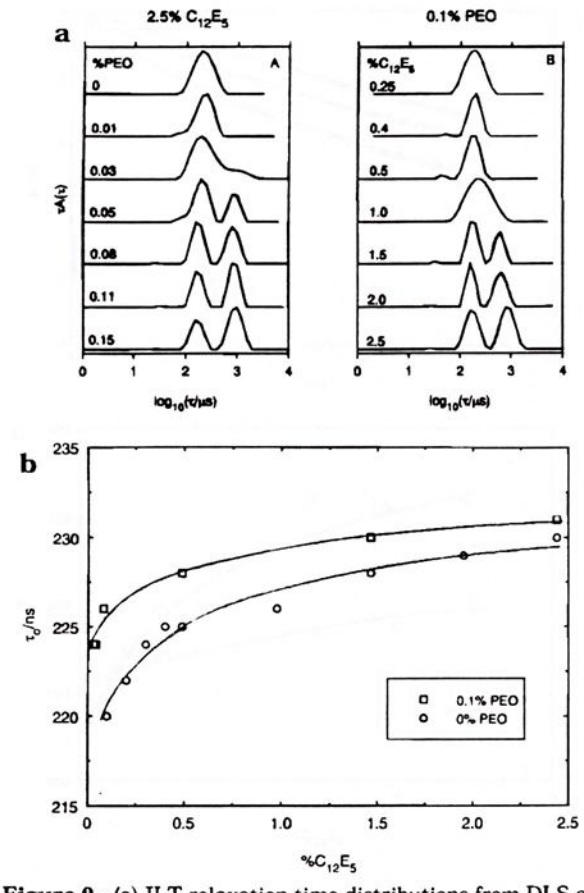


Figure 9. (a) ILT relaxation time distributions from DLS at 8 °C, showing the free micellar component and the coil/cluster complex development with PEO (panel A) and $C_{12}E_5$ concentration (panel B), keeping one of the respective components fixed. (b) Fluorescence liftetime (τ_0) spanning over a wide range of surfactant concentration in the absence and presence of 0.1% PEO at 8 °C.

The decay curves were fitted to the model of eqs 1 and 2. The results are shown in Figures 10b and 10c as average aggregation number (N) versus the surfactant concentration with and without 0.1% PEO and similarly in Figure 10d for samples with constant $C_{12}E_5$ but varied PEO concentration at $T = 8$ °C. The results presented in Figures 10b and 10c can be divided into two concentration zones for clarity: At low $C_{12}E_5$ concentrations (i.e. between 0.02 and 0.25%), the N of polymer-associated micelles is smaller than or equal to those in the corresponding PEO-free samples (i.e. within the micellar clusters inside or at the interface of the PEO coils). Similar results were also obtained at 15 °C (not shown) and 20 °C[11]. The smaller size of the micelles is due to the relatively stronger polymer−surfactant interaction at low concentrations arising mainly from steric effects and restrictions imposed by the PEO chain configuration in water. The DLS results shown in Figure 9a show that these samples are from a region characterized by a unimodal relaxation time distribution where the slightly more hydrophobic environment provided by the PEO coils compared to water favors association of $C_{12}E_5$ micelles mainly due to the excluded volume effect. Initially, the micelles are smaller in size compared to free micelles but grow with increasing surfactant to a similar size at 0.25% $C_{12}E_5$. We note that in a parallel study of the ternary system

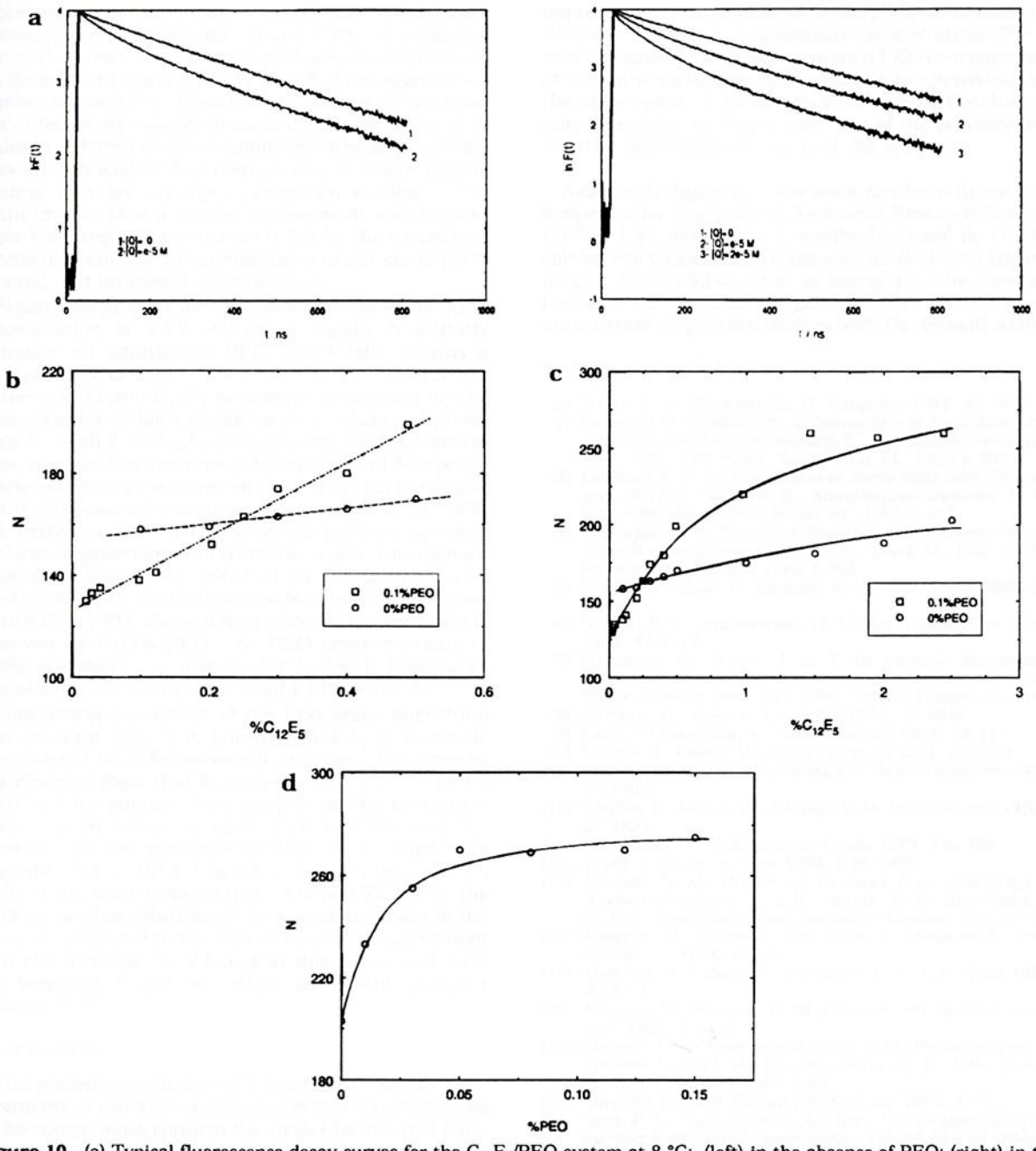


Figure 10. (a) Typical fluorescence decay curves for the $C_{12}E_5$/PEO system at 8 °C: (left) in the absence of PEO; (right) in the presence of PEO. (b) Dynamic fluorescence data. Average aggregation number (N) as a function of surfactant concentration, with and without polymer (0.1% PEO), at 8 °C. (c) Variation of the average aggregation number with surfactant concentration over an extended range of $C_{12}E_5$ concentration; PEO concentration = 0.1% , 8 °C. (d) Variation of the average aggregation number as a function of increasing PEO concentration at a fixed surfactant concentration of 2.5% ; data at 8 °C.

of the cationic surfactant CTAB and essentially neutral poly(acrylic acid) at low pH,[31] a lower N was found in the presence of the polymer. Figure 10c includes the variation of N for higher concentrations of $C_{12}E_5$ (0.3 to 2.5%) where the average N increases rapidly up to a plateau value of 270 monomers at 1.5% surfactant for the compositions containing 0.1% PEO at 8 °C. This large growth in the PEO-associated micelles (170−270) as opposed to the moderate growth found in polymer-free samples (155−203) can be connected to a significant lowering of the clouding temperature (about 3−4 °C) due to the presence of 0.1% PEO at surfactant concentrations above 0.25%.[11] Furthermore, the DLS results show that at concentrations above 1% $C_{12}E_5$ the broad relaxation time distribution becomes bimodal; this is attributed to a distribution of free $C_{12}E_5$ micelles (the faster mode) and a complex (PEO coils saturated with $C_{12}E_5$ micelles, slower mode). The micelles grow dramatically up to 1.5% $C_{12}E_5$, above which the onset of complex formation and the appearance of the free micellar peak in DLS (Figure 9a(B)) corresponds to a plateau value of N, i.e. 270 monomers (Figure 10c). The increase in aggregation number up to a plateau value is also due to the tendency for new surfactant molecules to prefer to pack in the environment of near-saturated PEO chains (both PEO and $C_{12}E_5$ become more hydro-

phobic as temperature increases; the saturation $C_{12}E_5$ concentration lies between 1.0 and 1.5%). A combination of the above two effects is probably responsible for the dramatic increase and leveling off of the aggregation number above 0.3%. Fluorescence studies do not show two different pyrene lifetimes arising from probe molecules in different microenvironments (free and polymer-associated micelles) but instead give a single pyrene lifetime and an average aggregation number. The result implies that a similar environment with respect to packing and microstructure is felt by the solubilized pyrene molecules at all compositions under study (both bimodal and unimodal distributions).

Figure 10d gives N for solutions with constant $C_{12}E_5$ concentration of 2.5% (60 mM). Again N initially increases on addition of PEO and finally attains a plateau value of about $N \approx 270$. Thus the interaction between PEO and $C_{12}E_5$ is strongly dependent on the concentration of both components as observed previously.[11] With 2.5% $C_{12}E_5$ and different PEO concentrations, the micelles are more polydisperse and N depends on the quencher concentration used. For this particular result, N varies with an uncertainty range of 10−15%. The variation in N has been considered at a constant surfactant/quencher concentration ratio throughout. From DLS (Figure 9a, panel A) for the samples with fixed 2.5% $C_{12}E_5$, the distribution is unimodal and broad up to 0.01% PEO, above which a second slower mode is observed at 0.03% PEO. At PEO concentrations of 0.05% and above, the distribution is clearly bimodal as it is above 1.5% $C_{12}E_5$ with fixed PEO (panel B).

Concerning the values of the first order quenching rate constant (k_q), it is known[21] that k_q is inversely proportional to N for spherical micelles. The present experiments show that k_q varies from 7.5×10^6 to 4.0×10^6 s^{-1} for polymer-free samples as the surfactant concentration increases from 0.1% to 2.5% at 8 °C. However, in the presence of PEO, k_q is practically constant: 8.4×10^6 s^{-1} to 7.6×10^6 s^{-1}, up to 0.25% $C_{12}E_5$ at the same temperature. Above 0.3% $C_{12}E_5$, the PEO-containing solutions show a small decrease in the k_q value compared to the PEO-free case, in agreement with the increase in N found in this range and with the behavior found for other surfactant−polymer systems.[27−30]

Conclusions

The present results from DLS and fluorescence measurements at different temperatures and concentrations of the components confirm the model for neutral polymer−surfactant interaction proposed in the previous communication:[11] i.e. micellar clusters are formed within the large PEO coils, leading to coil expansion. The overall hydrodynamic size of the coil/micellar cluster complex increases strongly with increasing temperature up to the clouding point and also with increasing concentration of each component. Above the saturation concentration, the complex co-exists with free micelles in solution.

From the fluorescence measurements, we conclude the following: In dilute solution, high molar mass PEO interacts with polar moieties of the surfactant molecule. The cmc or cac of the surfactant remains unchanged with increase in PEO concentration. At low surfactant concentrations, the aggregation number (N) of the $C_{12}E_5$ micelles within the clusters is smaller than in the polymer-free solution in the temperature range from 8 to 15 °C due to steric factors. N increases with increasing surfactant concentration in the presence of constant PEO concentration, to a plateau value of about 270. N also increases in a similar way with PEO concentration at constant surfactant concentration to approximately the same value. N for the micelles forming the clusters may be smaller or larger than that of the polymer-free micelles depending on the T_c of the system.

Acknowledgment. This work has been financially supported by the Swedish Technical Research Council (TFR). E.F. thanks the Conselho Nacional de Desenvolvimento Científico e Tecnológico (CNPq) for a stipend (Grant 201720/93-0). M.V. is grateful to the Swedish Institute for financial support. M.S.V. gratefully acknowledges helpful discussions with Dr. Elouafi Alami.

References and Notes

(1) Nikas, Y. J.; Blankschtein, D. *Langmuir* **1994**, *10*, 3512.
(2) Lindman, B.; Thalberg, K. In *Interactions of Surfactants with Polymers and Proteins*; Goddard, E., Ananthapadmanabhan, K. P., Eds.; CRC Press: Boca Raton, FL, 1993; p 203.
(3) Goddard, E. D. In *Interactions of Surfactants with Polymers and Proteins*; Goddard, E., Ananthapadmanabhan, K. P., Eds.; CRC Press: Boca Raton, FL, 1993; p 219.
(4) Degiorgio, V. In *Physics of Amphiphiles: Micelles, Vesicles and Microemulsions*; Degiorgio, V., Corti, M., Eds.; North-Holland: Amsterdam, 1985; p.303.
(5) Brown, W.; Zhou, P.; Rymdén, R. *J. Phys. Chem.* **1988**, *92*, 6086.
(6) Nilsson, P.-G.; Wennerström, H.; Lindman, B. *J. Phys. Chem.* **1983**, *87*, 1377.
(7) Hayakawa, K.; Kwak, J. C. T. In *Cationic Surfactants*; Surfactant Science Series; Rubingh, D. N., Holland, P., Eds.; Marcel Dekker: New York, 1991; Vol. 37, Chapter 5, p 189.
(8) Anthony, O.; Zana, R. *Langmuir* **1994**, *10*, 4048.
(9) Saito, S.; Kitamura, K. *Tenside Deterg.* **1981**, *18*, 117.
(10) Fundin, J.; Brown, W. *Macromolecules* **1994**, *27*, 5024.
(11) Feitosa, E.; Brown, W.; Hansson, P. *Macromolecules*, **1996**, *29*, 2169.
(12) Schillén, K.; Brown, W.; Johnsen, R. M. *Macromolecules* **1994**, *27*, 4825.
(13) Provencher, S. W. *Makromol. Chem.* **1979**, *180*, 201.
(14) Jakes, J. *Czech. J. Phys.* **1988**, *B38*, 1305.
(15) Johnsen, R. M.; Brown, W. In *Laser Light Scattering in Biochemistry*; Harding, S. E., Sattelle, D. B., Bloomfield, V. A., Eds.; Royal Society of Chemistry: London, 1992; p 77.
(16) Almgren, M.; Alsins, J.; van Stam, J.; Mukhtar, E. *Prog. Colloid Sci.* **1988**, *76*, 68.
(17) Almgren, M.; Löfroth, J.; van Stam, J. *J. Phys. Chem.* **1986**, *90*, 4431.
(18) Almgren, M.; Hansson, P.; Mukhtar, E.; van Stam, J. *Langmuir* **1992**, *8*, 2405.
(19) Almgren, M. In *Kinetics and Catalysis in Microheterogeneous Systems*, Gratzel, M., Kalyanasundaram, K., Eds.; Marcel Dekker: New York, 1991, p 63.
(20) Almgren, M. *Adv. Colloid Interface Sci.* **1992**, *41*, 9.
(21) Zana, R. In *Surfactants in Solution. New Methods of Investigation*; Surfactant Science Series; Vol. 22, Marcel Dekker: New York, 1987; Vol. 22, p 241.
(22) Infelta, P. P.; Grätzel, M.; Thomas, J. K. *J. Phys. Chem.* **1974**, *78*, 190.
(23) Almgren, M.; Alsins, J. *Prog. Colloid Polym. Sci.* **1987**, *74*, 55.
(24) Nilsson, P. G.; Wennerström, H.; Lindman, B. *J. Phys. Chem.* **1983**, *87*, 1377.
(25) Kato,T.; Anzai, S.; Seimiya, T. *J. Phys. Chem.* **1987**, *91*, 4655.
(26) Karlström, G. *J. Phys. Chem.* **1985**, *89*, 4962.
(27) Thalberg, K.; van Stam, J.; Lindblad, C.; Almgren, M.; Lindman, B. *J. Phys. Chem.* **1991**, *95*, 8975.
(28) van Stam, J.; Brown, W.; Fundin, J.; Almgren, M.; Lindblad, C. In *Colloid−Polymer Interactions. Particulate, Amphiphilic and Biological Surfaces*; Dubin, P., Tong, P., Eds.; American Chemical Society: Washinghton, DC, 1993; p 195.
(29) van Stam, J.; Almgren, M.; Lindblad, C. *Prog. Colloid Polym. Sci.* **1991**, *84*, 13.
(30) Winnik, F. M. *Langmuir* **1990**, *6*, 522.
(31) Fundin, J.; Hansson, P.; Brown, W.; Idegran, I. *Macromolecules*, submitted.

MA9600771

artigo V

Articles

Interaction of the Nonionic Surfactant $C_{12}E_8$ with High Molar Mass Poly(ethylene oxide) Studied by Dynamic Light Scattering and Fluorescence Quenching Methods

Eloi Feitosa,† Wyn Brown,* and Martin Swanson-Vethamuthu‡

Department of Physical Chemistry, University of Uppsala, P.O. Box 532, 751 21 Uppsala, Sweden

Received May 15, 1996. In Final Form: August 19, 1996[⊗]

Dynamic light scattering has been used to investigate ternary aqueous solutions of *n*-dodecyl octaoxyethylene glycol monoether ($C_{12}E_8$) with high molar mass poly(ethylene oxide) (PEO). The measurements were made at 20 °C, always below the cloud point temperature (T_c) of the mixed solutions. The relaxation time distributions are bimodal at higher PEO and surfactant concentrations, owing to the presence of free surfactant micelles, which coexist with the slower component, representing the polymer coil/micellar cluster complex. As the surfactant concentration is increased, the apparent hydrodynamic radius (R_H) of the coil becomes progressively larger. It is suggested that the complex structure consists of clusters of micelles sited within the polymer coil, as previously concluded for the PEO–$C_{12}E_5$–water system. However, $C_{12}E_8$ interacts less strongly than $C_{12}E_5$ with PEO; at low concentrations of surfactant the complex does not contribute significantly to the total scattered intensity. The perturbation of the PEO coil radius with $C_{12}E_8$ is also smaller than that in the $C_{12}E_5$ system. The addition of PEO strongly decreases the clouding temperature of the system, as previously observed for $C_{12}E_5$/PEO mixtures in solution. Addition of PEO up to 0.2% to $C_{12}E_8$ (10 wt %) solutions does not alter the aggregation number (N_{agg}) of the micelles probably because the surfactant monomers are equally partitioned as bound and unbound micelles. The critical micelle concentration (cmc), obtained from the I_1/I_3 ratio (a measure of the dependence of the vibronic band intensities on the pyrene probe environment), does not change when PEO is added, suggesting that for neutral polymer/surfactant systems the trends in N_{agg} and the cmc do not unambiguously reflect the strength of interaction.

Introduction

Ternary systems consisting of polymers and surfactants in aqueous solution are interesting since their properties usually differ substantially from those of the binary solutions of the pure components. Moreover, the rich variety of such systems encompasses many of biological and technological interest. The driving forces which lead to complex formation between polymer and surfactant are, however, still poorly understood, owing to the highly system-dependent nature of the interactions. The fact that anionic surfactants interact more strongly than cationic surfactants with neutral polymers cannot be explained only by competing electrostatic and hydrophobic forces: the size and nature of the surfactant head-group are also important in the interaction. The generality of such observations in addition to the common view that neutral polymers do not interact significantly with nonionic surfactants illustrates the complexity of the situation. For a recent review see ref 1. The investigations described in the literature deal moreover with a very limited range of systems.

Anthony and Zana[2] have recently determined the aggregation number (N_{agg}) of nonionic $C_{12}E_8$ micelles in the presence and absence of the neutral polymer poly(ethylene oxide) (PEO, M_w = 20 000) by fluorescence measurements up to 60 °C. For fixed surfactant and polymer concentrations, respectively of 0.3% (≈5 mM) and 3.0%, they found that the aggregation number of $C_{12}E_8$ micelles in the presence of PEO is unchanged up to 60 °C and they concluded that PEO does not interact with $C_{12}E_8$. Furthermore, no evidence for interaction was found for this system over a range of surfactant concentrations up to 2.6 wt % at a constant concentration of 0.5 wt % PEO (M = 20 000) according to recent light-scattering measurements.[3] The situation is apparently different with a high molar mass PEO.

This paper describes results of dynamic light-scattering measurements and fluorescence methods on the ternary PEO/$C_{12}E_8$/water system where the PEO has a high MW (here 5.94×10^5). The results are compared with those from a parallel investigation on the same polymer fraction with the surfactant $C_{12}E_5$.[4]

Materials and Methods

$C_{12}E_8$ (Nikko Chemicals, Japan) and PEO (Toya Soda, Ltd., Japan) were used as purchased. The critical micelle concentration (cmc) of $C_{12}E_8$ is 3.8×10^{-3} wt % (71 μM) at 25 °C.[5] The PEO has $M_w = 5.94 \times 10^5$ and $M_w/M_n = 1.03$.[6] All the concentrations are expressed in wt % units, where 1 wt % PEO or $C_{12}E_8$ corresponds to 1.69×10^{-3} M or 18.56 mM, respectively.

† Permanent address: Departamento de Física, IBILCE/UNESP, São José do Rio Preto, SP, Brazil.

‡ Present address: Department of Chemical Engineering, Colburn Laboratory, University of Delaware, Newark, DE 19716.

⊗ Abstract published in *Advance ACS Abstracts*, November 1, 1996.

(1) Goddard, E., Ananthapadmanabhan, K. P., Eds.; *Interactions of Surfactants with Polymers and Proteins*; CRC Press: Boca Raton, FL, 1993.

(2) Anthony, O.; Zana, R. *Langmuir* **1994**, *10*, 4048.

(3) Alami, E.; Almgren, M.; Brown, W.; François, J. *Macromolecules* **1996**, *29*, 2229.

(4) (a) Feitosa, E.; Brown, W.; Hansson, P. *Macromolecules* **1996**, *29*, 2169. (b) Feitosa, E.; Brown, W.; Vasilescu, M.; Swanson-Vethamuthu, M. *Macromolecules* **1996**, *29*, 6837.

(5) Degiorgio, V. In *Physics of Amphiphiles: Micelles, Vesicles and Microemulsions*; Degiorgio, V., Corti, M., Eds.; North-Holland: Amsterdam, 1985; p 303.

(6) PEO sample specification sheet, Toyo Soda, Ltd., Tokyo, Japan.

S0743-7463(96)00478-7 CCC: $12.00 © 1996 American Chemical Society

Dynamic light scattering (DLS) measurements have been made using the apparatus described earlier.[4a] An ALV wide-band, multi-τ, digital autocorrelator has been used for assembling the data. For polydisperse solutions the experimentally measured autocorrelation function of the scattered intensity, $g_2(t)$, is related to the field correlation function ($g_1(t)$) by the Siegert relationship:

$$g_2(t) = B[1 + \beta|g_1(t)|^2] \quad (1)$$

Here β is a constant reflecting the deviation from ideal correlation and B is a baseline. For an infinite range of particle sizes in a continuous distribution, the inverse Laplace transform (ILT) is used:[7]

$$g_1(t) = \int_{-\infty}^{\infty} \tau A(\tau) \exp(-t/\tau)\, d\ln\tau \quad (2)$$

where τ is the relaxation time which is obtained together with the corresponding relative amplitude using the inversion algorithm REPES.[8] The relaxation time distribution is plotted as $\tau A(\tau)$ versus $\log\tau$ to provide an equal area representation.[9] Unlike CONTIN,[10] REPES directly minimizes the sum of the squared difference between the experimental and fitted intensity correlation functions using a nonlinear algorithm which allows the choice of the "smoothing" (probability to reject) parameter.[11] Mean diffusion coefficients are obtained from the moments of the distributions, $D = \Gamma/q^2$ in the limit of zero angle. Here q is the scattering vector: $q = (4\pi n/\lambda)\sin(\theta/2)$, with n the refractive index, λ the wavelength, and θ the scattering angle. $\Gamma = \tau^{-1}$ is the relaxation rate.

The experimental details and method of analysis for time-resolved fluorescence quenching (TRFQ) decay data have been described earlier (ref 4). All measurements were performed in equilibrium with air at 20 °C using pyrene and dimethylbenzophenone as probe and quencher, respectively. The TRFQ data were fitted to the Infelta-Tachiya equations (see the previous paper[4a]):

$$F(t) = A_1 \exp[-A_2 t + A_3\{\exp(-A_4 t) - 1\}] \quad (3)$$

$F(t)$ describes the time evolution of the fluorescence intensity. The parameters A_1–A_4 are given as follows: $A_1 = F(0)$, the fluorescence intensity at time zero; $A_2 = 1/\tau_0$, where τ_0 is the natural lifetime of pyrene determined from separate experiments without quencher; $A_3 = \langle n\rangle$ and $A_4 = k_q$, where $\langle n\rangle$ is the average number of quenchers in a micelle and k_q is the psuedo-first-order quenching constant. This interpretation is valid if the micelles are small and monodisperse, if the probe and quenchers are stationary in the micelles during the lifetime of the probe, and if the quenchers are distributed Poisson-like over the micelles.

The surfactant aggregation number, N_{agg}, was calculated from $\langle n\rangle$ with the known values for the concentration of surfactant (S_m) and quenchers (Q_m) in the micelles.

$$N_{agg} = \frac{\langle n\rangle S_m}{Q_m} \quad (4)$$

The quencher has a low solubility in water and preferentially solubilizes into the hydrophobic environment provided by the micelle. The quencher molecules are very few compared to the surfactant monomers and have a Poisson distribution in the micelles, validating the use of eq 4. At the surfactant concentrations used in this study (10 wt %), the free concentrations of surfactant and quencher are negligible, so S_m and Q_m may be replaced by the total concentration of surfactant and quencher, respectively.

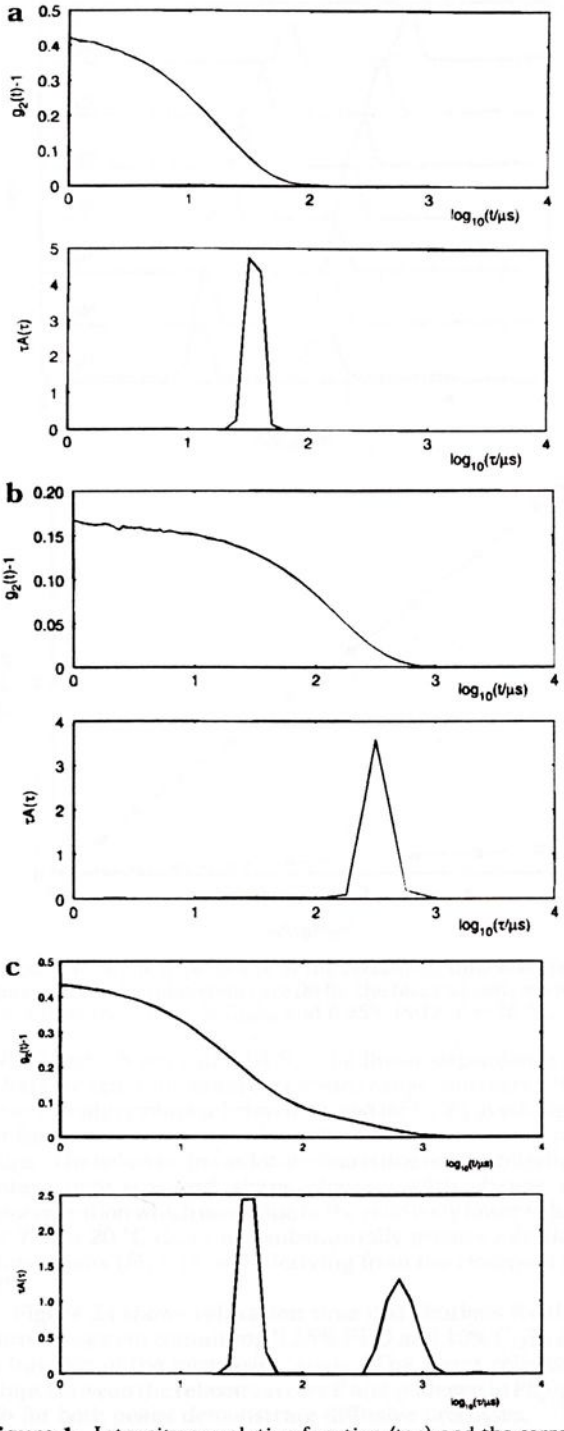


Figure 1. Intensity correlation function (top) and the corresponding relaxation time distribution (bottom) for (a) $C_{12}E_8$ and (b) PEO at concentrations of 10% and 0.5%, respectively, and (c) for a ternary $C_{12}E_8$/PEO mixture (10 wt %/0.25%) in aqueous solution; $T = 20$ °C and $\theta = 90°$.

Results and Discussion

Typical normalized intensity correlation functions and the corresponding relaxation time distributions for the ternary PEO $C_{12}E_8$ water system as well as the individual components are shown in Figure 1 at 20 °C. Up to at least

(7) Chu, B. *Laser Light Scattering*, 2nd ed.; Academic Press, New York, 1991.
(8) Schillén, K.; Brown, W.; Johnsen, R. M. *Macromolecules* **1994**, *27*, 4825.
(9) Johnsen, R. M.; Brown, W. In *Laser light scattering*; Harding, S. E., Sattelle, D. B., Bloomfield, V. A., Eds.; Royal Society of Chemistry: London, 1992; p 77.
(10) Jakes, J. *Czech. J. Phys.* **1988**, *B38*, 1305.
(11) Provencher, S. W. *Makromol. Chem.* **1979**, *180*, 201.

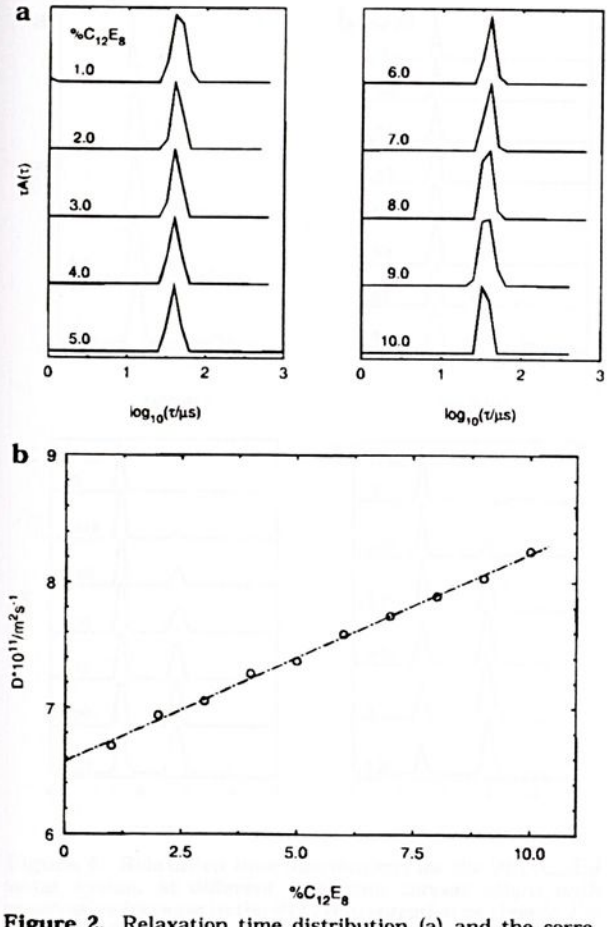


Figure 2. Relaxation time distribution (a) and the corresponding diffusion coefficients (b) for pure $C_{12}E_8$ in water as a function of surfactant concentration; $T = 20$ °C and $\theta = 90°$.

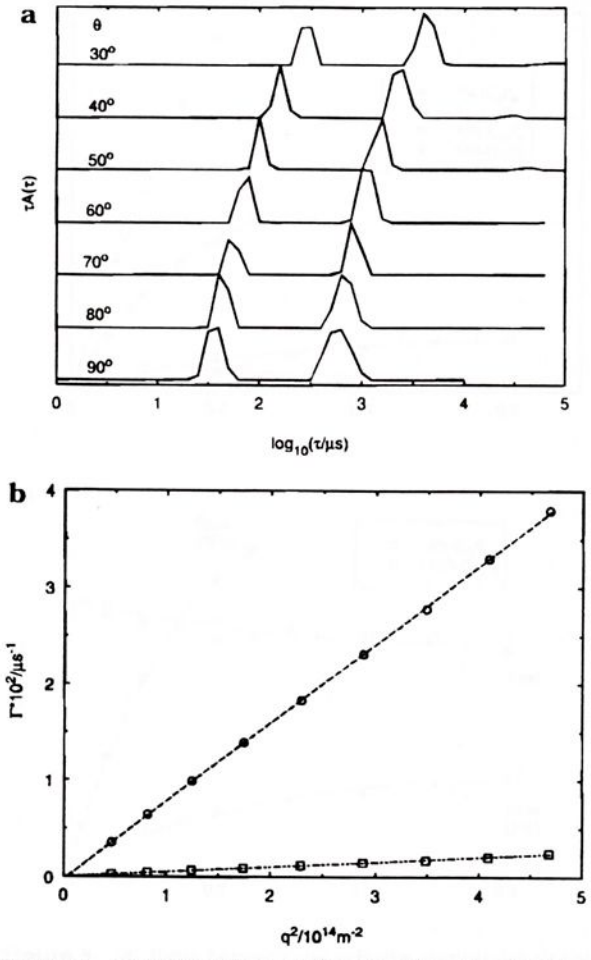


Figure 3. Angle dependence of the relaxation time distributions (a) and the relaxation rate (b) for the fast and slow modes for a mixture with 10% $C_{12}E_8$ and 0.25% PEO; T = 20 °C.

$C = 10\%$ the relaxation time distribution for $C_{12}E_8$ is unimodal (Figure 1a) as is that for PEO (Figure 1b). In the ternary mixture, however, the distribution is bimodal (Figure 1c). The aim of this article is to provide confirmatory evidence that, for the ternary mixture PEO/$C_{12}E_8$/water, the fast and slow modes derive, respectively, from free micelles and clusters of $C_{12}E_8$ micelles which are sited within the PEO coils, as was concluded for the PEO/$C_{12}E_5$/water system.[4] It will be noted that the scattered intensity from the pure PEO is very weak compared to that from the micelles: only when a high relative concentration of $C_{12}E_8$ is present is the complex formed in a significant amount, as is seen by comparing the effect of increasing surfactant concentration at, for example, a PEO concentration of 0.1% in Figures 4 and 5a, below. The changes which result on varying the concentrations of the components are discussed in the following sections.

Figure 2a shows relaxation time distributions for pure $C_{12}E_8$ in water, measured at 20 °C and at concentrations up to 10 wt %. The distributions are close to monodisperse. The mean hydrodynamic radius (R_H) of the $C_{12}E_8$ micelles at 20 °C was obtained from the diffusion coefficient at infinite dilution using the Stokes–Einstein relation together with the viscosity of water and gives $R_H = 3.3$ nm. The uncertainty in this value is estimated to be ±0.1 nm. This value is close to that earlier obtained by Nilsson et al.[12] (3.1 nm) and Brown et al.[13] (2.9 nm) using PFG-NMR and 3.8 nm using DLS. The linear dependence of D on $C_{12}E_8$ concentration over a wide range contrasts with the strongly nonlinear behavior noted for $C_{12}E_5$ in solution at concentrations below about 1% at the same temperature. The behavior in the latter case is due to intermicellar interactions/size and shape changes with change in concentration which occur due to the relatively lower value of T_c. At 20 °C $C_{12}E_5$ has substantially greater micellar dimensions ($R_H \approx 12$ nm)[4] deriving from the closeness to T_c.[5]

Figure 3a shows relaxation time distributions for the ternary system containing 0.25% PEO and 10% $C_{12}E_8$ as a function of the measuring angle. The linear relationships between the relaxation rate Γ and q^2 shown in Figure 3b for both peaks demonstrate diffusive processes.

Figure 4 shows the changes in the relaxation time distributions for the PEO/$C_{12}E_8$/water system at four surfactant concentrations between 1 and 15% as the concentration of PEO is progressively increased. At a given surfactant concentration above 1%, the relative amplitude of the slow mode associated with the PEO/$C_{12}E_8$ clusters increases significantly as the PEO concentration is increased. It is noted that the peak ascribed to the complex at low surfactant concentrations has a relaxation time similar to that for the pure PEO (Figure 1b). The complex relaxation time then increases as the

(12) Nilsson, P. G.; Wennerström, H., Lindman, B. *J. Phys. Chem.* **1983**, *87*, 1377.
(13) Brown, W.; Zhou, P.; Rymdén, R. *J. Phys. Chem.* **1988**, *92*, 6086.
(14) Kalashnikov, V. N.; Kudin, A. M. *Nature* **1973**, *23*, 63.
(15) Devanand, K.; Selser, J. C. *Nature* **1990**, *343*, 739.

unesp

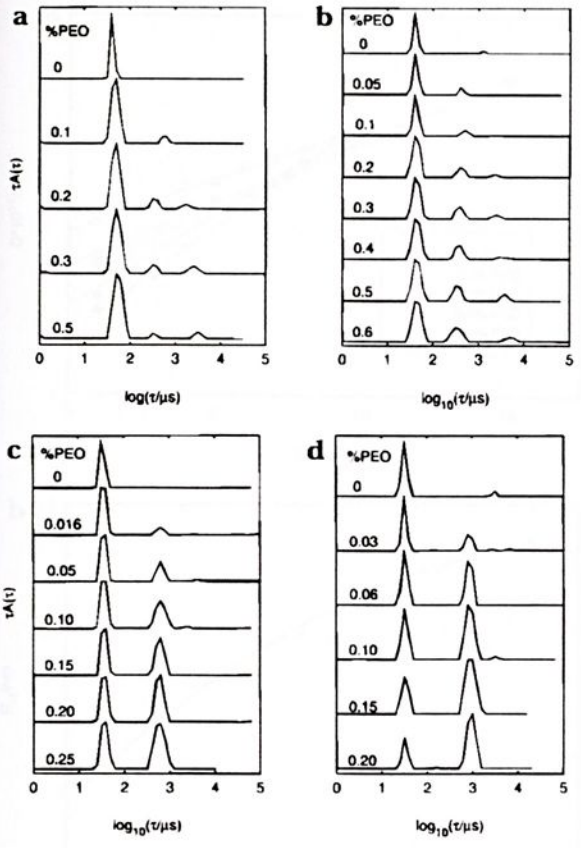


Figure 4. Relaxation time distributions for the PEO/$C_{12}E_8$/water system at different surfactant concentrations with progressive increase in the PEO concentration as shown; T = 20 °C and θ = 90°: (a) 1% $C_{12}E_8$; (b) 5% $C_{12}E_8$; (c) 10% $C_{12}E_8$; (d) 15% $C_{12}E_8$.

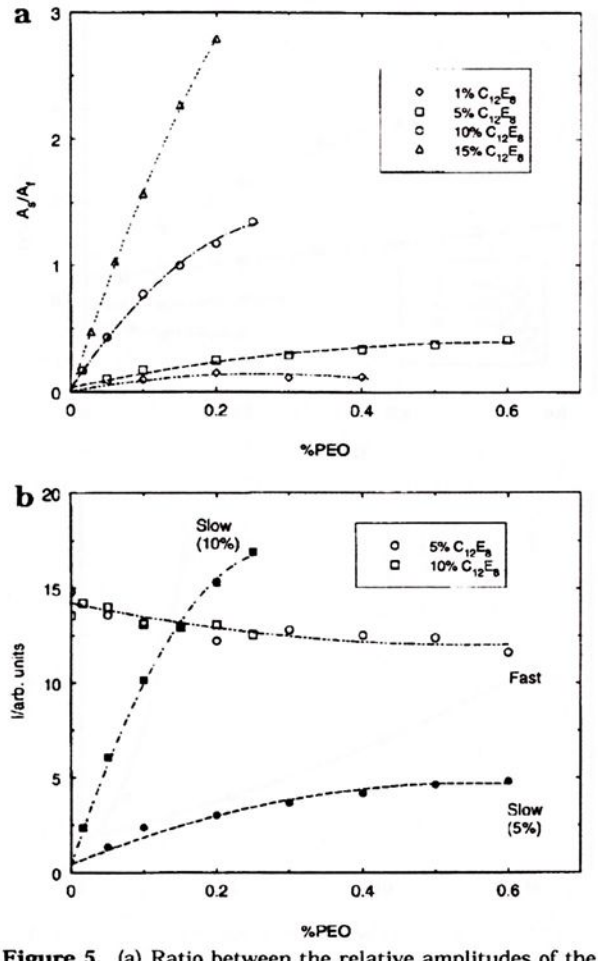


Figure 5. (a) Ratio between the relative amplitudes of the slow and fast modes as a function of PEO concentration at different $C_{12}E_8$ concentrations; T = 20 °C and θ = 90°. (b) Influence of PEO concentration on the scattered intensity of the fast and slow modes at two concentrations of $C_{12}E_8$, as shown; T = 20 °C and θ = 90°.

$C_{12}E_8$ concentration is increased at a constant level of PEO. But, clearly, the interaction between the surfactant and the polymer increases with the increasing concentration of both components. Similar behavior was observed for the $C_{12}E_5$/PEO mixtures.[4]

Figure 5a illustrates the effect on the ratio of the slow to fast mode amplitudes A_s/A_f of increasing the PEO concentration at different $C_{12}E_8$ concentrations; the effect is strongest at high surfactant concentration. Figure 5b shows the fast and slow mode scattering intensities at two $C_{12}E_8$ concentrations (5 and 10 wt %); the fast mode intensity is essentially independent of the PEO and surfactant concentrations whereas the slow mode intensity increases more strongly with the polymer concentration. It is assumed here that, at the highest surfactant concentration, the coil is saturated with surfactant and the surplus surfactant molecules aggregate as free micelles.

The dependence of the fast mode diffusion coefficient on the surfactant concentration at several constant PEO concentrations is shown in Figure 6a. At a given PEO concentration, the diffusion coefficient of the fast mode increases linearly with the $C_{12}E_8$ concentration. With a change in the PEO concentration the slope increases while the intercept decreases. The hydrodynamic radius of the free $C_{12}E_8$ micelles (obtained from the fast diffusion coefficient at infinite dilution of surfactant using Figure 6a) is shown as a function of the PEO concentration in Figure 6b. Assuming for simplicity, a constant interaction with change in PEO concentration, the results would suggest that R_H increases and approaches a limiting value of about 4.5 nm at high PEO concentration; i.e., there is an apparent micellar growth on adding the polymer. This behavior, which could be further elucidated using neutron-scattering experiments, stands in contrast to that found for the anionic surfactant SDS together with PEO, where the polymer chain apparently stabilizes smaller SDS micelles at a lower cac.[12] Neither was a similar apparent growth of the free micelles observed in the PEO/$C_{12}E_5$ system,[4] over the range of PEO concentration examined (C_{PEO} < 0.3 wt %). However, both the size and the intermicellar interactions may change in the presence of PEO, and it will then not be possible in the ternary system to unambiguously distinguish between changes in size and interactions using the present approach.

Data for the slow mode are depicted in Figure 7a. The diffusion coefficient at infinite dilution PEO decreases, as do the slopes with increasing surfactant concentration. Figure 7b shows the variation in apparent R_H for the PEO coil (data at zero concentration PEO from Figure 7a) as the $C_{12}E_8$ (respectively, $C_{12}E_5$) concentration is increased (the curve for $C_{12}E_5$ has been taken from ref 4a). Here again, there is unavoidable ambiguity, owing to possible concurrent changes in dimensions and interactions. It is also possible that the draining characteristics of the PEO coil change in the presence of surfactant clusters within the coil. It is important to note that in Figure 7b R_H increases, starting from the value found in the binary

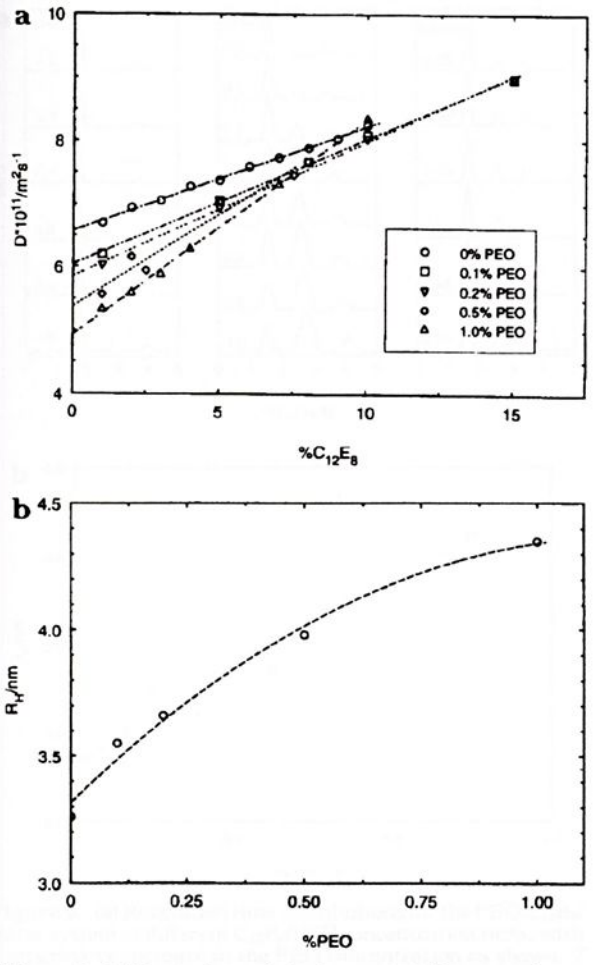


Figure 6. (a) Dependence of the fast mode diffusion coefficient on surfactant concentration for the PEO/$C_{12}E_8$ water system at different PEO concentrations; T = 20 °C and θ = 90°. (b) Dependence of the apparent hydrodynamic radius (obtained at zero surfactant concentration) of the free micelles (fast mode) on PEO concentration- data using the intercepts in part a.

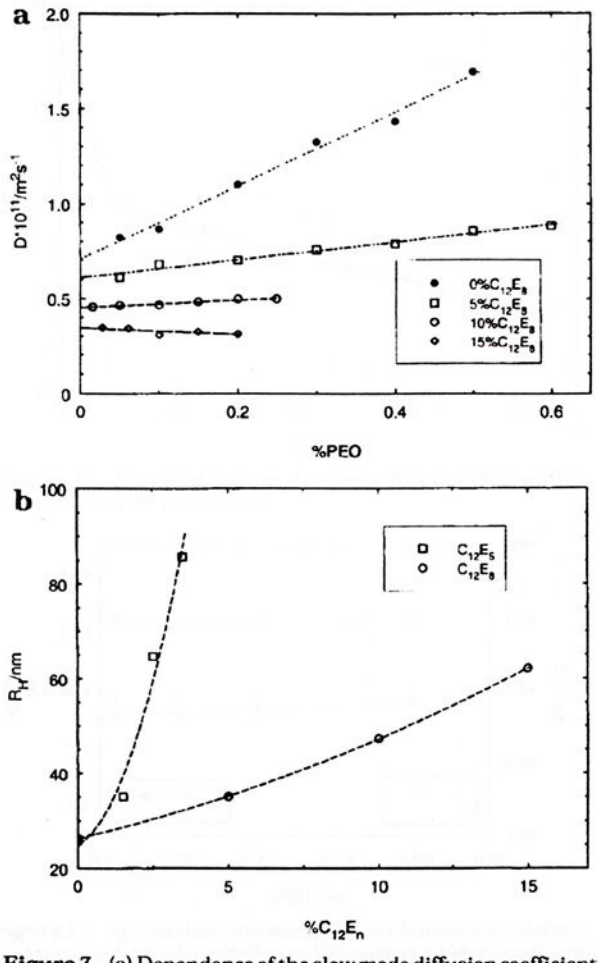


Figure 7. (a) Dependence of the slow mode diffusion coefficient on the PEO concentration for the PEO/$C_{12}E_8$/water system at different surfactant concentrations as shown; T = 20 °C and θ = 90°. (b) Dependence of the apparent hydrodynamic radius of the coil/micellar cluster complex (slow mode) on the $C_{12}E_8$ concentration; (data in part a extrapolated to zero PEO concentration). For comparison, data for the $C_{12}E_5$/PEO system taken from ref 4 are included

PEO/water system with both surfactants. Assuming, for argument, similarity in their interaction patterns, the major difference with $C_{12}E_8$ compared to the $C_{12}E_5$ system would be that the PEO coil expansion with $C_{12}E_8$ is much less pronounced. A lower level of interaction with $C_{12}E_8$ is supported by the observation that, at a similar composition (i.e. a similar ratio of components) and temperature, the relative amplitude of the slow complex mode is always much smaller in the $C_{12}E_8$ system compared to $C_{12}E_5$. This behavior is in agreement with the lower T_c value for $C_{12}E_5$. As would be anticipated, the tendency to form micellar clusters driven by the excluded volume of the added polymer is much lower with the small $C_{12}E_8$ micelles in comparison with bulky $C_{12}E_5$ micelles.

Figure 8 shows changes in the relaxation time distributions on increasing the $C_{12}E_8$ concentration at two PEO levels (0.1 and 0.2%). The relative amplitude of the more slowly relaxing PEO/$C_{12}E_8$ complex increases as the surfactant concentration is increased. The trend is analogous to the effect of adding PEO at constant surfactant concentration (Figure 4). Similar trends were observed for the PEO/$C_{12}E_5$ system.[4]

Figure 9a shows the relaxation time distributions for three R= $C_{12}E_8$/PEO concentration ratios with increasing PEO concentration. At R= 2.0 the distributions are close to single exponential, whereas at R = 10 and R = 15 the

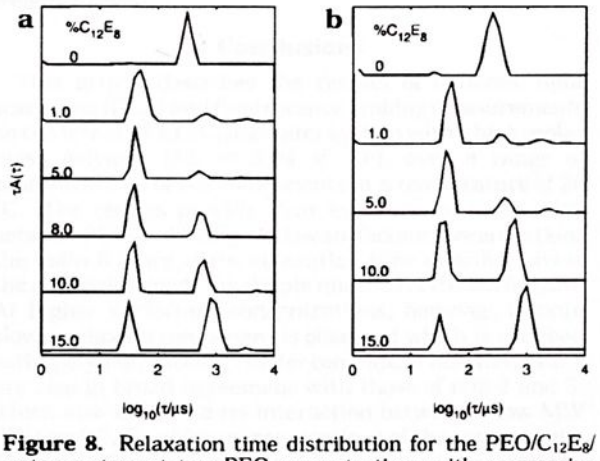


Figure 8. Relaxation time distribution for the PEO/$C_{12}E_8$/water system at two PEO concentrations with progressive increase of the surfactant concentration, as shown; T = 20 °C and θ = 90°. (a) 0.1%P EO; (b) 0.2% PEO.

PEO/micellar cluster complex is present together with an even slower component; see also Figure 4a and b. The presence of the slowest component in the relaxation time distribution was recognized in earlier studies (ref 4) and

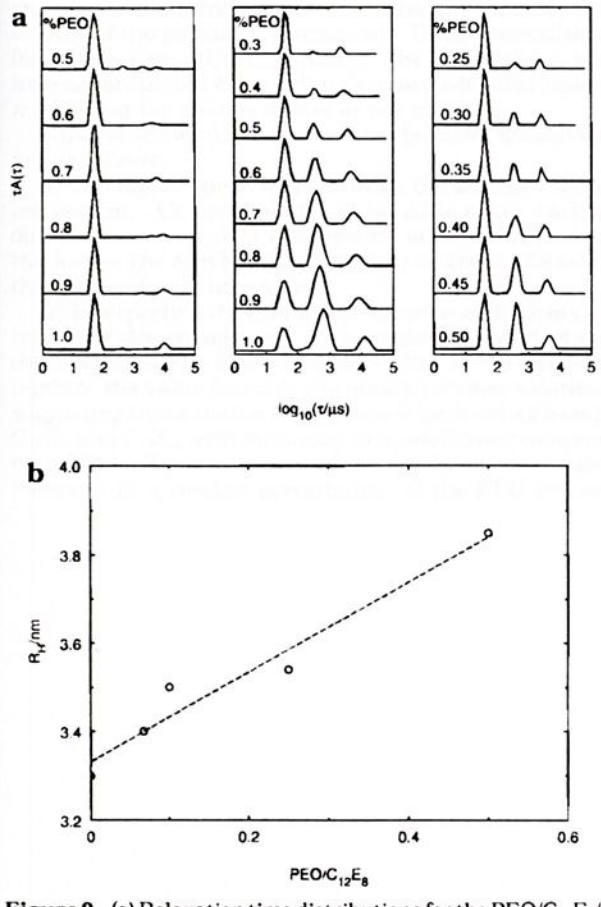


Figure 9. (a) Relaxation time distributions for the PEO/$C_{12}E_8$/water system at different $C_{12}E_8$/PEO concentration ratios with a progressive increase in the PEO concentration as shown; $T = 20$ °C and $\theta = 90°$: (left) $R = 2$; (center) $R = 10$; (right) $R = 15$. (b) Dependence of the apparent hydrodynamic radius of the free micelles (fast mode) on the PEO/$C_{12}E_8$ concentration ratio. Measurements at 20 °C and $\theta = 90°$.

possibly derives from $C_{12}E_8$ clusters existing outside the PEO coils. The approximate size of the latter is in the range 240−750 nm.

As discussed above, the amplitude of the complex mode increases with both the polymer concentration and the value of the ratio R.

The effect of the PEO/$C_{12}E_8$ ratio (R^{-1}) on the apparent hydrodynamic radius of the free micelles of $C_{12}E_8$ is shown in Figure 9b. R_H increases approximately linearly with R^{-1}, which is similar to the dependence of R_H on PEO concentration at zero surfactant concentration shown in Figure 6b.

As in the $C_{12}E_5$/PEO/water system,[4] the clouding temperature of the $C_{12}E_8$/PEO/water system decreases strongly on increasing the concentration of each component.

Figure 10 illustrates the change in T_c on adding PEO while holding constant the surfactant concentration at 15%. The higher the $C_{12}E_8$ concentration at a given PEO concentration, the lower is T_c.

Fluorescence quenching measurements were used to monitor possible changes in aggregation number (N_{agg}) on addition of high molecular weight PEO to 10 wt % $C_{12}E_8$ solutions at 20 °C. The results are summarized in Figure 11, which shows that, within the limits of experimental error, no significant change in N_{agg} is found on incorporation of up to 0.2% PEO. The fluorescence lifetime

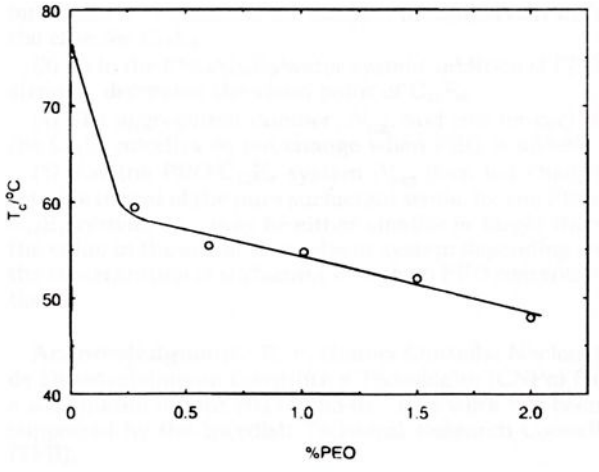


Figure 10. Clouding temperature as a function of the PEO concentration at 15% $C_{12}E_8$.

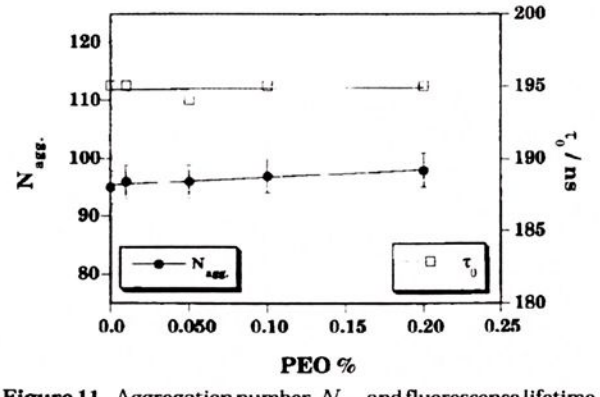


Figure 11. Aggregation number, N_{agg}, and fluorescence lifetime of pyrene, τ_0, for $C_{12}E_8$ micelles at 10% w/w as a function of high molecular weight PEO concentration at 20 °C.

of monomeric pyrene also remains nearly constant at 195 ns over the same concentration interval, showing that the presence of PEO does not significantly alter the microenvironment. These results are in agreement with the results of Anthony and Zana[2] using low molecular weight PEO.

Conclusions

This article describes the results of dynamic light scattering (DLS) and fluorescence probing measurements on the ternary PEO/$C_{12}E_8$/water system with a high molar mass polymer ($M_w = 5.94 \times 10^5$), over a range of concentrations of the components at a temperature of 20 °C. The results provide clear evidence for interaction between PEO and $C_{12}E_8$. At low surfactant concentrations the main feature of the relaxation time distributions is the relaxation mode for simple micelles of the surfactant. At higher surfactant concentrations, however, a more slowly relaxing component is observed which is ascribed to the polymer/micellar cluster complex. Thus, the results are also in broad agreement with those of refs 2 and 3, which also indicated no interaction between a low MW PEO and $C_{12}E_8$ at low concentrations of the components. The main difference between the present system and those of refs 2 and 3 is the high molar mass of the present polymer. Our results suggest that the higher the polymer molar mass, the greater its interaction with nonionic surfactants. This behavior is qualitatively similar to that earlier observed for the PEO/$C_{12}E_5$/water system.[4] We conclude that the underlying mechanism is that micellar

clusters form within the PEO coils, driven by the excluded volume of the polymeric component. Thus, generalizing for the system PEO/C_mE_n/water, the strength of the interaction should be found to decrease with increasing n following the change in size of the micelles.

Although drawn from limited data, the main conclusions are as follows:

(1) The higher the MW of the PEO, the stronger is the interaction. Comparing the data with those earlier obtained on the $C_{12}E_5$/PEO system,[4] one concludes that the longer the ethylene oxide moiety in the surfactant, the weaker is the interaction.

(2) Interpreting the changes in diffusion coefficients as reflecting size change only, on decreasing the surfactant concentration, the hydrodynamic radius of the complex tends to the value found in the binary polymer solution, suggesting that a similar mechanism is involved with both $C_{12}E_5$ and $C_{12}E_8$ with formation of a coil/cluster complex with PEO. The smaller size of the $C_{12}E_8$ micelles leads, however, to a smaller perturbation of the PEO coil on formation of the coil/cluster complex in comparison with the case for $C_{12}E_5$.

(3) As in the PEO/$C_{12}E_5$/water system, addition of PEO strongly decreases the cloud point of $C_{12}E_8$.

(4) The aggregation number, N_{agg}, and cmc (or cac) of the $C_{12}E_8$ micelles do not change when PEO is added.

(5) For the PEO/$C_{12}E_8$ system N_{agg} does not change relative to that of the pure surfactant while, for the PEO/$C_{12}E_5$ system, N_{agg} may be either smaller or larger than the value in the surfactant/solvent system depending on the concentration of surfactant at a given PEO concentration.

Acknowledgment. E. F. thanks Conselho Nacional de Desenvolvimento Científico e Tecnológico (CNPq) for a stipendium (Grant 201720/93-0). This work has been supported by the Swedish Technical Research Council (TFR).

LA960478+

artigo VI

cm 1 2 3 4 5 6 7 unesp 1 12 13 14 15 16 17 18

Articles

Fragment and Vesicle Structures in Sonicated Dispersions of Dioctadecyldimethylammonium Bromide

Eloi Feitosa[†] and Wyn Brown*[,‡]

Department of Physics, IBILCE/UNESP, São José do Rio Preto, SP, Brazil, and Institute of Physical Chemistry, University of Uppsala, Box 532, 751 21 Uppsala, Sweden

Received November 22, 1996. In Final Form: May 30, 1997[⊗]

Dynamic light scattering has been used to investigate sonicated aqueous dispersions of dioctadecyldimethylammonium bromide (DODAB). The hydrodynamic radius (R_H) of the scattering particles and the mean scattering intensity (I) have been monitored as functions of the DODAB concentration and temperature (T). In the dilute regime, the relaxation time distribution of the sonicated dispersion of DODAB is bimodal with the slow mode dominating the distribution. The slow and fast modes are respectively characteristic of vesicles and bilayer fragments with R_H values of 22 and 8.5 nm (25 °C) and 20 and 6 nm (50 °C), respectively. The total scattered intensity initially decreased with temperature up to 45 °C (T_c), above which it was constant; identical behavior was observed for the slow mode intensity, but the fast mode intensity was constant with temperature change, showing that T_c is a property of the vesicles and not of the bilayer fragments. At T_c the slow vesicle mode becomes narrower whereas the fast fragment mode shows no change. On aging, the dispersion showed a slow transition from bimodal to a rather broad single-modal relaxation time distribution. The corresponding R_H was 33.8 nm when measured 10 months after preparation. These results suggest that aqueous sonicated dispersions of DODAB are metastable.

Introduction

The function of vesicles or liposomes derived either from natural or synthetic amphiphiles, such as phospholipids or detergents, as models for biological membranes,[1] carriers of drugs,[2] or modifiers of the rates and mechanisms of chemical reactions[3] requires knowledge of the structural properties of these systems. Unlike phospholipid vesicles,[4] synthetic amphiphile vesicles are unstable in the presence of salts.[5] Such instability greatly limits the applicability of these aggregates. The water insolubility of long double-chained amphiphiles has led to the development of a number of methods of preparation of vesicle structures[6−9] possessing quite different physical properties, such as size, permeability, osmotic behavior, stability, capability for entrapping solutes, and so on.

Since the first use of dialkylated quaternary ammonium salts in the preparation of closed bilayer-like structures[10,11] called vesicles, in 1977, many research groups have sought improved methods for preparing vesicles which are stable and monodisperse. The success of vesicles as membrane model systems depends on these features. Useful vesicular systems should be long-lived and have narrow size distributions. In spite of many investigations, these aspects, as well as the vesicle size itself, are difficult to control. Recently two groups have emphasized the inefficiency of the probe sonication method for preparing vesicles from two widely-used amphiphiles: dioctadecyldimethylammonium chloride (DODAC)[12,13] and dihexadecyl phosphate (DHP).[14] They found that probe-sonicated dispersions consist mainly of bilayer fragments rather than closed vesicle structures. The present article shows that bath-sonicated dispersions of dioctadecyldimethylammonium bromide (DODAB) are metastable in the sense that they evolve slowly to a more polydisperse distribution and consist of a mixture of fragments and vesicle structures.

Different sizes of DODAX (X = Cl, Br) vesicles are described in the literature, measured either by dynamic light scattering or electron microscopy.[15−20] Such discrepancies are understandable, since differing physical conditions may be used during sample preparation, which influences the final properties of the dispersions. Furthermore in these references, either probe- or bath-type sonication methods have been used, which may yield

[†] IBILCE/UNESP.

[‡] University of Uppsala.

[⊗] Abstract published in *Advance ACS Abstracts,* July 15, 1997.

(1) Fendler, J. H. *Membrane Mimetic Chemistry*; Wiley-Interscience: New York, 1982.
(2) Ostro, M. J. *Sci. Am.* **1987**, *256*, 102.
(3) Kawamuro, M. K.; Chaimovich, H.; Abuin, E. B.; Lissi, E. A.; Cuccovia, I. M. *J. Phys. Chem.* **1991**, *95*, 1458.
(4) Ohki, S.; Roy, S.; Ohshima, H.; Leonards, K. *Biochemistry* **1984**, *23*, 6126.
(5) Carmona-Ribeiro, A. M.; Yoshida, L. S.; Chaimovich, H. *J. Phys. Chem.* **1985**, *89*, 2928.
(6) Szoka, F., Jr.; Papahadjopoulos, D. *Annu. Rev. Biophys. Bioeng.* **1980**, *9*, 467.
(7) Lasic, D. D. *Biochem. J.* **1988**, *256*, 1.
(8) Cuccovia, I. M.; Aleixo, R. M. V.; Mortara, R. A.; Berci Filho, P.; Bonilha, J. B. S. *Tetrahedron Lett.* **1979**, 3065.
(9) Carmona-Ribeiro, A. M.; Yoshida, L. S.; Sesso, A.; Chaimovich, H. *J. Colloid Interface Sci.* **1984**, *100*, 433.
(10) Kunitake, T.; Okahata, Y. *J. Am. Chem. Soc.* **1977**, *99*, 3860.
(11) Kunitake, T.; Okahata, Y.; Tamaki, K.; Kumamaru, F.; Takayanagi, M. *Chem. Lett.* **1977**, 387.
(12) (a) Pansu, R. B.; Lan, L.; Faure, J.; Roncin, J. *New J. Chem.* **1990**, *14*, 105. (b) Pansu, R. B.; Arrio, B.; Roncin, J.; Faure, J. *J. Phys. Chem.* **1990**, *94*, 796.
(13) Andersson, M.; Hammarström, L.; Edwards, K. *J. Phys. Chem.* **1995**, *99*, 14531.
(14) (a) Liu, L.; Pansu, R. B.; Faure, J.; Ronein, J.; Arrio, B.; Lapouyade, R. *Res. Chem. Intermed.* **1995**, *21*, 765. (b) Hammarström, L.; Velidian, I.; Karlsson, G.; Edwards, K. *Langmuir* **1995**, *11*, 408. (c) Liu, L.; Pansu, R. B.; Roncin, J.; Arrio, B.; Lapouyade, R. *Res. Chem. Intermed.* **1995**, *21*, 777.
(15) Herman, U.; Fendler, J. H. *Chem. Phys. Lett.* **1979**, *64*, 270.
(16) Regen, S. L.; Czech, B.; Singh, A. *J. Am. Chem. Soc.* **1980**, *102*, 6640.
(17) Pileni, M.-P. *Chem. Phys. Lett.* **1980**, *71*, 317.
(18) Carmona-Ribeiro, A. M.; Chaimovich, H. *Biophys. J.* **1986**, *50*, 621.
(19) Cuccovia, I. M.; Feitosa, E.; Chaimovich, H.; Sepulveda, L.; Reed, W. *J. Phys. Chem.* **1990**, *94*, 3722.
(20) Carmona-Ribeiro, A. M.; Midmore, B. R. *J. Phys. Chem.* **1992**, *96*, 3542.

S0743-7463(96)02034-3 CCC: $14.00 © 1997 American Chemical Society

unesp

Table 1. R_H Values from the Literature for Small Unilamellar Vesicles of DODAX in Water Prepared by Ultrasonic Irradiation Procedures

surfactant	sonication method	R_H/nm	ref
DODAC	probe	24.2	17
	bath	26.5	19
	probe	39.6	15
	probe	80.0	12b
DODAB	bath	32.5	19
	bath	22.0	this work

vesicles with quite different sizes and polydispersities. Table 1 summarizes some R_H values from the literature for small unilamellar vesicles of DODAX prepared by either the tip- or bath-sonification procedures. Different preparations may give significantly different vesicle sizes if a particular procedure for vesicle preparation is not followed rigorously. This constitutes a major difficulty of the sonication methods. Among the key conditions are the temperature, power, time and type of sonication, amphiphile concentration, volume of solution, filtering procedure (such as centrifugation or gel and membrane filtrations), type and pore size of the filtering membrane, purity of monomers, solvent quality, or even the flask geometry in the bath-sonication procedure. It is not well understood how or whether all of these conditions affect the vesicle structure. Concerning polydispersity and stability, there are references to mono-[21] and polydisperse,[12] stable,[14,22] metastable,[23] and unstable[20,24] vesicles. Attempts to improve vesicle stability include the use of aqueous or organic additives (*e.g.*, cholesterol, sucrose, etc.), buffer solutions, and also polymerized monomers.[1]

Light-scattering techniques are suitable for the investigation of supramolecular aggregates in suspension, *e.g.*, micelles,[25] microemulsions,[26] or vesicles.[14,16,18,19,27] Inverse Laplace transform (ILT) analysis of the intensity time correlation function may be used to obtain the relaxation time distribution for simple unimodal and more complex multicomponent systems, for example polydisperse macromolecular solutions.[28] This method has been applied in the study of complex association between ionic and nonionic micelle-forming surfactants and charged or neutral water-soluble polymers or block copolymers.[29-31] Here we report ILT analysis of bath-sonicated dispersions of DODAB in water. The results show that the dispersions are intrinsically polydisperse and that the main structure is vesicular. The degree of polydispersity represented by the number, relative amplitude, and width of the modes of the relaxation time distribution is a function of physical variables, such as the amphiphile concentration, ionic strength, temperature, and vesicle age. For many purposes, however, sonicated vesicles under conditions of low surfactant concentration, low ionic strength, or high temperature (above the T_c) are close to monodisperse and stable for several months.

Materials and Methods

Dioctadecyldimethylammonium bromide (DODAB) was used as purchased from Sigma without further purification; NaCl (Merck, Germany) was analytical grade. High-purity (MilliQ-plus) water was used for vesicle preparations. A volume (V) of DODAB solution (C_a molar) was prepared by magnetically stirring the dispersion (until complete dissolution of the crystals) at a temperature above the T_c of the surfactant. The solution was placed in a bath-type ultrasonic radiation apparatus (model Decon FS100, Ultrasonics Ltd., England) for time t and temperature above T_c (about 55 °C). Since the efficiency of sonication varies with time, we chose the sonication time needed to obtain a clear solution. A sonication time of 2.5 h and a temperature of 55 °C were used. The volume and concentration of the sonicated dispersion were, respectively, 10 mL and 10 mM. We have compared the efficiency of two different glass flasks, a round-bottomed cylinder (2 cm × 18 cm) and an Erlenmeyer-type flask. The cylindrical flask proved much more efficient, requiring a considerably shorter time of sonication. After sonication the stock solution was cooled and stored at room temperature. The samples were prepared by dilution of a stock solution and then filtered through 0.45 μm Millipore membranes; 0.20 μm pore-size membranes were also used for comparison. The nonsonicated dispersions were filtered using a 0.45 μm filter above T_c.

Surface tension (γ) measurements were done by the drop-volume technique.[32] A volume of solution was gradually extruded through a capillary by a step-motor connected to an oscillator which generates constant pulses. The drops were formed at the rate 100 Hz. The volume of a drop, $V = R^*P$, is obtained from the measured pulse number per drop (P), where R is the rate of drop formation (1.64×10^{-11} m^3/pulse). The surface tension (γ) is given by

$$\gamma = r^2 \Delta\rho g / \{2[\Phi(r/V^{1/3})]^2\} \qquad (1)$$

where $\Delta\rho$ is the difference in densities of the two phases, g is the local gravity acceleration, r is the tip's radius (1.75×10^{-3} m), and $\Phi(r/V^{1/3})$ is a correction factor which accounts for the nonsphericity of the drop.[33]

Dynamic light-scattering measurements were made using a 633 nm He/Ne laser as light source, and the detector system consists of an ITT FW 130 photomultiplier connected to an ALV-Langen Co. multibit, multitau autocorrelator through a digitalized Nuclear Enteprises amplifier/discriminator system. Details of the experimental arrangement may be found elsewhere.[30]

The ILT analysis of the measured intensity time correlation function, $g_2(t)$, was performed using the algorithm REPES[28,33] to obtain the relaxation time distribution, $A(\tau)$. The method consists in minimizing the squared difference between the experimental and calculated $g_2(t)$ values, which for polydisperse solutions of particles with a infinite range of size are related to $A(\tau)$ through a Laplace relation:

$$g_1(t) = \int_{-\infty}^{\infty} \tau A(\tau) \exp(-t/\tau)\, \mathrm{d} \ln \tau \qquad (2)$$

where τ is the relaxation time, $g_1(t)$ is the first-order electric field time correlation function, related to $g_2(t)$ according to $g_2(t) - 1 = \beta|g_1(t)|^2$, and β is a factor which accounts for deviations from ideal correlation. The relaxation time distribution is presented as a $\tau A(\tau)$ *versus* $\log_{10} \tau$ profile, with $\tau A(\tau)$ in arbitrary units to provide an equal area representation.[33] The relaxation rates are obtained from the second moment of each mode, $\Gamma = 1/\tau$, where Γ is the relaxation rate. The diffusion coefficient for each mode is calculated from the relation $D = \Gamma/q^2$, in the limit of zero scattering angle θ, where $q = (4\pi n_0/\lambda) \sin(\theta/2)$ is the scattering

(21) Talmon, Y.; Evans, D.; Ninham, B. *Science* **1983**, *221*, 1047.
(22) Carmona-Ribeiro, A. M. *J. Phys. Chem.* **1993**, *97*, 11843.
(23) Brady, J. E.; Evans, D. F.; Kachar, B.; Ninham, B. W. *J. Am. Chem. Soc.* **1984**, *106*, 4279.
(24) Carmona-Ribeiro, A. M. *Chem. Soc. Rev.* **1992**, *21*, 209.
(25) There is an extensive list of papers on the application of light-scattering techniques to micelles in solution. See, for example, the recent review: Magid, L. In *Dynamic Light Scattering. The Method and Some Applications*; Brown, W, Ed.; Clarendon Press: Oxford, 1993; Chapter 13.
(26) Dichrisna, T.; Roux, D.; Bellocq, A. M.; Bothorel, P. *J. Phys. Chem.* **1985**, *89*, 1433.
(27) Ostrowsky, N.; Sornette, D. In *Light Scattering in Liquids and Macromolecular Solutions*; Degiorgio, V., Corti, M., Giglio, M., Eds.; Plenum Press: New York, 1980; p 125.
(28) Johnsen, R. M.; Brown, W. In *Laser Light Scattering in Biochemistry*; Harding, S. E., Sattele, D. B., Bloomfield, V. A., Eds.; Royal Society of Chemistry: Herts, U.K., 1992; p 77.
(29) Schillén, K.; Brown, W.; Johnsen, R. M. *Macromolecules* **1994**, *27*, 4825.
(30) Feitosa, E.; Brown, W.; Hansson, P. *Macromolecules* **1996**, *29* (6), 2169.
(31) Brown, W., Ed. *Dynamic Light Scattering. The Method and Some Applications*; Clarendon Press: Oxford, 1993.
(32) Tornberg, E. *J. Colloid Interface Sci.* **1977**, *60*, 50.
(33) (a) Silkinson, M. C. *J. Colloid Interface Sci.* **1972**, *40*, 14. (b) Jakes, J. *Czech. J. Phys.* **1988**, *B38*, 1305.

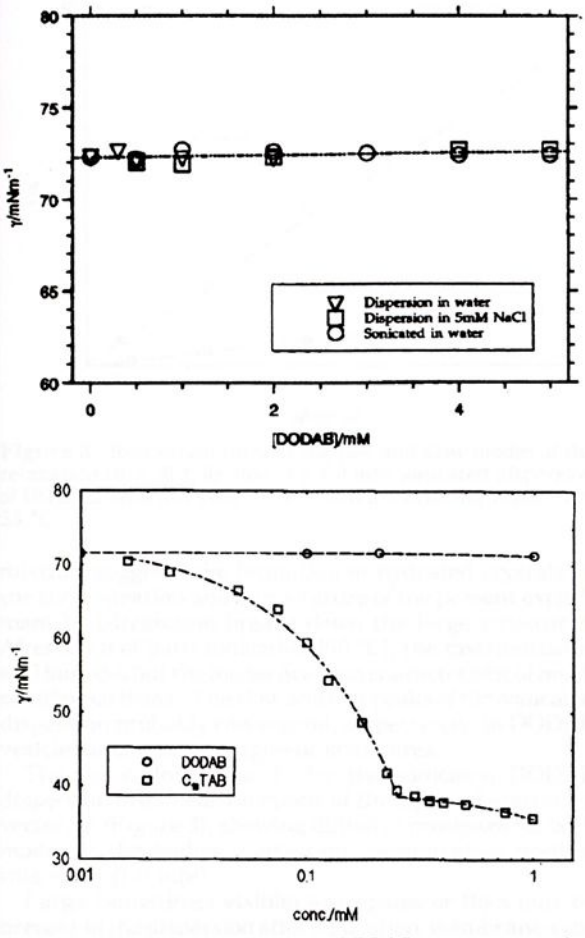


Figure 1. Surface tension *versus* DODAB concentration for the sonicated dispersion in aqueous solution, before and after 2.5 h of bath sonication at 25 °C (a, top) and 40 °C (b, bottom) in 5 mM NaBr.

vector, λ is the wavelength of the incident light, and n_0 is the solvent refractive index. The diffusion coefficient for small particles was shown to be independent of q and is related linearly to the particle concentration (C),

$$D = D_0(1 + k_D C + ...) \quad (3)$$

where k_D is the hydrodynamic "virial" coefficient. D_0 is the diffusion coefficient at infinite dilution, which is related to the hydrodynamic radius (R_H) through the Stokes–Einstein equation,

$$D_0 = k_B T/6\pi\eta_0 R_H \quad (4)$$

where k_B is the Boltzmann constant, T is the absolute temperature, and η_0 is the solvent viscosity.

Results and Discussion

In spite of being much less powerful compared to the probe-sonication method, bath sonication has some distinct advantages. Thus, the latter allows better control of sample temperature and sonication power and also eliminates the risk of contamination with organic solvents and titanium microparticles. The properties of the vesicles formed in this way have as yet not been extensively examined, however. Figure 1 depicts the surface tension (γ) of DODAB dispersions before and after 2.5 h of bath sonication in the presence and absence of monovalent salt (NaCl, 5 mM), as a function of the surfactant concentration, measured at 22 °C. Addition of DODAB up to 10 mM

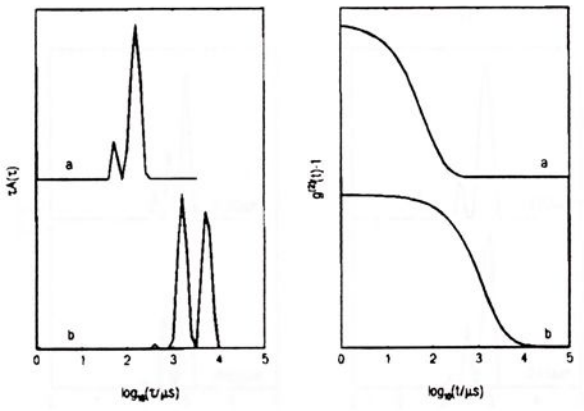


Figure 2. Relaxation time distributions and intensity correlation functions for a 0.1 mM DODAB dispersion in pure water after 2.5 h of sonication (a) and before sonication (b). For the nonsonicated dispersion the measurement was made 2 min after preparation, and the sonicated dispersion, 24 h after preparation. Measurements were made at 25 °C and $\theta = 90°$.

does not change the surface tension of the pure solvent (72.5 mN m^{-1}). The independence of γ on DODAB concentration and the ultrasonic irradiation time (Figure 1) reflects either a low surface activity of the DODAB molecules or a low sensitivity of the drop-volume technique, providing a rapid method but unsuitable for detection of the relatively slow migration of DODAB molecules from the bulk phase to the air/water interface. Recent measurements of γ using a wire loop dipping technique[34] show a decrease of no more than 6% of γ for pure water as DODAB was added up to a concentration of 1 mM, suggesting that usual techniques for determining the cmc of micelle-forming surfactants may be unsuitable for determination of the cmc of vesicle-forming surfactants. Above T_c, DODAB molecules in aqueous solution self-assemble into bilayer structures. The latter aggregated structures persist when the solution is cooled to room temperature. DODAB molecules thus exhibit a critical aggregation concentration (or critical vesicle concentration, cvc) close to zero, prohibiting measurements using a technique such as tensiometry. It has been shown[35a] that, as for the micelle-forming surfactants, there is a linear relationship between log(cvc) and the number of carbon atoms in the dialkyl chain (n), *i.e.*, log(cvc) = 3.495 − 0.6625n. Accordingly, the cvc for DODAB ($n = 18$) is extremely low, 3.7×10^{-9} M.[35b] Figure 1b compares the DODAB solution surface tension *versus* concentration curve with that for the homologous octadecyltrimethylammonium bromide (C_{18}TAB) at 40 °C (above the Krafft point of C_{18}TAB and close to the T_c of DODAB), for which cmc = 0.25 mM from the break point of the curve taken from ref 36.

Figure 2 shows typical normalized intensity correlation functions, $g_2(t) - 1$, and the corresponding relaxation time distributions, $\tau A(\tau)$, at 25 °C, for a 0.1 mM DODAB dispersion in water after 2.5 h of sonication (curves a) and, for comparison, before sonication (curve b). Both distributions are bimodal. The peaks for the nonsonicated dispersion have about the same relative amplitude and show that the solution contains large aggregates. The structures present in the nonsonicated dispersion are still being studied; the phase diagram of the DODAC/water

(34) Benatti, C. R.; Feitosa, E. In preparation.
(35) (a) Klevens, H. B. *J. Am. Oil Chem. Soc.* **1953**, *30*, 74. (b) Svitova, T. F.; Smirnova, Y. P.; Pisarev, S. A.; Berezina, N. A. *Colloids Surf. A* **1995**, *98*, 107.
(36) Swanson-Vathamuthu, M.; Feitosa, E.; Brown, W. *Langmuir*, submitted.

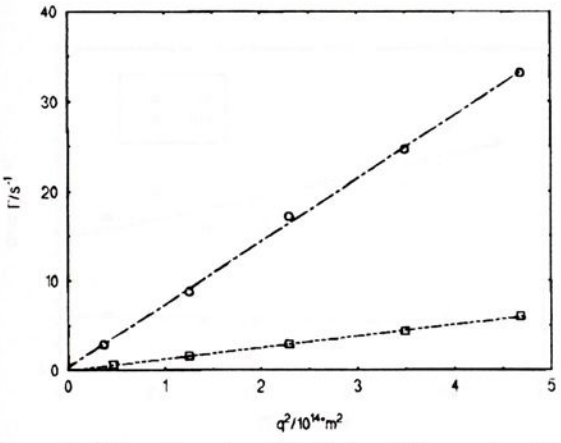


Figure 3. Relaxation rates of the fast and slow modes of the relaxation time distribution of a 1.0 mM sonicated dispersion of DODAB, as a function of the squared scattering vector. T = 35 °C.

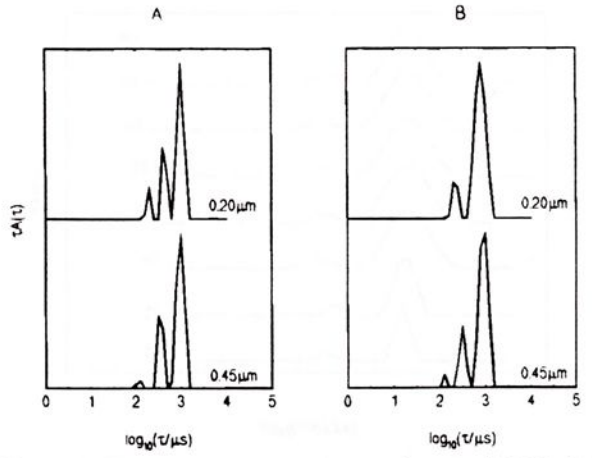


Figure 4. Relaxation time distributions for a 1 mM DODAB sonicated dispersion immediately after (A) and 18 h after (B) preparation, showing the effect of two sizes of Millipore membrane filters, as shown.

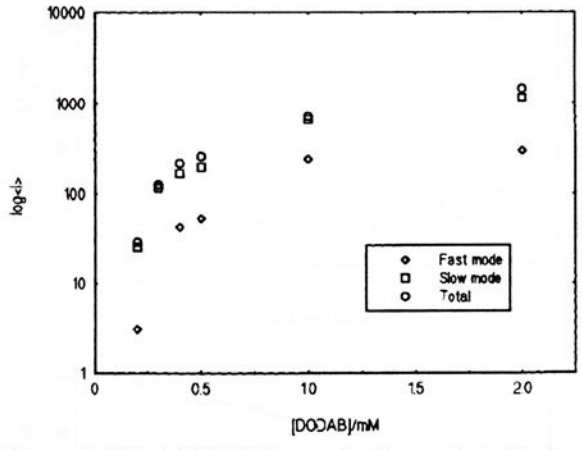


Figure 5. Effect of DODAB concentration on the total, slow, and fast mode scattered intensities of a 2.5 h bath-sonicated dispersion. T = 25 °C and θ = 90°.

mixture suggests the formation of hydrated crystals at the concentration and temperature of the present experiment.[37] Ultrasound breaks down the large structures. After 2.5 h of bath sonication (55 °C), the distribution is still bimodal but the modes are then characteristic of much smaller particles. The slow and fast peaks of the sonicated dispersion probably correspond, respectively, to DODAB vesicles and bilayer fragment structures.

The relaxation rates, Γ, for the sonicated DODAB dispersion are linear functions of the squared scattering vector, q^2 (Figure 3), showing diffusive processes for both modes at the highest surfactant concentration used in this work (1.0 mM).

Large (sometimes visible) aggregates or flocs may be present in the dispersion after sonication; membrane-type filters are commonly used to eliminate these aggregates as well as dust particles which disrupt scattering measurements. Nylon or Millipore filters are mostly used. However, the latter are inadequate for dispersions of cationic surfactants, since they retain considerable amounts of material and also may destroy the vesicle structure. We have compared the effects of filtering the sonicated dispersion of DODAB through two different pore sizes of Millipore membranes (0.20 and 0.45 μm) (Figure 4). It is observed that the smaller pore size retains much more material than the larger one, since the mean scattered intensity is about 60% smaller than when the 0.45 μm filter is used (results not shown). The loss of material, however, preserves the number of peaks and the relative sizes of the populations (Figure 4). Since the 0.45 μm membrane filter retains less material, we used this filter for all the samples. Filtering is important for preparing floc-free vesicle dispersions using the bath-sonication process. Figure 4 also compares the distributions immediately after (A) and 18 h after (B) vesicle preparation; the change in the distributions probably arises because some time is required for the dispersion to attain thermodynamic and mechanical equilibrium after sonication (annealing effect). There is no clear relationship between the apparent R_H or polydispersity and the membrane pore size. The third (fastest mode in Figure 4) peak is probably due to the high DODAB concentration (1.0 mM), which favors the formation of new structures in solution, as will be discussed below.

The contributions of the slow and fast modes in the relaxation time distributions for the scattered intensity of the DODAB sonicated dispersion, measured at 25 °C, are depicted in Figure 5 as a function of the DODAB concentration. The latter shows that the main contribution to the total scattered intensity comes from the slow mode associated with the vesicle structures.

Parts a and b of Figure 6 show, respectively, the effect of DODAB concentration on the diffusion coefficients of the fast and slow modes of the ILT distributions shown in Figure 6c for the sonicated dispersions in water, at 25 and 50 °C, *i.e.*, below and above T_c. At infinite dilution the following mean R_H values were obtained using the Stokes–Einstein relation (eq 4) for the slow and fast modes: 22.2 and 8.5 nm (25 °C) and 19.8 and 6.2 nm (50 °C), respectively. The R_H values obtained for the slow and fast modes are compatible, respectively, with the anticipated sizes of the vesicle and fragment structures. R_H for the fast mode is too small for vesicle structures which are defined by a minimum (critical) radius for the monomers to pack into closed bilayer structures.[38] The latter probably derives from two bilayer fragments of DODAB. Above T_c the effective R_H values of both the vesicles and the fragments are slightly smaller than those at room temperature (below T_c). Below T_c the relaxation

(37) Kunieda, H.; Shimoda, K. *J. Phys. Chem.* **1978**, *82*, 1710.

(38) Israelachvili, J. N. *Intermolecular and Surface Forces*, 2nd ed.; Academic Press: London, 1992.

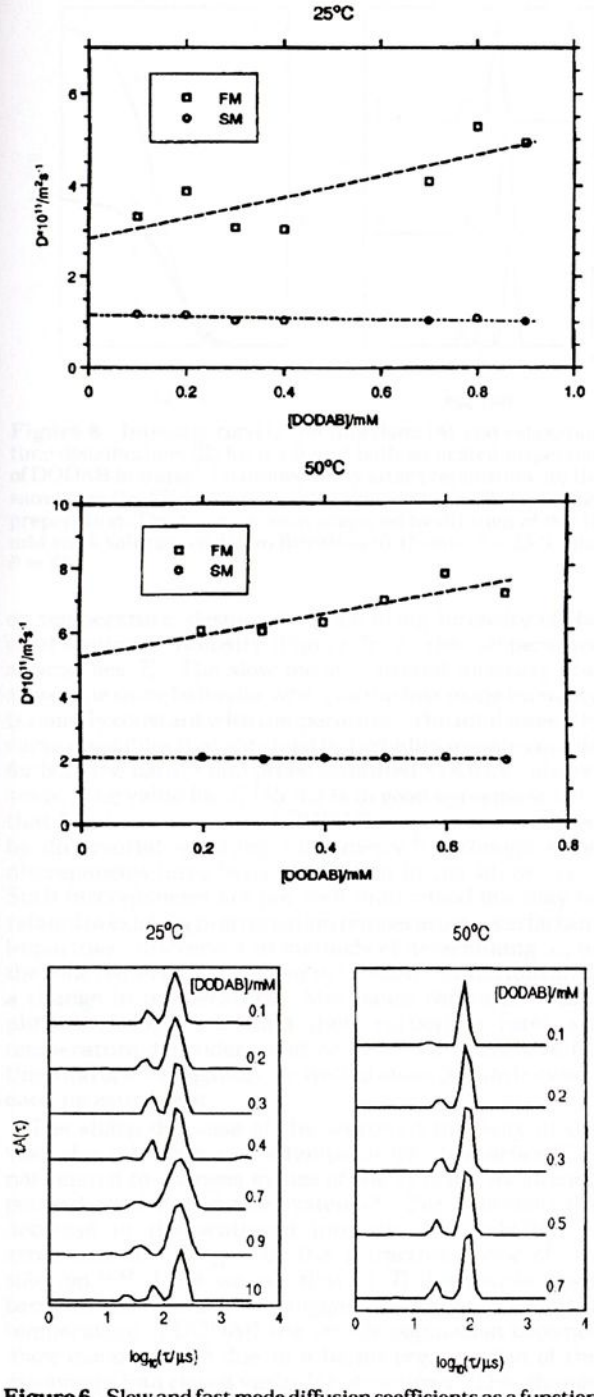


Figure 6. Slow and fast mode diffusion coefficients as a function of DODAB concentration at 25 °C (a, top) and 50 °C (b, middle). $\theta = 90°$. (c, bottom) Relaxation time distributions for a DODAB bath-sonicated dispersion at 25 and 50 °C and progressive increase of DODAB concentration, as shown. $\theta = 90°$.

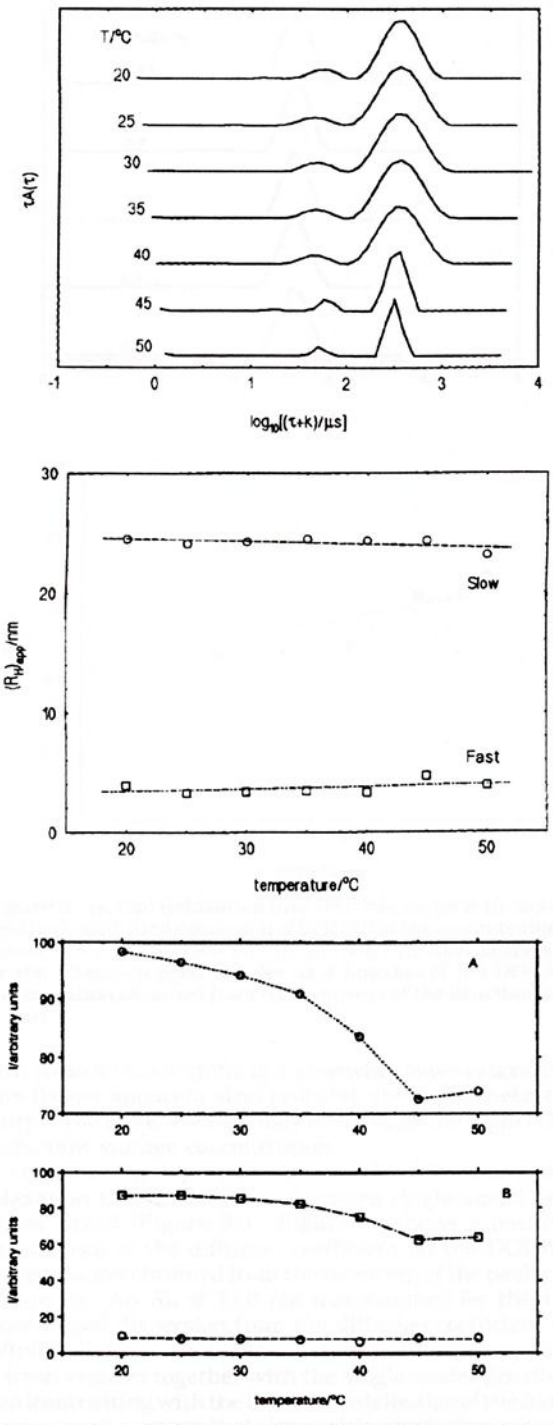


Figure 7. (a, top) Relaxation time distributions for a 1.0 mM bath-sonicated dispersion of DODAB, normalized for the temperature and viscosity, at increasing temperature, as shown. (b, middle) Effect of the temperature on the apparent hydrodynamic radius of the vesicles and fragments obtained, respectively, from the slow and fast modes of the distributions. $\theta = 90°$. (c, bottom) Effect of temperature on the total scattered intensity for a 1.0 mM bath-sonicated dispersion of DODAB (A) and on the slow (vesicle) and fast (fragment) mode scattered intensities (B).

time distribution is only bimodal within the dilute regime, *i.e.*, below ca. 1.0 mM; above this concentration a third (faster) peak appears (Figure 6c). Above T_c the distribution is essentially bimodal with the relative amplitude of the fast mode increasing with the surfactant concentration.

Figure 7a depicts the effect of temperature on the relaxation time distributions of the 2.5 h sonicated dispersion at the DODAB concentration of 1.0 mM. The distributions are shifted on the log τ axis by (T/η) to account for the solvent viscosity change with temperature. At each temperature the distribution is bimodal and the peaks are broadened below about 45 °C (T_c). The corresponding apparent R_H obtained from the moments of the slow and fast modes (Figure 7b) shows no significant dependence

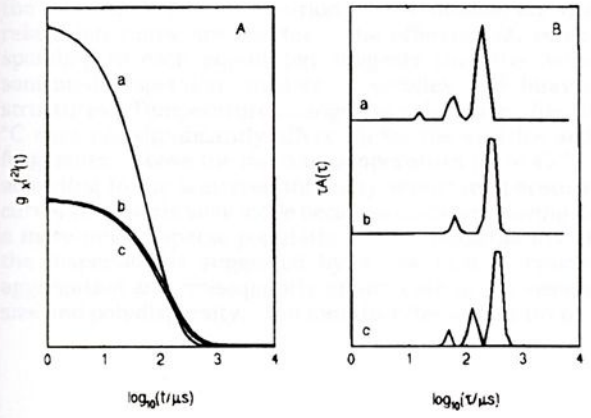


Figure 8. Intensity correlation functions (A) and relaxation time distributions (B) for a 1.0 mM bath-sonicated dispersion of DODAB in water: (a) immediately after preparation; (b) the same sample 17 days later; (c) a new sample 17 days after preparation. The samples were prepared by dilution of the 10 mM stock solution and then filtration (0.45 μm). $T = 25$ °C and $\theta = 90°$.

on temperature, despite the decreasing intensity of the total scattered intensity (Figure 7c) as the temperature approaches T_c. The slow mode scattered intensity also shows the same behavior whereas the fast mode intensity is roughly constant with temperature. The total intensity curve resembles that obtained by turbidity measurements for both the bath-[39] and probe-sonicated[18] DODAC dispersions. The value for T_c (45 °C) is in good agreement with that for the nonsonicated DODAB dispersion measured by differential scanning calorimetry,[40] although some discrepancies have been referred to in the literature.[13] Such discrepancies are not well understood but may be related to existing pretransition temperatures, surfactant impurities, differences in methods of determining T_c, or the time required for the system to reach equilibrium after a change in temperature. Also, since the relative amplitude of the peaks and their relaxation rates are temperature-dependent and equilibrium is decisive for this kind of investigation, we waited about 30 min between each measurement.

The sharp decrease of the scattered intensity of the vesicular solutions as the temperature approaches T_c is not related to changes in size of the vesicles, as already pointed out for liposome systems.[41] For liposomes the decrease in the scattered intensity (or turbidity) is attributed to changes in the refractive index of the solution.[41,42] Here we see that at T_c the vesicle mode becomes visibly narrower, suggesting that at the melting temperature of DODAB the vesicle population becomes more monodisperse due to a better organization of the monomers into closed vesicular structures. This change in the vesicle structure probably influences the solute polarizability.

Figure 8 shows the correlation functions and ILT distributions for the same 1.0 mM DODAB sonicated dispersion measured immediately and 17 days after sonication (curves a and b, respectively). Curve c corresponds to the dispersion stored at the stock concentration (10 mM), diluted to 1.0 mM 17 days after preparation, and then filtered (0.45 μm) before the measurement. The

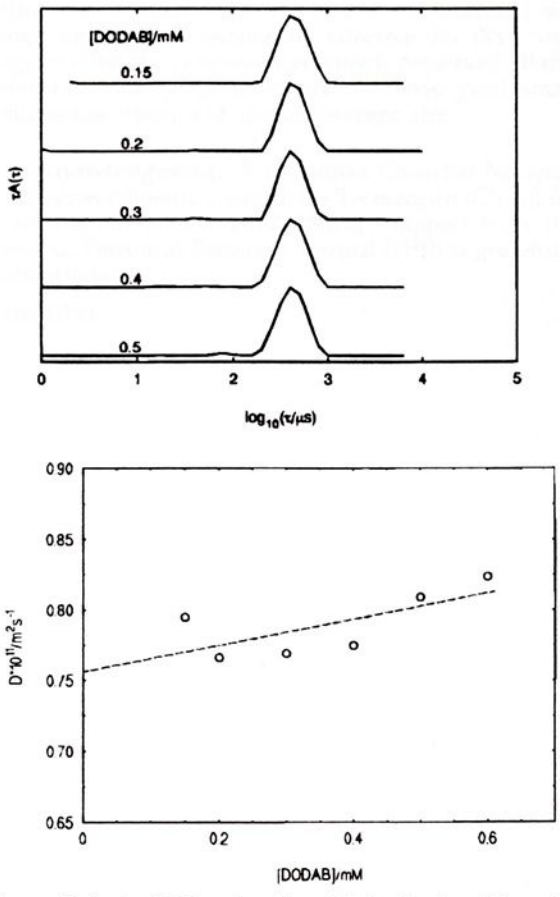


Figure 9. (a, top) Relaxation time distribution for a 10-month aged bath-sonicated dispersion of DODAB at the concentrations shown. $T = 25$ °C and $\theta = 90°$. (b, bottom) Diffusion coefficient for the 10-month aged vesicles as a function of the DODAB concentration obtained from the moments of the distributions in part a.

slow (vesicle) mode shifts to a somewhat lower relaxation rate (larger apparent size) probably due to the metastability of the system, which may be stronger the higher the surfactant storage concentration.

After storing the stock solution for 10 months the relaxation time distribution becomes single-modal and rather broad (Figure 9a). Figure 9b shows a positive dependence of the diffusion coefficient on the DODAB concentration obtained from the moments of the peaks in Figure 9a. An R_H of 33.8 nm was obtained for the 10-month aged dispersion from the diffusion coefficient at infinite dilution. This higher value of R_H relative to that of fresh vesicles together with the single-modal distribution (contrasting with the bimodal distribution of the fresh suspensions) suggests that slow vesicle aggregation occurs. The unfavorable energetic condition of the fragments, owing to the exposure of the hydrocarbon tails to water, contributes as well to the aggregation process.

Conclusions

According to the surface tension measurements, DODAB molecules self-assemble, above T_c, into giant bilayer structures, giving rise to bimodal relaxation time distributions with rather slow relaxation times (large apparent hydrodynamic radii). As a result, the surfactant does not significantly reduce the surface tension of the pure solvent, as is usual with micelle-forming surfactants. Under sonication the vesicle structures become smaller although

(39) Feitosa, E. Ph.D. Thesis, University of São Paulo, Brazil, 1990.
(40) Blandamer, M. J.; Briggs, B.; Cullis, P. M.; Green, J. A.; Waters, M.; Soldi, G.; Engberts, J. B. F. N.; Hoekstra, D. *J. Chem. Soc., Faraday Trans.* **1992**, *88*, 3431.
(41) Yi, P. N.; McDonald, R. C. *Chem. Phys. Lipids* **1973**, *11*, 114.
(42) Disalvo, E. A. *Chem. Phys. Lipids* **1991**, *59*, 199.

the relaxation time distribution is still bimodal but the relaxation times are shorter. The effective R_H corresponding to each population suggests that the bath-sonicated dispersion consists of vesicles and bilayer structures. Temperature change over the range 20−50 °C does not significantly affect R_H for the vesicles and fragments. Above the melting temperature (T_c = 45 °C, according to the scattered intensity *versus* temperature curve) the vesicle slow mode becomes narrower, owing to a more monodisperse population. The metastability of the dispersion is suggested by a low rate of vesicle aggregation and consequently an increase in the vesicle size and polydispersity. Ten months after vesicle preparation the relaxation time distribution is unimodal and broad and the corresponding effective R_H (33.8 nm) suggests that the vesicular structure is preserved. Bath-sonication and probe-sonication methods yield small unilamellar vesicles of similar average size.

Acknowledgment. E.F. thanks Conselho Nacional de Desenvolvimento Científico e Tecnológico (CNPq) for a stipendium (Grant 201720/93-0). Support from the Swedish Technical Research Council (TFR) is gratefully acknowledged.

LA962034J

artigo VII

Mixed Micelles of the Anionic Surfactant Sodium Dodecyl Sulfate and the Nonionic Pentaethylene Glycol Mono-*n*-dodecyl Ether in Solution

Eloi Feitosa[†] and Wyn Brown*[,‡]

Departamento de Física, IBILCE/UNESP, C.P. 136, 15054-000, São José do Rio Preto, SP, Brazil, and Department of Physical Chemistry, University of Uppsala, Box 532, 751 21, Uppsala, Sweden

Received February 5, 1998. In Final Form: May 20, 1998

Dynamic light scattering, surface tension, and clouding temperature have been monitored to elucidate the solution properties of mixed micelles formed between the anionic surfactant sodium dodecyl sulfate (SDS) and the nonionic surfactant pentaethylene glycol mono-*n*-dodecyl ether ($C_{12}E_5$) over a wide range of surfactant concentration and temperature. Addition of 0.1 M NaCl shifts the relaxational modes to higher frequency and lowers the clouding temperature (T_c) of the nonionic surfactant solution by about 1 °C compared to the salt-free system. T_c for the mixed surfactant solutions is higher than that of the binary $C_{12}E_5$ solutions and depends sensitively on the concentration of the two surfactants but increases only slightly when the total surfactant concentration is increased at a given molar $C_{12}E_5$/SDS concentration ratio. With $C_{12}E_5$/SDS = 5.7, for example, T_c is 46.0 and 47.5 °C, respectively, at 5 and 70 mM of $C_{12}E_5$. The mixed solutions are homogeneous and stable and contain nonspherical micelles, which are close to monodisperse over a range of surfactant concentrations and temperature. The mixed system has a lower Krafft point than binary SDS solutions and shows an approximately ideal behavior in contrast to the binary $C_{12}E_5$ solution. The hydrodynamic radius (R_H) of the mixed micelle increases with temperature as do $C_{12}E_5$ micelles in the binary solutions and also with increasing $C_{12}E_5$/SDS ratio. At 25 °C, the critical micelle concentration of the mixed solution lies between those of the individual surfactants and decreases as the $C_{12}E_5$/SDS ratio is increased.

Introduction

There is considerable interest in micellar structures and the solution behavior of surfactants having different hydrophobic/hydrophilic structures and/or charge. The so-called mixed micelles possess well-defined physical properties that typically are intermediate between those of the individual surfactants. Mixed micelles of surfactants having differing lengths of the alkyl chain and/or polarity of the headgroup have been extensively investigated.[1] Ionic/ionic, ionic/nonionic, or nonionic/nonionic surfactant mixtures have been studied by experimental[2-7] and theoretical[8] approaches. This work is concerned with mixed micelles of an anionic (SDS) and a nonionic surfactant ($C_{12}E_5$) in solution.

Hydrated salts of sodium dodecyl sulfate (SDS, $C_{12}H_{25}SO_4^-Na^+$) self-assemble above the critical micelle concentration (cmc) of the surfactant into small negatively charged micelles. The latter have been extensively investigated at different temperatures and concentrations of the surfactant and supporting electrolytes[9] as well as mixed with other surfactants,[10] polymers,[11] or proteins.[12] At low electrolyte and surfactant concentrations, SDS micelles are spherical in aqueous solution but become rodlike at high ionic strengths or high surfactant concentrations[9] although these changes have not as yet been well-characterized. Above the Krafft point (ca. 18 °C in salt-free solution)[13] there is no pronounced effect of temperature on the SDS micellar size or geometry.

$C_{12}E_5$ is a nonionic surfactant of the poly(ethylene oxide) monoether (C_mE_n, $C_mH_{2m+1}(OC_2H_4)_nOH$) series with a relatively low cloud point ($T_C \approx 32.5$ °C within the isotropic phase), which forms large nonspherical micelles when dissolved in water.[14,15] Owing to the low T_C, $C_{12}E_5$ solutions are strongly nonideal even in the dilute regime at temperatures well below T_c ($T - T_C \geq 20$ °C).[16] Such

[†] Departamento de Física, IBILCE/UNESP.

[‡] University of Uppsala.

(1) For a review, see: Ogino, K., Abe, M. Eds. *Mixed Surfactant Systems*; Marcel Dekker: New York, 1993.

(2) Penfold, J.; Staples, E.; Thompson, L.; Tucker, I.; Hines, J.; Thomas, R. K.; Lu, J. R. *Langmuir* **1995**, *11*, 2496.

(3) McDonald, J. A.; Rennie, A. *Langmuir* **1995**, *11*, 1493.

(4) Douglas, C. B.; Kaler, E. W. *Langmuir* **1994**, *10*, 1075.

(5) Hobson, R.; Grieser, F.; Healy, T. W. *J. Phys. Chem.* **1994**, *98*, 274.

(6) Lusvardi, K. M.; Full, A. P.; Kaler, E. W. *Langmuir* **1995**, *11*, 487.

(7) Furuya, H.; Moroi, Y.; Sugihama, G. *Langmuir* **1995**, *11*, 774.

(8) (a) Maeda, H.; Tsunoda, M.; Ikeda, S. *J. Phys. Chem.* **1974**, *78*, 1086. (b) Rubingh, D. N. In *Solution Chemistry of Surfactants*; Mittal, K. L., Ed.; Plenum Press: New York, 1979; Vol. 1, p 337. (c) Hoffmann, H.; Possnecker, G. *Langmuir* **1994**, *10*, 381. (d) Maeda, H. *J. Colloid Interface Sci.* **1995**, *172*, 98.

(9) (a) Mazer, N. A.; Benedek, G. B.; Carey, M. C. *J. Phys. Chem.* **1976**, *80*, 1075. (b) Missel, P. J.; Mazer, N. A.; Benedek, G. B.; Carey, M. C. *J. Phys. Chem.* **1983**, *87*, 1264. (c) Young, C. Y.; Missel, P. J.; Mazer, N. A.; Benedek, G. B.; Carey, M. C. *J. Phys. Chem.* **1978**, *82*, 1375. (d) Corti, M.; Degiorgio, V. *J. Phys. Chem.* **1981**, *85*, 711. (e) Mishic, J. R.; Fisch, M. R. *J. Chem. Phys.* **1990**, *92*, 3222.

(10) Abe, M.; Ogino, K. In *Mixed Surfactant Systems*; Ogino, K., Abe, M., Eds.; Marcel Dekker: New York, 1993; p 1.

(11) van Stam, J.; Brown, W.; Fundin, J.; Almgren, M.; Lindblad, C. In *Colloid-Polymer Interactions*; Dubin, P., Tong, P., Eds.; ACS Symposium Series 532; American Chemical Society: Washinghton, DC, 1993.

(12) Brown, W.; Gimel, J.-C. *J. Chem. Phys.* **1996**, *104*, 8112.

(13) Lindman, B.; Wennerstrom, H. *Topics in Current Chemistry*; Springer-Verlag: Berlin, 1980; Vol. 87.

(14) (a) Brown, W.; Zhou, P.; Rymdén, R. *J. Phys. Chem.* **1988**, *92*, 6086. (b) Kato, T.; Anzai, S.; Seimiya, T. *J. Phys. Chem.* **1987**, *91*, 4655; **1990**, *94*, 7255.

(15) (a) Feitosa, E.; Brown, W.; Hansson, P. *Macromolecules* **1996**, *29*, 2169. (b) Feitosa, E.; Brown, W.; Vasilescu, M.; Swanson-Vethamuthu, M. *Macromolecules* **1996**, *29*, 6837.

(16) Degiorgio, V. In *Physics of Amphiphiles. Micelles, Vesicles and Microemulsions*; Corti, M., Ed.; North-Holland: Amsterdam, 1985; p 303.

S0743-7463(98)00142-5 CCC: $15.00 © 1998 American Chemical Society
Published on Web 07/17/1998

nonideality, with accompanying polydispersity, complicates investigations of $C_{12}E_5$ micellar properties in solution, for example, when determining the molecular weight or the hydrodynamic radius using light scattering. Unlike SDS, the micellar size of $C_{12}E_5$ is highly sensitive to temperature but not to ionic strength.[15,16]

Depending on the ratio of the two surfactants, the total concentration, and the presence or otherwise of simple salt, one anticipates changes in the micellar size/shape as the interaction pattern is changed. Mixed micelles of SDS and surfactants of the C_mE_n series have already been studied using a number of techniques, including light scattering and NMR.[10,17] Abe et al.[10] found no relationship between the macro- and the microscopic viscosities of the mixed surfactant solutions and also that the microscopic viscosity is larger and the polarity is smaller in the interior of the mixed micelles compared to the single-surfactant micelles.[10] Guéring et al.[17] studied the salt-free systems as a function of added SDS up to a total surfactant concentration of 50 wt %. They observed that the correlation functions were bimodal at different $C_{12}E_5$/SDS ratios (up to 50 wt %) in D_2O and, by comparison with NMR data, identified the slow mode as the self-diffusion coefficient for the mixed micelles. They interpreted the fast decay as a collective diffusion coefficient arising from unscreened electrostatic interactions.

The aim of this work was to further elucidate the dynamic behavior of mixed micelles, and we have applied dynamic light scattering (DLS) to the $C_{12}E_5$/SDS/water system in 0.1 M NaCl over a range of temperatures and a wider range of relative surfactant concentrations than hitherto. We show the effect of surfactant concentration on the cloud point and surface tension of the mixed micellar system. The work was motivated by some unresolved questions about the properties of the binary surfactant systems that influence the utility of the mixed micellar solutions.. These concern the effects of the relatively low Krafft point of SDS (around 18 °C)[13] and the low cloud point (ca. 32.5 °C in the isotropic phase) of the binary $C_{12}E_5$ solution, which make the solutions rather nonideal.[14] Mixtures of SDS and $C_{12}E_5$ are also relevant in conjunction with polyelectrolyte utilization since the lower (and controlled) surface charge density of the mixed micelles can inhibit polyelectrolyte precipitation.[18]

Materials and Methods

Sodium dodecyl sulfate (SDS) and pentaethylene glycol mono-*n*-dodecyl ether ($C_{12}E_5$) were used as purchased, respectively, from BDH, England, and Nikko Chemicals, Japan. NaCl (Merck, Germany) was analytical grade. The solutions were prepared with (Milli-Q plus) ultrapure water. The cmc's of SDS and $C_{12}E_5$ in pure water are respectively 8.1 mM and 65 μM at 25 °C.[13,14] In the presence of 0.1 M NaCl, the cmc of SDS decreases to 0.43 mM,[19] whereas the cmc of $C_{12}E_5$ is almost insensitive to the ionic strength.[15]

T_C was measured by slowly increasing the temperature and visually observing the temperature at which the solution clouds. The surface tension (γ) measurements were made using the drop volume technique.[20] The cmc was obtained as the break point of the γ vs surfactant concentration curve (see, for example, Figure 1).

Dynamic Light Scattering. The light scattering setup consists, as described previously,[14,15] of a 633 nm He−Ne laser light source and the detector optics with an ITT FW 130 photomultiplier and ALV-PM-PD amplifier-discriminator connected to an ALV-5000 autocorrelator/computer. The cylindrical scattering cells were sealed after filtration through 0.22 μm Millipore filters and immersed in a large-diameter thermostated bath containing Decalin placed at the axis of a goniometer. Measurements were made at different angles, sample concentrations, and temperatures.

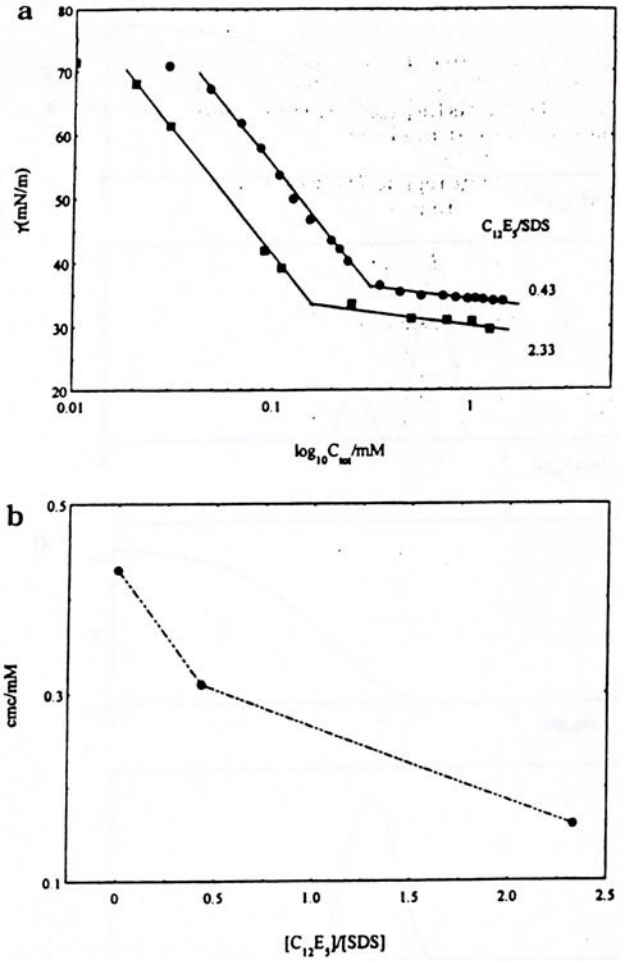


Figure 1. (a) Surface tension, γ, as a function of the total surfactant concentration at the $C_{12}E_5$/SDS molar ratios shown (25 °C). (b) Critical micelle concentration (cmc) as a function of the $C_{12}E_5$/SDS molar ratio for the mixed surfactant solution in 0.1 M NaCl (25 °C).

Analysis of the data was performed by fitting the experimentally measured $g_2(t)$, the normalized intensity autocorrelation function, which is related to the electrical field correlation function, $g_1(t)$, by the Siegert relation[21]

$$g_2(t) - 1 = \beta|g_1(t)|^2 \quad (1)$$

where β is a factor accounting for deviation from ideal correlation. For polydisperse samples, $g_1(t)$ can be written as the inverse Laplace transform (ILT) of the relaxation time distribution, $\tau A(\tau)$[22]

$$g_1(t) = \int \tau A(\tau) \exp(-t/\tau) \mathrm{d} \ln \tau \quad (2)$$

where t is the lag time. The relaxation time distribution, $\tau A(\tau)$, is obtained by performing the inverse Laplace transform (ILT) wth the aid of a constrained regularization algorithm (REPES),[23]

(17) (a) Guéring, P.; Nilsson, P.-G.; Lindman, B. *J. Colloid Interface Sci.* **1985**, *105*, 41. (b) Nilsson, P.-G.; Lindman, B. *J. Phys. Chem.* **1984**, *88*, 5391.

(18) (a) Dubin, P. L.; Rigsbee, D. R.; McQuigg, D. W. *J. Colloid Interface Sci.* **1985**, *105*, 509. (b) Bergfeldt, K.; Piculell, L. *J. Phys. Chem.* **1996**, *100*, 5935.

(19) Emerson, M. F.; Holtzer, H. *J. Phys. Chem.* **1967**, *71*, 1898.

(20) Tornberg, E. *J. Colloid Interface Sci.* **1977**, *60*, 50.

(21) Schillén, K.; Brown, W.; Johnsen R. M. *Macromolecules* **1988**, *27*, 4825.

(22) Chu, B. *Laser Light Scattering*, 2nd ed.; Academic Press: New York, 1991.

(23) Jakes, J. *Czech. J. Phys.* **1988**, *B38*, 1305.

cm 1 2 3 4 5 6 7 8 unesp 12 13 14 15 16 17 18 19

which minimizes the sum of the squared differences between the experimental and calculated $g_2(t)$. The mean diffusion coefficient (D) is calculated from the second moments of the peaks as $D = \Gamma/q^2$, where $q = (4\pi n_o/\lambda) \sin \theta/2$ is the magnitude of the scattering vector and $\Gamma = 1/\tau$ is the relaxation rate. Here θ is the scattering angle, n_o the refractive index of pure solvent, and λ the wavelength of the incident light.

Within the dilute regime, D varies linearly with the surfactant concentration (C), that is

$$D = D_o(1 + k_D C + ...) \quad (3)$$

where D_o is the diffusion coefficient at infinite dilution and k_D is the hydrodynamic "virial" coefficient related to the solute–solute and solute–solvent interactions. The Stokes–Einstein equation relates the infinite dilution diffusion coefficient to the hydrodynamic radius (R_H)

$$D_o = k_B T/6\pi\eta_o R_H \quad (4)$$

where $k_B T$ is the thermal energy factor and η_o is the temperature-dependent viscosity of the solvent.

Static light scattering measurements were made using a Hamamatsu photon-counting device, with a 3 mW He–Ne laser. Toluene was used as the reference ($R_{toluene} = 13.59 \times 10^{-4}$ m^{-1} at 633 nm). dn/dc was measured in a differential refractometer with Rayleigh optics at 25 °C. At $C_{12}E_5$/SDS molar ratio 0.43, dn/dc was 0.116 mLg^{-1} and at ratio 2.33 dn/dc = 0.126 mLg^{-1}.

Results and Discussion

A value of R_H = 2.7 nm at 25 °C for the SDS micelle in 0.1 M NaCl obtained previously in our laboratory[11] is used here for comparisons. The strong increase in the hydrodynamic radius (R_H) of SDS micelles on increasing the ionic strength has been attributed to a sphere to rod transition and/or changes in the intermicellar interactions due to electrostatic screening effects.[9] It is also known that the radius of SDS micelles decreases on increasing the temperature.[9c,d]

Light scattering measurements on $C_{12}E_5$ micelles in aqueous solution are, on the other hand, complicated by the nonideal behavior of the solutions specially at temperatures close to the cloud point (T_C) of the surfactant. We have previously estimated R_H = 12 nm at 20 °C.[14] In this work we have also determined R_H=12 nm in 0.1 M NaCl (see below). It was shown that, after an initial decrease, R_H for $C_{12}E_5$ increases strongly as the temperature increases up to T_C.[15] The increase in R_H as well as the increase in the scattered intensity with the temperature may be attributed either to changes in size and/or asymmetric growth possibly into branched cylinder networks at high concentrations and/or to changes in the intermicellar interactions (critical concentration fluctuations).[24]

The cmc values of the $C_{12}E_5$/SDS mixtures in 0.1 M NaCl were estimated as 0.31 and 0.16 mM for $C_{12}E_5$/SDS mixtures at the molar concentration ratios of 0.47 and 2.3, respectively (25 °C), using surface tension measurements (Figure 1a). These values lie between those of the binary component solutions SDS (0.43 mM in the presence of 0.1 M NaCl) and $C_{12}E_5$ (65 μM) as predicted by theory and also as experimentally observed for similar mixed micellar systems.[8b] The surface tension curves have about the same slope within the concentration range immediately below the cmc, suggesting that the area per headgroup of the monomer (or the surface excess) does not change with the $C_{12}E_5$/SDS ratio, according to the Gibbs adsorption equation.[25] Figure 1b shows that the cmc decreases with increasing ratio from that of pure SDS toward that for pure $C_{12}E_5$.

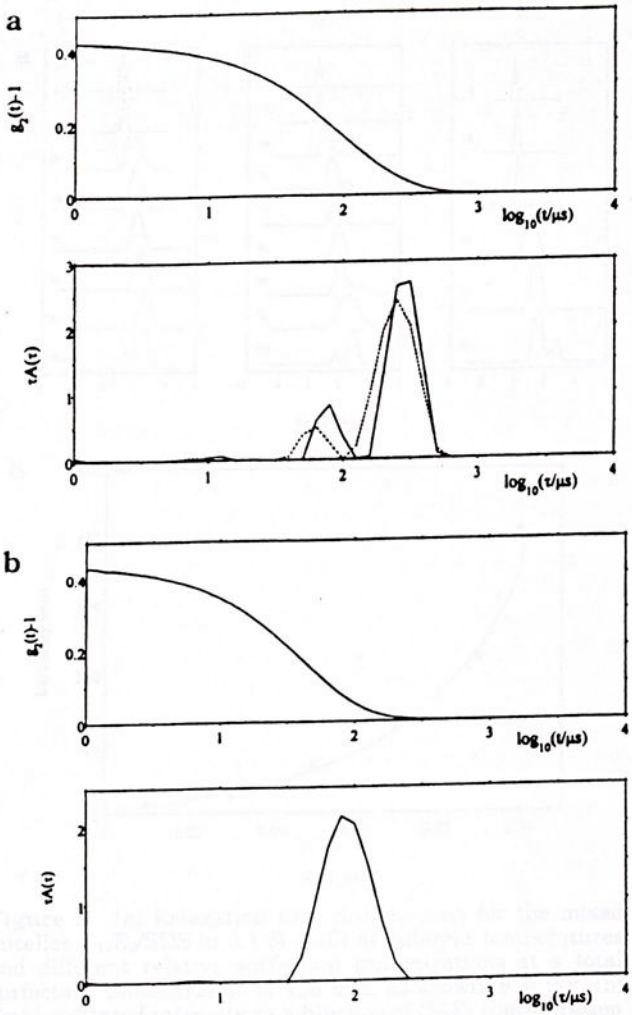


Figure 2. (a) Intensity correlation function (top) and the corresponding relaxation time distribution (bottom) for a binary solution of $C_{12}E_5$ (100 mM) at 25 °C, in the absence (dotted) and presence (full) of 0.1 M NaCl; θ = 90°. (b) Same as Figure 2a, but for the mixture of $C_{12}E_5$/SDS = 7/3 (total surfactant concentration 100 mM) in 0.1 M NaCl.

Figure 2a shows a typical intensity correlation function, $g_2(t) - 1$, together with the corresponding relaxation time distribution for a binary $C_{12}E_5$ micellar solution in the absence (dotted line) and in the presence (full line) of 0.1 M NaCl, at 25 °C. The bimodal distributions for pure $C_{12}E_5$ are always dominated by the slow mode. Furthermore, above about 10 °C, there is always a faster, low intensity, component present at all $C_{12}E_5$/SDS ratios.[14] In contrast, binary SDS micellar solutions invariably have unimodal ILT distributions, as already shown previously.[11] The relaxation time distributions for mixed $C_{12}E_5$/SDS solutions in 0.1 M NaCl are, perhaps surprisingly, also unimodal over a wide range of surfactant concentrations and temperatures (Figure 2b) with an average relaxation time intermediate between those for the fast and slow modes observed in pure $C_{12}E_5$ solutions. Thus we conclude that the mixed micelles are a homogeneous and well-defined species and that the system does not simply contain a mixture of the ionic and nonionic species. Figure 2b shows an example of a correlation function and the

(24) Nilsson, P. G.; Wennerstrom, H.; Lindman, B. *J. Phys. Chem.* **1983**, *87*, 1377.

(25) Hunter, R. J. *Foundations of Colloid Science*; Clarendon Press: Oxford, 1987; Vol. 1, p 250.

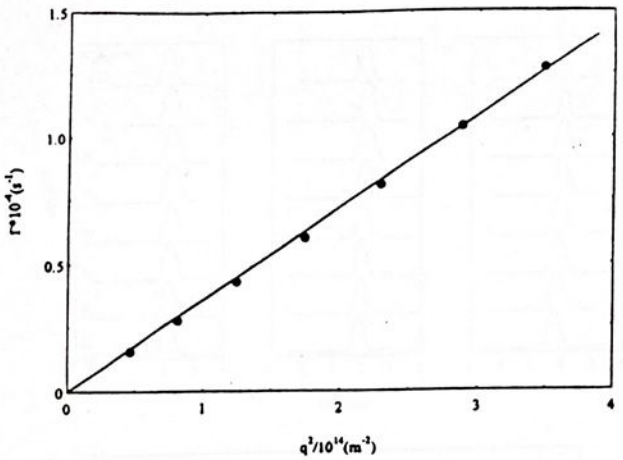


Figure 3. Relaxation rate, Γ, as a function of the squared scattering vector, q^2, for the mixed micellar system with $C_{12}E_5$/SDS molar ratio = 7/3 in 0.1 M NaCl at 25 °C.

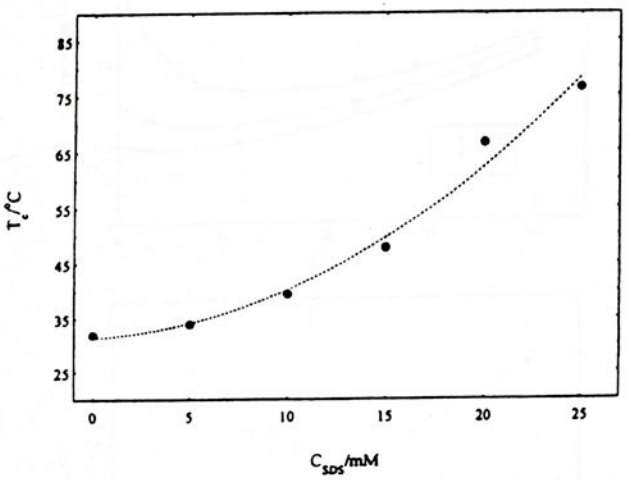
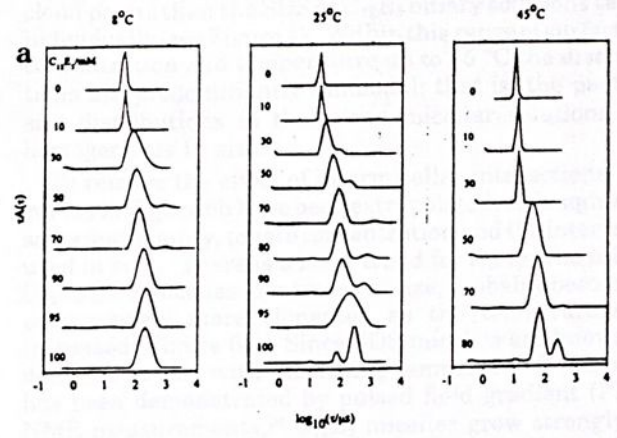


Figure 4. Clouding temperature for $C_{12}E_5$/SDS mixtures in 0.1 M NaCl as a function of the SDS concentration at constant total surfactant concentration of 100 mM.

corresponding relaxation time distribution for the mixture containing 70 and 30 mM of $C_{12}E_5$ and SDS, respectively, in 0.1 M NaCl solution at 25 °C. As seen in Figure 3, there is a linear relationship between the mean relaxation rate (Γ) of this single mode and the squared scattering vector (q^2) showing a diffusive process.

The clouding temperature (T_c) for $C_{12}E_5$/SDS mixtures in 0.1 M NaCl increases considerably when the relative concentration of SDS is increased maintaining a constant total surfactant concentration of 100 mM as shown in Figure 4. The added salt screens the charge effects deriving from the surfactant and which were shown to complicate the behavior of surfactant mixtures in D_2O in the absence of added salt.[17] The measured T_c of pure $C_{12}E_5$ (C = 0.1 M) is 33.1 °C in water and 32.0 °C in the presence of 0.1 M of NaCl. T_c for $C_{12}E_5$ was found to be strongly lowered on addition of poly(ethylene oxide) (PEO) owing to micellar cluster formation.[14,15] A decrease in T_c for the $C_{12}E_5$/PEO/water system was also observed both when the surfactant/polymer concentration ratio was increased and when the total surfactant concentration was increased at a constant surfactant/polymer concentration ratio. Similar behavior has been observed on addition of a high[26] or low[27] molar mass PEO to the surfactant $C_{12}E_8$.

(26) Feitosa, E.; Brown, W.; Swanson-Vethamuthu, M. *Langmuir* **1996**, *12*, 5985.
(27) Feitosa, E.; Brown, W.; Wang, K. In preparation.



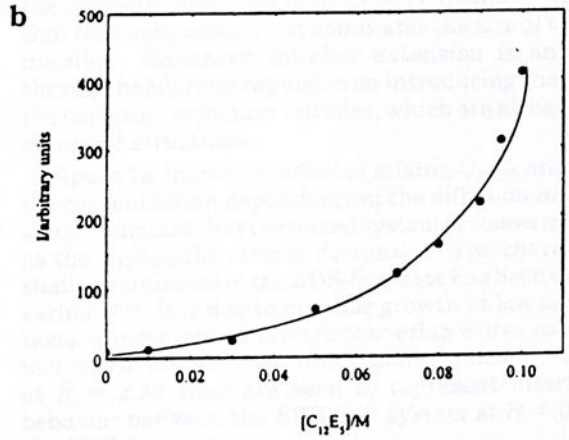


Figure 5. (a) Relaxation time distributions for the mixed micelles $C_{12}E_5$/SDS in 0.1 M NaCl at different temperatures and different relative surfactant concentrations at a total surfactant concentration of 100 mM, as shown; θ = 90°. (b) Total scattered intensity as a function of $C_{12}E_5$ concentration for the $C_{12}E_5$/SDS mixture at total surfactant concentration 100 mM; T = 25 °C, θ = 90°.

However, the T_c of the $C_{12}E_5$/SDS mixtures changes only slightly when the total concentration is changed, holding the $C_{12}E_5$/SDS ratio constant; for example, at $C_{12}E_5$/SDS = 85/15 (mM) (ratio 5.7), T_c = 47.5 °C, which decreases only slightly to 46.0 °C on dilution of the solution to 5.1/0.9 mM. The stronger dependence of T_c on the $C_{12}E_5$/SDS ratio rather than on the total surfactant concentration at a given surfactant ratio suggests that the structure of the mixed micelle aggregates in solution is preserved when varying the total surfactant concentration at constant surfactant concentration ratio.

In 0.1 M NaCl, T_c for the mixture of 30 mM SDS with 70 mM $C_{12}E_5$ (i.e., $C_{12}E_5$/SDS = 7/3) is about 100 °C. At this ratio, or higher ones, the relaxation time distribution is close to unimodal over the range of temperature investigated (8−45 °C) but then broadens and eventually becomes bimodal at higher relative concentrations of $C_{12}E_5$ (Figure 5a). This change is probably related to a clustering of the micelles in solution as T_c is approached, eventually leading to critical scattering. In these experiments all the concentrations were kept above the cmc of the surfactants and the total surfactant concentration was held constant at 100 mM.

Figure 5b shows the effect of the $C_{12}E_5$ concentration on the total scattered intensity (25 °C) for $C_{12}E_5$/SDS mixtures in 0.1 M NaCl at a total surfactant concentration of 100 mM, showing that 100 mM $C_{12}E_5$ scatters much more than the same concentration of SDS. A progressive increase in the scattered intensity is found for the mixtures

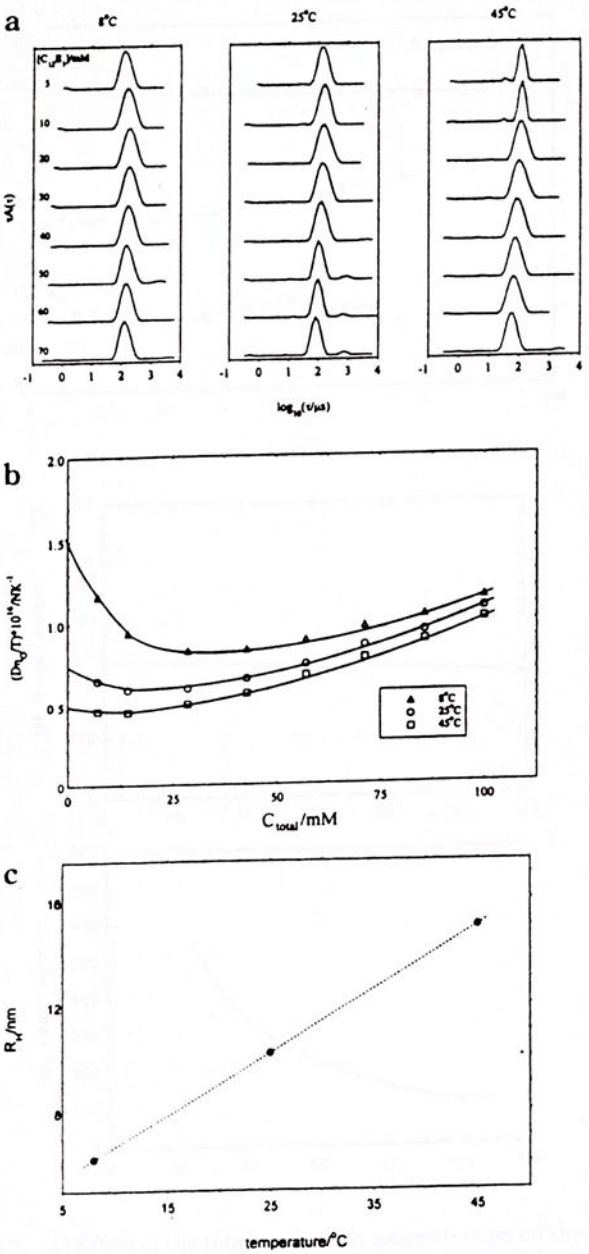


Figure 6. (a) Relaxation time distributions for the mixed $C_{12}E_5$/SDS micelles in 0.1 M NaCl at constant $C_{12}E5$/SDS molar ratio = 7/3 and at the surfactant concentrations and temperatures shown; $\theta = 90°$. (b) Dependence of the reduced diffusion coefficient ($D\eta_0/T$) on the total surfactant concentration for $C_{12}E_5$/SDS = 7/3 and the temperatures shown. Data correspond to the distributions in Figure 6a. (c) Effect of temperature on the hydrodynamic radius derived from the intercepts in Figure 6b.

as the $C_{12}E_5$/SDS concentration ratio is raised at a fixed total surfactant concentration (100 mM), showing that larger, possibly branched, structures progressively form.

Figure 6a shows relaxation time distributions obtained on increasing the total surfactant concentration at the fixed $C_{12}E_5$/SDS molar concentration ratio of 7/3 at three different temperatures: 8, 25, and 45 °C. The peak position changes little with change in surfactant concentration, as is also observed in Figure 6b for the corresponding normalized diffusion coefficients. Unlike the $C_{12}E_5$/SDS mixtures, SDS molecules are insoluble in water below ca. 18 °C (the Krafft point of pure SDS), whereas $C_{12}E_5$ binary solutions first cloud at about 31.5 °C. The mixed micelles have both a higher solubility and higher cloud points than the SDS or $C_{12}E_5$ binary solutions taken individually (see Figure 4). Within this range of surfactant concentration and temperature up to 45 °C the distributions are predominantly unimodal; that is, the particle size distributions in the mixed micellar solutions are homogeneous in size.

To remove the effect of intermicellar interactions, the curves in Figure 6b have been extrapolated, although with some uncertainty, to zero concentration and the intercepts used in eq 4. There is a clear trend for R_H for the mixed $C_{12}E_5$/SDS micelles to increase in size, probably becoming progressively more elongated as the temperature is increased (Figure 6c). Since SDS micelles are known to decrease in size with increasing temperature[9] while, as has been demonstrated by pulsed field gradient (PFG) NMR measurements,[24] $C_{12}E_5$ micelles grow strongly in the opposite sense and become more flexible,[15] it is clear that the $C_{12}E_5$ component dominates the size of the mixed micelles. Enhanced micellar extension is anticipated through headgroup repulsion on introducing charges into the nonionic surfactant micelles, which are already highly extended structures.

Figure 7a shows the effect of mixing $C_{12}E_5$ and SDS on the concentration dependence of the diffusion coefficient, which indicates that the mixed system becomes more ideal as the $C_{12}E_5$/SDS ratio is decreased. The characteristic shallow minimum in the SDS-free data has been discussed earlier.[14,15] It is due to micellar growth at low concentrations, which eventually leads to overlap with a subsequent increase in the cooperative diffusion coefficient. The data at $R = 2.33$ thus are seen to represent intermediate behavior between the SDS-rich system at $R = 0.43$ and the SDS-free system.

The influence of the $C_{12}E_5$ content is also seen in static light scattering measurements in 0.1 M NaCl (Figure 7b). Both at $R = 0.43$ and 2.33 the reduced scattered intensity Kc/R_θ is angle-independent over the range 20−150° at all concentrations, as anticipated for compact particles of radius < 20 nm. At $R = 0.43$ (Figure 7b(upper)) the apparent molecular weight $(R_\theta/Kc)_{\theta=0} = 1/M_w$, that is, the value obtained at each total surfactant concentration, is concentration-independent with a molecular weight at infinite dilution of 47×10^3. $R_H = 2.7$ nm from the relaxation rate at infinite dilution in Figure 7a, and this is close to the R_H value for the pure SDS micelle. At $R = 2.33$ (Figure 7b(lower)), however, M_w-apparent decreases from 500×10^3 at $c = 27$ mM to 120×10^3 at 100 mM. By plotting log M_w versus concentration, an approximate value of 900×10^3 is obtained at infinite dilution. The data are consistent with the trend in D in Figure 7a at this ratio. The strong curvature shows that the interactions at $R = 2.33$ are strongly dependent on the total surfactant concentration in this range. At infinite dilution the value of $R_H = 11$ nm.

The addition of $C_{12}E_5$ to an SDS solution increases the cloud point and increases the micellar size (Figure 7c) since $C_{12}E_5$ dominates the size of the mixed micelle. We note that the effect of added salt is also important. The measurements of Guéring et al.[17] show that in the absence of salt, the hydrodynamic radius of mixed micelles is less sensitive to the $C_{12}E_5$ content and also, as expected, that the micelles are larger ($R_H \approx 12$ nm at 50% (w/w) SDS compared with $R_H \approx 5$ nm in 0.1 M NaCl at the same ratio). Figure 7d compares relaxation time distributions for the binary $C_{12}E_5$ solution and the ternary mixture at the $C_{12}E_5$/SDS ratio 3/7; that is, the mixed system is unimodal like the binary SDS solution, whereas the binary $C_{12}E_5$ solution is bimodal.

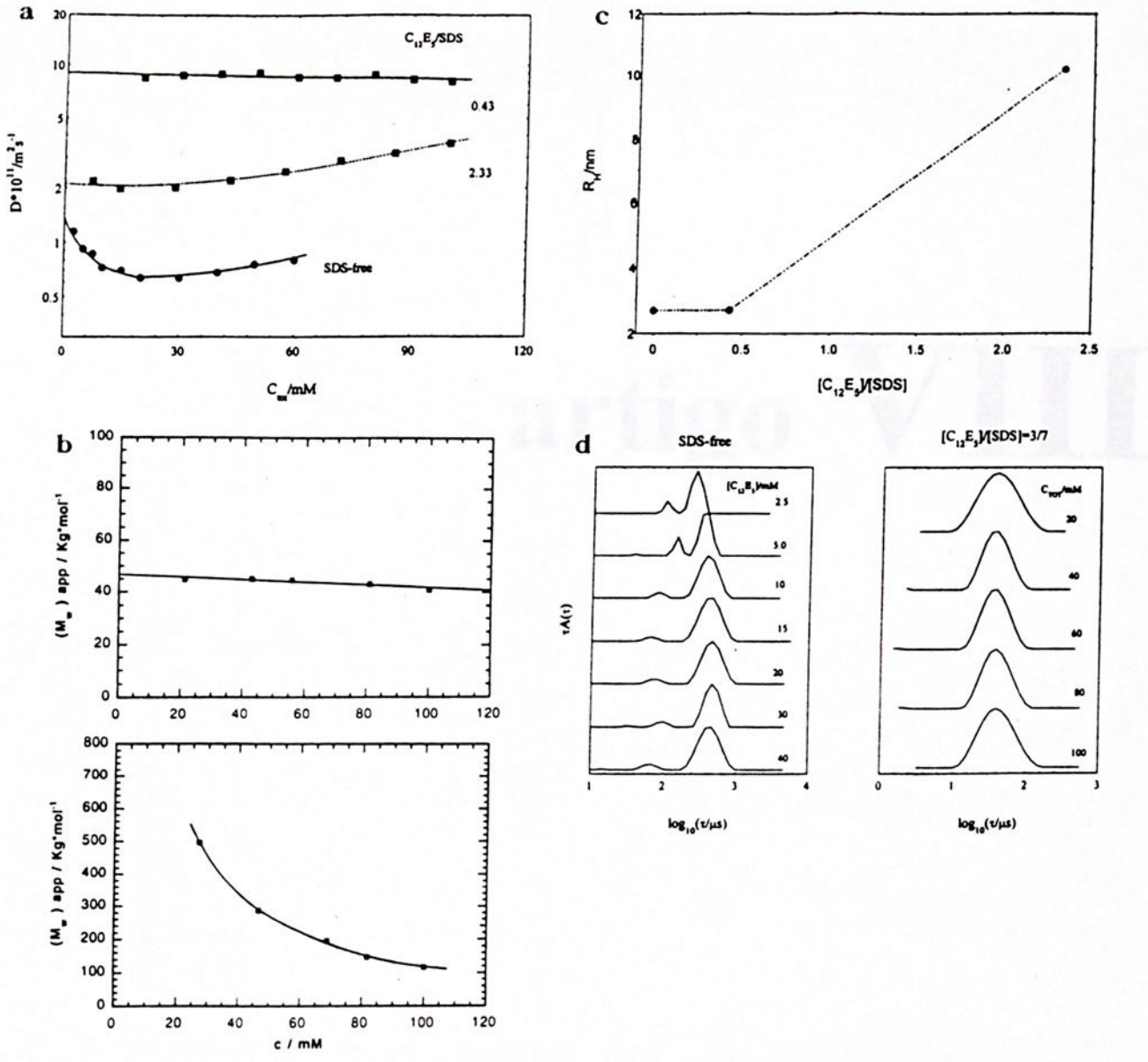


Figure 7. (a) Effect of the total surfactant concentration on the diffusion coefficient for the selected $C_{12}E_5$/SDS molar ratios shown. Measurements at 90 and 25 °C in 0.1 M NaCl. (b) Static light scattering data (apparent molecular weight, $(R_\theta/Kc)_{\theta=0}$) as a function of total surfactant concentration at (a) $R = 0.43$ and (b) $R = 2.33$. (c) Hydrodynamic radius as a function of the $C_{12}E_5$/SDS molar ratio obtained from data in Figure 7a. (d) Relaxation time distributions for the binary $C_{12}E_5$ and ternary $C_{12}E_5$/SDS solutions at the selected concentrations of the surfactants shown.

Conclusions

It is shown that mixtures of anionic SDS and nonionic $C_{12}E_5$ surfactants self-assemble above the cmc of the surfactant mixture over a broad range of temperatures to form mixed micelles of homogeneous size as demonstrated by the single-modal relaxation time distributions for the ternary system. The cmc of the mixed surfactants lies between the values of the individual compounds and decreases as the ratio $C_{12}E_5$/SDS is increased. The clouding temperatures of the mixed micellar systems are higher than those of the binary $C_{12}E_5$ solutions. At the $C_{12}E_5$/SDS molar concentration ratio of 2.33, R_H for the mixed micelles increases linearly with temperature over the range investigated (8−45 °C). R_H also increases as the $C_{12}E_5$/SDS ratio increases. The mixed micelle solutions become more ideal as the $C_{12}E_5$/SDS ratio is decreased whereas the binary solutions of $C_{12}E_5$ become less ideal as the temperature is increased up to the clouding point. At the $C_{12}E_5$/SDS molar ratio of 2.33, the relaxation time distribution for mixed micellar solutions is unimodal in contrast to binary $C_{12}E_5$ solutions, which are bimodal. Relative to the SDS micelles the mixed micelles show a lower Krafft point and a higher cloud point relative to $C_{12}E_5$ micelles

Acknowledgment. This work was supported financially by the Swedish Technical Research Council (TFR). E.F. thanks the Conselho Nacional de Desenvolvimento Científico e Tecnológico (CNPq) for a stipendium (Grant 201720/93-0) and Fundacao Coordenacao de Aperfeicoamento de Pessal de Nivel Superior (CAPES) for partial support.

LA980142V

artigo VIII

ELSEVIER

Thermochimica Acta 328 (1999) 137–142

thermochimica acta

Phase behavior of synthetic amphiphile vesicles investigated by calorimetry and fluorescence methods[1]

C.R. Benatti[a], M.J. Tiera[b], E. Feitosa[a,*], G. Olofsson[c]

[a]*Physics Department, IBILCE/UNESP, C.P. 136-15054-000, São José do Rio Preto-SP, Brazil*
[b]*Chemistry and Geoscience Department, IBILCE/UNESP, C.P. 136-15054-000, São José do Rio Preto-SP, Brazil*
[c]*Division of Thermochemistry, Chemical Center, Lund University, S-221 00, Lund, Sweden*

Accepted 1 October 1998

Abstract

The understanding of biological membranes may be improved by investigating physical properties of vesicles from natural or synthetic amphiphiles. The application of vesicles as mimetic agents depends on the knowledgment of their structure and properties. Vesicles having different curvature and size may be obtained using different preparation protocols. We have used differential scanning calorimetry (DSC) and steady-state fluorescence to investigate the gel to liquid-crystal phase transition of vesicles prepared by sonication (SUV) and non-sonication (GUV) of the synthetic dioctadecyldimethylammonium bromide (DODAB) in aqueous solution. DSC thermograms for a non-sonicated dispersion show a well-defined pre- and main transition corresponding to two narrow peaks at 36 and 45°C in the first upscan, while in a second upscan, only the main peak was observed. The sharpness of the peaks indicate a cooperative phase behavior for GUV. For a sonicated DODAB dispersion, the first upscan shows a third peak at 40.3°C, whereas for the second upscan the peaks are not well-defined, indicating a less cooperative phase behavior. Alternatively, the fluorescence quantum yield (Φ_f) and the anisotropy (r) of *trans, trans, trans*-1-[4-(3-carboxypropyl)-phenyl]-6-[4-butylphenyl]-1,3,5-hexatriene (4H4A) and the ratio I_1/I_3 of the first to the third vibronic peaks of the pyrene emission spectrum as function of temperature are used as well to describe the phase behavior of DODAB sonicated and non-sonicated dispersions. It is in good agreement with the DSC results that the cooperativity of the thermotropic process is diminished under sonication of the DODAB dispersion, meaning that sonication changes from homogeneous to heterogeneous populations of the amphiphile aggregates. The pre- and main transitions obtained from these techniques are in fairly good accord with results from the literature. © 1999 Elsevier Science B.V. All rights reserved.

Keywords: Differential scanning calorimetry; Steady-state fluorescence; Melting temperature; Thermotropic phase behavior; Synthetic amphiphile vesicles

1. Introduction

Vesicles or liposomes consist of closed bilayers formed from hydrated natural or synthetic amphiphiles. Small, large or giant unilamellar vesicles are easily obtained using appropriate methods such as sonication or extrusion [1]. The vesicle structure depends on the preparation protocol, as well as on the amount and nature of the amphiphiles and additives [1].

DODAX (dioctadecyldimethylammonium halide) molecules are double, long-chained, synthetic vesicle-forming amphiphiles, widely used in studies of

*Corresponding author. Tel:. +55-17-221-22-40; fax: +55-17-224-86-92; e-mail: eloi@df.ibilce.unesp.br

[1]Presented at the IUPAC International Symposium on Calorimetry and Chemical Thermodynamics, April 5–9, 1998, Campinas, Brazil.

0040-6031/99/$ – see front matter © 1999 Elsevier Science B.V. All rights reserved.
PII: S0040-6031(98)00634-0

association colloid systems [2–9]. In the presence of water, they assemble as small (SUV) or large vesicles (LUV) when treated, respectively, with sonication or chloroform-injection [2]. Recently, we reported that within the diluted regime, DODAB molecules self-assemble spontaneously as a bipopulation of large and giant unilamellar vesicles (GUV) [3,4]. At higher concentrations, however, the vesicle structure becomes multilamellar [5]. The mean hydrodynamic radii of SUV, LUV and GUV measured by dynamic light scattering are, respectively, 22–33 [4], 275 [6] and 337 nm [3].

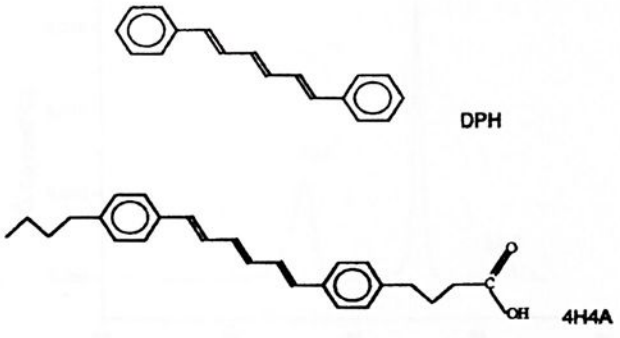
The thermotropic phase behavior of DODAB vesicles is not well understood. Different values for the melting temperature of DODAB (or derivatives) in water solution are found in the literature [4,7–10] and, in addition, pre-transition temperatures are not usually detected for these vesicular systems [8,9]. Fluorescence [10–12], light scattering [3,4], EPR [7] and calorimetry [8,9] are the most commonly used methods for these type of studies. In general, the melting temperature (T_M), around which the gel to liquid-crystal phase transition occurs, depends on the particular experimental method used to determine it. Typical T_M values for DODAB vesicles are 36 and 45°C for the pre- and main transition, respectively.

We have used differential scanning calorimetry (DSC) and steady-state fluorescence methods to investigate the thermotropic phase behavior in vesicle systems prepared by sonication or by simply mixing (non-sonication) of DODAB–water dispersions above the amphiphile T_M. Using these techniques, pre- and main transitions of about 36 and 45°C were detected and the cooperativity of the phase behavior is dependent on the vesicle curvature or preparation protocol.

2. Materials and methods

2.1. Chemicals

DODAB (Eastman Kodak), pyrene (Sigma) and *trans, trans, trans*-1,6-diphenyl-1,3,5-hexatriene (DPH) (Aldrich) were recrystallized twice from acetone. *Trans, trans, trans*-1-[4-(3-carboxypropyl)-phenyl]-6-[4-butylphenyl]-1,3,5-hexatriene (4H4A) was prepared as reported previously [11,12]. The chemical structures of DPH and 4H4A are shown below.



2.2. Vesicle preparation

Giant unilamellar vesicles (GUV) from DODAB were prepared by mixing the DODAB–water mixture at 55°C (above T_M) till the amphiphile present at low concentration (up to ca. 1.0 mM) was completely dissolved. To prepare small unilamellar vesicles (DODAB), the non-sonicated DODAB dispersion was sonicated at 55°C until it became optically clear. A bath-type cell disrupter (Microsonic, SX-10) was used in the sonication process. After preparation the DODAB stock, dispersions were cooled to room temperature and stored at it for the experiments. The vesicles so prepared are stable for months [3,4]. The properties of giant and small DODAB vesicles are described elsewhere [3,4,6]. The term 'giant' is used here to distinguish the non-sonicated vesicles from those large ones obtained by chloroform injection [6].

2.3. Probed vesicle preparation

A small amount of 1.0 mM 4H4A/$CHCl_3$, or pyrene/$CHCl_3$ solution was placed on the bottom of a cylindrical glass flask and the chloroform evaporated under a constant N_2 flux. The sonicated or non-sonicated sample was than added to the flask and the solution was stirred for about 24 h in a light protected container.

2.4. Differential Scanning Calorimetry (DSC)

The DSC measurements were made in a high sensitive differential microcalorimeter (Microcal, MC-2) using twin 1.2 ml total-fill cells to heat the sample and the reference (water) simultaneously and

independently. At a phase transition, heat is applied to the DODAB sample (endothermic process) to maintain the same temperature in both the sample and reference. The samples were scanned at the rate of 1°C/min. The collection and analysis of the data were made with the ORIGIN™ (version 2.9) software supplied by the manufacturer.

2.5. Fluorescence

All measurements were performed using a Hitachi 4500 fluorescence spectrofluorimeter. The temperature of the water-jacketed cell holder was controlled with a circulating bath and monitored by a thermistor probe. The fluorescence quantum yield was determined using DPH in cyclohexane as reference ($\Phi_{f(ref)} = 0.80$) [12]. The reference solution was prepared with the same optical density as the probe-containing vesicle dispersion and its integrated emission band compared at the same wavelength region [11].

The fluorescence anisotropy results were determined using a polarization accessory (right-angle geometry) through the relationship [13]:

$$r = \frac{I_{\parallel} - GI_{\perp}}{I_{\parallel} + 2GI_{\perp}} \quad (1)$$

where $G = i_{\perp}/i_{\parallel}$ is an instrumental correction factor for the equipment set up, and the fluorescence intensity parameters (i and I) account for the ordinary polarization of the excitation and emission light. The subscript symbols $\parallel$ and $\perp$ refer to the position of the polarizers, whether parallel or perpendicular, respectively, to the plane of polarization of the excitation or emission light.

We have obtained the ratio between the intensities of the first and the third vibronic peaks of the emission spectrum of pyrene (I_1/I_3), which is highly sensitive to the polarity of the probe microenvironment [13], to monitor the DODAB vesicle bilayer core. Pyrene was excited at 310 nm and the emission spectra detected at a right angle to the excitation radiation.

3. Results and discussion

3.1. DSC results

All the DSC and fluorescence measurements were made at least 24 h after the sample preparation to ensure the kinetic and mechanical equilibrium of the vesicle suspensions. Fig. 1 (A) shows, after a first scan, the effect of increasing temperature on the heat excess capacity (ΔC_P) of the DODAB (1.0 mM) non-sonicated vesicle sample within the range of 25–55°C. It shows two main peaks, one at 36 and the other at 45°C, corresponding respectively to the pre- and main transition, in good agreement with DSC results from the literature [8,9]. After the first upscan, the sample was quickly cooled and then heated again. The second DSC heating thermogram made about 1.5 h after the first scan shows only the main transition at 45°C (Fig. 1 (B)), suggesting that the first peak in Fig. 1 (A) corresponds to a pre-transition which is a kinetically slow process.

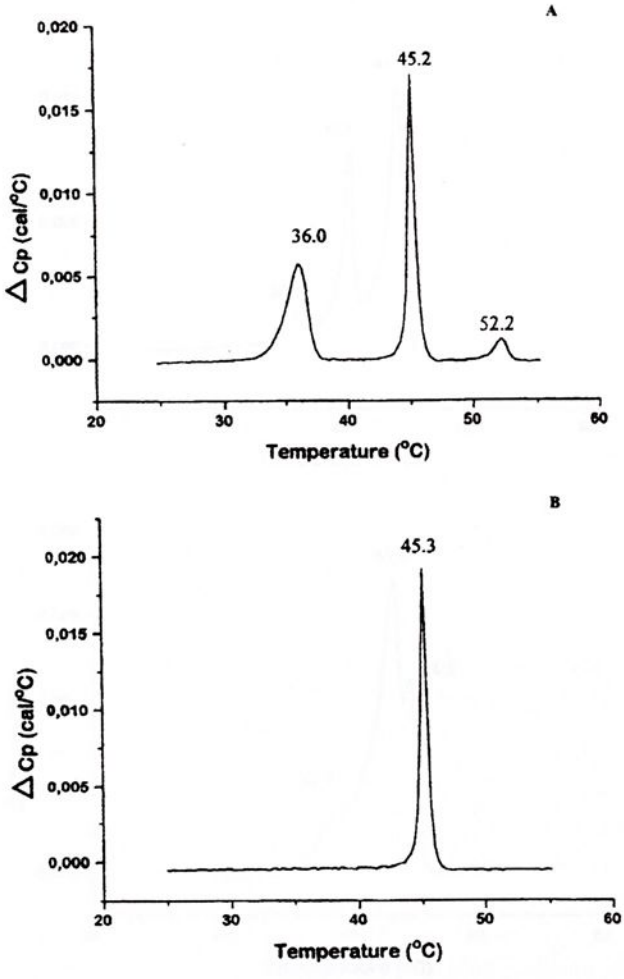


Fig. 1. Change in excess heat capacity with increasing temperature of 1.0 mM DODAB non-sonicated vesicles in water. (A) First upscan, and (B) second upscan. The scan rate was 1°C/min.

The origin of the pre-transition either in lipid or synthetic amphiphile vesicles is not clear. It has been attributed either to changes in the chain conformations [14] or to structural transformations within the amphiphile head groups [15]. Blandamer et al. [8,9], on the other hand, using DSC reported that the addition of ionic surfactants to a non-sonicated DODAB vesicle dispersion eliminates the pre-transition peak and linked it to intervesicular interactions. In this work, the time (1.5 h) to cooling and reheat the sample was not enough for the vesicles to attain the kinetic equilibrium, since the second upscan does not reveal the pre-transition peak.

After 60 min sonication of the non-sonicated DODAB dispersion, the DSC thermograms change considerably in comparison to those obtained before sonication (Fig. 2 (A) and Fig. 2 (B)). The pre-transition peak at 36°C is considerably weakened and the main transition temperature is lowered by about one degree ($T_M \approx 44.4$°C) relative to the non-sonicated sample (Fig. 2 (A)). The sonicated dispersion presents a third intermediate peak at 40.3°C probably due to the co-existing populations of structurally different aggregates, such as bilayer fragments and vesicles as already reported in a previous communication [4]. A second upscan reveals a broad peak which dominates the thermogram indicating that the gel to liquid-crystalline phase transition is not well-defined (Fig. 2 (B)). The mixture of two populations of DODAB supramolecular aggregates having different structures (fragments and vesicles) for the sonicated dispersion is probably responsible for the loss of cooperativity relative to the non-sonicated dispersion which consist not only of two populations but also of vesicle structure with differing size [3].

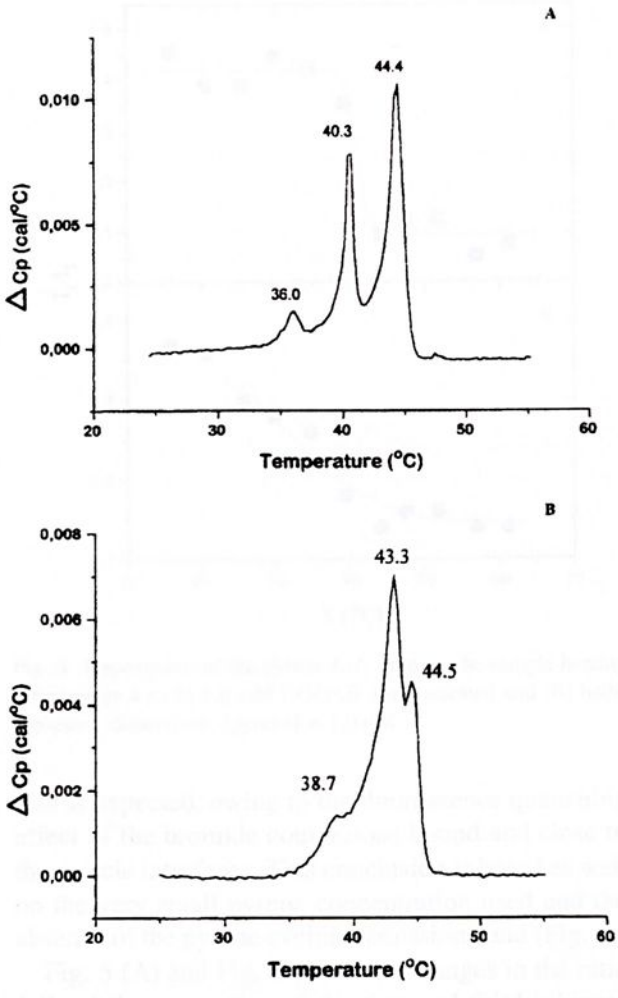


Fig. 2. Change in excess heat capacity with increasing temperature of 1.0 mM 90 min sonicated DODAB vesicles in water. (A) First upscan and (B) second upscan. The scan rate was 1°C/min.

3.2. Fluorescence results

The fluorescence results corroborate the calorimetric ones shown above. 4H4A is a very sensitive amphiphile-like probe suitable to investigate the properties of natural or synthetic amphiphile like micelles or vesicles [11,12]. Fig. 3 shows the effect of increasing the temperature on the fluorescence quantum yield (Φ_f) for 4H4A solubilized in a small (sonicated) and giant (non-sonicated) DODAB unilamellar vesicle in water. The curve for non-sonicated vesicles have two break points, at about 35 and 42°C, suggesting that both a pre- and main transitions can be detected from the Φ_f curve for 4H4A. Sonicated vesicles, on the other hand, show a single less defined break point around 43°C, characteristic of a non-cooperative phase transition as observed from the DSC experiments. Assuming that the 4H4A is solubilized inside the vesicle bilayer because of the amphiphilic characteristics of the prove, as already observed for phospholipid vesicles [11], the existence of intervesicular interactions could slightly change the packing state of the DODAB bilayer causing the appearance of the first (pre-transition) break point in non-sonicated vesicles.

Fig. 4 illustrates typical emission spectra for pyrene in water and in a 1.0 mM DODAB dispersion showing the vibronic peaks. For comparison, it also shows the

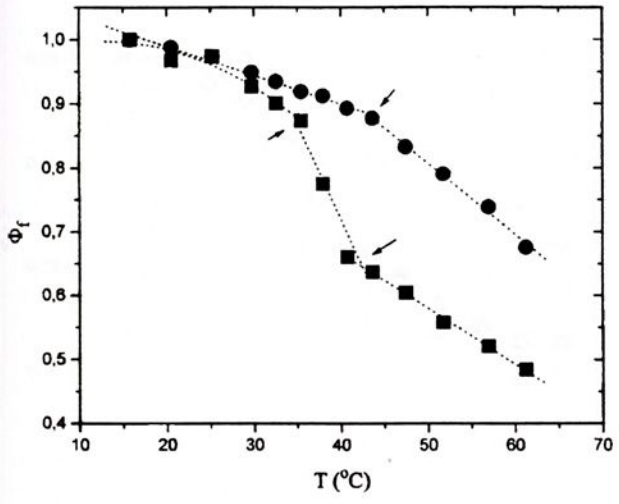


Fig. 3. Dependence of the fluorescence quantum yield for 4H4A (2.2 μM) on the sample heating temperature for 1.0 mM DODAB 90 min. sonicated (●) and non-sonicated (■) dispersions. The arrows indicate the phase transitions.

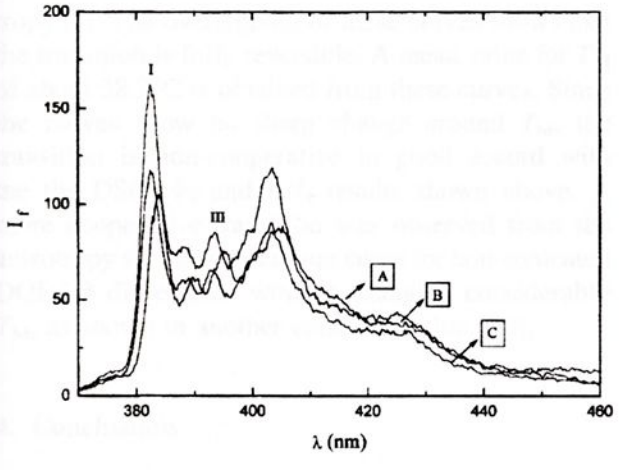


Fig. 4. Emission spectra for pyrene in (A) pure water, (B) 1.0 mM DODAB and (C)NaBr solutions showing the first (I) and third (III) vibronic peaks.

spectrum for a 1.0 mM NaBr aqueous solution. Note that 1.0 mM NaBr does not change the pyrene I_1/I_3 (≈1.85, from Fig. 4) in pure water but it has a stronger quenching effect than the same amount of DODAB molecules because only the bound Br^- counterions (ca. 80% of the whole amount of the amphiphile) quench the fluorescence signal. Pyrene incorporated either in sonicated or non-sonicated vesicles decreases Φ_f relative to that in pure water and slightly shifts the vibronic peaks to a higher wavelength. Such a beha-

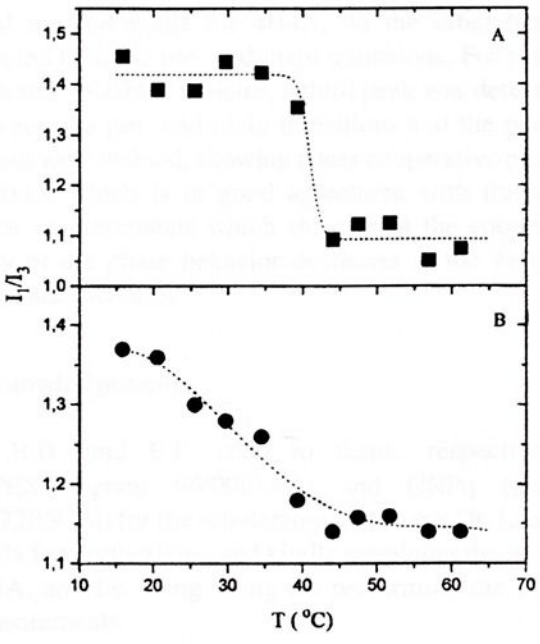


Fig. 5. Dependence of the pyrene I_1/I_3 ratio on the sample heating temperature for (A) 1.0 mM DODAB non-sonicated and (B) bath-sonicated dispersions. [pyrene] = 1.0 μM.

vior is expected, owing to the fluorescence quenching effect of the bromide counterions bound and close to the vesicle interfaces. This conclusion is based as well on the very small pyrene concentration used and the absence of the pyrene excimer emission band (Fig. 4).

Fig. 5 (A) and Fig. 5 (B) show changes in the ratio I_1/I_3 of the intensities of the first and third vibronic peaks of the pyrene fluorescence emission spectra for increasing temperature. The I_1/I_3 value at 20°C ($I_1/I_3 \approx 1.4$) is similar to that for the micelle-forming cationic surfactants like hexadecyltrimethylammonium bromide (CTAB) or dodecyltrimethylammonium chloride (DTAC) [16], indicating that pyrene is placed near the interface where water molecules are present to some extent. The ratio I_1/I_3 as a function of temperature gives a slightly lower T_M value (ca. 40.3°C) for non-sonicated vesicles (Fig. 5 (A)). The sharpness of the curve around T_M indicates a cooperative process for the non-sonicated but not for the sonicated DODAB vesicles (Fig. 5 (B)). Fig. 5 (B) also stresses that T_M for sonicated DODAB vesicles is not well defined and a value of about 43°C is obtained, corroborating the DSC and Φ_f results.

Fig. 6 shows the effect of heating and cooling the sonicated DODAB vesicle on the fluorescence aniso-

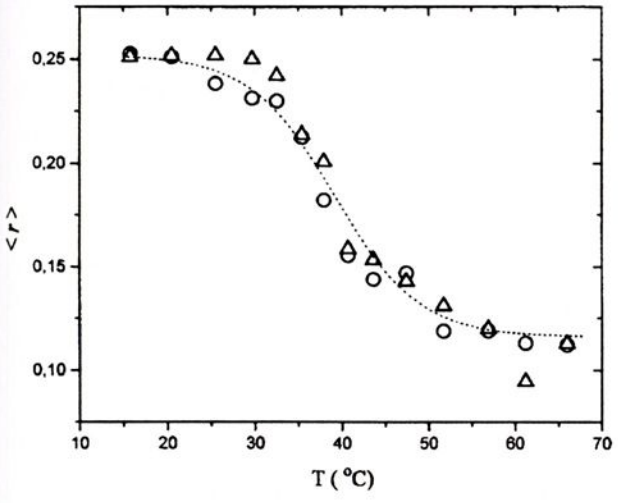


Fig. 6. Dependence of the 4H4A probe fluorescence anisotropy on sample temperature for 90 min. sonicated DODAB aqueous dispersion under heating (O) and cooling (Δ), as shown. [4H4A] = 2.5 μM.

tropy (r). The overlapping of these curves shows that the transition is fully reversible. A mean value for T_M of about 38.2°C is obtained from these curves. Since the curves show no sharp change around T_M, the transition is non-cooperative in good accord with the the DSC, Φ_f and I_1/I_3 results shown above. A more cooperative transition was observed from the anisotropy versus temperature curve for non-sonicated DODAB dispersions without changing considerably T_M, as shown in another communication [10].

4. Conclusions

Different experimental methods show that sonicated and non-sonicated DODAB vesicles have different thermotropic phase behavior. The gel to liquid crystal phase transition is cooperative for giant (non-sonicated) vesicles and non-cooperative for small (sonicated) vesicles as the sonicated dispersions consist of mixed aggregate structures in suspensions, whereas the non-sonicated dispersions contain only vesicle structures. For kinetically equilibrated giant DODAB vesicles in water, the DSC thermograms reveal a pre- and a main transition, whereas pyrene fluorescence shows only the main transition corresponding to the melting temperature (T_M). Quantum yield measurements for 4H4A, on the other hand, detected both the pre- and main transitions. For small sonicated DODAB vesicles, a third peak was detected between the pre- and main transitions and the peaks are not well-defined, showing a less cooperative phase behavior which is in good agreement with fluorescence measurements which shows that the cooperativity of the phase behavior decreases as the vesicle curvature increases.

Acknowledgements

C.R.B. and E.F. wish to thank, respectively, FAPESP (grant 96/00613-5) and CNPq (grant 201720/93-0) for the scholarship. We thank Dr. Laerte Miola for synthesizing and kindly supplying the probe 4H4A, and Dr. Geng Wang for performing the DSC measurements.

References

[1] M. Rosoff (Ed.), Vesicles: Surfactant Science Series, vol. 62, Marcel Dekker, New York, 1996, p. 151.
[2] A.M. Carmona-Ribeiro, Chem. Soc. Rev. 21 (1992) 209.
[3] E. Feitosa, K. Edwards, G. Karlsson, manuscript in preparation.
[4] E. Feitosa, W. Brown, Langmuir 13 (1997) 4810.
[5] E. Feitosa, L.Q. Amaral, Condensed Matter Physics Meeting, Caxambu, MG, Brazil, 1998.
[6] I.M. Cuccovia, E. Feitosa, H. Chaimovich, L. Sepulveda, W.F. Reed, J. Phys. Chem. 94 (1990) 3722.
[7] R.B. Pansu, B. Arrio, J. Roncin, J. Faure, J. Phys. Chem. 94 (1990) 796.
[8] M.J. Blandamer, B. Briggs, P.M. Cullis, J.B.F.N. Engberts, D. Hoekstra, J. Chem. Soc., Faraday Trans. 90 (1994) 1905.
[9] M.J. Blandamer, B. Briggs, P.M. Cullis, J.B.F.N. Engberts, A. Kacperska, J. Chem. Soc., Faraday Trans. 91 (1995) 4275.
[10] C.R. Benatti, M.J. Tiera, E. Feitosa, manuscript in preparation.
[11] M. T Allen, L. Miola, D.G. Whitten, J. Am. Chem. Soc. 110 (1988) 3198.
[12] M.T. Allen, L. Miola, D.G. Whitten, J. Phys. Chem. 24 (1991) 6099.
[13] J. Lakowics, Principles of Fluorescence Spectroscopy. Plenum Press, New York, 1983.
[14] R.P. Rand, D. Chapman, K. Larsson, Biophys. J. 15 (1975) 1117.
[15] M.J. Janiak, D.M. Small, G.G. Shipley, Biochemistry 15 (1976) 4575.
[16] K. Kalyanasundaram, Photochemistry in Microheterogeneous Systems, Academic Press, New York, 1987, p. 40.

unesp

artigo IX

ELSEVIER

Chemistry and Physics of Lipids
105 (2000) 201–213

CPL
CHEMISTRY AND PHYSICS OF LIPIDS

www.elsevier.com/locate/chemphyslip

Phase transition in dioctadecyldimethylammonium bromide and chloride vesicles prepared by different methods

E. Feitosa [a,*], P.C.A. Barreleiro [b], G. Olofsson [b]

[a] *Department of Physics, IBILCE/UNESP, C.P. 136, 15054-000 São José do Rio Preto, SP, Brazil*
[b] *Physical Chemistry 1, Center for Chemistry and Chemical Engineering, University of Lund, PO Box 124, S-221 00 Lund, Sweden*

Received 7 June 1999; received in revised form 25 January 2000; accepted 25 January 2000

Abstract

The gel to liquid crystalline phase transition of the double-chained cationic dioctadecyldimethylammonium chloride and bromide (DODAX, X = Cl^- or Br^-) in aqueous vesicle dispersions prepared by non-sonication, sonication and extrusion has been investigated using high-sensitivity differential scanning calorimetry (DSC). The transition temperature (T_m) is a function of the preparation method, amphiphile concentration, vesicle curvature and nature of the counterion. DSC thermograms for DODAB and DODAC non-sonicated vesicle dispersions exhibit a single endothermic peak at T_m roughly independent of concentration up to 10 mM. Extrusion broadens the transition peak and shifts T_m downwards. Sonication, however, broadens slightly the transition peak and tends to shift T_m upwards suggesting that extrusion and sonication form vesicles with different characteristics. DODAC always exhibits higher T_m than DODAB irrespective of the preparation method. T_m changes as follows: T_m (sonicated) $\geq T_m$ (non-sonicated) $> T_m$ (extruded). Hysteresis of about 7°C was observed for DODAB vesicle dispersions. © 2000 Elsevier Science Ireland Ltd. All rights reserved.

Keywords: Differential scanning calorimetry; Transition temperature; Sonicated vesicles; Non-sonicated vesicles; Extruded vesicles

1. Introduction

The assembling of hydrated synthetic or natural amphiphiles into vesicle structures offers unique opportunities to mimic complex biomembranes and to develop artificial drug carriers. The knowledge of the structure and properties will be essential for the application of vesicles as mimetic agents or drug delivery vehicles (e.g. gene therapy). For example, it is necessary that vesicles have a narrow size distribution and long term stability (Fendler, 1982).

Abbreviations: $DODA^+$, dioctadecyldimethylammonium ion; DODAB, dioctadecyldimethylammonium bromide; DODAC, dioctadecyldimethylammonium chloride; DSC, differential scanning calorimetry; GUV, giant unilamellar vesicles; LUV, large unilamellar vesicles; SUV, small unilamellar vesicles; T_m, transition temperature.

* Corresponding author. Tel.: +55-17-2212240; fax: +55-17-2248692.
E-mail address: eloi@df.ibilce.unesp.br (E. Feitosa)

0009-3084/00/$ - see front matter © 2000 Elsevier Science Ireland Ltd. All rights reserved.
PII: S0009-3084(00)00127-4

unesp

In spite of being one of the most investigated vesicle-forming cationic synthetic amphiphiles, the structure and properties of dioctadecyldimethylammonium bromide (DODAB) and chloride (DODAC) vesicles are still not fully understood. Overall, vesicle size, polydispersity, thermotropic phase behavior, surface potential, degree of ionization, permeability and physical stability depend on the preparation protocol and physical conditions of the bulk solution, such as temperature or ionic strength (Szoka and Papahadjopoulos, 1980; Fendler, 1982; Lasic, 1993). Bath- or probe-type sonication (Kunitake and Okahata, 1977; Carmona-Ribeiro and Chaimovich, 1983; Cuccovia et al., 1990) and chloroform slow injection (Carmona-Ribeiro and Chaimovich, 1983; Nascimento et al., 1998) are by far the most commonly used methods to prepare small and large unilamellar vesicles, respectively, of DODA*X* ($X = Cl^-$ or Br^-) and other synthetic amphiphiles. Chloroform slow injection gives large and (meta)stable unilamellar vesicles whereas ethanol quick injection gives small and unstable unilamellar vesicles (Cuccovia et al., 1979). More recently, dichloromethane injection was used to prepare stable large unilamellar vesicles (LUVs) from DODAC with the advantage that the boiling temperature of CH_2Cl_2 is lower than that of $CHCl_3$ (Cuccovia et al., 1997). Above the main transition temperature (T_m) DODAX molecules self-assemble in aqueous solution into stable giant unilamellar vesicles (GUVs) (Feitosa and Brown, 1997; Feitosa et al., manuscript submitted for publication) whereas extrusion yields vesicles with size controlled by the pore size of the membrane filter (Cuccovia et al., 1997; Lopes et al., unpublished data). However, the relatively high T_m of DODAX has limited the applicability of extrusion to prepare vesicles of these synthetic amphiphiles. In spite of the extrusion method being ordinarily used in the preparation of phospholipid liposomes (Hunter and Frisken, 1998), to our knowledge properties like size or transition temperature of extruded DODAB or DODAC vesicles have been only poorly investigated.

Calorimetry (Blandamer et al., 1992, 1994, 1995; Benatti et al., 1999), light scattering (Feitosa and Brown, 1997), turbidity (Carmona-Ribeiro and Chaimovich, 1983, 1986), fluorescence (Sarpal and Durocher, 1994; Benatti et al., 1999), surface tension (Gugliotti et al., 1998), and electron spin resonance (Lan et al., 1992) are the most often used techniques to determine T_m of natural or synthetic amphiphiles in vesicle dispersions. Since different methods may explore different physical phenomena related to the change in conformation of the amphiphilic chains within the vesicle bilayer, it is not surprising that different or even conflicting values of T_m for analogous amphiphilic systems have been reported. Table 1 summarizes values of T_m reported in the literature for DODAX vesicles prepared by different methods under different solvent conditions. T_m also depends on the source of the amphiphiles which, depending on the degree of purity (e.g. chain length distribution), may or may not yield a pretransition (Ladbrooke and Chapman, 1969).

Differential scanning calorimetry (DSC) is a useful tool to investigate the thermotropic phase behavior and determine T_m of amphiphiles in vesicle and liquid–crystal systems (Ladbrooke and Chapman, 1969; Kodama et al., 1981, 1990; Linseisen et al., 1996; Schulz et al., 1998). The major advantage of DSC is that it does not require the addition of spectroscopic probes to the system. T_m values for DODAB (Blandamer et al., 1992, 1994, 1995; Schulz et al., 1998; Benatti et al., 1999), and DODAC (Kodama et al., 1981, 1990; Linseisen et al., 1996) in water obtained by DSC have been reported. However, detailed investigations of T_m for DODAX vesicle systems within the dilute and semi-dilute concentration regimes as a function of the preparation method is scarce in the literature. Blandamer et al. (1992, 1994, 1995) used DSC to investigate T_m of DODAB in the presence and absence of micelle-forming cationic and anionic surfactants. These authors, however, limited their investigations to a fixed concentration of the amphiphile and the vesicles were prepared using the non-sonication and ethanol injection protocols. More recently, Gugliotti et al. (1998) reported T_m values from surface pressure measurements for DODAC which are lower (37.5°C) than those obtained by DSC shown here and in previous communications (Blandamer et al., 1992, 1994, 1995; Linseisen et



al., 1996; Benatti et al., 1999). Lan et al. (1992) used electron spin resonance (ESR) and pyrene excimer formation and obtained T_m values of 38 and 40°C, respectively, for DODAB. Kodama et al. (1981, 1990) and Schulz et al. (1998) reported T_m values for DODAX obtained by DSC at higher concentrations of the amphiphile in the crystalline phase. Our results on T_m of DODAX from DSC measurements are in very good agreement with those measured previously by the same technique (Blandamer et al., 1992, 1994, 1995; Linseisen et al., 1996; Benatti et al., 1999). Since T_m indicates the vesicle stability and permeability (Lasic, 1993) it is perhaps, besides the size and surface electrostatic potentials, the most characteristic property which can be used to characterize the dispersions. The aim of this work is to use DSC to investigate how the vesicle preparation protocol, size, nature of counterion and amphiphile concentration influence the transition temperature of DODAX in vesicle dispersions.

Values of T_m reported here for DODAX vesicles prepared by different protocols may be useful to those who make practical or scientific use of these synthetic vesicles in particular and of amphiphilic vesicles in general. We also hope that our findings may stimulate further investigations on the phase behavior in this kind of vesicle systems.

2. Materials and methods

2.1. Reagents

High purity DODAB from Avanti Polar Lipids (purity better than 99%) was used as purchased; recrystallized DODAC, obtained by counterion exchange from DODAB (Eastman Kodak, purity 99.5%) as described elsewhere (Cuccovia et al., 1997), was kindly supplied by Dr I.M. Cuccovia to whom we are indebted. Ultra pure water of

Table 1
Values of T_m found in the literature for DODAX vesicles and the preparation methods used

Amphiphile	Solvent	Protocol	T_m (°C)[a]	Methodology	Ref.*
DODAC	NaCl 5.0 mM	Tip-sonication	37.5	Surface pressure	c
DODAC	NaCl 42 mM	Tip-sonication	38.6	Turbidity	d
DODAC	Water	Tip-sonication	38.0	ESR	e
DODAC	Water	Tip-sonication	40.0	Pyrene excimer	e
DODAC	Water	Tip-sonication	37.5 (34.8)[a]	Turbidity	f[a]
DODAC	Water	$CHCl_3$-injection	38.6 (34.4)[a]	Turbidity	f[a]
DODAC	Water	$CHCl_3$-injection	47.5 (42.0)[a]	Turbidity	g[b]
DODAC	Water	Non-sonication	46[b]	DSC	h[a]
DODAB	HEPES 50 mM pH = 7	Non-sonication	47.8	DSC	i
DODAB	Water	Bath-sonication	45.0	Light scattering	j
DODAB	Water	Tip-sonication	36.0	Fluorescence	k
DODAB	Water	Tip-sonication	36.0	Anisotropy	l
DODAB	Water	Sonication	43.0	Quantum yield	m
DODAB	Water	Bath-sonication	44.4	DSC	m
DODAB	Water	Non-sonication	42.0	Quantum yield	m
DODAB	Water	Non-sonication	45.2	DSC	m
DODAB	Water	Non-sonication	44.8	DSC	m[b]
DODAB	Water	$CHCl_3$-injection	43.5(39.0°C)[a]	Turbidity	f[b]
DODAB	Water	Tip-sonication	35.0	Anisotropy	o

[a] Measurement made under cooling the sample.
[b] Value of T_m obtained at 14.3 wt.% (~0.24 M) DODAC.
* c = Gugliotti et al. (1998); d = Carmona-Ribeiro and Chaimovich (1986); e = Lan et al. (1992); f = Carmona-Ribeiro and Chaimovich (1983); g = Nascimento et al. (1998); h = Schulz et al. (1998); i = Linseisen et al. (1996); j = Feitosa and Brown (1997); k = Sarpal and Durocher (1994); l = Andersson et al. (1995); m = Benatti et al. (1999); n = Blandamer et al. (1992); o = Guillame et al. (1991).

cm 1 2 3 4 5 6 7 8 unesp 12 13 14 15 16 17 18 19

Milli-Q-Plus quality was used to prepare the samples.

2.2. Preparation of vesicles

Giant unilamellar vesicles (GUVs) were prepared by simply mixing DODAX and water to a desired final concentration (usually below 5 mM) and warming the mixture to 60°C (above T_m) to obtain a homogeneous solution (Feitosa and Brown, 1997; Feitosa et al., manuscript submitted for publication). Small unilamellar vesicles (SUVs) were prepared using a bath-type sonicator (Starsonic 90, Liarre) with a temperature controlled water bath. The dispersion was placed in a sealed cylindrical glass tube at 60°C and sonicated to give a clear (slightly bluish) dispersion (Feitosa and Brown, 1997). The cylindrical glass tube is required to improve the sonication efficiency. The time required to form a clear dispersion depends primarily on the sonicator power supply, on the amphiphile concentration, volume of solution and shape of the tube (Feitosa and Brown, 1997). One hour is a typical time required to form clear dispersions of DODAX. The effect of sonication temperature on the physico-chemical properties is not yet well understood, but it is likely that it has only minor effects on the structure of sonicated vesicles. The extruded size-controlled vesicles were obtained using an extrusion system (Avanti Polar Lipids, Alabaster, AL). Extrusions were performed manually through two stacked 13 mm polycarbonate filters with nominal pore diameters (ϕ) of 50, 100, 200 and 400 nm. The dispersions of DODAX were extruded at 60°C which is safely above T_m of the amphiphile. After being prepared the vesicle dispersions were stored at room temperature for at least 2 h before starting the DSC scans.

2.3. DSC measurements

A high-sensitive differential scanning calorimeter MicroCal MC-2 (MicroCal, Northampton, MA) was used for the DSC measurements. It is equipped with twin cells of 1.2 ml for the reference and sample solutions. The Origin™ software (version 2.9) was used for data acquisition and analyses. The sample and reference cells were filled with the vesicle solution and solvent. The solutions were degassed (Nueva II stirrer, Termolyne) before being transferred to the cells using a Hamilton syringe. The instrument measures the power required to keep the temperature of the sample and reference cells equal while the temperature is raised (upscan) or lowered (downscan) at a constant rate. The reference thermogram for both cells filled with the same solvent was recorded under the same conditions. The difference between the sample and reference thermograms is proportional to the excess heat capacity, ΔC_p. The transition enthalpy, ΔH_m, was calculated from the area under the peak, and the temperature at the peak maximum was taken to indicate the transition temperature, T_m. The shape of the curve gives additional information about the phase transition and the width at half-height ($\Delta T_{1/2}$) is related to the cooperativity of the transition, which is higher the narrower is the peak. Downscan thermograms were obtained as well and the existence of hysteresis detected. The DSC scans were repeated at least twice to check the reproducibility.

3. Results and discussion

The main phase transition in vesicle systems observed by DSC is characterized by the transition temperature (T_m), enthalpy of transition (ΔH_m), and shape and width at half-height ($\Delta T_{1/2}$), of the transition peak. The DSC traces were the same whether the vesicle dispersions were prepared directly at the concentration for the DSC measurements, or prepared at a higher concentration and then diluted (results not shown). The effect of the scan rate on the thermograms of DODAB is shown in Fig. 1A and the parameters T_m, ΔH_m and $\Delta T_{1/2}$ are summarized in Table 2. As seen from Fig. 1B, T_m of DODAB increases in a roughly sigmoidal way with the scan rate while the width of the peak increases only slightly and the transition enthalpy is roughly constant at the mean value of 10.5 kcal/mol. Thus, the effect of varying scan rate is small and regular. Except otherwise noted, all the DSC upscans were made at a rate of 53°C/h.



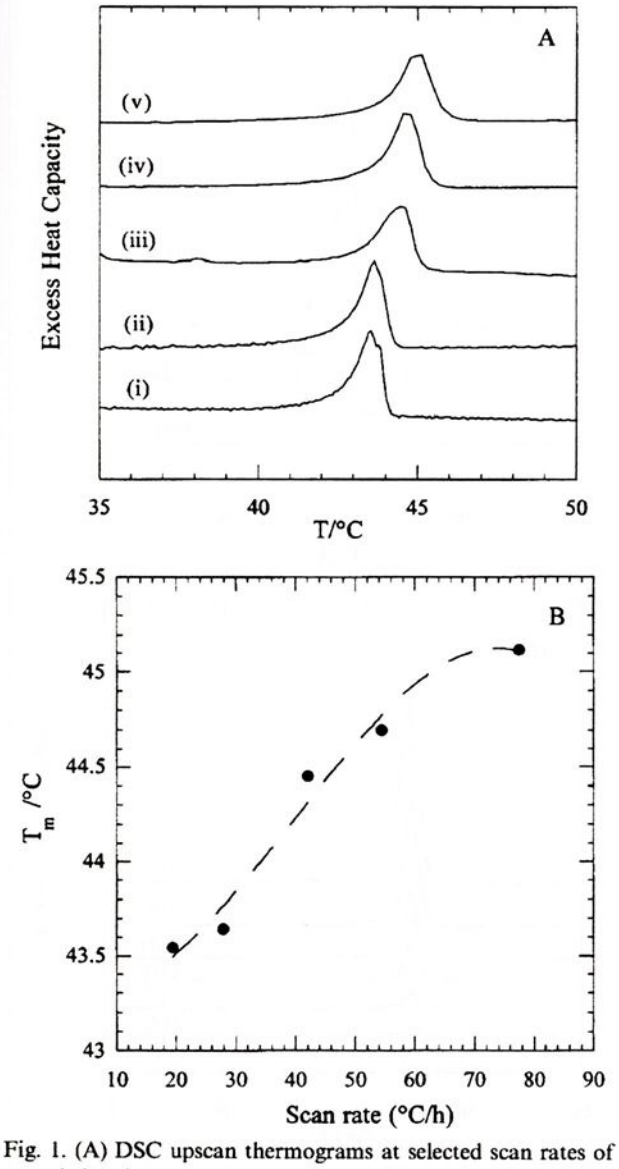


Fig. 1. (A) DSC upscan thermograms at selected scan rates of extruded DODAB vesicles in aqueous dispersions prepared using a membrane with 200 nm pore diameter: (i) 19.4°C/h (ii) 27.9°C/h (iii) 42.0°C/h (iv) 54.4°C/h and (v) 77.4°C/h. (B) Effect of the scan rate on the transition temperature of these vesicles.

The thermograms for DODAX vesicles prepared by non-sonication, sonication and extrusion through a membrane filter of $\phi = 100$ nm at selected concentrations of the amphiphiles are shown in Figs. 2–4. The curves in these diagrams are shown at the same amplification to clearly show that the peak intensity increases with concentration. The thermograms for DODAX vesicles prepared by extrusion using membrane filters with different pore diameters are shown in Fig. 5. Table 3 summarizes the values of T_m, $\Delta T_{1/2}$ and ΔH_m for DODAX vesicles in 1.0 mM dispersions prepared by different protocols. Fig. 6 shows the effect of DODAX concentration on T_m for vesicles prepared by the three methods. The effect of the pore diameter (ϕ) on T_m of DODAX 1.0 mM in extruded dispersions is shown in Fig. 7. Downscan traces for DODAB vesicles prepared in different ways are shown in Fig. 8.

3.1. Effects of vesicle preparation method

3.1.1. Non-sonication

The thermograms for DODAX in non-sonicated vesicle dispersions exhibit a single and relatively sharp endothermic peak with $\Delta T_{1/2} \approx 0.65$°C (Fig. 2A and B) characteristic of structurally homogeneous dispersions and of a cooperative gel-to-liquid-crystalline phase transition. The peaks are relatively sharp up to ca. 10 mM. At about this concentration DODAB (but not DODAC) exhibits two additional small but well-defined peaks at $T_s = 36.3$°C and $T_p = 52.6$°C, whereas T_m remains at about 45°C. Here T_s and T_p denote the pre- and post-transition temperatures. The dependence of T_m on the concentration of DODAX in the non-sonicated dispersions is shown in Fig. 6A and B. Below ca. 1.0 mM for DODAB and 0.5 mM for DODAC, T_m decreases slightly when the concentration is increased but above these concentrations T_m remains roughly constant.

Table 2
Thermodynamic parameters for 1.0 mM DODAB vesicles prepared by extrusion (pore filter $\phi = 200$ nm) at different scan rates

Scan rate (C/h)	T_m (°C)[a]	$T_{1/2}$ (°C)	ΔH_m (kcal/mol)[a]
19.4	43.5	0.71	10.4
27.9	43.6	0.72	10.4
42.0	44.4	0.82	11.0
54.4	44.7	0.88	10.6
77.4	45.1	1.01	9.9

[a] Estimated error in T_m and ΔH_m: ± 0.1°C and ± 0.5 kcal/mol, respectively.

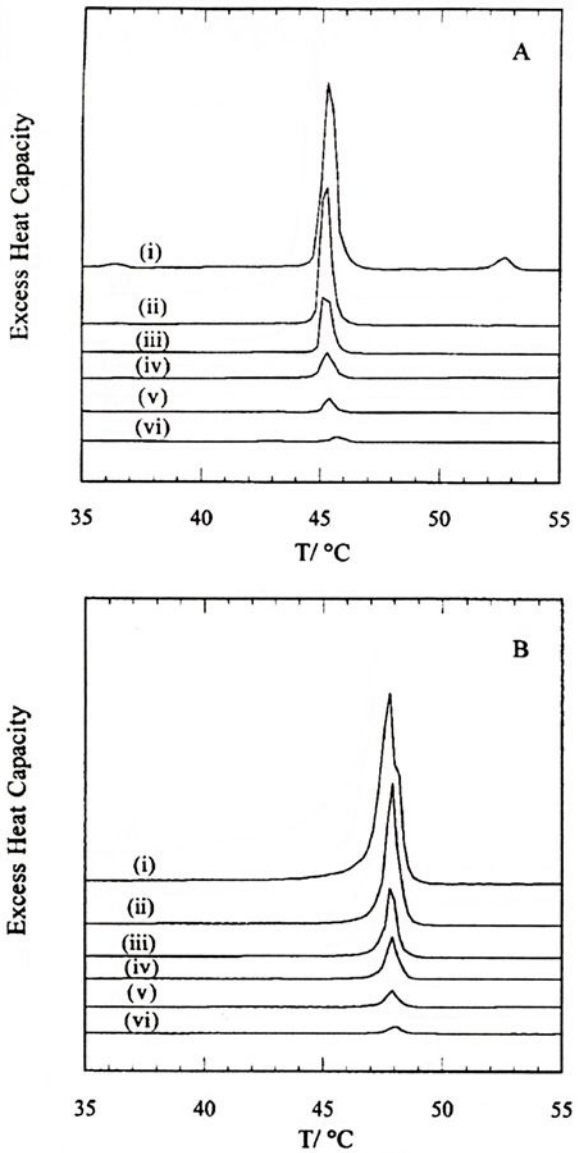


Fig. 2. DSC upscan thermograms of DODAB (A) and DODAC (B) aqueous vesicle dispersions prepared by non-sonication, at selected concentrations of the amphiphiles: (i) 10 mM (ii) 5 mM (iii) 2 mM (iv) 1 mM (v) 0.5 mM and (vi) 0.25 mM.

For all concentrations (up to 10 mM) T_m is always higher for DODAC than for DODAB in non-sonicated vesicle dispersions as well as in sonicated and extruded dispersions, as shown below. It is an observation not so clear from the literature (see Table 1). The higher T_m for DODAC relative to DODAB cannot be explained only on the basis of the vesicle curvature, since for a given vesicle preparation method, DODAB vesicles exhibit lower curvature than DODAC vesicles (Lopes et al.; Feitosa et al., unpublished data) and, as shown below, T_m decreases when the curvature is increased (see Table 3). Vesicles of saturated phospholipids also show decreasing T_m with increasing curvature of the liposomes. According to Brady et al. (1986), the stiffness of the hydrocarbon chains within the bilayer depends on the counterion binding to the vesicle interfaces.

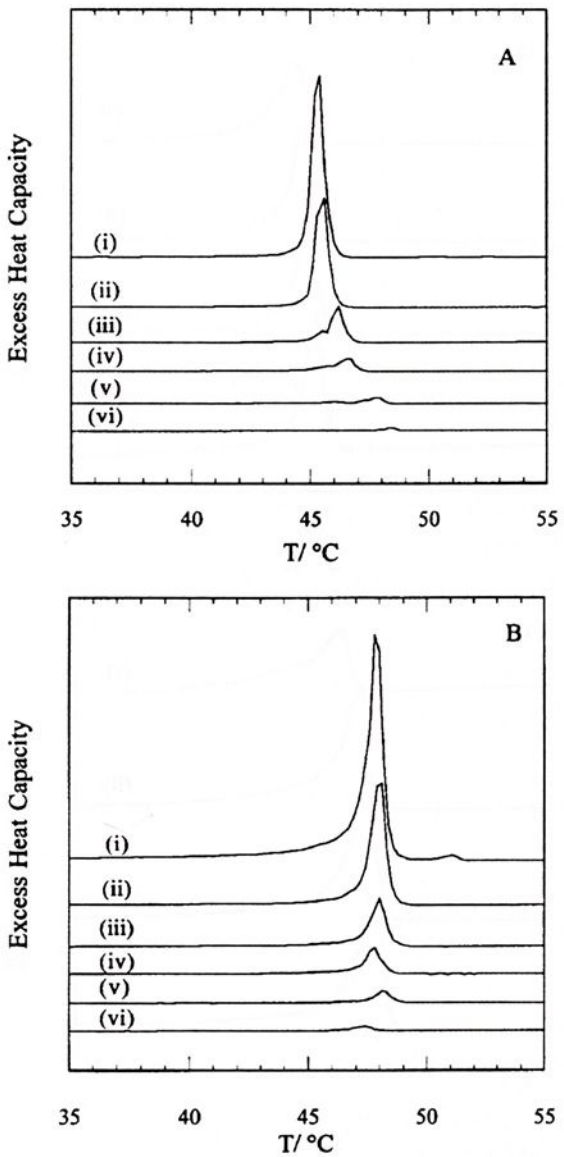


Fig. 3. DSC upscan thermograms of DODAB (A) and DODAC (B) aqueous vesicle dispersions prepared by sonication, at selected concentrations of the amphiphiles: (i) 10 mM (ii) 5 mM (iii) 2 mM (iv) 1 mM (v) 0.5 mM and (vi) 0.25 mM.

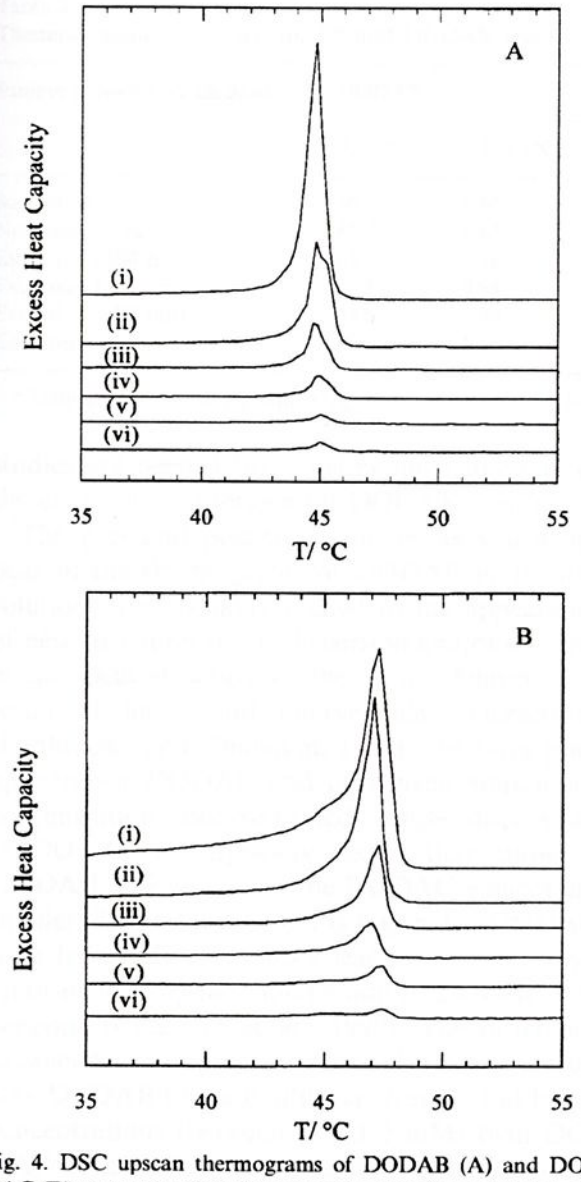


Fig. 4. DSC upscan thermograms of DODAB (A) and DODAC (B) aqueous vesicle dispersions prepared by extrusion, at selected concentrations of the amphiphiles: (i) 10 mM (ii) 5 mM (iii) 2 mM (iv) 1 mM (v) 0.5 mM and (vi) 0.25 mM.

Underwood and Anacker (1987) concluded from their study of the effect of various counterions on decyltrimethylammonium micelles that counterions that are highly effective in promoting micellization are those that interact the least strongly with water. The most effective ions also bind most closely to the amphiphile aggregates. The CMC values correlated best with the lyotropic numbers of the anions. In general, not only the radius of the hydrated counterion but also its polarizability and lyotropicity determine the structure and properties of the micellar or vesicular aggregates. Since Br^- and Cl^- have about the same hydrated radius (2.06 and 1.82 Å, respectively) but differing polarizability (4.27 and 3.01 $Å^3$, respectively) (Cacace et al., 1997), the polarizability instead is probably the most important factor of the higher T_m of DODAC relative to DODAB. Further

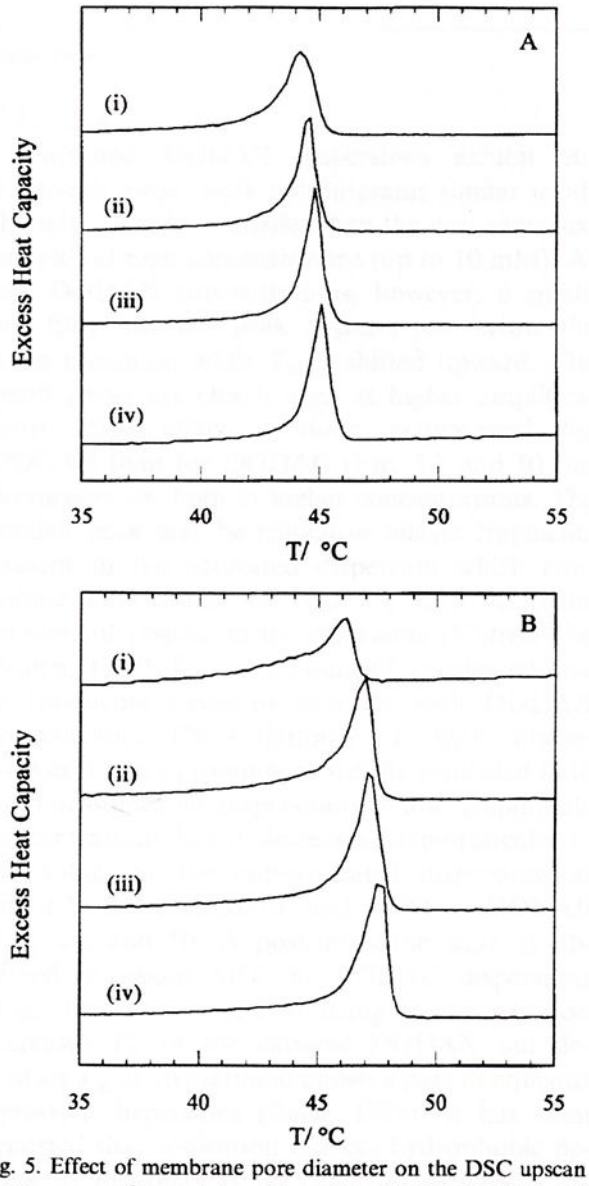


Fig. 5. Effect of membrane pore diameter on the DSC upscan thermograms of extruded vesicles of 1 mM DODAB (A) and DODAC (B): (i) 50 nm (ii) 100 nm (iii) 200 nm and (iv) 400 nm.

Table 3
Thermodynamic parameters for 1.0 mM DODAX vesicles in water prepared by different methods

Sample preparation method	DODAB			DODAC		
	T_m (°C)[a]	$\Delta T_{1/2}$ (°C)	ΔH_m (kcal/mol)[a]	T_m (°C)[a]	$\Delta T_{1/2}$ (°C)	ΔH_m (kcal/mol)[a]
Sonication	46.7	0.66	10.0	47.8	0.66	10.4
Non-sonication	45.3	0.65	10.7	47.9	0.65	13.0
Extrusion (400 nm)	45.2	0.88	10.8	47.6	1.10	13.1
Extrusion (200 nm)	44.8	0.88	10.6	47.1	1.10	12.8
Extrusion (100 nm)	44.6	0.88	10.3	46.9	1.10	12.7
Extrusion (50 nm)	44.3	1.32	9.9	46.2	1.55	10.8

[a] Estimated error in T_m and ΔH_m: ± 0.1°C and ± 0.5 kcal/mol, respectively.

studies are needed for a better understanding of the effect of counterions on DODAX vesicles.

The pre- and post-transition peaks which appear in the thermograms of DODAB in 10 mM solutions are probably related to the appearance of new structures in the dispersion and/or changes in the local structure of the vesicle bilayer as a result of intra- and intervesicular interactions (Ladbrooke and Chapman, 1969). No extra peak appears for DODAC and at a given amphiphile concentration, non-sonicated vesicle dispersions of DODAC are optically clearer than those of DODAB indicating that the DODAC vesicles are smaller. The zeta potential is higher for DODAC than for DODAB vesicles leading to a stronger repulsive electrostatic interaction in DODAC dispersions (Cuccovia et al., 1990). The difference between the zeta potentials may also be the reason why DODAB forms multilayer structures at lower concentrations (between 1 and 5 mM) than DODAC (above 10 mM) (Feitosa et al., manuscript submitted to publication; Feitosa and Amaral, unpublished data). As the concentration is increased the weaker intervesicular electrostatic repulsion in DODAB dispersions favors the formation of multilamellar instead of new unilamellar vesicles (Feitosa and Amaral, unpublished data). The transition from giant unilamellar vesicles to multilamellar structures gives no significant change in bilayer curvature (Feitosa et al., manuscript submitted to publication) and, therefore, the transition temperature T_m remains unchanged.

3.1.2. Sonication

Sonicated DODAX dispersions exhibit endothermic single-peak thermograms similar to although somewhat broader than the non-sonicated samples at high concentrations (up to 10 mM). At low DODAX concentrations, however, a small, not fully resolved peak appears just below the main transition while T_m is shifted upward. The small peaks are clearly seen at higher amplifications. This effect is more pronounced for DODAB than for DODAC (Fig. 3A and B) but disappears for both at higher concentrations. The smaller peak may be related to bilayer fragments present in the sonicated dispersion which contribute more to the pre-transition the lower is the amount of vesicles in the dispersion (Feitosa and Brown, 1997), for the amount of vesicles relative to fragments seems to increases with DODAX concentration The variation of T_m with concentration is more pronounced for the sonicated than for non-sonicated dispersions at low amphiphile concentrations but it decreases asymptotically to the value for the non-sonicated dispersions at about 1 mM for DODAC and 4 mM for DODAB (Fig. 6A and B). A post-transition peak is observed at about 51°C in DODAC dispersions (Fig. 3B). It is worth noticing that sonication increases T_m of the cationic DODAX but decreases T_m of zwitterionic phosholipids in aqueous liposome dispersions (Bach, 1984). It has been reported that sonication induces hydrophobic defects in the bilayers of DODAC vesicles (Carmona-Ribeiro and Chaimovich, 1986; Andersson et al., 1995), which may result in the formation of

SUVs having a 'lens-like' shape as a result of fragmentation of the larger bilayer structures. The arrangement of the alkyl chains may be more compact in this structure, which may be the reason for the surprising increase in T_m we observed. However, $\Delta T_{1/2}$ of the main transition was not significantly changed (Table 3), which indicates that sonication does not affect the cooperativity

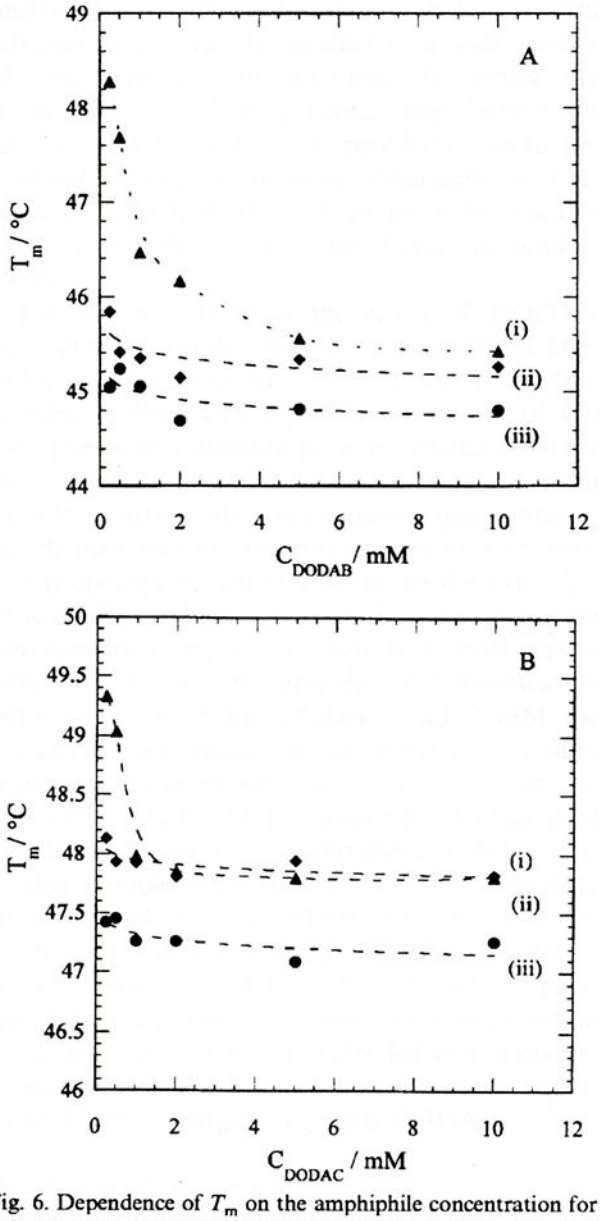


Fig. 6. Dependence of T_m on the amphiphile concentration for DODAB (A) and DODAC (B) unilamellar vesicles prepared by different protocols: (i) sonication (ii) non-sonication and (iii) extrusion.

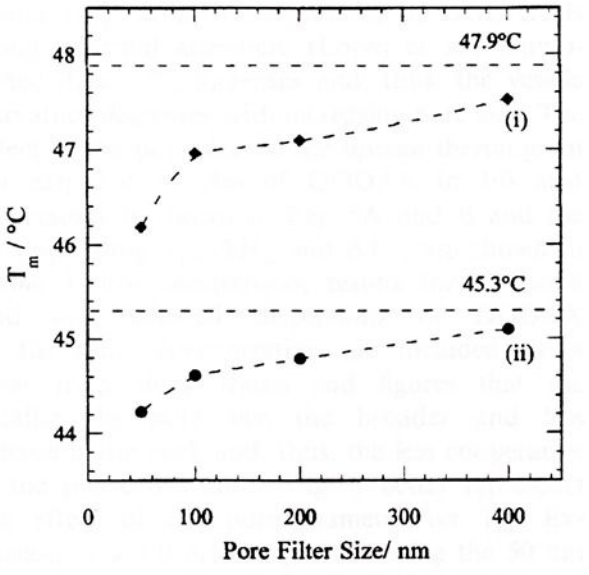


Fig. 7. Effect of membrane filter pore diameter on T_m of (i) DODAB and (ii) DODAC (1.0 mM) in extruded vesicle dispersions. T_m of DODAB (45.3°C) and DODAC (47.9°C) are indicated in the diagram by the dashed lines.

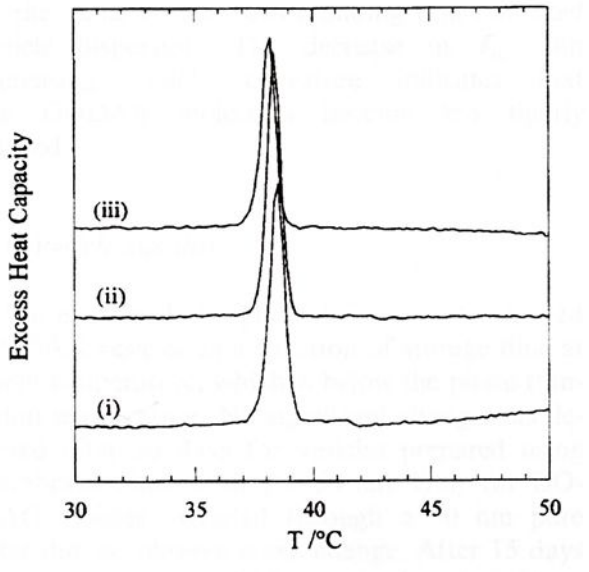


Fig. 8. DSC downscan thermograms obtained at the scan rate of 42°C/h for DODAB in aqueous vesicle dispersions prepared by (i) non-sonication, (ii) sonication and (iii) extrusion using a membrane with 200 nm pore diameter.

of the phase transition in vesicles of DODAB supplied by Avanti Polar Lipids. The significant broadening of the main transition and pre-transition peaks we observed for DODAB supplied by

Sigma in an earlier study probably was caused by impurities in the sample (Benatti et al., 1999). DODAC in sonicated dispersions like in the non-sonicated dispersions always exhibits higher T_m than DODAB.

3.1.3. Extrusion

Extrusion is currently one of the most common methods for reducing vesicle size and producing unilamellar vesicles. The technique has several advantages and can be applied to a wide variety of lipid species and mixtures. It allows the preparation of homogeneous populations of LUVs or SUVs and avoids problems due to the removal of organic solvents, detergents or titanium artifacts from the final preparations used in other protocols (Szoka and Papahadjopoulos, 1980).

Fig. 4A and B show the effect of DODAX concentration on the upscan thermogram of DODAX vesicles prepared by extrusion through a membrane filter with a pore diameter (ϕ) of 100 nm. The main transition peak is broader than for the corresponding sonicated or non-sonicated samples, particularly toward lower temperatures, which may indicate the presence of smaller vesicles (polydisperse sample) owing to the extrusion process. Fig. 6A and B also show that like the non-sonicated dispersions there is a small dependence of T_m on the amphiphile concentration below ca. 1 mM for DODAC and 2 mM for DODAB. Like sonication, the effect of extrusion is not only of increasing the vesicle curvature, but also of modifying the polydispersity (Cuccovia et al., 1997; Lopes et al., unpublished data). Extruded samples of DODAC exhibit a slightly broader peak than DODAB (Fig. 4A and B), suggesting that the transition is more cooperative for DODAB than for DODAC. No pre- or post-transitions are observed within the concentration range studied. DODAC in extruded vesicle dispersions like in sonicated and non-sonicated dispersions exhibits a higher T_m than DODAB.

3.2. Effect of vesicle size

A detailed study on the effect of the pore size of the extrusion membrane on the hydrodynamic radius (R_H) of extruded vesicles of DODAX is being reported elsewhere (Lopes et al., unpublished data). R_H increases and, thus, the vesicle curvature decreases with increasing pore size. The effect of the pore size on the upscan thermogram for extruded vesicles of DODAX in 1.0 mM dispersions is shown in Fig. 5A and B and the corresponding T_m, ΔH_m and $\Delta T_{1/2}$ are shown in Table 3. For comparison, results for sonicated and non-sonicated dispersions of DODAX at the same concentration are included. It is clear from these traces and figures that the smaller the pore size the broader and less intense is the peak and, thus, the less cooperative is the phase transition. Fig. 7 better represents the effect of the pore diameter on T_m. Extrusion of a 1.0 mM dispersion using the 50 nm filter decreases T_m of DODAB by 2.4°C and of DODAC by 1.6°C relative to T_m of the non-sonicated dispersions. As seen from Table 3 and Fig. 7, T_m increases as the pore size is increased (or the vesicle curvature is decreased) to the value of the corresponding non-sonicated vesicle dispersion. The decrease in T_m with increasing vesicle curvature indicates that the DODAB molecules become less tightly packed.

3.3. Vesicle stability

We examined the phase behavior of extruded DODAX vesicles as a function of storage time at room temperature, which is below the phase transition temperature. No significant change was detected after 30 days for vesicles prepared using membrane filters with $\phi > 50$ nm. Only for DODAC vesicles extruded through a 50 nm pore filter did we observe some change. After 15 days T_m had increased 1.3°C but no further change was observed after one month. Values of ΔH_m and $\Delta T_{1/2}$ were unchanged. Thus, only the smallest extruded DODAC vesicles prepared using the 50 nm filter showed any change with time. Further investigations on DODAX vesicle stability, for instance in the presence of electrolytes, are underway by our group (Barreleiro et al., unpublished data).



3.4. T_m obtained in the DSC downscan mode

Fig. 8 depicts some downscan thermograms for DODAB in 1.0 mM dispersions and Table 4 summarizes the thermodynamic parameters obtained from the corresponding transition peaks. T_m of DODAB observed in the downscan mode is about 7.0°C lower (hysteresis) than the corresponding value obtained in the upscan mode independent of the preparation method (Table 4). Values of $\Delta T_{1/2}$ and ΔH_m, however, are about the same for both the up- and downscans (see Tables 3 and 4). Hysteresis of ca. 3.5°C for DODAB (and higher for DODAC) has been observed from turbidity measurements (Nascimento et al., 1998) and recently we observed no hysteresis for non-sonicated DODAB using steady state fluorescence (Benatti et al., 1999) suggesting that the hysteresis phenomenon may be sensitive to the method and experimental procedure used. Since T_m depends on the scan rate (Table 2) it is likely that smaller hysteresis may be observed at lower scan rates. Probably, the phase transition is not momentaneous and the different hysteresis observed by different methods stems from differences in observation times.

4. Summary and conclusions

Our DSC results show that T_m depends on the vesicle preparation protocol, vesicle size or curvature, amphiphile concentration and nature of the counterion. Sonication and extrusion give vesicles with different size and structure distribution (e.g. bilayer fragments, smooth or unsmooth 'lens-like' structures, etc.) as confirmed by light scattering and cryo-TEM (Andersson et al., 1995; Lopes et al., unpublished data;).

For both DODAB and DODAC, T_m decreases in the sequence sonication $\geq$ non-sonication > extrusion. For non-sonicated and extruded dispersions T_m is roughly independent on DODAX concentration, but for sonicated dispersions it decreases monotonically to a plateau value corresponding to that for non-sonicated dispersions as the concentration increases. The DSC results for extruded DODAX dispersions clearly suggest that T_m increases with increasing size (or decreasing curvature) of the vesicles. Surprisingly, sonication of DODAX dispersions at low concentrations gave a significant increase in T_m, probably due to defects in the bilayer and/or the presence of bilayer fragments caused by the sonication process rather than to curvature effects (Carmona-Ribeiro and Chaimovich, 1986; Feitosa and Brown, 1997). The results suggest that extrusion is the best method to prepare small unilamellar vesicles.

Within the investigated concentration range (up to 10 mM) DODAB always exhibits lower T_m than DODAC, irrespective of the method used to prepare the dispersions. The width of the main transition peak ($\Delta T_{1/2}$) is larger for extruded DODAC than for DODAB samples, suggesting that the transition from the gel-to-liquid crystalline phase is more cooperative for DODAB. T_m of DODAX in vesicle dispersions depends on whether the traces are made in the up- or downscan mode and exhibits a hysteresis of 6 to 7°C.

Our findings suggest that T_m can be used as a vesicle 'finger print'. T_m is an important physical parameter, which characterizes the state of aggregation of the amphiphilic vesicles, as suggested by Biltonen and Lichtenberg (1993) for phospholipid liposomes. Deviations from its regular value may be an indication of sample contamination or improper preparation of the vesicles. A better understanding of the effect of Br^- and Cl^- counterions on T_m of DODAX requires further investigation, for example on the effect of supporting electrolytes in vesicle systems. Such work is currently underway (Barreleiro et al., unpublished data).

Table 4
Downscan thermodynamic parameters for 1.0 mM DODAB vesicles prepared by different methods

Preparation method	T_m (°C)[a]	$T_{1/2}$ (°C)	ΔH_m (kcal/mol)[a]
Non-sonication	38.4	0.63	10.3
Sonication	38.5	0.67	10.3
Extrusion (200 nm)	38.2	0.83	10.4

[a] Estimated error for T_m and ΔH_m: ± 0.1°C and ± 0.5 kcal/mol, respectively.

Acknowledgements

E.F. thanks Fundação de Amparo à Pesquisa do Estado de São Paulo (FAPESP) for granting his visit to Sweden (Proc. 98/09772-4). P.C.A.B. acknowledges the PRAXIS XXI, JNICT for financial support, scholarship BD/13788/97.

References

Andersson, M., Hammarström, L., Edwards, K., 1995. Effect of bilayer phase transitions on vesicle structure and its influence on the kinetics of viologen reduction. J. Phys. Chem. 99, 14531–14538.

Bach, D., 1984. In: Chapman, D. (Ed.), Biomembrane Structure and Function. Verlag Chemie, Deerfield Beach, FLA.

Benatti, C.R., Feitosa, E., Tiera, M.J., Olofsson, G., 1999. Phase behavior of synthetic amphiphile vesicles investigated by calorimetry and fluorescence. Thermochim. Acta 328, 137–142.

Biltonen, R.L., Lichtenberg, D., 1993. The use of differential scanning calorimetry as a tool to characterize liposome preparations. Chem. Phys. Lipids 64, 129–142.

Blandamer, M.J., Briggs, B., Cullis, P.M., Engberts, J.B.F.N., Hoekstra, D., 1994. Differential scanning microcalorimetric study of sodium di-*n*-dodecylphosphate vesicles in aqueous solution. J. Chem. Soc. Faraday Trans. 90, 1905–1907.

Blandamer, M.J., Briggs, B., Cullis, P.M., Engberts, J.B.F.N., Kacperska, A., 1995. Vesicle-surfactant interactions-effects of added surfactants on the gel to liquid crystal transition for two vesicular systems. J. Chem. Soc. Faraday Trans. 91, 4275–4278.

Blandamer, M.J., Briggs, B., Cullis, P.M., Green, J.A., Waters, M., Soldi, G., Engberts, J.B.F.N., Hoekstra, D., 1992. Differential scanning microcalorimetric study of vesicles in aqueous solutions formed by dimethyldioctadecylammonium bromide. J. Chem. Soc. Faraday Trans. 88, 3431–3434.

Brady, J.E., Evans, D.F., Warr, G.G., Grieser, F., Ninham, B., 1986. Counterion specificity as the determinant of surfactant aggregation. J. Phys. Chem. 90, 1853–1859.

Cacace, M.G., Landau, E.M., Ramsden, J.J., 1997. The Hofmeiester series: salt and solvent effects on interfacial phenomena. Q. Rev. Biophys. 30, 241–277.

Carmona-Ribeiro, A.M., Chaimovich, H., 1983. Preparation and characterization of large dioctadecyldimethylammonium chloride liposomes and comparison with small sonicated vesicles. Biochim. Biophys. Acta 733, 172–179.

Carmona-Ribeiro, A.M., Chaimovich, H., 1986. Salt-induced aggregation and fusion of dioctadecyldimethylammonium chloride and sodium dihexadecylphosphate. Biophys. J. 50, 621–628.

Cuccovia, I.M., Aleixo, R.M.V., Mortara, R.A., Berci Filho, P., Bonilha, J.B.S., Quina, F.H., Chaimovich, H., 1979. Effect of dialkyldimethylammonium vesicles on the thiolysis of *p*-nitrophenyl acetate. Tetrahedron Lett. 3065–3068.

Cuccovia, I.M., Feitosa, E., Chaimovich, H., Sepulveda, L., Reed, W., 1990. Size, electrophoretic mobility, and ion dissociation of vesicles prepared with synthetic amphiphiles. J. Phys. Chem. 94, 3722–3725.

Cuccovia, I.M., Sesso, A., Abuin, E.B., Okino, P.F., Tavares, P.G., Campos, J.F.S., Florenzano, F.H., Chaimovich, H., 1997. Characterization of dioctadecyldimethylammonium chloride vesicles prepared by membrane extrusion and dichloromethane injection. J. Mol. Liquids 72, 323–386.

Feitosa, E., Brown, W., 1997. Fragment and vesicle structures in sonicated dispersions of dioctadecyldimethylammonium bromide. Langmuir 13, 4810–4816.

Fendler, J.H., 1982. Membrane Mimetic Chemistry. Wiley-Interscience, New York.

Gugliotti, M., Politi, M.J., Chaimovich, H., 1998. Phase transition temperature of vesicles determined by surface tension: a fast method. J. Colloid Interface Sci. 198, 1–5.

Guillame, B.C.R., Yogev, D., Fendler, J.H., 1991. Twisted intramolecular charge-transfer emissions of fluorescence probes in didodecyldimethylammonium bromide, dioctadecyldimethylammonium bromide and didodecylphosphate vesicles undergoing fusion. J. Phys. Chem. 95, 7489–7494.

Hunter, D.G., Frisken, B.J., 1998. Effect of extrusion pressure and lipid properties on the size and polydispersity of lipid vesicles. Biophys. J. 74, 2996–3002.

Kodama, M., Kunitake, T., Seki, S., 1990. Thermal characterization of the mode of phase transition in the dioctadecyldimethylammonium bromide water system in relation to the stability of its gel phase. J. Phys. Chem. 94, 1550–1554.

Kodama, M., Kuwabara, M., Seki, S., 1981. Thermal study on the interaction of crystalline surfactant with water: the dioctadecyldimethylammonium chloride-water system. Thermochim. Acta 50, 81–91.

Kunitake, T., Okahata, Y., 1977. A totally synthetic bilayer membrane. J. Am. Chem. Soc. 99, 3860–3861.

Ladbrooke, B.D., Chapman, D., 1969. Thermal analysis of lipids, proteins and biological membranes. A review and summary of some recent studies. Chem. Phys. Lipids 3, 304–367.

Lasic, D.D., 1993. Liposomes. From Physics to Applications. Elsevier, Amsterdam.

Lan, L., Pansu, R., Roncin, J., Faure, J., Arai, T., Tokumaru, K., 1992. Molecular organization in DODAC membrane fragments. J. Colloid Interface Sci. 148, 118–128.

Linseisen, F.M., Bayerl, S., Bayerl, T.M., 1996. ^{2}H NMR and DSC study of DPPC-DODAB mixtures. Chem. Phys. Lipids 83, 9–23.

Nascimento, D.B., Rapuano, R., Lessa, M.M., Carmona-Ribeiro, A.M., 1998. Counterion effects on properties of cationic vesicles. Langmuir 14, 7387–7391.

Sarpal, R.S., Durocher, G., 1994. Temperature-induced structural and permeability changes in dioctadecyldimethylammonium bromide (DODAB) vesicles: a fluorescence

cm 1 2 3 4 5 6 7 8 unesp 12 13 14 15 16 17 18 19

investigation using 2-[(*p*-methylamino)phenyl]-3,3-dimethyl-5-carboethoxy-^{3}H-iodole as a probe. J. Photochem. Photobiol. A: Chem. 80, 307–314.

Schulz, P.L., Rodriguez, J.L., Soltero-Martinez, F.A., Puig, J.E., Proverbio, Z.E., 1998. Phase behavior of the dioctadecyldimethylammonium bromide-water system. J. Therm. Anal. 51, 49–62.

Szoka, F. Jr., Papahadjopoulos, D., 1980. Comparative properties and methods of preparation of lipid vesicles (liposomes). Annu. Rev. Biophys. Bioeng. 9, 467–508.

Underwood, A.L., Anacker, E.W., 1987. Counterion lyotropy and micelle formation. J. Colloid Interface Sci. 117, 242–250.

artigo X



Progr Colloid Polym Sci (2000) 116: 33–36
© Springer-Verlag 2000

P. C. A. Barreleiro
G. Olofsson
E. Feitosa

Vesicle-to-micelle transition in dioctadecyldimethylammonium bromide and dioctadecyldimethylammonium chloride dispersions induced by octaethylene glycol *n*-dodecyl monoether. An isothermal titration calorimetry study

Abstract We have used isothermal titration calorimetry to investigate the vesicle-to-micelle transition in dioctadecyldimethylammonium bromide (DODAB) and chloride (DODAC) vesicle dispersions induced by the nonionic surfactant octaethylene glycol *n*-dodecyl monoether ($C_{12}E_8$) at room temperature. Small and giant unilamellar vesicles were prepared by sonication and without sonication, respectively, of the pure cationic surfactants at low concentrations in water. The titration of 1.0 mM DODA*X* (*X* = Cl^- and Br^-) by a concentrated micellar solution of $C_{12}E_8$ shows that the enthalpy of interaction (ΔH_{obs}) of $C_{12}E_8$ in micellar form with DODA*X* is always endothermic. The titration curves are understood on the basis of superposition of the enthalpies of partitioning of $C_{12}E_8$ into the bilayer, of micelle formation and of vesicle-to-micelle transformation. The enthalpy, ΔH_{obs}, initially increases owing to the incorporation of $C_{12}E_8$ into the vesicle bilayer until the $C_{12}E_8$/DODA*X* saturation ratio (R_{sat}) is reached, then ΔH_{obs} decreases, in different ways for DODAB and DODAC, owing to degradation of vesicles and formation of mixed micelles and intermediary structures up to the $C_{12}E_8$/DODA*X* solubilization ratio, R_{sol}. Above R_{sol} only mixed micelles exist. The surfactant solubilization takes place in three stages. All the critical ratios are lower for DODAB than for DODAC, meaning that $C_{12}E_8$ solubilizes more strongly in DODAB; for example, R_{sat} is 0.8 for DODAB and 1.2 for DODAC. Sonication has no significant effect on the transition.

Key words · Cationic vesicles · Dioctadecyldimethylammonium bromide · Dioctadecyldimethylammonium chloride · Isothermal titration calorimetry · Surfactant solubilization

P. C. A. Barreleiro · G. Olofsson
Physical Chemistry 1,
Center for Chemistry
and Chemical Engineering
University of Lund
P.O. Box 124, 221 00 Lund, Sweden

E. Feitosa (✉)
Physics Department
IBILCE/UNESP, 15054-000
São José do Rio Preto, SP, Brazil
e-mail: eloi@df.ibilce.unesp.br

This work is part of the results presented at the First Nordic–Baltic Meeting on Surface and Colloid Science, in Vilnius, Lithuania, from 21–25 August 1999

Introduction

Dioctadecyldimethylammonium bromide (DODAB) and chloride (DODAC) have been the most investigated long-chain (C18) vesicle-forming cationic surfactants since the first preparation and characterization of small unilamellar DODAB vesicles in 1977 by Kunitake and Okahata [1]. Since then a number of methods to prepare cationic vesicles from these and homologous surfactants have been developed to give long-term stability and size-controlled structures to be used in specific applications, such as membrane mimetic systems [2], drug and DNA carrier vehicles [3] or as catalysts [4].

The methods commonly used to prepare DODA*X* (here *X* denotes Br^- or Cl^-) vesicles are the same as used to prepare phospholipid liposomes [3]. They include tip- or bath-type sonication [1, 5], ethanol- [6], chloroform- [7] or dichloromethane-injection [8], extrusion [8] and the novel nonsonication (nonextrusion or noninjection) method, which gives giant unilamellar vesicles (GUVs)

[9–11]. Small amounts of DODAB or DODAC are simply mixed with the aqueous solvent above the gel-to-liquid-crystalline phase transition temperature (T_m) (around 45 °C for DODAB and 48 °C for DODAC in water) to prepare GUV dispersions, as reported recently by our group [9–11]. The physical properties of these vesicles are described in the literature [1, 5–11].

In our attempt to obtain "high-quality" DODA*X* vesicles by reducing their structure and size polydispersity as well as to search for new methods to prepare stabilized vesicles with well-controlled size distribution we have been investigating the effects of mixing DODA*X* with micelle-forming surfactants, such as octaethylene glycol *n*-dodecyl monoether ($C_{12}E_8$). Isothermal titration calorimetry is suitable for obtaining critical composition and thermodynamic parameters related to the surfactant solubilization [12]. Our results indicate that these surfactants mix together according to the "three-stage" model [13–15] to form stabilized structures like mixed vesicles and micelles or intermediary structures depending on the relative amount of the compounds in the mixture and on the nature of the counterion.

Materials and methods

Chemicals

DODAB with purity better than 99% (Avanti Polar Lipids, Alabaster, Ala.) was used as purchased. DODAC was obtained by counterion exchange from DODAB (Eastman Kodak) and recrystallized as described elsewhere [8]. $C_{12}E_8$ (Nikko Chemicals) was used as purchased. Ultrapure water of Milli-Q-Plus quality was used in the sample preparations.

Vesicle preparation

GUV dispersions were prepared by simply mixing DODAB or DODAC and water at a concentration of 1.0 mM at 60 °C (above the critical transition temperature, T_m) to obtain a homogeneous dispersion [9–11]. Small unilamellar vesicle (SUV) dispersions were prepared by bath-sonicating the GUV dispersion at 60 °C using a bath-type sonicator (Starsonic 90, Liarre) to obtain optically clear dispersions. After preparation the vesicle dispersions were cooled to room temperature and stored for at least 24 h before the calorimetric measurements.

Titration calorimetry measurements

The enthalpies of reaction (ΔH_{obs}) in the $C_{12}E_8$/DODA*X*/water system were measured in a stainless-steel titration vessel of 3 cm^3 in the prototype of the thermal activity monitor four-channel microcalorimeter at 25 °C [16]. The calorimetric signal was calibrated electrically [16]. Small aliquots of a concentrated $C_{12}E_8$ micellar solution were added to a 2.7-cm^3 aqueous DODA*X* vesicle dispersion of 1.0 mM placed in the vessel of the calorimeter. The additions were made using a gas-tight Hamilton syringe connected with a computer-operated syringe drive for good control of the injection volume and injection rates. Typically, 10-μl aliquots were injected over 120 s, with a time period between injections of at least 100 min. All measurements were made at least twice to ensure reproducibility.

Results and discussion

The vesicle-to-micelle transition of DODAB and DODAC vesicles in nonsonicated (GUV) and sonicated (SUV) dispersions induced by the nonionic amphiphile $C_{12}E_8$ was studied by isothermal titration calorimetry. The results of the calorimetric titration of a 1 mM DODAB vesicle dispersion with 54 mM $C_{12}E_8$ solution are shown in Fig. 1, where the observed enthalpy changes ΔH_{obs} (calculated per mole of $C_{12}E_8$ added) are plotted against the $C_{12}E_8$/DODAB molar ratio (R) in the final solution. When repeating the titration series but using pure water in the calorimetric vessel, the first injection gave a significant exothermic peak owing to demicellization but after a couple of injections the concentration is well above the critical micelle concentration (cmc) and only a weekly exothermic dilution enthalpy of −1.0 kJ mol^{-1} was seen. The cmc of $C_{12}E_8$ is 9.1×10^{-5} M^{-1} and the enthalpy of micelle formation, ΔH_{mic}, is 16.3 ± 0.4 kJ mol^{-1} at 25 °C [17]. With DODAB vesicles present in the solution, the first injection gave a weekly exothermic enthalpy change but then ΔH_{obs} increased steeply to a peak value of about 17.5 kJ mol^{-1} at $R = 0.6$. This indicates that a critical concentration of $C_{12}E_8$ must be reached before solubi-

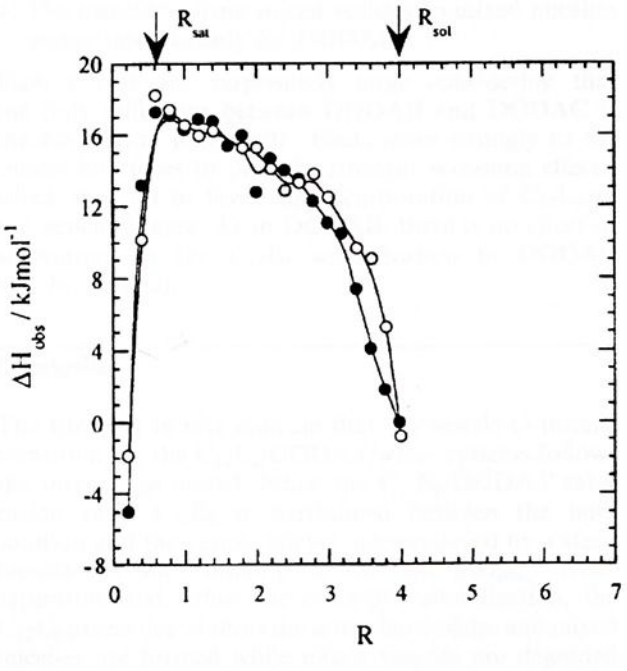


Fig. 1 Enthalpy of interaction as a function of octaethylene glycol *n*-dodecyl monoether ($C_{12}E_8$)/dioctadecyldimethylammonium bromide (*DODAB*) molar ratio, R, obtained by consecutive additions of aliquots of concentrated (54 mM) $C_{12}E_8$ solution to 1.0 mM DODAB dispersion. Dispersion prepared by sonication (●) and without sonication (○) (25 °C)

lization in DODAB vesicles takes place. After the peak ΔH_{obs} decreased steadily to R about 3.2, after which it dropped to close to zero. As seen from Fig. 1, sonication did not significantly change the titration curves. The results of addition of $C_{12}E_8$ solution to a 1 mM DODAC vesicle dispersion are shown in Fig. 2. After reaching a maximum value of about 6.0 kJ mol^{-1} at $R = 1.2$, ΔH_{obs} stays roughly constant till R is about 3.2, after which it gradually decreases to become close to zero at R around 5.8. Thus, the calorimetric titration curves show the same general features but the changes are more gradual and the enthalpic effects are smaller in the DODAC system than in the DODAB one.

The $C_{12}E_8$/DODAB/water system

When the $C_{12}E_8$ micellar solution is added to the DODAB vesicle dispersion, three stages can be discerned. In the first stage, $C_{12}E_8$ is partitioned between the bulk solution and the vesicle bilayers, resulting in a progressive increase in ΔH_{obs} to around 17.5 kJ mol^{-1} at the $C_{12}E_8$/DODAB mole ratio, R_{sat}, of about 0.6. In the second stage, above R_{sat}, the vesicles become unstable and start to degrade to form mixed micelles with the added $C_{12}E_8$. Dynamic light scattering results to be reported by our group show the existence in this stage of two populations with characteristic sizes of vesicles and micelles. As R is further increased the vesicle population decreases, whereas the micelle population increases continuously until R_{sol} is reached. Above R_{sol} (in the third stage) the vesicle-to-micelle transition is complete and only mixed micelles exist. Considering the ease with which cationic and nonionic surfactants mix nearly ideally to form mixed micelles [18], the formation of a homogeneous population of mixed micelles is more likely than a mixture of pure $C_{12}E_8$ and mixed micelles. The rapidly vanishing ΔH_{obs} indicates that the enthalpy content of $C_{12}E_8$ is approximately the same in the pure and in the mixed micelles.

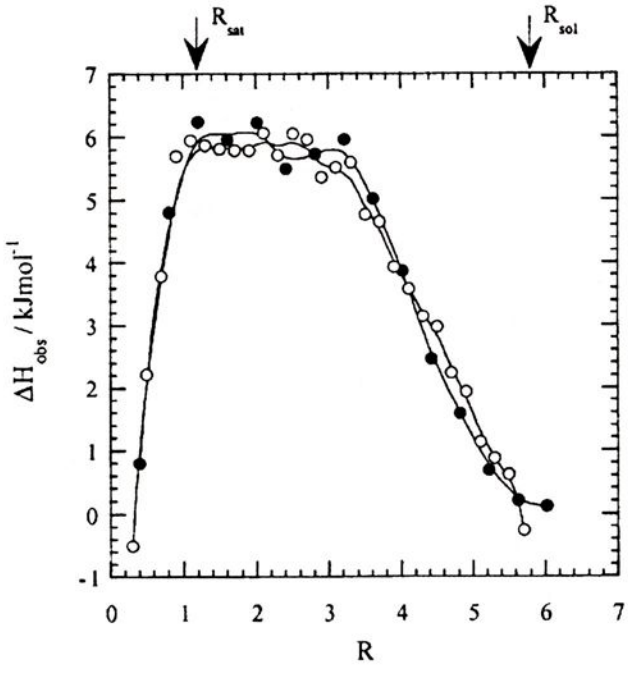


Fig. 2 Enthalpy of interaction as a function of $C_{12}E_8$/dioctadecyldimethylammonium chloride (*DODAC*) molar ratio, R, obtained by consecutive additions of aliquots of concentrated (54 mM) $C_{12}E_8$ solution to 1.0 mM DODAC dispersion. Dispersion prepared by sonication (●) and without sonication (○) (25 °C)

The $C_{12}E_8$/DODAC/water system

About the same general behavior was observed for the addition of $C_{12}E_8$ to a DODAC vesicle dispersion, except in the following respects (see Fig. 2):

1. The interaction enthalpy, ΔH_{obs}, is lower for DODAC than for DODAB.
2. Just above R_{sat} the enthalpy change reaches a plateau for DODAC but decreases for DODAB.
3. The critical ratios R_{sat} and R_{sol} are higher for DODAC than for DODAB.
4. The transition from mixed vesicles to mixed micelles occurs more steeply for DODAB.

Such effects are surprisingly large considering that the only difference between DODAB and DODAC is the counterion nature. Br^- binds more strongly to the vesicle interfaces to produce stronger screening effects, which appears to favor the incorporation of $C_{12}E_8$ in the vesicle bilayer. As in DODAB, there is no effect of sonication on the $C_{12}E_8$ solubilization in DODAC vesicles (Fig. 2).

Conclusion

The titration results indicate that the vesicle-to-micelle transition for the $C_{12}E_8$/DODA*X*/water systems follows the three-stage model: below the $C_{12}E_8$/DODA*X* saturation ratio $C_{12}E_8$ is partitioned between the bulk solution and the vesicle bilayer, accompanied by a steep increase in the enthalpy of reaction (ΔH_{obs}). After saturation and below the complete solubilization, the $C_{12}E_8$ excess destabilizes the saturated vesicles and mixed micelles are formed while mixed vesicles are degraded continuously. Above the solubilization ratio, all vesicles have been degraded and only mixed micelles remain. For both the DODAB and DODAC systems, there is no significant effect of sonication on the titration curve. A detailed investigation of solubilization phenomena in

$C_{12}E_8$/DODAX/water systems is currently underway by our group using different experimental techniques to providing a better understanding of the vesicle-to-micelle transition mechanism and morphology of the aggregates in each stage of the transition.

Acknowledgements E.F. wishes to thank FUNDUNESP for partially granting his participation in the "First Nordic–Baltic Meeting on Surface and Colloid Science". P.C.A.B. acknowledges the PRAXIS XXI, JNICT for financial support, scholarship BD/13788/97. We express our gratitude to I. M. Cuccovia for supplying the DODAC samples.

References

1. Kunitake T, Okahata Y (1977) J Am Chem Soc 99:3860
2. Fendler JH (1982) Membrane mimetic chemistry. Wiley–Interscience, New York
3. Lasic DD (1993) Liposomes. From physics to applications. Elsevier, Amsterdan
4. Bunton CA (1991) In: Rubingh DN, Holland PM (eds) Cationic surfactants. Physical chemistry. Surfactant science series, vol 37. Dekker, New York, p 323
5. Cuccovia IM, Feitosa E, Chaimovich H, Sepulveda L, Reed WF (1990) J Phys Chem 94:3722
6. Cuccovia IM, Aleixo RMV, Mortara RA, Berci Filho P, Bonilha JBS, Quina FH, Chaimovich H (1979) Tetrahedron Lett 3065
7. Carmona-Ribeiro AM (1992) Chem Soc Rev 21:209
8. Cuccovia IM, Sesso A, Abuin E, Okino PF, Tavares PG, Campos JFS, Florenzano FH, Chaimovich H (1997) J Mol Liq 72:323
9. Feitosa E, Brown W (1997) Langmuir 13:4810
10. Benatti CR, Tiera MJ, Feitosa E, Olofsson G (1999) Thermochim Acta 328:137
11. Feitosa E, Barreleiro PCA, Olofsson G (2000) Chem Phys Lipids 105:210
12. Heerklotz H, Lantzcsch G, Binder H, Klose G, Blume A (1995) Chem Phys Lett 235:517
13. (a) Lichtenberg D, Robson RJ, Dennis EA (1983) Biochim Biophys Acta 737:285; (b) Lichtenberg D (1985) Biochim Biophys Acta 821:470
14. Dennis EA (1974) Arch Biochim Biophys 165:764
15. Helenius A, Simons K (1975) Biochim Biophys Acta 415:29
16. Bäckman P, Bastos M, Briggner L-E, Hägg S, Hallén D, Lönnbro P, Nilsson S-O, Olofsson G, Schön A, Suurkuusk J, Teixeira C, Wadsö I (1994) Pure Appl Chem 66:375
17. Olofsson G (1985) J Phys Chem 89:1473
18. Holland PM, Rubingh DN (1991) In: Rubingh DN, Holland PM (ed) Cationic surfactants. Physical chemistry. Surfactant science series, vol 37. Dekker, New York, p 141

artigo XI

ELSEVIER

Chemistry and Physics of Lipids
111 (2001) 93–104

CPL
CHEMISTRY AND PHYSICS OF LIPIDS

www.elsevier.com/locate/chemphyslip

Structural and thermal characterization of dioctadecyldimethylammonium bromide dispersions by spin labels

Carlos R. Benatti [a], Eloi Feitosa [a,*], Roberto M. Fernandez [b], M. Teresa Lamy-Freund [b]

[a] *Physics Department, IBILCE/UNESP, Rua Cristóvão Colombo, 2265 Sao Jose do Rio Preto SP, CEP 15054-000, Brazil*
[b] *Instituto de Física, Universidade de S. Paulo, CP 66318, CEP 05315-970, S. Paulo, SP, Brazil*

Received 19 September 2000; received in revised form 22 January 2001; accepted 22 January 2001

Abstract

Dioctadecyldimethylammonium bromide (DODAB) dispersions obtained by simply mixing the amphiphile in water, and by bath-sonication, were investigated by electron spin resonance (ESR) of stearic acids and their methyl ester derivatives, labeled at the 5th and 16th carbons of the acyl chain. The ESR spectra indicate that the non-sonicated dispersions are formed mainly by one population of DODAB vesicles, either in the gel ($T < T_m$) or in the liquid–crystalline ($T > T_m$) state. Around T_m there is a co-existence of the two phases, with a thermal hysteresis of about 3.2°C. In sonicated DODAB dispersions, spin labels indicate two different environments even for temperatures far below T_m: one similar to that obtained with non-sonicated samples, a gel phase, and another one in the liquid–crystalline state. The fluid phase domain present below T_m could correspond to either the periphery of bilayer fragments, reported to be present in sonicated DODAB dispersions, or to high curvature vesicles. © 2001 Elsevier Science Ireland Ltd. All rights reserved.

Keywords: Dioctadecyldimethylammonium bromide; Spin label; Cationic vesicle; Thermal analyses; Melting temperature

1. Introduction

Since the first formation in 1977 of cationic unilamellar vesicles of long double-chain quaternary ammonium surfactants (Kunitake and Okahata, 1977), several methods have been used to prepare stabilized vesicles with well-defined size distribution, which may be suitable as membrane mimetic systems (Fendler, 1982; Carmona-Ribeiro, 1992; Feitosa et al., 2000), catalysts (Kawamuro et al., 1991), drug delivery vehicles or carriers in gene therapy (Lasic, 1993). Several research groups have been investigating the properties of these synthetic vesicles, and searching new applications for them (Carmona-Ribeiro and Chaimovich, 1983; Cuccovia et al., 1990; Car-

* Corresponding author. Tel.: +55-17-2212238; fax: +55-17-2212247.
E-mail address: eloi@df.ibilce.unesp.br (E. Feitosa).

0009-3084/01/$ - see front matter © 2001 Elsevier Science Ireland Ltd. All rights reserved.
PII: S0009-3084(01)00134-7

mona-Ribeiro, 1992; Engberts and Hoekstra, 1995; Cuccovia et al., 1997; Carvalho and Carmona-Ribeiro, 1998; Blandamer et al., 1999; Kikuchi and Carmona-Ribeiro, 2000).

It has been shown that the physical and morphological properties of dioctadecyldimethylammonium chloride (DODAC) or bromide vesicles (DODAX; X being C for Cl^- or B for Br^-), such as the degree of counterion dissociation, hydrodynamic radius, polydispersity and melting temperature, depend on the preparation protocol and the solvent conditions, including the presence of additives (Cuccovia et al., 1990; Feitosa and Brown, 1997; Benatti et al., 1999; Feitosa et al., 2000). Large unilamellar vesicles are formed by simply mixing DODAX with water, at low surfactant concentration (Blandamer et al., 1999; Feitosa et al., 2000). DODAX unilamellar vesicles with higher curvature are then prepared using one of the protocols available, such as extrusion or sonication, the latter being the most used method for preparing high curvature vesicles. Overall, the mean diameter of sonicated DODAX vesicles ranges from 20 to 100 nm, depending on the surfactant chemical structure, solvent composition or sonication conditions. Sonication, however, not only increases the vesicle curvature, but also forms smaller aggregates (with diameter less than 20 nm), possibly bilayer fragments (Liu et al., 1992; Feitosa and Brown, 1997) or lens-like structures (Andersson et al., 1995).

A number of techniques have been used to investigate the phase behavior of DODAX dispersions prepared by different methods. It includes turbidity (Nascimento et al., 1998), static light scattering (Feitosa and Brown, 1997), static fluorescence (Benatti et al., 1999), surface pressure (Gugliotti et al., 1998), differential scanning calorimetry (DSC) (Feitosa et al., 2000), and electron spin resonance (ESR; Liu et al., 1992). Though DSC is the preferred method for measuring the gel to liquid–crystalline phase transition temperature, T_m, several other techniques can give important complementary information on the thermal behavior of lipid systems. Below T_m, the hydrocarbon chains are in a more rigid and extended gel state, whereas above T_m they are in a more flexible and disordered liquid–crystalline phase. Therefore, the cooperativity of the gel to liquid–crystalline phase transition may depend on the vesicle structure and curvature, which, in turn, are determined by the method of vesicle preparation, lipid composition and solvent conditions (ionic strength, pH, presence of additives, etc.). Fluorescence probes incorporated in DODAX aggregates showed that the dispersions prepared by simply mixing DODAX with water (here called non-sonicated dispersion) display a sharp temperature transition at $T_m \approx 42°C$, indicating a highly cooperative gel to liquid–crystalline phase transition. The bath-sonicated samples exhibit a broader temperature transition profile, centered at a somewhat lower transition temperature (Benatti et al., 1999).

The ESR of spin labels incorporated in amphiphilic aggregates have been extensively used to monitor the viscosity and polarity of the microenvironment where the probes are localized (see, for instance, Schreier et al. (1978), Marsh (1981), and references therein). In the present work, we monitored by ESR two differently prepared dioctadecyldimethylammonium bromide (DODAB) dispersions, namely, non-sonicated and bath-sonicated, using four types of spin labels: stearic acid derivatives (SASL) and their methyl ester (MESL), labeled at the 5th and the 16th carbon of the acyl chain (5-SASL, 16-SASL, 5-MESL and 16-MESL). Although the labels display different degrees of hydrophobicity, they exhibit a low solubility in aqueous medium, thus incorporating in the DODAB aggregates. The amphiphiles labeled at the 5th carbon atom monitor the DODAB aggregates closer to their water interface, whereas the 16 C-atom labels give information about the bilayer core, close to the end of the DODAB hydrocarbon chains. Owing to their distinct chemical characteristics, the stearic acid (probably negatively charged in the cationic DODAB aggregates; Ptak et al., 1980) and the methyl ester derivatives (neutral and less polar than the acid) may partition diversely among the structurally different aggregates or bilayer domains present in the samples.

The ESR results presented here bring a new contribution to the understanding of the structure of the DODAB aggregates. They show that below

T_m, in sonicated dispersions, DODAB aggregates share a two-phase (gel and liquid–crystalline) state, whereas in non-sonicated dispersions the coexistence of the two phases is only observed close to the transition temperature. The results are discussed on the basis of the curvature and structure of the aggregates.

2. Materials and methods

2.1. Materials

DODAB from Eastman Kodak, and octadecyltrimethylammonium bromide (C_{18}TAB), from Fluka, were used as purchased. DODAC was obtained from DODAB by ion exchange and recrystallized as described elsewhere (Cuccovia et al., 1997). The 5- and 16-doxyl stearic acid spin labels (5- and 16-SASL) and their methyl ester derivatives, 5- and 16-MESL, were used as purchased from Sigma Chemical Co. Fig. 1 shows the molecular formula of 16-SALS. 5-SALS contains the doxyl group at the 5th C-atom, and the *n*-MELS has the H^+ replaced by the methyl ester group.

2.2. DODAB dispersions and C_{18}TAB micelle preparation

Non-sonicated dispersions were prepared by mixing DODAB crystals with water at 58°C (above T_m) to the final concentration of 5 mM. Bath-sonicated dispersions were obtained by sonicating the 5 mM DODAB dispersions with a Branson 1210 bath-type cell disrupter at 58°C. Fig. 2 shows the effect of bath-sonication time on the optical density (OD) of DODAB dispersions (time $t = 0$ corresponds to the non-sonicated dispersion). It clearly shows that after about 60 min sonication the turbidity attains a plateau, suggesting that the bilayer structures in the dispersion have reached a minimum size. We have sonicated the dispersions for 90 min, safely above the 60 min necessary to achieve the plateau. After preparation, the DODAB dispersions were stored at room temperature, and found to be stable for months, as monitored by light scattering (Feitosa and Brown, 1997). C_{18}TAB micelles were prepared by simply mixing the surfactant crystals (5 mM) in water above the Krafft point of the surfactant (≈ 38°C) and stored at room temperature. Turbidity measurements were made in an UV–visible spectrophotometer (Hitachi, model U-2001) equipped with two quartz square cells (1 cm of optical path-length) for vesicle and reference samples.

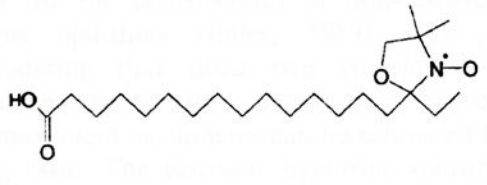


Fig. 1. Molecular formula of 16-doxyl stearic acid spin label (16-SASL).

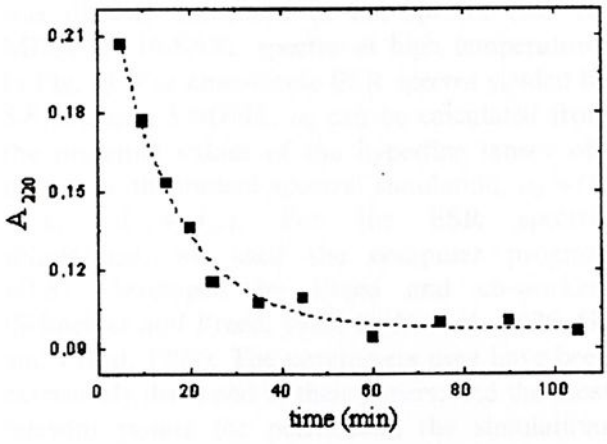


Fig. 2. Effect of bath-sonication time on the turbidity of DODAB aqueous dispersion. Measurements made at $\lambda = 220$ nm.

2.3. Spin labeled sample preparations

Films were formed from chloroform solutions of the spin labels, dried under a N_2 stream and left under reduced pressure for at least 2 h to remove all traces of the organic solvent. Spin labeled dispersions of DODAB and C_{18}TAB were prepared by adding the amphiphilic dispersion to the dried film of spin labels (to a final concentration of no more than 0.8 mol% of label relative to amphiphile, to avoid spin–spin interactions), and

the sample smoothly stirred for 5 min. The ESR measurements were always started within 1 h after the addition of the spin labels to the dispersions.

2.4. ESR spectroscopy

ESR measurements were performed with a Bruker EMX spectrometer. Field-modulation amplitude of 1 G and microwave power of 5 mW were used. The temperature was controlled to about 0.2°C with a Bruker BVT-2000 variable temperature device, and monitored with a Fluke 51 K/J thermometer with the probe placed just above the cavity. The magnetic field was measured with a Bruker ER 035 NMR Gaussmeter, and, when desired, the spectra were converted to a g-value scale with the WINEPR software (Bruker).

2.5. ESR parameters

The empirical parameter A_{max} is the maximum hyperfine splitting directly measured in the spectrum (Fig. 3), which increases with the label microenvironment viscosity and/or order (Freed, 1976). At high temperatures, the parameters of the ESR spectra of the more mobile probes, labeled at the 16th carbon atom, were found by fitting each line to a Gaussian–Lorentzian sum function (Halpern et al., 1993), taking advantage of the fact that the sum function is an accurate representation of a Gaussian–Lorentzian convolution, the Voigt function (Bales, 1989). Due to the difficulty in postulating a preferential rotational axis for the probes (Marsh, 1989), rotational correlation times, τ_B and τ_C, were calculated by the fitting of the ESR spectra, using the principal components of the g and hyperfine tensors of doxyl-propane, and 3300 G for the magnetic field (Schreier et al., 1978). The corrections for the contribution of non-resolved hyperfine splittings (Bales, 1989) were made. Considering that these two correlation times should be identical for rapid, isotropic movement, the movement asymmetry can be estimated by the τ_C/τ_B ratio. The isotropic hyperfine splitting, a_0, was taken to be one-half the difference in the resonance fields of the high- and low-field lines, or was directly measured in the spectra (see 16-MESL or 16-SASL spectra at high temperatures in Fig. 3). For anisotropic ESR spectra yielded by 5-SASL and 5-MESL, a_0 can be calculated from the principal values of the hyperfine tensor obtained by theoretical spectral simulation, $a_0 = (1/3)(A_{xx} + A_{yy} + A_{zz})$. For the ESR spectral simulations, we used the computer program NLSL developed by Freed and co-workers (Schneider and Freed, 1989; Budil et al., 1996; Ge and Freed, 1999). The parameters used have been extensively discussed in their papers, and the most relevant points for performing the simulations have been recently reviewed (Fernandez and Lamy-Freund, 2000). The g-tensor components

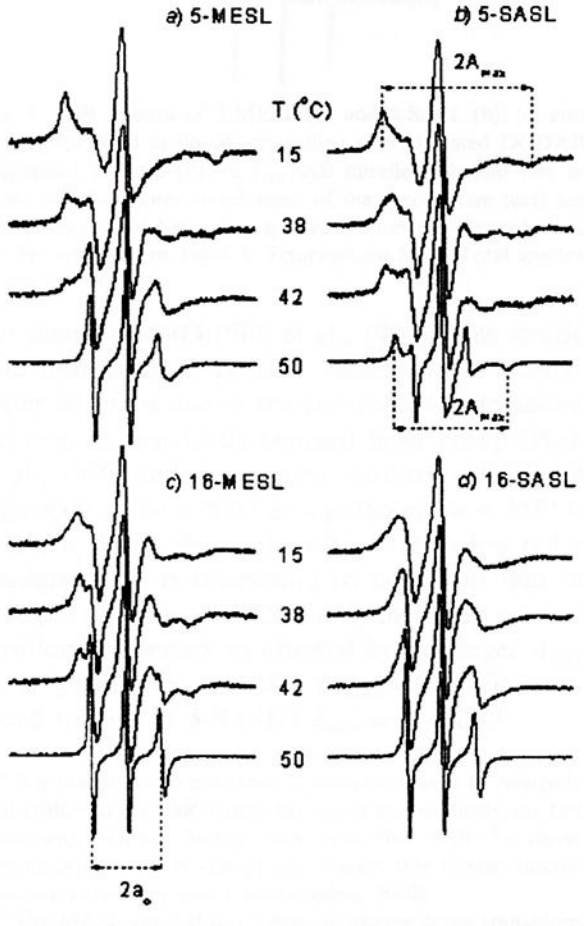


Fig. 3. ESR spectra of 5- and 16-MESL and SASL in non-sonicated DODAB dispersions at 15, 38, 42 and 50°C. Total spectra width 100 G. The outer hyperfine splitting (A_{max}) and the isotropic hyperfine splitting (a_0) are indicated.

were kept as $g_{xx} = 2.0089$, $g_{yy} = 2.0058$ and $g_{zz} = 2.0021$ (Earle et al., 1994; Ge and Freed, 1999). The hyperfine splitting tensor was considered to be axial, $A_{xx} = A_{yy} = A_{\perp}$, and the $A_{\perp}$ and A_{zz} values were allowed to vary within a reasonable interval (Earle et al., 1994). Rotational correlation times ($\tau_{\perp}$ and $\tau_{\parallel}$) were calculated based on the best results obtained for the principal values of an axially symmetric rotational diffusion tensor for the nitroxide moiety attached to the chain segment. The microscopic orientational ordering of the spin label is characterized here by two terms of the restoring potential (Schneider and Freed, 1989), S_{20} and S_{22}, related to the amplitude of the rotational motion.

2.6. Relative vertical position of the SASL and MESL in DODAB bilayers

It is interesting to note that 5-SASL in DODAB aggregates monitors a highly ordered region, as indicated by the rather large A_{max} value measured in the ESR signal (Fig. 3). Accordingly, the theoretical simulation of the 5-SASL signal at 50°C (dashed lines in Fig. 4(b)) indicates that its movement is relatively fast and highly ordered, as evidenced by the fairly low correlation times (mainly a low $\tau_{\parallel}$) and high order parameters (S_{20} and S_{22}; Table 1). The simulation of the 5-MESL signal (dashed lines in Fig. 4(a)) indicates that this label is localized in a less packed bilayer region, presenting lower correlation times and order parameters, relative to 5-SASL (Table 1). Therefore, assuming that the two label molecules incorporate in similar structural regions, and considering the known flexibility gradient towards the membrane center (Hubbell and McConnell, 1971), it can be concluded that, at 50°C, the SASL is localized in a shallower position in the bilayer than the MESL. Hence, for the former, both the correlation time and the order parameter measured in the ESR spectra of the N–O moiety are higher than those obtained for the methyl ester derivative. That is in accord with the somewhat larger isotropic hyperfine splitting, a_0, obtained for 5-SASL as compared to 5-MESL (Table 1), indicating a microenvironment of higher dielectric constant for the N–O group in

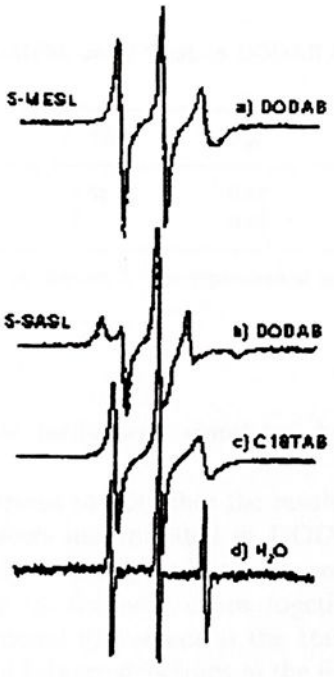


Fig. 4. ESR spectra of 5-MESL (a) and 5-SASL (b), (c) and (d) incorporated in liquid–crystalline non-sonicated DODAB aggregates (a) and (b), in C_{18}TAB micelles (c), and free in water (d). Computer simulations of the spectra (see text) are shown by dashed lines. The spectral parameters derived from the fits are given in Table 1. Temperature 50°C. Total spectra width 100 G.

the stearic acid (Griffith et al., 1974).[1] The stearic acid headgroup is possibly closer to the bilayer/water interface due to the electrostatic interaction between its negatively charged head group (Ptak et al., 1980) and the cationic surface of DODAB aggregates. The methyl group makes the *n*-MESL a very hydrophobic probe with a rather low polar headgroup. It is interesting to point out that in the lipid gel phase (15°C, Fig. 3) the labels relative position is inverted, as attested by the larger A_{max} value yielded by 5-MESL ($A_{max} = 61.4$ G) compared to that of 5-SASL ($A_{max} = 60.4$ G).[2]

[1] It is important to note that a_0 values can only be relatively well evaluated for ESR signals typical of probes displaying fast movement, with correlation times lower than $\sim 10^{-9}$ s, therefore incorporated in fluid phase bilayers (for further discussion, see Fernandez and Lamy-Freund, 2000).

[2] The MESL vertical movement at bilayer phase transitions has been previously observed (Fernandez and Lamy-Freund, 2000; Turchiello et al., 2000) and should be taken into consideration when the information from the different labels is compared.

Table 1
Parameters obtained from non-linear least-squares fitting [a] of the ESR spectra of 5-MESL and 5-SASL in DODAB dispersions at 50°C

	$A_{\parallel}$ (G)	A_{zz} (G)	a_0 (G)	$\tau_{\parallel}$ (ns)	$\tau_{\perp}$ (ns)	S_{20}	S_{22}
5-MESL	5.12	33.84	14.69	0.028	0.61	0.12	−0.15
5-SASL	5.00	34.50	14.83	0.52	17	0.42	−0.57

[a] For the discussion of the simulating program used and the spectral parameters, see Section 2. The experimental and theoretical spectra are shown in Fig. 4.

3. Results and discussion

3.1. Non-sonicated DODAB dispersions

The ESR spectra yielded by the labels 5- and 16-SASL, and 5- and 16-MESL, incorporated in non-sonicated DODAB dispersions, at four different temperatures, are shown in Fig. 3. Due to the flexibility gradient towards the bilayer core (Hubbell and McConnell, 1971), at a certain temperature, the spectra yielded by the 5th carbon labeled amphiphiles are much more anisotropic than those yielded by the probes labeled at the 16th carbon of the acyl chain, which monitor the bilayer core (Fig. 3). Yet, the ESR signals of all four labels can be interpreted as monitoring a highly packed environment at 15°C, typical of amphiphiles in the gel phase, and a much more mobile environment at 50°C, consistent with a bilayer liquid–crystalline state. In the intermediate temperatures, 38 and 42°C, the ESR spectra seem to be due to a mixture of these two phases with distinct degrees of fluidity (this point will be further discussed below).

At 50°C, above T_m, the spectra yielded by the 16 C-atom labels in DODAB non-sonicated dispersion are characteristic of the motionally narrowing region, with a low order parameter (Marsh, 1981). As expected, 5-MESL and 5-SASL, which monitor a relatively organized environment close to the bilayer surface, present anisotropic signals even at high temperatures (large A_{max} values). The simulations shown in Fig. 4 strongly indicate that the bilayer domains present in non-sonicated DODAB dispersions are homogeneous, as the ESR spectrum of each spin label can be fairly well simulated by a single signal.

It is important to note that the results obtained with spin labels incorporated in DODAB aggregates, namely, a highly ordered movement at the 5th position of the acyl chain together with a rather disordered movement at the 16th position, are typical of bilayer structures in the liquid–crystalline state, never yielded by micelles. For comparison, Fig. 4 shows the spectra of 5-SASL incorporated in micelles of the homologue surfactant C_{18}TAB and in water (c and d, respectively). It is evident from the ESR spectrum that 5-SASL in micelles (Fig. 4(c)) undergoes a much more isotropic movement than in DODAB aggregates (Fig. 4(b)), displaying three relatively narrow hyperfine lines, though much broader than those obtained for the spin label tumbling free in water (Fig. 4(d)).

As mentioned before, the ESR spectra of spin labels incorporated in non-sonicated DODAB aggregates at temperatures around 40°C (close to T_m) can be interpreted as the sum of two signals, corresponding to labels in different bilayer structural domains: a gel and a liquid–crystalline phase. This is an indication that the DODAB main phase transition occurs over a range of temperature, with the coexistence of the two phases[3]. Since the use of labels always brings

[3] It is interesting to point out that the fact that two well-separated spectra are obtained shows that the exchange rate between the labels in the two different phase domains is slow on the ESR time scale (lower than about 10^8 s^{-1}). This is more evident for the 16-MESL than for the other spin labels used.



Table 2
Parameters obtained from the fitting of the ESR spectra of 16-MESL and 16-SASL in different samples at 50°C[a]

Sample	16-MESL			16-SASL		
	τ_B (ns)	τ_C (ns)	a_0 (G)	τ_B (ns)	τ_C (ns)	a_0 (G)
NS-DODAB[b]	0.38	0.28	14.35	0.45	0.35	14.24
SO-DODAB[c]	0.37	0.31	14.40	0.49	0.42	14.37
C_{18}TAB	0.21	0.20	14.90	0.15	0.16	14.96
H_2O	–	–	–	0.04	0.04	15.75

[a] For the discussion of the spectral parameters, see Section 2.
[b] Non-sonicated DODAB dispersion.
[c] Sonicated DODAB dispersion. The estimated errors for τ and a_0 are around ± 0.03 ns and ± 0.03 G, respectively.

some uncertainty about their exact location in the membrane, it is interesting to point out that the ESR parameter a_0 indicates that the more mobile signal is also yielded by the nitroxide moiety inside the hydrophobic bilayer core and not at the bilayer/water interface. For example, in the 16-MESL spectrum at 42°C (Fig. 3(c)), where the presence of the two different signals is rather evident, it is possible to estimate the value of the isotropic hyperfine constant of the more mobile signal by direct measurement at the ESR spectrum, $a_0 = 14.16$ G. This low value, compared to the one obtained with 16-SASL in aqueous solution at the same temperature, $a_0 = 15.73$ G (spectrum not shown), indicates that in DODAB dispersions, the spin labels responsible for the two different ESR signals are incorporated inside the aggregates. Moreover, the a_0 value obtained for the mobile signal at 42°C (14.16 G) is close to that yielded by the same sample at 50°C, in the fluid phase, $a_0 = 14.35$ (Table 2). (Usually, the a_0 values do not change much with temperature, varying less than 0.3% from 35 to 50°C, in aqueous solution).

Interestingly, the phase transition shows a hysteresis effect as indicated by the 16-MESL spectra in Fig. 5: at a given temperature, the DODAB bilayer is more fluid under cooling than heating. In order to monitor the phase transition, an empirical parameter is plotted versus the sample temperature (Fig. 6(a)). It is the ratio of the 16-MESL ESR spectrum amplitudes at positions b and a (Fig. 5), where a and b are mainly related to the gel and liquid–crystalline phases, respectively. The gel to liquid–crystalline phase transition temperatures (T_m) were found to be around 39.5 and 42.7°C, under cooling and heating, respectively. No alteration in the two different ESR spectra obtained under heating or cooling the DODAB sample was observed up to 15 min of incubating the sample at 40°C, suggesting that in both cases the surfactant suspension is in a metastable equilibrium.

Another ESR parameter that can be used to monitor the thermal phase transition is the line width of the central field line, ΔH_0 (Fig. 5). Fig.

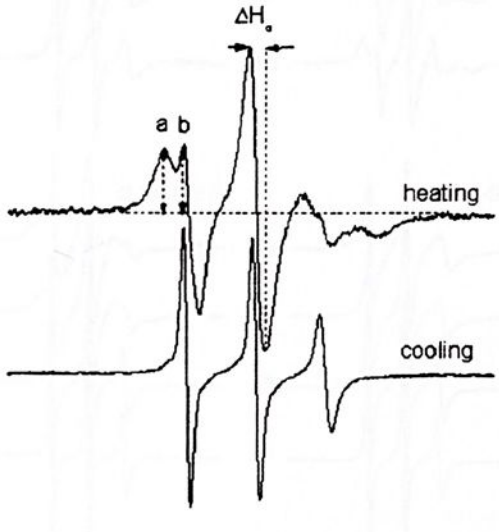


Fig. 5. The hysteresis effect in non-sonicated DODAB dispersions at 40°C, evidenced by the different 5-MESL ESR spectra obtained upon cooling and heating the sample. Total spectra width 100 G. (a) and (b) are the amplitudes at the two indicated positions. ΔH_0 is the line width of the central field line.

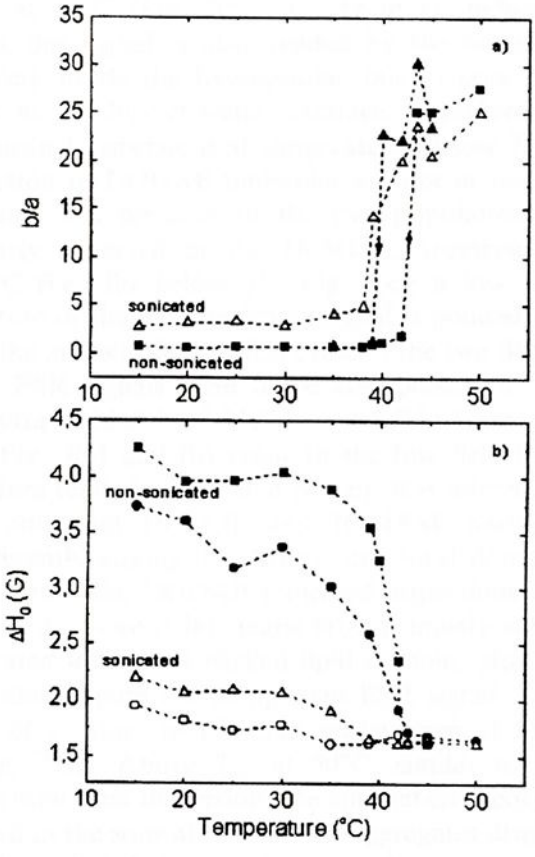


Fig. 6. Temperature dependence of the ratio b/a and the central field line width (ΔH_0; see Fig. 5). The parameters were measured in the ESR spectra of 16-MESL (△, ■, □) and 16-SASL (●,○), in non-sonicated (solid symbols) and sonicated (open symbols) DODAB dispersions. All but (□) were obtained by heating the samples.

6(b) shows the ΔH_0 variation with temperature for both 16-MESL and 16-SASL incorporated in DODAB bilayers. As this is an average parameter, which does not distinguish the two lipid phases, the thermal transition seems to be slightly broader than when monitored by the b/a ratio in the 16-MESL spectra (Fig. 6(a); the 16-SASL monitors an even broader temperature transition, and the b/a ratio cannot be measured in the spectra). The information yielded by this parameter could be similar to those produced by the fluorescent probes that partition among the different bilayer domains, giving an average value of the membrane viscosity (Benatti et al., 1999). For instance, similar to the ESR results presented here, steady-state fluorescence studies revealed a rather sharp (cooperative) main transition for DODAB in non-sonicated dispersions ($T_m \approx$ 42°C), but could not monitor the coexistence of the gel and the fluid phases around T_m (mainly monitored here by the b/a ratio of the 16-MESL ESR spectra).

3.2. Sonicated DODAB dispersions

Unlike the results for non-sonicated DODAB dispersions, spin labels incorporated in DODAB sonicated samples indicate the presence of two distinct lipid populations at 15°C (below T_m): one highly packed, probably in the gel state, and the other one rather mobile. Here, again, the low a_0 parameter measured in the 16-MESL mobile sig-

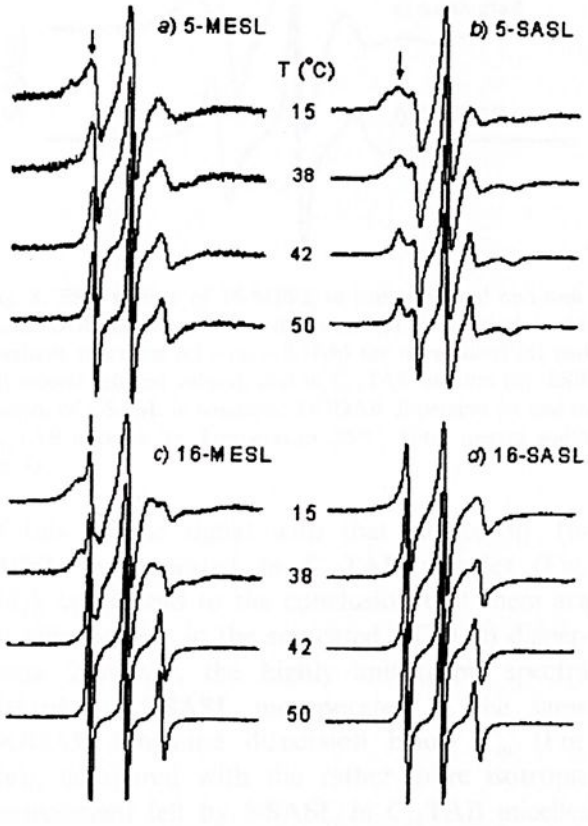


Fig. 7. ESR spectra of spin labels (5- and 16-MESL and SASL) in sonicated DODAB dispersions at different temperatures (15, 38, 42 and 50°C). Total spectra width 100 G. The arrows indicate the low field feature of the more fluid component.

nal at 38°C (Fig. 7(c)), $a_0 \approx 14.46$ G, indicates that this signal is also yielded by the nitroxide moiety inside the hydrophobic bilayer core and not at the bilayer/water interface. Therefore, in sonicated dispersions at temperatures below T_m, a fraction of DODAB molecules are not in the gel phase. The presence of the two populations is clearly observed in the 16-MESL spectrum at 15°C (i.e., far below T_m; Fig. 7(c); a low field feature of the more isotropic signal is pointed out by the arrow). Though less evident, the two different ESR signals seem to be also present in the spectra yielded by 5-MESL and 5-SASL (arrows in Fig. 7(a) and (b) point to the low field ESR feature related to the fluid phase). It is interesting to note that 16-SASL and 16-MESL partition differently among the diverse structural domains present in the DODAB sonicated dispersions. Indeed, the more polar stearic label is mostly incorporated in the less packed lipid domain, yielding an almost pure one-component ESR signal, typical of a rather mobile spin probe, even at 15°C (Fig. 7(d)). Above T_m, at 50°C, similar to the non-sonicated dispersion, the spin labels incorporated in the sonicated DODAB aggregates display ESR spectra that can be interpreted as a one-component signal, typical of a liquid–crystalline sample. Although not discussed here, the results obtained with the four spin labels (5- and 16-SASL and MESL) incorporated in non-sonicated and sonicated DODAC aggregates were found to be very similar to those obtained for DODAB.

It is shown in Fig. 8 that it is possible to decompose the spectrum of 16-MESL in sonicated DODAB dispersions, below the lipid T_m (Fig. 8(a)), in two components: one similar to that obtained with the label in non-sonicated DODAB dispersions (Fig. 8(b)), corresponding to a gel phase (78%), and the other one being a rather mobile signal (22%; Fig. 8(c)).[4] The comparison

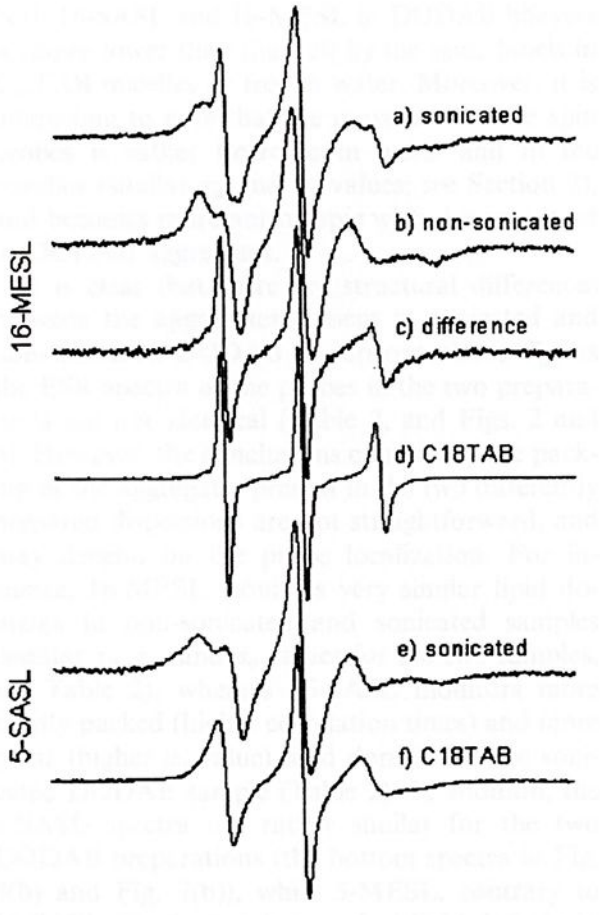


Fig. 8. ESR spectra of 16-MESL in sonicated and non-sonicated DODAB dispersions ((a) and (b), respectively), the resultant spectrum (c) = (a) − 0.78(b) for normalized (a) and (b) second integral values), and in C_{18}TAB micelles (d). ESR spectra of 5-SASL in sonicated DODAB dispersion (e) and in C_{18}TAB micelles (f). Temperature 35°C. Total spectra width 100 G.

of this mobile signal with that yielded by 16-MESL incorporated in C_{18}TAB micelles (Fig. 8(d)), could lead to the conclusion that there are micelles present in the sonicated DODAB dispersions. However, the highly anisotropic spectra yielded by 5-SASL incorporated in the same DODAB sonicated dispersion below T_m (Fig. 8(e)), compared with the rather more isotropic environment felt by 5-SASL in C_{18}TAB micelles (Fig. 8(f)), at the same temperature, indicates that most of the lipid domains monitored in DODAB sonicated dispersion are organized in bilayers and not in micelles.

[4] Spectrum (c) is the resulting signal, (c) = (a) − 0.78(b), after normalizing the areas of the (a) and (b) spectra. The subtraction proceeded by trial and error, judging by eye the quality of the resultant spectrum (Fig. 8(c)), until it looked like a one-component signal and could be reasonably fitted by a Voigt line shape (Bales, 1989). Here, again, the fact that two well-separated spectra are obtained shows that the exchange

Similar to the analysis made for the non-sonicated dispersions, the gel to liquid–crystalline phase transition in the sonicated samples can also be monitored by the b/a ratio measured in the 16-MESL ESR spectra, or the line width of the central field line, ΔH_0, measured in the spectra of both 16-MESL or 16-SASL (Fig. 5). Probably, due to the presence of the two species at low temperatures, the measured phase transition is not so sharp as that observed with the non-sonicated samples (Fig. 6(a)), and can be barely monitored with the ΔH_0 parameter (Fig. 6(b)). Besides, the temperature transition yielded by the b/a ratio (Fig. 6(a)) in sonicated vesicles occurs at about 3°C lower (39°C) than that obtained with the non-sonicated sample (42°C), and no hysteresis could be clearly detected with spin labels. Fluorescent probes have also indicated that in sonicated DODAB dispersions the gel to liquid–crystalline transition is broader and occurs at a lower temperature as compared to the non-sonicated samples (Benatti et al., 1999). However, only the ESR of spin probes can clearly monitor the presence of both the gel and the fluid phases below T_m, in sonicated DODAB and DODAC (not shown) dispersions. It is interesting to point out that the presence of the two phases could possibly explain the different local viscosities measured by the fluorescent and the spin labels in probe-sonicated DODAC dispersions (Liu et al., 1992).

3.3. Comparing the structures of the sonicated and non-sonicated DODAB fluid bilayers

In order to structurally characterize the aggregates present in DODAB dispersions at high temperatures, allowing a comparison between those yielded by non-sonicated and sonicated samples, some spectral parameters of the 16th labeled amphiphiles (16-MESL and 16-SASL) were calculated (Table 2): the correlation times τ_B and τ_C, and the isotropic hyperfine splitting a_0. (The ESR spectra are typical of the motional narrowing region and can be well fitted with Voigt functions; Bales, 1989; see Section 2). Since the isotropic hyperfine constant a_0 increases with the spin label microenvironment polarity (Griffith et al., 1974), Table 2 shows that the bilayer polarity felt by both 16-SASL and 16-MESL in DODAB bilayers is rather lower than that felt by the same labels in C_{18}TAB micelles or free in water. Moreover, it is interesting to note that the movement of the spin probes is rather isotropic in water and in the micelles (similar τ_B and τ_C values; see Section 2), and becomes more anisotropic when incorporated in DODAB aggregates.

It is clear that there are structural differences between the aggregates present in sonicated and non-sonicated DODAB dispersions above T_m, as the ESR spectra of the probes in the two preparations are not identical (Table 2, and Figs. 2 and 6). However, the conclusions concerning the packing of the aggregates present in the two differently prepared dispersions are not straightforward, and may depend on the probe localization. For instance, 16-MESL monitors very similar lipid domains in non-sonicated and sonicated samples (similar τ_B, τ_C, and a_0 values for the two samples, see Table 2), whereas 16-SASL monitors more tightly packed (higher correlation times) and more polar (higher a_0 value) lipid domains in the sonicated DODAB sample (Table 2). In addition, the 5-SASL spectra are rather similar for the two DODAB preparations (the bottom spectra in Fig. 3(b) and Fig. 7(b)), while 5-MESL, contrary to 16-SASL, monitors a less packed lipid domain in the sonicated than in the non-sonicated DODAB dispersion (compare the anisotropy of the bottom spectra in Fig. 3(a) and Fig. 6(a)).

4. Conclusions

Spin labels incorporated in 5 mM DODAB aqueous dispersions indicate that both non-sonicated and bath-sonicated aggregates are mostly organized in bilayers, presenting a well-defined gel to liquid–crystalline phase transition. The lower T_m value yielded by the sonicated samples (39.5°C), compared to the non-sonicated (42.7°C), is in accordance with the presence of smaller vesicles in the former (Feitosa and Brown, 1997; Benatti et al., 1999). Chemically distinct spin labels partition differently among structurally distinct DODAB bilayer domains, therefore monitoring several local environments in the bi-



layer, giving comprehensive information about the system. The time-scale of the ESR spectroscopy, together with its high sensitivity to bilayer viscosity, were also essential for the detection of the coexistence of the gel and liquid–crystalline phases in sonicated and non-sonicated dispersions, at temperatures below or around T_m, respectively. To our best knowledge, ESR of spin labels is the first technique capable of detecting the coexistence of the two phases in DODAX bilayer systems. Below T_m, in sonicated dispersions, DODAX molecules in the liquid–crystalline state could be present in vesicles with high curvature, in the periphery of bilayer fragments (Feitosa and Brown, 1997), or in non-smoothed (lens-like) vesicle structures (Andersson et al., 1995). The presence of a fluid phase in DODAX bilayers below or around T_m, may be important for the different characteristics attributed to these synthetic amphiphilic aggregates, for instance, for the efficient incorporation of proteins or DNA (Lasic, 1993; Carvalho and Carmona-Ribeiro, 1998; Kikuchi and Carmona-Ribeiro, 2000), or peculiar reactions found for bilayer adsorbed molecules (Kawamuro et al., 1991; Andersson et al., 1995).

Acknowledgements

This work was supported by USP, FAPESP and CNPq. Fellowships for R.M.F. and C.R.B. (FAPESP) and M.T.L.F. (CNPq, research) are acknowledged.

References

Andersson, M., Hammarström, L., Edwards, K., 1995. Effect of bilayer phase transitions on vesicle structure and its influence on the kinetics of viologen reduction. J. Phys. Chem. 99, 14531–14538.

Bales, B.L., 1989. Inhomogeneously broadened spin-label spectra. In: Berliner, L.J., Reuben, J. (Eds.), Spin Labeling. Theory and Applications, vol. 8. Plenum Press, New York, pp. 77–130.

Benatti, C.R., Tiera, M.J., Feitosa, E., Olofsson, G., 1999. Phase behavior of synthetic amphiphile vesicles investigated by calorimetry and fluorescence methods. Thermochim. Acta 328, 137–142.

Blandamer, M.J., Briggs, B., Cullis, P.M., Last, P., Engberts, J.B.F.N., Kacperska, A., 1999. Effects of added urea and alkylureas on gel to liquid–crystal transitions in DOAB vesicles. J. Therm. Anal. Calorimetry 55, 29–35.

Budil, D.E., Lee, S., Saxena, S., Freed, J.H., 1996. Nonlinear-least-squares analysis of slow-motion EPR spectra in one and two dimensions using a modified Levenberg-Marquardt algorithm. J. Mag. Res. 120, 155–189.

Carmona-Ribeiro, A.M., Chaimovich, H., 1983. Preparation and characterization of large dioctadecyldimethylammonium chloride liposomes and comparison with small sonicated vesicles. Biochim. Biophys. Acta 733, 172–179.

Carmona-Ribeiro, A.M., 1992. Synthetic amphiphile vesicles. Chem. Soc. Rev. 21, 209–214.

Carvalho, L.A., Carmona-Ribeiro, A.M., 1998. Interaction between cationic vesicles and serum proteins. Langmuir 14, 6077–6081.

Cuccovia, I.M., Feitosa, E., Chaimovich, H., Sepulveda, L., Reed, W., 1990. Size, electrophoretic mobility and ion dissociation of vesicles prepared with synthetic amphiphiles. J. Phys. Chem. 94, 3722–3725.

Cuccovia, I.M., Sesso, A., Abuin, E.B., Okino, P.F., Tavares, P.G., Campos, J.F.S., Florenzano, F.H., Chaimovich, H., 1997. Characterization of dioctadecyldimethylammonium chloride vesicles prepared by membrane extrusion and dichloromethane injection. J. Mol. Liquids 72, 323–336.

Earle, K.A., Moscicki, J.K., Ge, M., Budil, D.E., Freed, J.H., 1994. 250-GHz electron spin resonance studies of polarity gradients along the aliphatic chains in phospholipid membranes. Biophys. J. 66, 1213–1221.

Engberts, J.B.F.N., Hoekstra, D., 1995. Vesicle-forming synthetic amphiphiles. Biochim. Biophys. Acta 1241, 323–340.

Feitosa, E., Brown, W., 1997. Fragment and vesicle structures in sonicated dispersions of dioctadecyldimethylammonium bromide. Langmuir 13, 4810–4816.

Feitosa, E., Barreleiro, P.C.A., Olofsson, G., 2000. Phase transition in dioctadecyldimethylammonium bromide and chloride vesicles prepared by different methods. Chem. Phys. Lipids 105, 210–213.

Fendler, J.H., 1982. Membrane Mimetic Chemistry. Wiley-Interscience, New York.

Fernandez, R.M., Lamy-Freund, M.T., 2000. Correlation between the effects of a cationic peptide on the hydration and fluidity of anionic lipid bilayers: a comparative study with sodium ions and cholesterol. Biophys. Chem. 87, 87–102.

Freed, J.H., 1976. Theory of slow tumbling ESR spectra for nitroxides. In: Berliner, L.J. (Ed.), Spin Labeling: Theory and Applications, vol. 1. Academic Press, New York, pp. 53–132.

Ge, M., Freed, J.H., 1999. Electron-spin resonance study of aggregation of gramicidin in dipalmitoylphosphatidylcholine bilayers and hydrophobic mismatch. Biophys. J. 76, 264–280.

Griffith, O.H., Dehlinger, P.J., Van, S.P., 1974. Shape of the hydrophobic barrier of phospholipid bilayers (evidence for water penetration in biological membranes). J. Membrane Biol. 15, 159–192.

cm 1 2 3 4 5 6 7 8 unesp 12 13 14 15 16 17 18 19

Gugliotti, M., Politi, M.J., Chaimovich, H., 1998. Phase transition temperature of vesicles determined by surface tension: a fast method. J. Colloid Interf. Sci. 198, 1–5.

Halpern, H.J., Peric, M., Yu, C., Bales, B.L., 1993. Rapid quantitation of parameters from inhomogeneously broadened EPR-spectra. J. Magn. Reson. 103, 13–22.

Hubbell, W.L., McConnell, H.M., 1971. Molecular motion in spin-labeled phospholipids and membranes. J. Am. Chem. Soc. 93, 314–326.

Kawamuro, K., Chaimovich, H., Abuin, E., Lissi, E.A., Cuccovia, I., 1991. Evidence that the effects of synthetic amphiphile vesicles on reaction rates depend on vesicle size. J. Phys. Chem. 95, 1458–1463.

Kikuchi, I.S., Carmona-Ribeiro, A.M., 2000. Interactions between DNA and synthetic cationic liposomes. J. Phys. Chem. B 104, 2829–2835.

Kunitake, T., Okahata, Y., 1977. A totally synthetic bilayer membrane. J. Am. Chem. Soc. 99, 3860–3861.

Lasic, D.D., 1993. Liposomes. From Physics to Applications. Elsevier, Amsterdam.

Liu, L., Pansu, R., Roncin, J., Faure, J., Arai, T., Tokumaru, K., 1992. Molecular organization in DODAC membrane fragments. J. Colloid Interf. Sci. 148, 118–128.

Marsh, D., 1981. Electron spin resonance: spin labels. In: Grell, E. (Ed.), Membrane Spectroscopy. Springer, Berlin, pp. 51–142.

Marsh, D., 1989. Experimental methods in spin-label spectral analysis. In: Berliner, L.J., Reuben, J. (Eds.), Spin Labeling. Theory and Applications, vol. 8. Plenum Press, New York, pp. 255–303.

Nascimento, D.B., Rapuano, R., Lessa, M.M., Carmona-Ribeiro, A.M., 1998. Counterion effects on properties of cationic vesicles. Langmuir 14, 7387–7391.

Ptak, M., Egret-Charlier, M., Sanson, A., Boloussa, O., 1980. An NMR study of the ionization of fatty acids, fatty amines and N-acylamino acids incorporated in phosphatidylcholine vesicles. Biochim. Biophys. Acta 600, 387–397.

Schneider, D.J., Freed, J.H., 1989. Calculating slow motional magnetic resonance spectra: a user's guide. In: Berliner, L.J., Reuben, J. (Eds.), Spin Labeling. Theory and Applications, vol. 8. Plenum Press, New York, pp. 1–76.

Schreier, S., Polnaszek, C.F., Smith, I.C.P., 1978. Spin labels in membranes. Problems in practice. Biochim. Biophys. Acta 515, 375–436.

Turchiello, R.F., Juliano, L., Ito, A.S., Lamy-Freund, M.T., 2000. How bradykinin alters the lipid membrane structure. A spin label comparative study with bradykinin fragments and other cations. Biopolymers 54, 211–221.

unesp

artigo XII

20 April 2001

ELSEVIER

Chemical Physics Letters 338 (2001) 88–94

CHEMICAL PHYSICS LETTERS

www.elsevier.nl/locate/cplett

Using an effective surface charge to explain surface potentials of Langmuir monolayers from dialkyldimethylammonium halides with the Gouy–Chapman theory

A. Cavalli [a], P. Dynarowicz-Łątka [b], O.N. Oliveira Jr. [c,*], E. Feitosa [a]

[a] *Departamento de Fisica, IBILCE/UNESP, 15055-000, São José do Rio Preto, SP, Brazil*

[b] *Jagiellonian University, Faculty of Chemistry, Kraków, Poland*

[c] *Instituto de Fisica de São Carlos, Universidade de Sao Paulo, Av. Dr. Carlos Botelho 1465, 13560 970 São Carlos, SP, Brazil*

Received 10 August 2000; in final form 20 February 2001

Abstract

The use of an effective surface charge density has allowed the Gouy–Chapman (GC) theory to explain surface potential isotherms of Langmuir monolayers of dioctadecyldimethylammonium bromide (DODAB). The effective surface charge density of DODAB monolayer increases with the electronegativity of the counterions in the subphase. The pressure–area isotherms indicate a very condensed monolayer for DODAB spread on an I^--containing subphase, which exhibits the lowest surface charge density, whereas the monolayer on a F^--containing subphase is extremely expanded owing to the high surface charge density or electrostatic repulsion between headgroups. © 2001 Published by Elsevier Science B.V.

1. Introduction

Dialkyldimethylammonium halides (DODAX) are synthetic double-chain cationic surfactants extensively investigated in mono- and bilayer structures, that is, at interfaces and bulk solution.Various physicochemical methods [1–7] confirm the similarity of their molecular assembly to those of phospholipids found in cellular walls, thus justifying the use of the quaternary dialkylammonium salts as model systems for the simulation of biomembranes. The hydrophilic–hydrophobic balance in long alkyl double-chain quaternary ammonium salts (like DODAX) is responsible for their ability to form stable Langmuir monolayers at the air/water interface [8–15]. Also, when dispersed in aqueous solution, they can readily form bilayer structures such as lamellae, vesicles or liposomes [14–18]. It is well known that the structure and properties of colloidal systems as well as monolayers are modified by the environment. Many investigations have concentrated on the influence of various factors on dialkyldimethylammonium assemblies. Concerning colloidal structures, not only the composition of the medium but also the dispersion method applied has been found to play an important role in their properties and stability [17]. Langmuir monolayers of dialkylammonium salts, on the other hand, have mainly been studied in view of their behavior on subphases containing different ions. Ahuja et al. [11] showed that the monolayer characteristics as

* Corresponding author. Fax: +55-16-272-2218.
E-mail address: chu@if.sc.usp.br (O.N. Oliveira Jr.).

0009-2614/01/$ - see front matter © 2001 Published by Elsevier Science B.V.
PII: S0009-2614(01)00272-X

well as its morphology depend strongly on the nature of the monovalent anion in the subphase. Also, the phase transition of the liquid expanded to liquid condensed (LE–LC) phases, observed for dioctadecyldimethylammonium chloride (DODAC) monolayers on a pure water subphase only below 26°C, was found to be more pronounced on subphases containing NaCl and appeared at a lower surface pressure [12]. The influence of hydrophobic ions (namely hexafluorophosphate, picrate and tetraphenylborate) on dioctadecyldimethylammonium bromide (DODAB) monolayers has been investigated by Shapovalov [14,15]. In this Letter we analyze surface pressure and surface potential data, where the latter are semi-quantitatively explained using the Gouy–Chapman (GC) theory with a discussion on the possible maximum charge distribution at the interface.

2. Materials and methods

DODAB (Eastman Kodak) was used as received. KBr and KI (both Mallinckrodt Baker, purity 99%+), NaCl (Merck, 99.5% purity), NaF (Merck, 99%) were used without further purification. The surface pressure and potential vs. area per molecule isotherms were measured simultaneously on a KSV 5000 Langmuir trough, housed in a class 10 000 clean room at ca. 20°C, equipped with a Wilhelmy plate (made of filter paper) and a Kelvin probe. Surface pressure was measured with an accuracy of ±0.1 mN/m and the electric surface potential was recorded within an experimental error of ±20 mV. Langmuir monolayers of DODAB were obtained by spreading a chloroform (Sigma, HPLC grade) solution of DODAB on the aqueous subphase prepared by dissolving 10^{-2}, 10^{-3} or 10^{-4} M of a particular inorganic salt in ultrapure water supplied by a Milli-Q system (resistivity = 18.2 MΩ cm). Monolayers spread onto NaOH (Mallinckrodt, 99.5% purity) solution were also investigated. After spreading the monolayer, a few minutes were allowed for chloroform evaporation before starting the monolayer compression. In the text DODAX means DODAB organized as a monolayer on a subphase containing the counterion X^-.

3. Results and discussion

Fig. 1a–c display surface pressure and surface potential vs. area per molecule isotherms for DODAB monolayers spread on pure water and aqueous subphases containing 10^{-4}, 10^{-3} and 10^{-2} M of the monovalent counterions F^-, Cl^-, Br^-, I^- and OH^-. It is worth noticing that for all concentrations investigated, the surface pressure for molecular areas larger than 50 Å^2 increases with the electronegativity of the counterion, i.e., it follows the order $F^- > OH^- > Cl^- > Br^- > I^-$. The isotherm of DODAB spread on the aqueous KI subphase is the only one that does not exhibit any plateau region, in addition to having the most condensed character. Even at large areas per molecule, the surface pressure has non-zero value for monolayers spread on the F^--containing aqueous subphases.

A detailed investigation of the structure of DODAC monolayers has already been done by Adolf et al. [19]. The calculation of the order parameter of alkyl tails using anisotropic noncovalent interactions and the Steele torsional potential show that the structure of hydrophobic tails goes from a quite disordered (77 Å^2) to an ordered phase (57 Å^2). These areas coincide with those observed in this work in the plateau regions for all concentrations of Br^- and Cl^- in the subphase. Thus, it is likely that the energy necessary for the ordering of hydrophobic chains depends on the electronegativity of the counterion, but not on the counterion concentration. Ahuja et al. [11] investigated DODAB monolayers on aqueous solutions with different monovalent counterions by Brewster angle microscopy (BAM) and observed the appearance of aggregates in the expanded monolayer ($\pi = 0$) in the presence of ions I^- in the subphase. By considering the geometrical dimensions of DODAB molecules, the area available for one molecule in the aggregate is small, suggesting that the hydrophobic chains are already ordered even at large areas per molecule (low pressure). From our results, the DODAB monolayer becomes increasingly expanded as the electronegativity of the counterion is augmented, being most expanded for F^- and least expanded for I^- in the subphase.



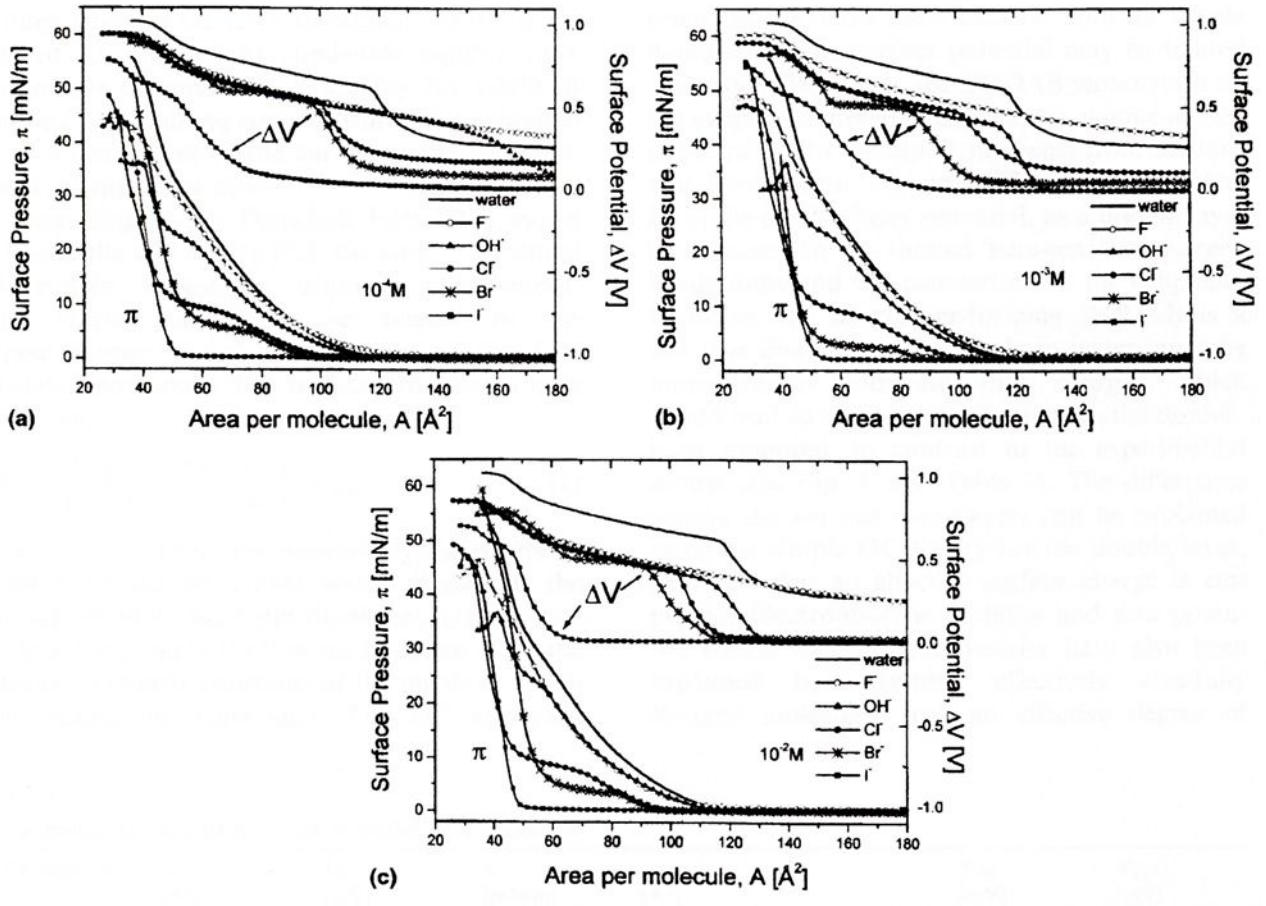


Fig. 1. Pressure–area and surface potential isotherms of DODAB on pure water and on subphases containing monovalent ions: water (solid), F (open circle), OH (triangle), Cl (solid circle), Br (star), I (square). Concentration of ions in the subphase: 10^{-4} mol/L (a), 10^{-3} mol/L (b), and 10^{-2} mol/L (a).

This can be explained by the electrostatic repulsion between the charged headgroups, which depends on the screening effects by the adsorbed counterions. Such differences in repulsion should not exist if the monolayers were fully charged. However, the analysis of the surface potential data (shown below) indicates that the effective charge – which actually contributes to the double-layer potential – may be considerably lower than the fully ionized monolayer charge, as is the case for DODAB and analogous vesicles in solution [23].

Fig. 1a–c also show the surface potential isotherms of DODAB on subphases containing monovalent salts. Unlike most of the film-forming molecules which show zero surface potential at large areas per molecule (zero pressure), the initial surface potential for DODAB monolayers is not zero, but increases with the electronegativity of the counterion at low surface densities of DODAB. The presence of ions in the subphase also affects the critical areas at which the surface potential starts to increase, as well as the maximum surface potential. An exception is the isotherm for the monolayer spread on the F^--containing subphase, for which no clear critical area can be distinguished and the surface potential increases steeplessly. The steep increase in the surface potentials is related to an abrupt decrease of the local dielectric constant in the vicinity of polar head

groups from 80 (at large molecular areas) to 6.4 [20] or 7.6 [21] (in the condensed region) upon monolayer compression. Especially for DODAB on the F^--containing aqueous solution the double-layer contribution to the surface potential dominates, as discussed below.

According to the Demchak–Fort (DF) model [21] and the GC theory [22], the surface potential of simple long-chain aliphatic compounds, e.g., stearic acid, may be related to the dipole moments of the molecules, and the double-layer potentials. The surface potential is then given by:

$$\Delta V = \frac{1}{A\varepsilon_0}\left(\frac{\mu_1}{\varepsilon_1}+\frac{\mu_2}{\varepsilon_2}+\frac{\mu_3}{\varepsilon_3}\right)+\psi_0, \quad (1)$$

where μ_1, μ_2 and μ_3 are respectively the contributions from the reoriented water dipoles at the monolayer interface, from dipoles at the film–water interface, and at the film–air interface. ε_i are the effective dielectric constants of the media in which the dipoles are embedded. The DF approach points out that the contributions from the dipole moments to the surface potential may be treated separately. Therefore, for DODAB monolayers on the subphases investigated here, we assume a fixed contribution to the dipole moments from the tails and headgroups. The only difference would then be in the double-layer potential, as a double layer is expected to be formed between the charged headgroups and the counterions in the subphase. However, the monolayer-forming DODAB is a salt that dissociates completely in water, and the monolayer is nominally fully charged, which would lead to similar contributions to the double-layer potential, in contrast to the experimental results (see Fig. 1 and Table 1). The differences among the various monolayers can be explained using the simple GC theory for the double layer, provided that an effective surface charge is employed. Electrophoretic mobility and zeta potential results for DODAB vesicles have also been explained by assuming effectively non-fully charged molecules, and an effective degree of

Table 1
Experimental and calculated values of double-layer potentials[a]

Counterion	C (M)	V_m (mV)	π (mN/m)	A (Å^2)	α	Ψ_{645} (mV)	$\Psi_0(\alpha)$ (mV)
Water	3.3×10^{-6}	1012	50	42	0.3	367	350
F^-	10^{-4}	979	43	35	1	334	334
	10^{-3}	940	46			295	276
	10^{-2}	857	46			212	218
Cl^-	10^{-4}	930	43	35	0.4	285	288
	10^{-3}	885	43			240	231
	10^{-2}	839	43			194	172
OH^-	10^{-4}	917	36	41	0.3	272	266
	10^{-3}	837	36			192	208
	10^{-2}	780	36			135	150
Br^-	10^{-5}	892	49	45	0.2	247	299
	10^{-4}	870	47			225	240
	10^{-3}	848	46			203	182
	10^{-2}	789	48			144	125
	10^{-1}	729	49			84	70
I^-	10^{-4}	744	44	33	0.015	99	126
	10^{-3}	709	45			64	71
	10^{-2}	688	45			43	29

[a] C is the subphase ion concentration, V_m is the maximum potential, π is the surface pressure, A is the collapse area, α is related to the effective surface charge density, Ψ_{645} is the potential of GC double layer subtracting 645 mV due to the molecular dipole moments of DODAB and $\Psi_0(\alpha)$ is the calculated value of GC using the effective α.



dissociation below 0.35 for DODAB vesicles in NaCl and 0.13 in NaBr solution [23].

Within the GC model, the basic assumptions are: (i) the charged surface is impenetrable, (ii) the charge is uniformly spread over it, (iii) the counterions behave as point charges, being able to approach up to the plane of the surface charges, and (iv) the solvent is assumed to be a uniform medium with a fixed dielectric constant. Using the Boltzmann equation for the ionic distribution, together with Poisson equation, the potential difference across the double layer, Ψ_0, at 293 K is found [22,24] to be:

$$\Psi_0 = 50.4 \sinh^{-1}(134 \cdot \alpha / A\sqrt{c}), \quad (2)$$

where A is the area per molecule in the monolayer, c is the bulk molar concentration of counterions, and α is the degree of dissociation of the film-forming molecules. Eq. (2) relates the surface potential with the bulk concentration of counterion and α. In order to apply the GC theory, the picture we envisage is one in which the counterions may be adsorbed under the charged monolayer, thus reducing the effective surface charge contributing to the double-layer potential. The data available do not suffice to determine whether the ion adsorption obeys a simple adsorption isotherm, e.g., Langmuir-type adsorption equation. In principle, a more quantitative treatment of the double-layer potential distribution should take into account the Stern layer in addition to the chemical activity of the counterions, but these effects are difficult to parameterize. Nevertheless, since the simple GC theory seems accurate enough to explain the double-layer potentials with monovalent counterions in a variety of situations where it was expected to fail [25], we have tried this model in the analyses of our data. The results are summarized in Table 1. By assuming that all DODAB molecules on subphases containing monovalent inorganic counterions have the same contribution to the dipole moment, we obtained the double-layer contributions for the various counterions and ionic concentrations. The experimentally determined double-layer potentials agree reasonably well with those calculated using the GC theory, provided that the surface charge density (represented by α) is allowed to vary from one compound to the other, indicating some specificity of the counterion binding. Accordingly, F^- appears to be the only ion leading to an effectively fully ionized DODAB monolayer (Table 1). I^-, on the other hand, displays a very small effective surface charge, which is consistent with the condensed nature of DODAI monolayers. By the same reason, the DODAF monolayer is the most expanded while the other ones display an intermediate expansion behavior.

There are a few points worthy of attention in the values of α (Table 1). First, it cannot be considered as the actual degree of dissociation, as it usually is in the GC theory, for the monolayers under investigation are nominally fully charged. Therefore, α simply reflects an effective charge density for the counterion adsorption causing the surface charge to decrease. Strictly speaking, if α were merely the degree of dissociation, it should increase with the ionic concentration according to the Henderson–Hasselbach equation [26], as is the case for stearic acid monolayers [22]. Using an α that is independent of the ion concentration, as we have done, is certainly an approximation. For instance, taking the potential values for Br^- in Table 1, one notes that the surface potential decreases as the salt concentration (ionic strength) is increased, as expected. However, a tenfold decrease in the counterion concentration does not correspond, on average, to a 58 mV increase in the measured potential, which implies that the effective charge density is altered with concentration. The values of α reported here confirm that colloidal or interfacial systems containing Br^- counterions are less charged than those containing Cl^-, in good agreement with the findings of [23] for DODAB vesicle suspensions. The use of an effective surface charge density was indeed expected on the basis of Monte Carlo simulations for interactions between charged macroions [27]. A further advantage of using an effective surface charge was that we did not need to consider the Stern layer of adsorbed counterions, which would require determination of adsorption parameters for the different ions. When data become available for a wide range of ion concentrations, the results using an effective surface charge can be compared to those employing a Stern model, as has been done for *n*-dodecyl sulfate adsorbed at air–salt solution interfaces [28].



Also, α appears to increase with the size of the hydrated counterion ($F^- > Cl^- > Br^- > I^-$ [29]), with the largest ions (F^-) displaying no binding to the monolayer and therefore leading to an effectively fully ionized monolayer, consistent with the results for bilayers of dioctadecyldimethylammonium salt surfactants [30].

For large areas (low pressure), the non-zero surface potentials for most DODAX monolayers (DODAB on different counterion subphases) can be explained by the double-layer potentials, which are positive for positively charged film-forming molecules. In fact, the large double-layer potential for DODAF (F^- in the subphase) at large areas per molecule prevents the steep increase in the surface potential at a critical area, for in this case the area-dependence of the double-layer potential predominates. For the other monolayers with less effective charge, a steep increase is observed.

4. Conclusion

Contrary to what one may have expected, Langmuir monolayers of DODAB are not fully ionized at the air/water interface. The effective surface charge density increases with the electronegativity of the counterions in the subphase owing to a selective binding to the interface, which affects not only the monolayer surface potential – via electrical double layer – but also the pressure–area isotherms. In practice, the use of an effective surface charge density corresponds to relaxing an important limitation of the GC theory that assumes no penetration of counterions into the charged surface, which is the reason why the simple GC model can be employed to explain surface potential data. Actually, a reduction of surface charge was described by Monte Carlo simulations, although in a different context [27].

Acknowledgements

The authors are grateful to FAPESP (proc. no. 98/04798) and CNPq (Brazil) for their financial assistance. We also thank Mark Robbins (Johns Hopkins University) for having drawn our attention to the importance of an effective charge in Poisson–Boltzmann equations.

References

[1] T. Kajiyama, A. Kumano, M. Takanagi, Y. Okahata, T. Kunitake, in: W.J. Bailey, T. Tsuruta (Eds.), Contemporary Topics in Polymer Science, vol. 4, Plenum Press, New York, 1984, p. 829.
[2] K. Okuyama, K. Hoso, N. Maki, H. Hamatsu, Thin Solid Films 203 (1991) 161.
[3] E. Alami, H. Levy, R. Zana, P. Weber, A. Skoulios, Liq. Cryst. 13 (1993) 201.
[4] K. Okuyama, Y. Soboi, N. Iijima, K. Hirabayashi, T. Kunitake, T. Kajiyama, Bull. Chem. Soc. Jpn. 61 (1988) 1485.
[5] T. Kunitake, Y. Okahata, K. Tamaki, F. Kumamaru, M. Takayanagi, Chem. Lett. (1977) 387.
[6] T. Kunitake, Y. Okahata, J. Am. Chem. Soc. 99 (1977) 3860.
[7] E. Feitosa, P.C.A. Barreleiro, G. Olofsson, Chem. Phys. Lipids 105 (2000) 210.
[8] L.G.T. Eriksson, P.L. Claesson, S. Ohnishi, M. Hato, Thin Solid Films 300 (1997) 240.
[9] P. Dynarowicz, N. Vila Romeu, J. Miñones Trillo, Colloid Surf. A 131 (1998) 249.
[10] F. Bonosi, G. Gabrielli, Colloid and Surf. 52 (1991) 277.
[11] R.C. Ahuja, P.L. Caruso, D. Möbius, Thin Solid Films 242 (1994) 195.
[12] D.M. Taylor, Y. Dong, C.C. Jones, Thin Solid Films 284–285 (1996) 130.
[13] O. Mori, T. Imae, J. Colloid Interface Sci. 198 (1998) 11.
[14] V.L. Shapovalov, Russ. Chem. Bull. 45 (1996) 1611.
[15] V. Shapovalov, A. Tronin, Langmuir 13 (1997) 4870.
[16] K. Deguchi, J. Mino, J. Colloid Interface Sci. 65 (1978) 155.
[17] A.M. Carmona-Ribeiro, B.R. Midmore, J. Phys. Chem. 96 (1992) 3542.
[18] M. Stelzle, G. Weissmüller, E. Sackmann, J. Phys. Chem. 97 (1993) 2974.
[19] D.B. Adolf, D.J. Tildesley, M.R.S. Pinches, J.B. Kingdon, T. Madden, A. Clark, Langmuir 11 (1995) 237.
[20] O.N. Oliveira Jr., D.M. Taylor, T.J. Lewis, S. Salvagno, C.J.M. Stirling, J. Chem. Soc. Faraday Trans. I 85 (1989) 1009.
[21] R.J. Demchak, T.J. Fort Jr., J. Colloid Interface Sci. 46 (1974) 191.
[22] D.M. Taylor, O.N. Oliveira Jr., H. Morgan, Chem. Phys. Lett. 161 (1989) 147.
[23] I.M. Cuccovia, E. Feitosa, H. Chaimovich, L. Sepulveda, W. Reed, J. Phys. Chem. 94 (1990) 3722.
[24] J.T. Davies, E.K. Rideal, in: Interfacial Phenomena, Academic Press, London, 1963.

cm 1 2 3 4 5 6 7 8 unesp 12 13 14 15 16 17 18 19

[25] O.N. Oliveira, Jr., PhD Thesis, University of Wales, Bangor, 1990.
[26] P. Dynarowicz-Łątka, A. Cavalli, O.N. Oliveira Jr., Thin Solid Films 360 (2000) 261.
[27] M.J. Stevens, M.L. Falk, M.O. Robbins, J. Chem. Phys. 104 (1996) 5209.
[28] P. Warszyński, W. Barzyk, K. Lunkenheimer, H. Fruhner, J. Phys. Chem. B 102 (1998) 10948.
[29] J. Burgess, in: Ions in Solutions. Basic Principles and Chemical Introduction, Ellis Horwood, New York, 1988.
[30] J. Marra, J. Phys. Chem. 90 (1986) 2145.





cm 1 2 3 4 5 6 7 8 unesp 12 13 14 15 16 17 18 19